NASA/TM–2015-218780
NESC-RP-14-00948

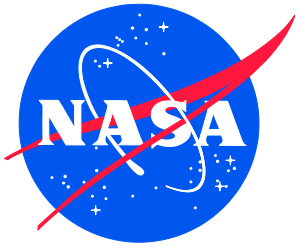

Joint Polar Satellite System (JPSS) Micrometeoroid and Orbital Debris (MMOD) Assessment

Michael D. Squire/NESC
Langley Research Center, Hampton, Virginia

William J. Cooke
Marshall Space Flight Center, Huntsville, Alabama

Joel Williamsen
Institute for Defense Analyses, Alexandria, Virginia

Donald Kessler
Independent Consultant, Asheville, North Carolina

William E. Vesely
NASA Headquarters, Washington DC

Scott H. Hull
Goddard Space Flight Center, Beltsville, Maryland

William Schonberg
Missouri University of Science and Technology, Rolla, Missouri

Glenn E. Peterson, and Alan B. Jenkin
The Aerospace Corporation, El Segundo, California

Steven L. Cornford
Jet Propulsion Laboratory, Pasadena, California

July 2015

NASA STI Program . . . in Profile

Since its founding, NASA has been dedicated to the advancement of aeronautics and space science. The NASA scientific and technical information (STI) program plays a key part in helping NASA maintain this important role.

The NASA STI program operates under the auspices of the Agency Chief Information Officer. It collects, organizes, provides for archiving, and disseminates NASA's STI. The NASA STI program provides access to the NTRS Registered and its public interface, the NASA Technical Reports Server, thus providing one of the largest collections of aeronautical and space science STI in the world. Results are published in both non-NASA channels and by NASA in the NASA STI Report Series, which includes the following report types:

- TECHNICAL PUBLICATION. Reports of completed research or a major significant phase of research that present the results of NASA Programs and include extensive data or theoretical analysis. Includes compilations of significant scientific and technical data and information deemed to be of continuing reference value. NASA counter-part of peer-reviewed formal professional papers but has less stringent limitations on manuscript length and extent of graphic presentations.

- TECHNICAL MEMORANDUM. Scientific and technical findings that are preliminary or of specialized interest, e.g., quick release reports, working papers, and bibliographies that contain minimal annotation. Does not contain extensive analysis.

- CONTRACTOR REPORT. Scientific and technical findings by NASA-sponsored contractors and grantees.

- CONFERENCE PUBLICATION. Collected papers from scientific and technical conferences, symposia, seminars, or other meetings sponsored or co-sponsored by NASA.

- SPECIAL PUBLICATION. Scientific, technical, or historical information from NASA programs, projects, and missions, often concerned with subjects having substantial public interest.

- TECHNICAL TRANSLATION. English-language translations of foreign scientific and technical material pertinent to NASA's mission.

Specialized services also include organizing and publishing research results, distributing specialized research announcements and feeds, providing information desk and personal search support, and enabling data exchange services.

For more information about the NASA STI program, see the following:

- Access the NASA STI program home page at *http://www.sti.nasa.gov*

- E-mail your question to help@sti.nasa.gov

- Phone the NASA STI Information Desk at 757-864-9658

- Write to:
  NASA STI Information Desk
  Mail Stop 148
  NASA Langley Research Center
  Hampton, VA 23681-2199

NASA/TM–2015-218780
NESC-RP-14-00948

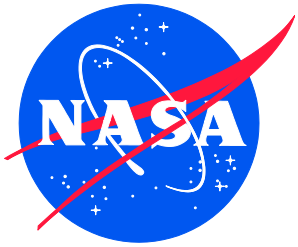

Joint Polar Satellite System (JPSS) Micrometeoroid and Orbital Debris (MMOD) Assessment

Michael D. Squire/NESC
Langley Research Center, Hampton, Virginia

William J. Cooke
Marshall Space Flight Center, Huntsville, Alabama

Joel Williamsen
Institute for Defense Analyses, Alexandria, Virginia

Donald Kessler
Independent Consultant, Asheville, North Carolina

William E. Vesely
NASA Headquarters, Washington DC

Scott H. Hull
Goddard Space Flight Center, Beltsville, Maryland

William Schonberg
Missouri University of Science and Technology, Rolla, Missouri

Glenn E. Peterson, and Alan B. Jenkin
The Aerospace Corporation, El Segundo, California

Steven L. Cornford
Jet Propulsion Laboratory, Pasadena, California

National Aeronautics and
Space Administration

Langley Research Center
Hampton, Virginia 23681-2199

July 2015

Acknowledgments

The NESC team would like to recognize the contributions of the following people in support of this assessment:

Ivonne Rodriguez, GSFC – Debris Assessment Software (DAS) and Bumper Support and JPSS-1 Assessment Support

Genevieve Devaud, Ball Aerospace and Technologies Corporation – JPSS-1 Construction Details

Steven Evans, Marshall Space Flight Center (MSFC) – Hydrocode Simulations

James Hyde, Johnson Space Center (JSC) – Bumper and Shielding Design Support

Dana Lear, JSC – Bumper and Shielding Design Support

Iain Miller, Stinger Ghaffarian Technologies/GSFC – JPSS-1 Wiring Harness Design Details

Available from:

NASA STI Program / Mail Stop 148
NASA Langley Research Center
Hampton, VA 23681-2199
Fax: 757-864-6500

Joint Polar Satellite System (JPSS) Micrometeoroid and Orbital Debris (MMOD) Assessment

April 23, 2015

Report Approval and Revision History

NOTE: This document was approved at the April 23, 2015, NRB. This document was submitted to the NESC Director on May 18, 2015, for configuration control.

Approved:	*Original Signature on File*	5/18/15
	NESC Director	Date

Version	Description of Revision	Office of Primary Responsibility	Effective Date
1.0	Initial Release	Michael Squire, NESC Principal Engineer, LaRC	4/23/15
1.1	Added an additional name to the signature sheet. *(No signature required)*	Michael Squire, NESC Principal Engineer, LaRC	4/23/15

Table of Contents

Technical Assessment Report

List of Figures

List of Tables

Technical Assessment Report

1.0 Notification and Authorization

Andre Dress, Joint Polar Satellite System (JPSS) Deputy Project Manager at Goddard Space Flight Center (GSFC), requested an independent evaluation of the Micrometeoroid and Orbital Debris (MMOD) models used in the latest JPSS MMOD risk assessment. The principal focus of the assessment was to compare Orbital Debris Engineering Model version 3 (ORDEM 3.0) with the Meteoroid and Space Debris Terrestrial Environment Reference version 2009 (MASTER-2009) and Aerospace Debris Environment Projection Tool (ADEPT) and provide recommendations to the JPSS Project regarding MMOD protection.

Michael Squire, NASA Engineering and Safety Center (NESC) Principal Engineer at Langley Research Center, was assigned to lead this assessment.

The key stakeholders for this assessment were Andre Dress, JPSS Deputy Project Manager; Kenneth Yienger, JPSS Chief Engineer; and Glenn Iona, JPSS Flight Project Mission System Engineer.

Other interested organizations included the Office of Safety and Mission Assurance (OSMA), the Office of the Chief Engineer, and other satellite missions with orbital locations that result in high MMOD risk.

2.0 Signature Page

Submitted by:

Team Signature Page on File – 5/28/15

Mr. Michael D. Squire Date

Significant Contributors:

Dr. William J. Cooke Date

Dr. Joel Williamsen Date

Mr. Donald Kessler Date

Dr. William E. Vesely Date

Mr. Scott M. Hull Date

Dr. William Schonberg Date

Dr. Glenn E. Peterson Date

Mr. Alan B. Jenkin Date

Dr. Steven L. Cornford Date

Signatories declare the findings, observations, and NESC recommendations compiled in the report are factually based from data extracted from program/project documents, contractor reports, and open literature, and/or generated from independently conducted tests, analyses, and inspections.

3.0 Team List

Name	Discipline	Organization
Core Team		
Michael Squire	NESC Lead	NESC/LaRC
Joe Pellicciotti	Former NESC Chief Engineer	NESC/GSFC
Steven Cornford	Systems Analysis	JPL
Scott Hull	Orbital Debris	GSFC
Alan Jenkin	MMOD Simulation	The Aerospace Corporation
Don Kessler	Orbital Debris	Independent Consultant
Glenn Peterson	MMOD Simulation	The Aerospace Corporation
William Schonberg	MMOD	Missouri University of Science and Technology
Roger Thompson	MMOD Simulation	Chantilly Aerospace
William Vesely	OSMA	NASA HQ
Joel Williamsen	MMOD	Institute for Defense Analyses
Roy Savage	MTSO Program Analyst	NESC/LaRC
Consultants		
Eric Christiansen	Hypervelocity Impact Technology	JSC
William Cooke	Micrometeoroid Environment	MSFC
Mark Matney	Orbital Debris Environment	JSC
Administrative Support		
Melinda Meredith	Project Coordinator	AMA/LaRC
Linda Burgess	Planning and Control Analyst	AMA/LaRC
Christina Williams	Technical Writer	AMA/LaRC

3.1 Acknowledgements

The NESC team would like to recognize the contributions of the following people in support of this assessment:

Ivonne Rodriguez, GSFC – Debris Assessment Software (DAS) and Bumper Support and JPSS-1 Assessment Support

Genevieve Devaud, Ball Aerospace and Technologies Corporation – JPSS-1 Construction Details

Steven Evans, Marshall Space Flight Center (MSFC) – Hydrocode Simulations

James Hyde, Johnson Space Center (JSC) – Bumper and Shielding Design Support

Dana Lear, JSC – Bumper and Shielding Design Support

Iain Miller, Stinger Ghaffarian Technologies/GSFC – JPSS-1 Wiring Harness Design Details

4.0 Executive Summary

Micrometeoroid and orbital debris (MMOD) risk assessments that use the newest orbital debris environment model, the Orbital Debris Engineering Model version 3.0 (ORDEM 3.0), will likely result in higher risk predictions than assessments performed with the previous model, ORDEM2000, for spacecraft operating between 600 and 1000 km and not shielded against debris up to 3 mm in size. This was the case for the Joint Polar Satellite System (JPSS), where assessed MMOD risk was up to 26 times higher using ORDEM 3.0 on JPSS-1 (the second satellite in the JPSS constellation) components considered critical to supporting post-mission disposal. The JPSS Project requested that the NESC assess ORDEM 3.0 relative to other orbital debris environment models and assist in mitigating the JPSS-1 MMOD risk.

The NESC team compared the orbital debris flux for ORDEM 3.0 to that of three other models: ORDEM2000, the European Space Agency's (ESA) Meteoroid and Space Debris Terrestrial Environment Reference version 2009 (MASTER-2009), and The Aerospace Corporation's Aerospace Debris Environment Projection Tool (ADEPT). Using JPSS-1 orbital parameters, the four models agree to within a factor of two for most particle sizes larger than 3 mm, but diverge significantly for smaller particles. In the 1 mm size range, ORDEM 3.0 has a flux at the JPSS-1 altitude (824 km) ~13 times greater than the ORDEM2000 flux and ~400 times the ADEPT and MASTER-2009 fluxes. Predictions of damage (penetration) fluence on a generic 1-meter/side cube in the JPSS-1 orbit were also compared for the four models. Damage fluence for ORDEM 3.0 was ~30 times the ORDEM2000 damage fluence, ~85 times the ADEPT damage fluence, and ~160 times the MASTER-2009 damage fluence. The combination of higher flux and the presence of high density (i.e., density of steel) particles were the primary contributors to the higher fluence for ORDEM 3.0.

These comparisons verified that ORDEM 3.0 has a higher flux in general and that using it results in higher assessed risk for JPSS-1. The NESC team also sought to understand the underlying reasons for the differences between the models and if the assumptions and methodology used in the development of ORDEM 3.0 were valid. ORDEM 3.0 uses radar measurements for particles as small as ~3 mm and observations of impact damage on the Space Shuttle orbiters' radiator panels and windows to ground the model in direct measurements for particles less than ~3 mm. The Space Shuttle impact data represent debris in only 400 to 600 km altitudes, which is the orbital range for the Space Shuttle. The NESC team has a higher confidence in risk predictions for these regimes because of the direct measurements that were made on returned Space Shuttle surfaces. The LEO-to-GEO Environment Debris (LEGEND) model is used in ORDEM 3.0 to predict the environment mostly in the size range above 3 mm in orbital regimes with no direct measurements and is used to extrapolate the environment into the future. Both ORDEM 3.0 and ORDEM2000 use surface degradation models to represent the source of the majority of debris particles smaller than 3 mm. These models are tuned to reproduce observed surface impacts. In ORDEM 3.0, most of these particles come from satellites and rocket bodies in near-circular, high inclination orbits. In ORDEM2000, a larger fraction of these particles come from satellites and rocket bodies in highly eccentric orbits. One key resulting difference between ORDEM 3.0 and

ORDEM2000 is a much higher concentration of 1 mm diameter particles for ORDEM 3.0 at orbits higher than ~600 km. This difference is a result of the assumptions made concerning the source of orbital debris particles and how large a population would be necessary at higher altitudes to produce the observed Space Shuttle impact damage. The assumptions in ORDEM 3.0 are different, but not judged to be either more or less valid, than those used in the development of ORDEM2000, and are the basis for the higher fluxes and damage fluence for ORDEM 3.0. The physical source of this higher population of 1 mm particles has not yet been explained by either the Orbital Debris Program Office or the NESC team. Another important difference in the models is many of the particles are high density in ORDEM 3.0 while all are assumed aluminum (i.e., medium density in ORDEM3.0) in ORDEM2000. The high density component increases risk because the higher density will cause greater damage than aluminum of the same size.

When compared to the other models, ORDEM 3.0 has several advantages: (1) by using the Space Shuttle impact data, ORDEM 3.0 incorporates the most extensive use of direct measurement data, (2) of the three other models evaluated, only ORDEM2000 reasonably predicts the observed shuttle impact data, (3) ORDEM 3.0 contains high density (i.e., material density of steel) particles not included in the other models, and (4) ORDEM 3.0 contains contributions from recent debris-producing events, only also included completely in ADEPT. There are still substantial uncertainties with ORDEM 3.0 because of the lack of available direct measurement data for < 3 mm particles at altitudes above 600 km, but these are challenges faced by all of the orbital debris environment models. The NESC team recommended that the JPSS-1 Project use ORDEM 3.0 for MMOD risk assessments, while acknowledging the uncertainties inherent to orbital debris environment models (there is an alternate opinion on this topic in Section 9 of this report). Because the uncertainties are large and not characterized, the NESC team recommended that the uncertainties need to be characterized and efforts made to reduce the uncertainties. Also, the NESC team did not make any recommendation as to the general use of ORDEM 3.0 beyond JPSS-1 since this was beyond the defined scope of this activity.

The JPSS Project also asked that the NESC team consider how using the newest meteoroid model, the Meteoroid Engineering Model (MEM) Release 2 (MEMR2), affected the MMOD risk assessments. MEMR2 was evaluated against three versions of the Divine-Staubach model (used in MASTER-2009). Fluxes produced by the four meteoroid models were shown to be in close agreement over the range of the altitudes considered. It is important to note that the contribution from MEMR2 to the overall assessed risk is an order of magnitude less than that of ORDEM 3.0.

The NESC team evaluated other elements of the MMOD risk assessment process that contribute to the overall uncertainty in assessed risk values. Refinement in these areas as described below will reduce uncertainty and, in some cases, possibly reduce assessed MMOD risk.

- The ballistic limit equations (BLEs) used for JPSS-1 risk assessments were not developed for the specific shield configurations used on JPSS-1 or for high density impactors. Existing BLEs were modified for use on JPSS-1. As a result, conservatisms might be associated with the BLEs used by JPSS and how they are applied. The variation of

damage fluence on the generic 1 meter/side cube using some candidate alternative BLEs was quantitatively evaluated.

- The NESC team evaluated failure criteria used for avionics boxes. The results showed that it may be possible for assessed risk to be reduced by addressing the failure of individual cards within an avionics box rather than assuming any penetration of the box results in a failure.
- The wire harnesses were not represented in the initial JPSS-1 risk assessments and may be a factor that would increase the assessed risk. A methodology was developed using hydrocode simulation software to assess risk to wire bundles based on individual wire failures. With the aid of the NESC team, JPSS implemented design modifications to increase protection for the wire bundles and other components. Additional protection included a heavier insulating blanket incorporating layers of Kevlar®, and spacers to increase the gap between the blanket and vulnerable surfaces.
- The failure criteria used for pressure vessels are outdated and not applied consistently within the MMOD risk assessment community. There may be conservatisms associated with how these failure criteria are used by JPSS.
- Orbital debris particle shape is not included in the orbital debris environment nor in the overall risk assessment. The assumption that all particles are spherical adds to uncertainty in the risk assessment process and resulting values of assessed risk.

In summary, given the known uncertainties in the orbital debris environment models, the NESC recommends the JPSS Project use ORDEM 3.0 for MMOD risk assessments related to JPSS-1. However, the use of ORDEM 3.0 beyond JPSS-1 was not assessed as this was beyond the defined scope of this activity. Finally, uncertainties associated with the MMOD risk assessment process, including those associated with the orbital debris environment models, damage prediction, and failure criteria should be understood and investigated to refine overall assessed MMOD risk for all spacecraft.

5.0 Background and Problem Description

5.1 Stakeholder Request and Assessment Plan

The Joint Polar Satellite System (JPSS)[1] Project requested an independent evaluation of the micrometeoroid and orbital debris (MMOD) models used in JPSS-1 MMOD risk assessments. Initial risk assessments performed using the newest MMOD environment models resulted in a substantial increase in assessed risk for several JPSS components compared to assessments performed using older models. For example, the probability for catastrophic damage to the JPSS-1 propellant tank increased from 1.1 percent to 26.0 percent over the life of the spacecraft when switching to the newest models. As a result, the JPSS Project increased MMOD shielding to the propellant tank in order to satisfy requirements to preserve end-of-mission controlled reentry capability. Several of the science instruments onboard JPSS-1 may also have elevated MMOD risk estimates. The science instruments had not been assessed because it was not required to do so to satisfy reentry requirements, but this may call into question the viability of the JPSS-1 science-gathering mission for the designed 7-year mission lifetime.

The increased MMOD assessed risk is due primarily to the use of the newest NASA orbital debris model, the Orbital Debris Engineering Model, version 3.0 (ORDEM 3.0). For this NESC assessment, the NESC was asked to provide an independent evaluation of ORDEM 3.0 and the meteoroid environment model, Meteoroid Engineering Model Release 2 (MEMR2), and compare them to other models, such as the Meteoroid And Space Debris Terrestrial Environment Reference version 2009 (MASTER-2009) used by the European Space Agency (ESA) and the ADEPT used by The Aerospace Corporation. The NESC team was also asked to provide recommendations concerning current JPSS MMOD protection and the methodology used to perform its MMOD risk assessment.

5.2 JPSS-1 Description

The JPSS Project is a series of polar-orbiting environmental satellites, formed through a partnership between NASA and the National Oceanographic and Atmospheric Administration (NOAA). NASA has the responsibility for developing and building the JPSS spacecraft, and NOAA will operate them. The mission of JPSS is to gather a variety of global sea, land, and atmospheric measurements to forecast weather conditions, assess environmental hazards, and provide continuity of critical weather satellite assets through 2025. The first satellite in the JPSS constellation, the Suomi National Polar-orbiting Partnership (S-NPP), was launched in October 2011 with a designed mission life of 5 years. The second satellite is JPSS-1. JPSS-1 is essentially the same design as S-NPP and will be launched in 2017 on a 7-year mission. The third satellite of the JPSS constellation will be JPSS-2, which is scheduled to be launched to provide operational continuity for JPSS after JPSS-1. All three spacecraft will be in a 98.7°

[1] JPSS is the restructured program formerly known as the National Polar-orbiting Operational Environmental Satellite System (NPOESS). JPSS is the project, while JPSS-1 is the second mission in the series.

circular orbit at a nominal altitude of 824 km. The focus of this assessment was JPSS-1 (see Figure 5.2-1).

Figure 5.2-1. The JPSS-1 Spacecraft

5.3 JPSS Preliminary MMOD Risk Assessments

The risk of MMOD penetration was evaluated for JPSS-1 as part of the Orbital Debris Assessment Report (ODAR) required by NPR 8715.6A, *NASA Procedural Requirements for Limiting Orbital Debris*. The assessment methods and technical requirements to support that NPR are found in NASA-STD 8719.14A, *Process for Limiting Orbital Debris*. The MMOD penetration risk is addressed in Requirement 4.5-2:

"*Requirement 4.5-2. Limiting debris generated by collisions with small objects when operating in Earth or lunar orbit:* For each spacecraft, the program or project shall demonstrate that, during the mission of the spacecraft, the probability of accidental collision with orbital debris and meteoroids sufficient to prevent compliance with the applicable post-mission disposal requirements is less than 0.01 (Requirement 56507)."

JPSS will comply with the disposal requirement by performing a controlled reentry following the completion of the scientific mission. Critical JPSS-1 components required to perform the controlled reentry were identified and assessed as described in Section 5.4, using the Debris Assessment Software (DAS) version 2.0.2 tool for preliminary evaluation, followed by the Bumper II risk assessment tool for refinement of the risk assessments for most vulnerable

components. Both DAS and Bumper assessments used the ORDEM2000 orbital debris and Space Station Program (SSP) 30425 meteoroid environment models. Most initial DAS assessment inputs were imported from the similar S-NPP prelaunch assessment, edited as necessary to reflect design changes between the two spacecraft (e.g., relocation of components, addition of new components). Throughout the entire assessment, input information details were refined, not only as the design changed, but also as the details of the design became better known to the analysts. A thorough understanding of the spacecraft construction early in the process is crucial to obtaining a meaningful assessment.

Early DAS assessments of the JPSS-1 penetration risk (performed through mid-2013) indicated that the overall risk would exceed the requirement by a factor of ~3, with the propulsion module accounting for over 80 percent of the risk. The propulsion tank was believed to be particularly exposed (continuously oriented into the velocity direction) whenever the spacecraft entered sun safe mode, estimated as one day per year throughout the mission (this was later revised to half that time) (see Figure 5.3-1). In light of this, the propulsion module became the focus of a detailed evaluation using Bumper II. The assessed risk was revised from 2.7 percent with DAS to 1.2 percent using Bumper II, still exceeding the required 1 percent spacecraft risk with this single component. The JSC Hypervelocity Impact Technology (HVIT) group was consulted to confirm the results and to help determine what supplemental shielding could be added to afford sufficient protection over the propulsion module. An updated DAS assessment showed significant vulnerability for several additional components, which were added to the HVIT Bumper II assessment.

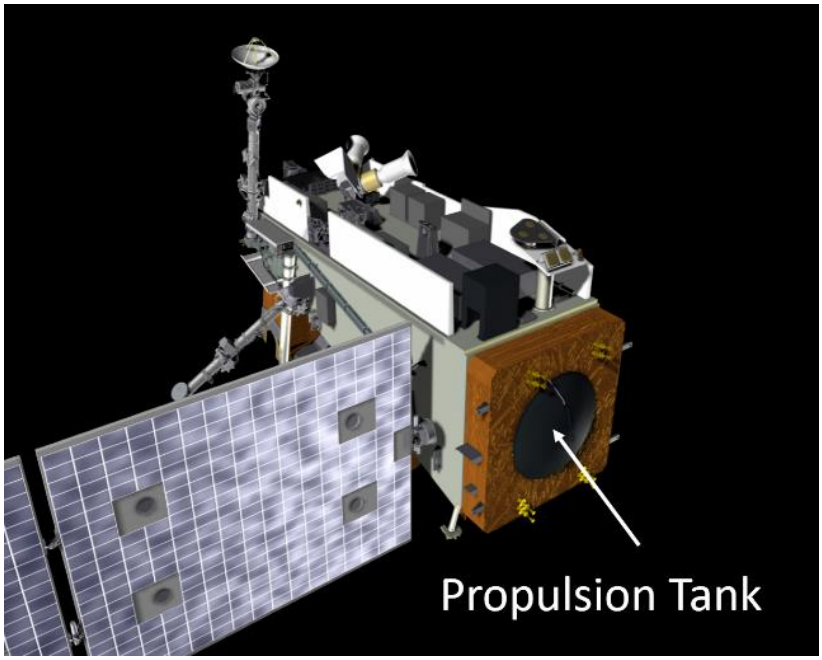

Figure 5.3-1. Location of Propulsion Tank on JPSS-1

During the assessment process, the ORDEM 3.0 debris environment model and Bumper III risk assessment tool (updated to incorporate ORDEM 3.0) became available for use. JPSS decided to use the updated model (as well as the latest meteoroid model, MEMR2) for further assessments. The new models and tools were adopted because the JPSS-1 mission is intended to operate for a relatively long time, in a very aggressive debris environment, performing an extremely high value function for weather forecasting. It was agreed that this was the most appropriate course of action to ensure that this national asset would be adequately protected against penetration risks. The Bumper III assessment indicated risks as much as 30 times higher than the previous Bumper II/ORDEM2000 assessment, invoking questions regarding the applicability of the ORDEM 3.0 environment model and the ways in which it was being used for JPSS-1.

Table 5.3-1 shows the relative MMOD risk assessments using the ORDEM2000/SSP 30425 versus ORDEM 3.0/MEMR2 for five of the critical JPSS-1 component types.

Table 5.3-1. Risk Assessments for JPSS-1 Critical Components

Component	Probability of Penetration	
	ORDEM2000/ SSP 30425	ORDEM 3.0/ MEMR2
Propellant Tank*	1.1%	26.0%
Propellant Lines	3.2%	49.7%
Battery #1 (Stbd)	1.2%	40.9%
Battery #2 (Port)	1.3%	43.4%
Command and Telemetry Unit (CTU)	0.5%	9.7%
Power Control and Distributor Unit (PCDU) #1 (Stbd)	0.1%	0.3%
PCDU #2 (Port)	0.1%	0.3%
Spacecraft Control Processor (SCP) #1 (Forward)	0.7%	14.5%
SCP #2 (Aft)	0.2%	2.9%

5.4 NASA's MMOD Risk Assessment Process

The first step in the risk assessment process, as defined in NASA-STD-8719.14A, is to identify those components critical to the planned disposal. For the JPSS-1 assessment, a reliability block diagram was examined to identify all components necessary to perform the planned controlled reentry disposal and the role of redundancy in the design. In addition to the entire propulsion module, 31 individual components were identified as critical to the disposal maneuvers and potentially vulnerable to MMOD damage. As many as a dozen additional component types were considered to be "robust by design," based on their construction, location, or redundancy, so no further assessment was deemed necessary for those.

The physical location on the spacecraft of each critical component was then examined to determine which surfaces are vulnerable to penetration by a hypervelocity projectile. All components are shadowed on at least one side by either the spacecraft itself or by other substantial components that would prevent a projectile from reaching the critical component (probability of penetration is assumed to be zero for that side). In many cases, a critical surface is partially shadowed, leaving some percentage of its area vulnerable to penetration. This vulnerable area is calculated or estimated by the analyst. For the purposes of the DAS assessments, these surfaces were evaluated with respect to six principal directions (velocity, anti-velocity, port, starboard, nadir, and zenith); this differs from the Bumper tool, which uses a detailed three-dimensional model to consider angled trajectories. The critical surface itself is considered to be the inside surface of a component – for the purposes of this evaluation, any penetration of a projectile through a component wall is considered to cause failure of the component. The exception is for the propellant tank, which as a pressure vessel DAS considers the wall thickness to be only one-fifth as thick, to account for the increased stress in the component wall.

When all critical surfaces are identified, the area, orientation, and shielding of each critical surface is determined, using engineering drawings and designer-supplied dimensions. Shielding is expressed in terms of areal density (material bulk density multiplied by the shield thickness) and distance from the critical surface. All shielding layers between the critical surface and space are identified (e.g., multi-layer insulation (MLI) blankets, thermal fins, or composite panel face sheets), following assessment guidelines defined by the GSFC Orbital Debris Group for details beyond those specified in NASA-STD 8719.14A.

The DAS assessment tool is available online from the Orbital Debris Program Office (ODPO) at http://orbitaldebris.jsc.nasa.gov/mitigate/das.html. A block diagram showing the data flow in and out of DAS is shown in Figures 5.4-1 and 5.4-2. DAS uses an algorithm based on areal density and distance from the critical surface for all shielding layers to determine the minimum penetrating particle size for a range of angles and velocities. The algorithm includes two tests to determine the effectiveness of each shielding layer, adjusting a correction factor accordingly through a range between the fixed minimum and maximum effectiveness values. DAS then uses ORDEM2000 and SSP 30425 to determine the cumulative flux of particles equal to or larger than the minimum penetrating size in each direction/velocity bin, arriving at the expected number of penetrating impacts for that critical surface during the mission. The expected number of penetrations is then converted to a probability of penetration for that critical surface.

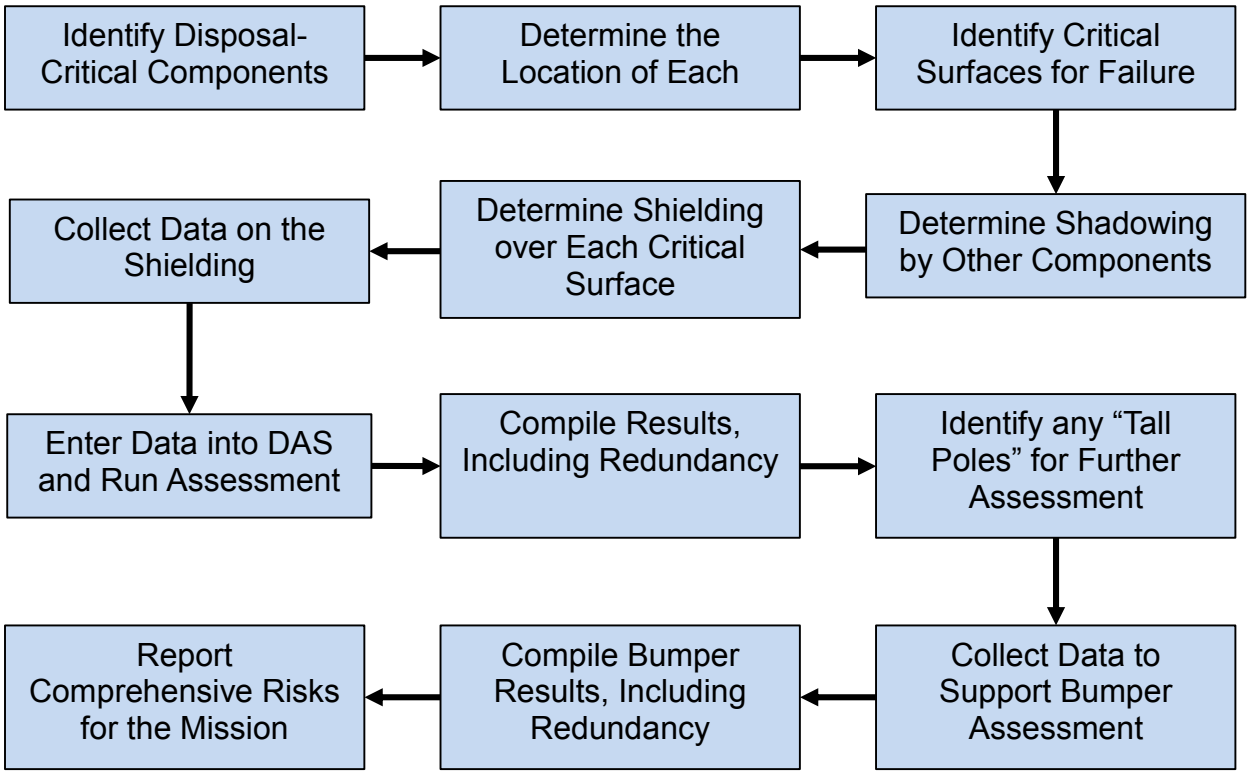

Figure 5.4-1. MMOD Risk Assessment Process

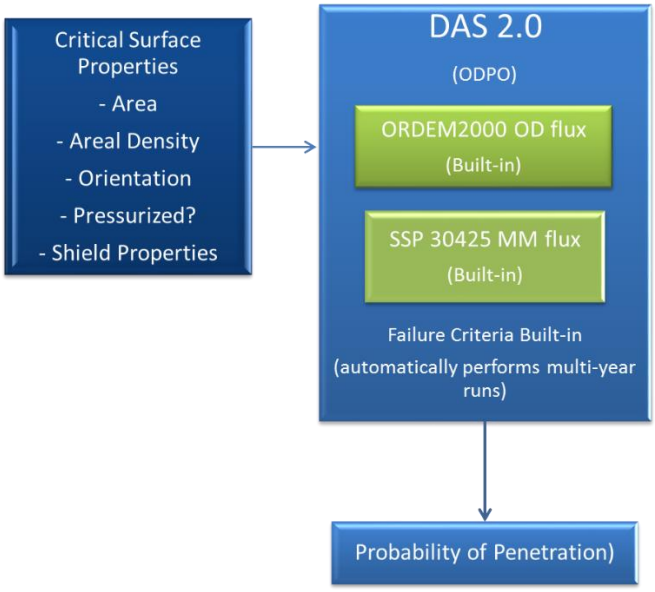

Figure 5.4-2. DAS 2.0 Data Flow

Results for each component must be accumulated and manipulated separately to determine the total risk for each component and to account for redundancy. The DAS assessment often identifies very low vulnerability for some components, but much higher vulnerability for others. It may, therefore, be necessary to refine the assessment of the components at higher assessed risk using a higher fidelity assessment tool. For NASA assessments, the higher fidelity MMOD penetration risk assessment tool is Bumper, which is available from the HVIT. Note that while the DAS algorithm is intended to yield more conservative risk assessments than Bumper, conditions have been identified when that is not always the case.

The higher fidelity Bumper assessment tool functions differently from the DAS in several important ways. First, the orbital debris and meteoroid environment models are run externally. Bumper also uses a three-dimensional finite element model (FEM) of the spacecraft to determine the exposure to each discrete element, allowing shadowing to be incorporated more completely. Bumper offers a selection of BLEs to address a variety of possible shielding configurations and failure criteria, as opposed to the single algorithm built into DAS. Finally, the output from the Bumper tool is more detailed than that from DAS, giving information on the risks from various populations of projectiles as well as the total expected number of impacts. The more complex process of performing a Bumper assessment is evident in Figure 5.4-3.

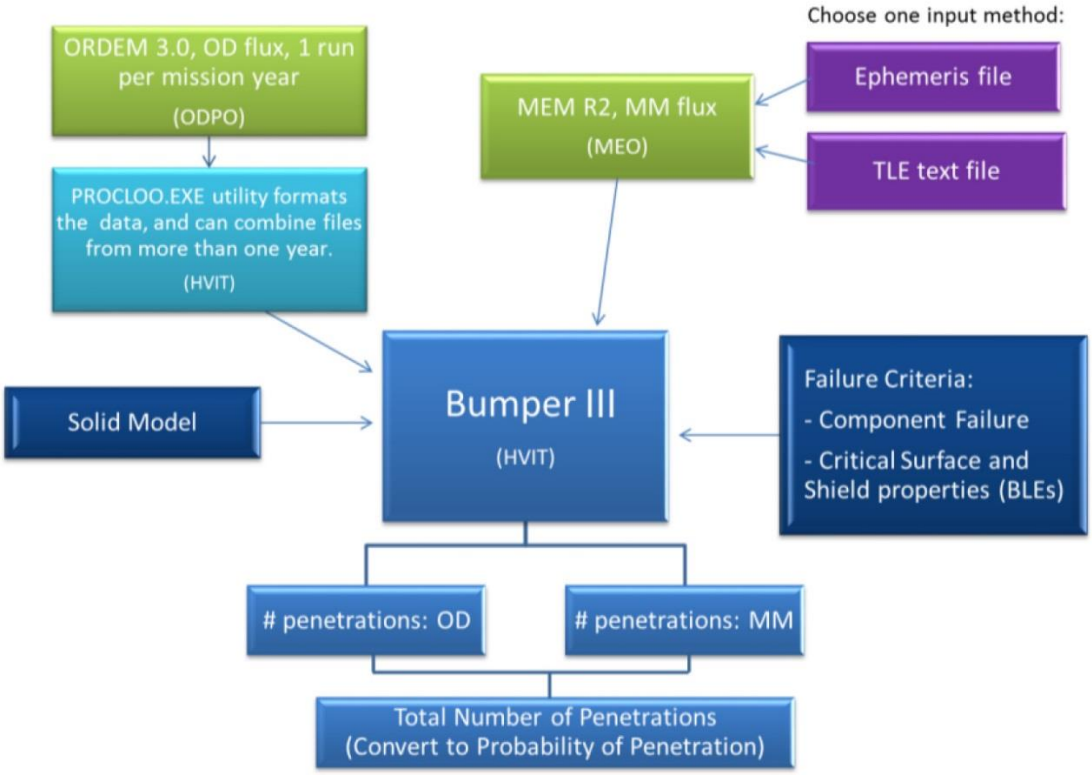

Figure 5.4-3. Bumper III Data Flow

The process for employing the Bumper tool begins with constructing a simplified solid model of the spacecraft, including FEMs for all critical components and shielding or shadowing features. The environment models are then run externally, and a conversion program is used to combine multiple years and to generate a Bumper-compatible format; note that either the newest NASA environment models or previous versions can be used for this step. The critical surface input information collected above is reinterpreted as layer thicknesses (as opposed to areal density) and specific material properties can be considered. Finally, an experienced operator interprets which BLE is appropriate for a given construction. Bumper is run in three modules, the first determining the exposure of each element in the FEM, the second defining the shield construction and appropriate BLEs, and the third introducing the environment model to determine the expected number of penetrations. Bumper must be run separately for orbital debris and meteoroid penetration risks.

6.0 MMOD Environment Models

The NASA OSMA supports the development and maintenance of NASA's MMOD environment models. The meteoroid model is maintained at MSFC by the Meteoroid Environment Office (MEO), and the orbital debris environment model is maintained at JSC by the ODPO. These two models together describe the MMOD environment. The MMOD environment models are used as input to tools, such as DAS and Bumper, that predict the orbital debris or micrometeoroid flux as a function of size and location in space.

6.1 Orbital Debris Models

The development of orbital debris models has tended to follow the same development pattern as older meteoroid models. However, unlike meteoroid models, the orbital debris models have become more complex due to an increasing amount of debris, which includes newly found sources. The ODPO maintains two major orbital debris models, where each serves a different purpose:

1. LEO-to-GEO Environment Debris Model (LEGEND), also known as the Long-term Evolutionary Model. The LEGEND model consists of a number of sub-models, which include a launch traffic model, an atmospheric drag model, orbit propagation models, satellite breakup models, surface degradation models, and mission-related models to account for unique sources of debris such as aluminum oxide from solid rocket firings and sodium-potassium (NaK) droplets from radiator coolant. These models were developed from a combination of ground testing and historical trends. LEGEND uses Monte Carlo simulations to predict possible future environments as a result of various traffic models, and it can simulate mitigation and remediation options to manage the orbital debris environment. It also serves as a data input source for the ORDEM model.

2. ORDEM is also known as the Engineering Model. The ORDEM model allows engineers to determine the expected population of man-made debris objects for a given orbit and timeframe and is used by other applications to ensure spacecraft are protected against debris damage to some predetermined reliability. The model relies on direct measurements of the environment as much as possible, but uses LEGEND as a predictor when interpolations or extrapolations of the data are required. LEGEND can be thought of as a source of data for ORDEM when it is used to predict future changes in the environment and fill in the data gaps in measurements of the current environment. If all the debris sources were completely understood, then the ORDEM model would agree with the LEGEND model; if the models disagree, then either some measurements have been misinterpreted, there is an unidentified source of debris, or the known debris sources are not behaving as expected.

6.1.1 ORDEM 3.0 Structure, Assumptions and Supporting Data

ORDEM 3.0 represents the latest ORDEM model, which is an update from ORDEM2000, released over 10 years ago. This update was overdue and necessitated by a series of events including the 2007 Chinese Fengyun-1C (FY-1C) antisatellite test and the Iridium 33/Cosmos 2251 collision. More importantly, an accumulation of MMOD impact data on the Space Shuttle orbiter up through 2011 was available, which was three times greater than the number of impacts used for ORDEM2000. It is the analysis and interpretation of the Space Shuttle impacts that are most important to the orbital debris environment affecting the JPSS Project.

Four sets of direct measurements of the debris environment went into ORDEM 3.0:

1. The United States Space Surveillance Network (SSN): A catalog of Earth-orbiting objects larger than ~10 cm in low Earth orbit (LEO).
2. The Massachusetts Institute of Technology's Lincoln Laboratory Long Range Imaging Radar (aka Haystack) and Haystack Auxiliary (HAX) Radar: Narrow beam, short wavelength mono-static radars in Massachusetts that sample the LEO debris environment for sizes greater than 6 mm.
3. The Goldstone Radar System: Narrow beam, short wavelength bi-static radars in Southern California that sample the LEO debris environment for sizes greater than 3 mm.

   To convert radar cross-section (RCS) to debris size, the ODPO calibrates debris fragments on a radar range to relate debris size to RCS. These fragments were produced in 1992 by a Department of Defense (DoD) hypervelocity ground test, designed to catastrophically break up a 35 kg spacecraft [ref. 1].

3. Space Shuttle orbiter surfaces: Between 1995 and 2011, a total 1.94 flight-years of 3.6 m^2 of window surfaces, and a total of 1.87 flight-years of 117 m^2 of radiator surface were examined in detail for hypervelocity impact damage. Most of that data was obtained at flight altitudes between 350 km and 400 km, but a few flights were as high as 600 km. This source will be referred to as "shuttle data" in this report.

   Hypervelocity damage to the Shuttle surfaces was examined and catalogued by location, crater or hole size, and chemistry of residue associated with the damage. Scanning electron microscope techniques developed in the 1990's from meteoroid and debris research at JSC were used to determine the chemistry of the impacting objects and separate orbital debris impacts from meteoroid impacts [ref. 2].

This accumulation of data represented a significant increase over the amount of data going into previous models.

Constructing ORDEM 3.0, Radar Data

Constructing an ORDEM model from radar data is relatively straightforward, with the largest uncertainty resulting from converting the measured RCS to size or mass. The process essentially

consists of adjusting the amount of debris in various orbits in the model to match the measured data. These measurements have been nearly continuous since the mid 1990's and are made by pointing the radar in a fixed direction for many hours. In Figures 6.1-1 through 6.1-3, the Haystack was pointed east, 75° above the horizon [ref. 3]. Flux is measured relative to the radar beam; it is converted to the flux relative to a spacecraft by assigning orbits to the flux from either the SSN, the LEGEND model, or the measured inclination from the Haystack measurements, then testing the orbits against the measurements.

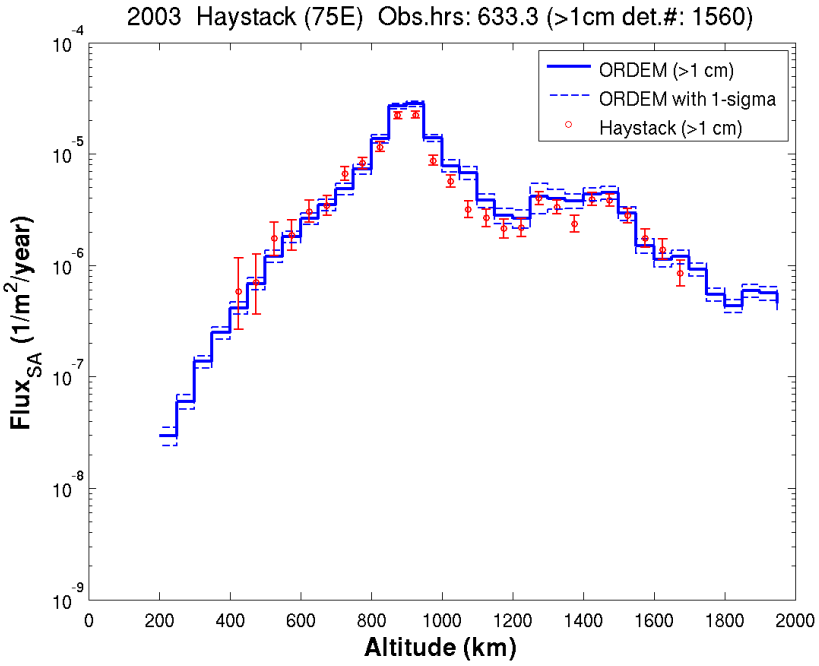

Figure 6.1-1. Flux of 1 cm Debris Measured through the Haystack Radar Beam at Altitudes up to 2000 km in 2003, Compared to an ORDEM 3.0 Prediction of the Flux

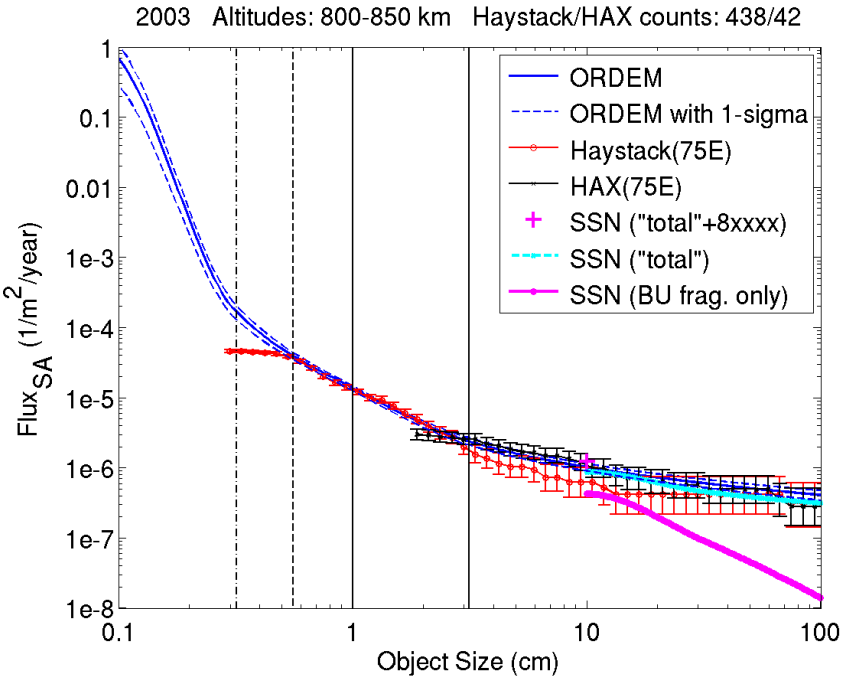

Figure 6.1-2. Flux measured between 800 km and 850 km in 2003 by Haystack and HAX as a function of debris size compared to ORDEM 3.0 predicted flux and the flux predicted by the SSN. For sizes less than about 0.6 cm, the radar begins to lose sensitivity and those data are not used. The ORDEM 3.0 curve was fit to the SSN total +8xxxx data[2], since the official SSN catalog is incomplete and does not include detected objects detected that are waiting to be cataloged.

[2] 8xxxx data refers to orbiting objects that have been tracked, but are not yet in the SSN catalog. To be in the catalog, an object must be identified with a specific launch and a country of origin. This information may not always be available for all tracked objects, especially those recently discovered.

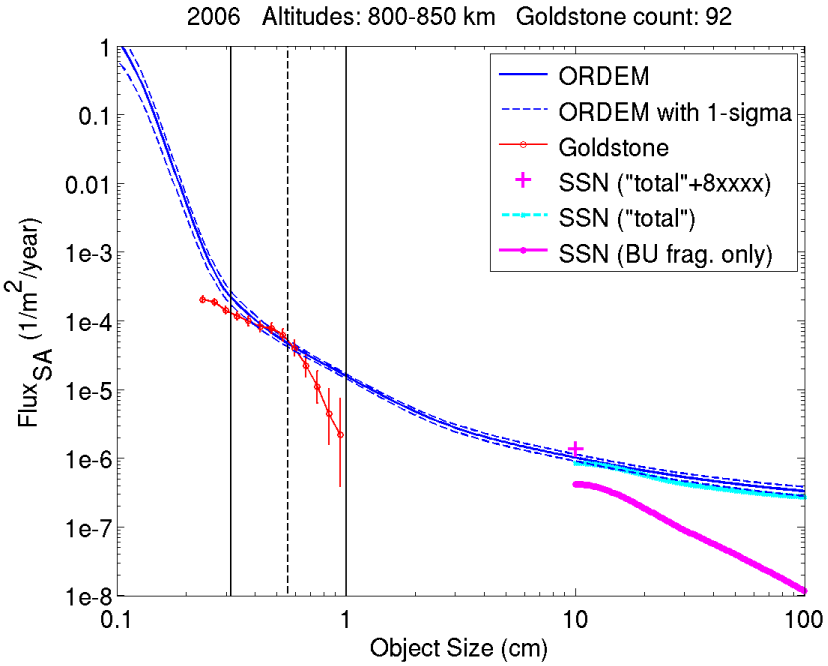

Figure 6.1-3. Flux measured between 800 km and 850 km in 2003 by Goldstone as a function of debris size compared to ORDEM 3.0 predicted flux and the flux predicted by the SSN. The Goldstone radar fills in the 0.03 cm to 0.06 cm flux measurements.

Constructing ORDEM 3.0, Space Shuttle Surface Impact Data

Using direct impact damage on any spacecraft surface has less uncertainty than measurements by radar since no matter what the actual size, velocity, or mass density, the measurement is essentially a "damage flux" on spacecraft surfaces. However, it has one major disadvantage: it is only valid for the altitude where the damage occurred. Like the radar measurements, this damage flux is converted to a damage flux that other orbits might experience by assigning orbits from other data that may be contributing the flux, then testing predicted damage against the damage measurements. However, unlike the radar measurements, there are very little data on how the flux might vary with altitude since all the shuttle flights were below 600 km, with 90 percent of the data being below 400 km [ref. 4]. Any effort to apply these data to higher altitudes requires an understanding of the source of the debris, with the only clues within the shuttle data being the chemistry of residue associated with the damage.

A total of 640 hypervelocity impact features were found on the Space Shuttle orbiter payload bay door radiators, and another 1986 impact craters were found on the Space Shuttle orbiter windows. Figure 6.1-4 is an example of a crater caused by a paint impact on a shuttle window, and Figure 6.1-5 is an example of a penetration hole through a shuttle radiator facesheet caused by a stainless steel impact. Approximately 70 percent of the impact features were classified as unknown, either because they were not fully analyzed or no impact residue could be identified

relative to the surface that was being examined (e.g., no identifiable residue could be expected from an aluminum impact into an aluminum surface). On those surfaces where residue was identified, about half were identified as orbital debris and the other half meteoroid; therefore, the unknowns were assumed to be likewise equally divided. The orbital debris impacts were divided into three groups: those originating from high density (>6g/cm³), medium density (2 to 6g/cm³), and low density debris (<2g/cm³) [ref. 5].

JSC 28033 Orbiter Meteoroid/Orbital Debris Impacts: Space Shuttle-50 (6/92) through Space Shuttle-86 (10/97)
SEM 059 Space Shuttle-59 Scanning Electron Microscope Analysis of Hypervelocity Impact on Side Hatch Window

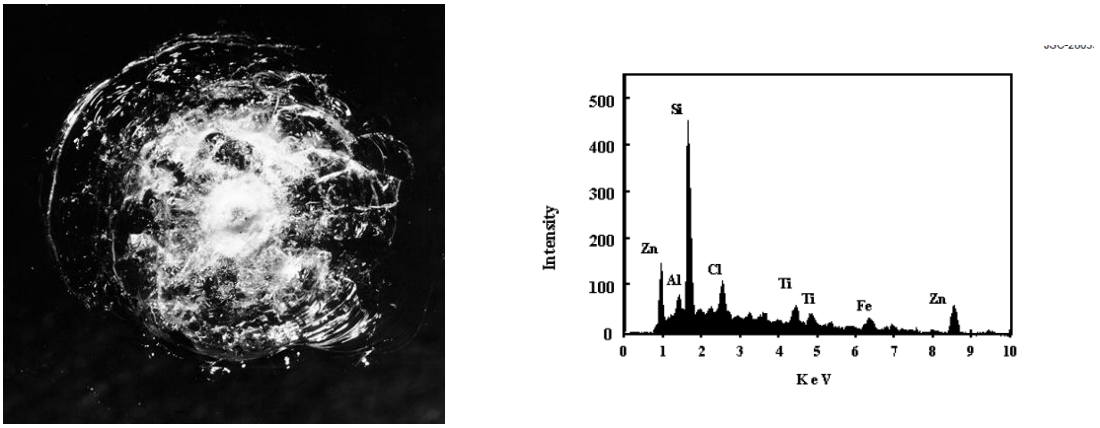

Figure 6.1-4. Example of Crater Found on Windows Caused by Paint Flake, 7.8 x 6.1mm in Diameter, estimated Particle Size is 0.26mm

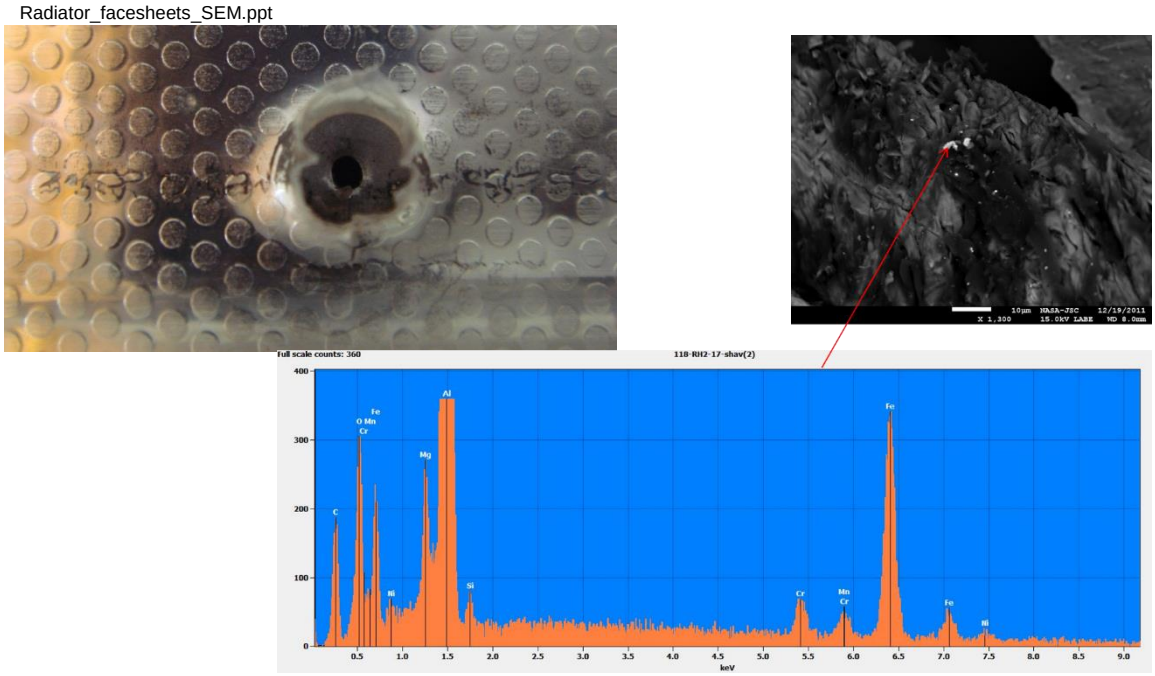

Figure 6.1-5. Example of Impact Hole found on Shuttle Radiator Facesheet caused by Stainless Steel: Facesheet 0.72 x 0.57mm hole Diameter, Estimated Impactor Size 0.15mm

The sizes of the impacting particles were not directly determined from the damage characteristics, rather the ORDEM 3.0 model combined with the Bumper model was used to determine the flux model that would cause the damage found on the Space Shuttle given its orbit and orientation as a function of time. Figure 6.1-6 shows the ORDEM 3.0 model fit to the radiator holes caused by high density and medium density debris. Similar curves were made for the craters on other surfaces for all three density groups.

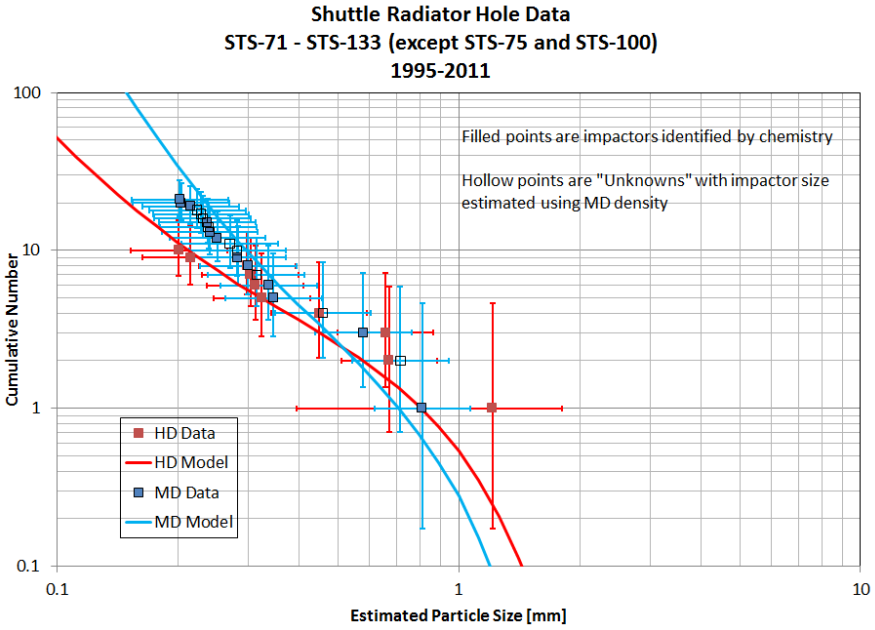

Figure 6.1-6. Example of ORDEM 3.0 Model Fit for Radiator Holes caused by High and Medium Density Debris

It is important to note that debris sizes between 0.5 mm and 1 mm were found to be dominated by high density debris consisting of stainless steel, copper and other high density metals. The higher density debris becomes more important because it also has both greater penetration capabilities and longer orbital lifetimes than lower density materials.

When the shuttle data were combined with the radar data, it produced a plot similar to that shown in Figure 6.1-7. While there was a relatively small gap in the available data between 1 and 3 mm debris, it represented an unexpected large change in the flux (i.e., larger than would be expected by any known debris source). This large increase in flux at the 1 mm size, combined with an unexpected dominant high density population, led the ODPO to conclude that there must exist an un-modeled source of orbital debris. This un-modeled source would have the characteristics of producing a large population of 1 mm debris and smaller, with very little production of debris larger than 3 mm. While interpolation of the flux between 1 and 3 mm may give adequate results for spacecraft operating near 400 km altitude, determination of the source of debris smaller than 1 mm is required before applying these results to other altitudes.

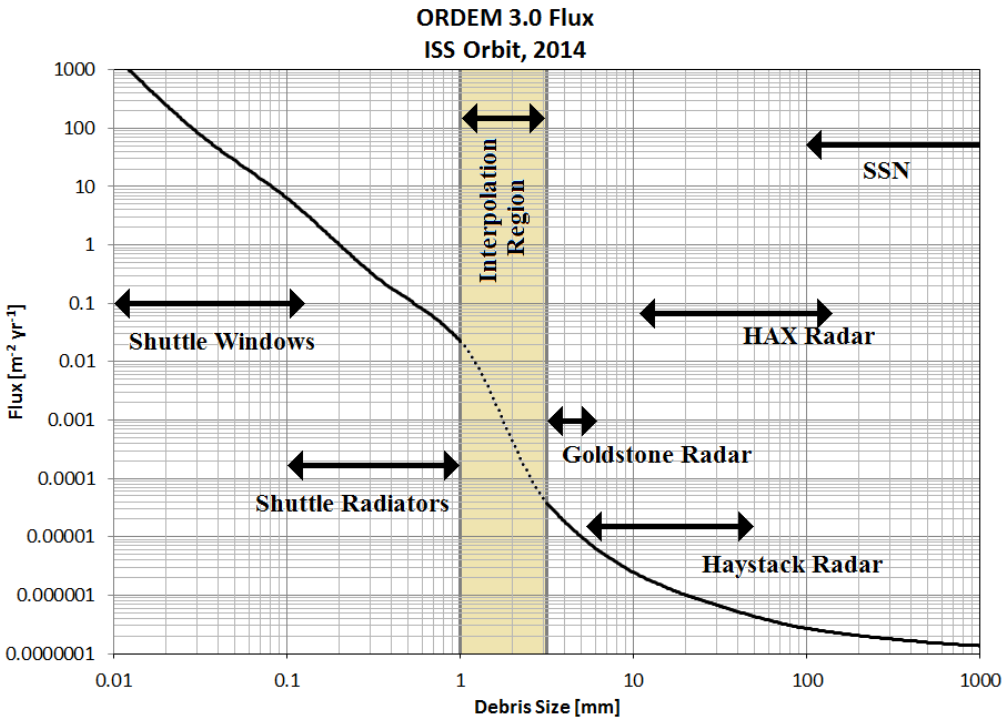

Figure 6.1-7. ORDEM 3.0 Data Sources; No Data Exist between 1 mm and 3 mm and must be Modeled

Constructing ORDEM 3.0, LEGEND and the Surface Degradation Model

As previously described, the LEGEND model depends on identifying a debris source along with the amount of debris it produces, then propagates that debris to predict the resulting long-term flux. The data supporting the collision breakup models in LEGEND have been tested by both ground- and space-based experiments, though these tests have been limited to catastrophic breakup tests of payloads. LEGEND accurately predicts the measured environment for sizes down to about 10 cm, but fails to accurately predict measurements for smaller sizes, possibly due to a lack of data to support upper stage rocket explosions and non-catastrophic collision models.

Some debris sources require special models to address them; examples are NaK coolant released from Russian RORSATs[3], Al_2O_4 from solid rocket firings in orbit, and paint from spacecraft surfaces. The source required to produce the 1 mm and smaller flux measured by the shuttle data is illustrated in Figure 6.1-8. The shape of the curve matches the surface degradation model used in LEGEND to model paint from spacecraft surfaces, except the composition of the material is high density metals and the largest debris size is near 1 mm. The surface degradation model was

[3] The Radar Ocean Reconnaissance Satellite (RORSAT) program was a series of Russian satellites powered by nuclear reactors that were cooled using a liquid NaK coolant. As RORSATs broke up in orbit, the NaK coolant was released forming spherical droplets.

then modified to fit the shuttle data, resulting in the ORDEM 3.0 model prediction at 400 km, illustrated for the ISS altitude in Figure 6.1-9.

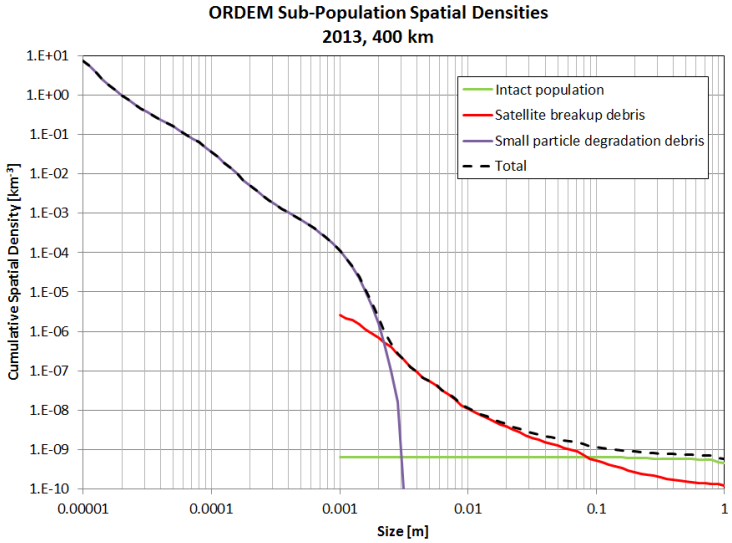

Figure 6.1-8. Combining Shuttle Data with Radar Data at 400 km. The shuttle data are assumed to originate from what is called a surface degradation model, where debris sizes less than about 1 mm follow a different size distribution law. This model is then added to the debris size distribution resulting from satellite breakups.

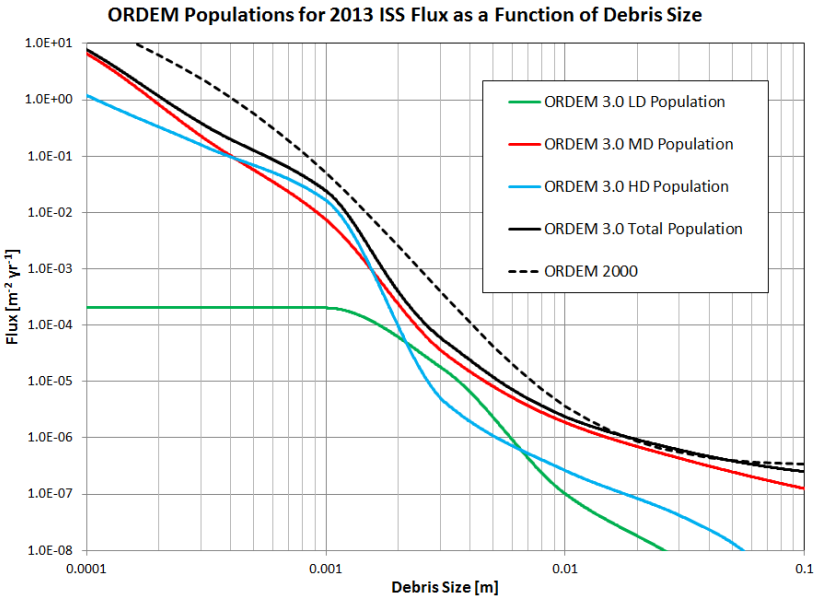

Figure 6.1-9. ORDEM 3.0 Model Prediction for the ISS at 400 km Altitude

The ODPO did not identify a particular source for this debris, but noted that many spacecraft surfaces are about 1 mm thick, and those surfaces are subject to erosion by numerous impacts by both small debris and meteoroids, possibly leading to a slow loss in spacecraft surfaces and a growth in the 1 mm debris population. Having not identified any particular class of objects generating this debris, the ODPO made the neutral assumption that all spacecraft surfaces were continually generating this distribution of small debris at a rate that would produce the flux measured by the shuttle surfaces. To do this, the LEGEND model was used to predict the flux at various altitudes and inclinations as the orbits of the newly generated debris decayed due to atmospheric drag. The results of this assumption are shown in Figure 6.1-10 for the JPSS-1 mission.

As a result of the assumption that all satellite and rocket body surfaces were generating the 1 mm and smaller debris, the increase in flux with altitude follows the general orbit element distribution of existing intact objects. However, this assumption has implications for the resulting debris environment. For example, if the source of debris were in highly elliptical orbits rather than following the near-circular orbits of the general object population, then the resulting altitude distribution of the 1 mm flux could be much different. Depending on the perigee distribution of the elliptical orbits, the flux at JPSS-1 altitude could be either higher or lower than predicted by ORDEM 3.0 by an order of magnitude or more.

The following findings and observations are related to the construction of ORDEM 3.0.

F-1. The degree of uncertainty present in the prediction of the 3 mm orbital debris flux by any orbital debris model at altitudes higher than 600 km has not been characterized, but is expected to be large because of the lack of direct measurements of orbital debris particles smaller than 3 mm at altitudes higher than where the Space Shuttle orbiter operated.

F-2. For the flux for particles < 3 mm, orbital debris model validation for altitudes above 600 km is most effective using *in situ* data (e.g., Space Shuttle impact data).

O-1. The NASA standard break-up model used by LEGEND does not account for the 1 mm population observed in Space Shuttle impact data.

O-2. The surface degradation model in ORDEM 3.0 dominates the population of particles smaller than 3 mm.

- This is based on a default assumption that intact object surface degradation generates particles that caused the Space Shuttle impacts.
- Because of the orbital distribution of the source intact objects, most debris-producing surfaces are located in near-circular orbits between 700 and 1000 km altitude.

O-3. The generation of 1 mm stainless steel debris via surface degradation in ORDEM 3.0 is assumed to continue into the future beyond the dates of Space Shuttle impact data.

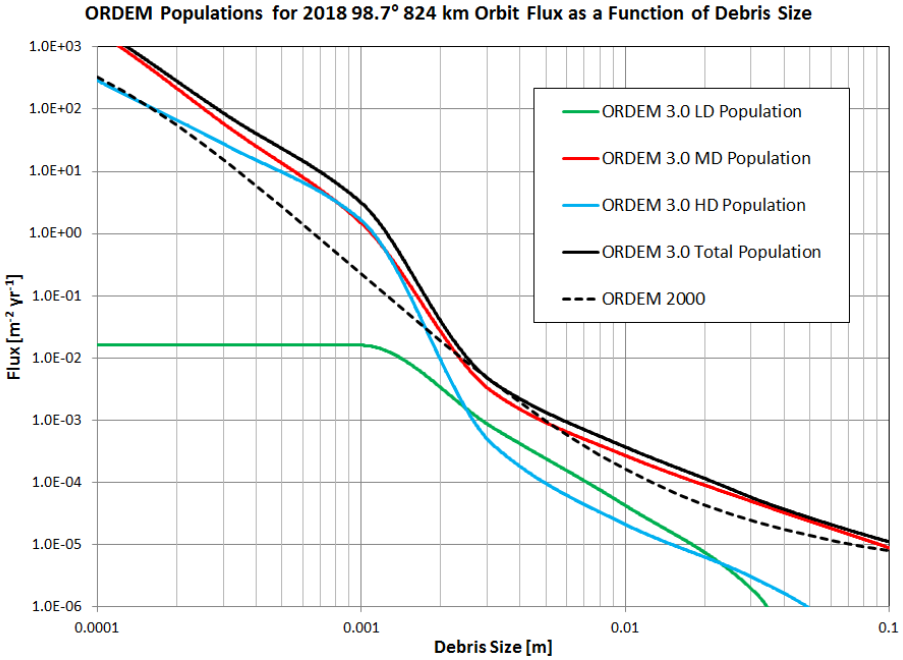

Figure 6.1-10. ORDEM 3.0 Model Prediction for JPSS-1 at 824 km Altitude

6.1.2 Orbital Debris Model Flux Comparisons

Various MMOD models are available for use in spacecraft risk assessment. ODPO has produced various versions of ORDEM (e.g., ORDEM96, ORDEM2000, and ORDEM 3.0). ESA has also produced an environment model called Meteoroid and Space Debris Terrestrial Environment Reference (MASTER), with the most recent version being MASTER-2009 (earlier models were MASTER-2001 and MASTER-2005). The Aerospace Corporation has also developed an orbital debris model, ADEPT, with the latest version originating in 2012. The NESC completed an analysis to gauge the differences in flux between ORDEM 3.0 and several of these other models in order to determine how the results for ORDEM 3.0 should be viewed.

Figure 6.1-11 shows the orbital debris flux for ORDEM 3.0 and ORDEM2000. Three years are depicted: 2017, 2021, and 2024 for the JPSS-1 nominal orbit altitude of 824 km. Values between years for both ORDEM 3.0 and ORDEM2000 are similar (<35 percent difference at 0.1 mm particle size) indicating that there is little difference between the intra-model flux values over the expected JPSS mission. However, there is a noticeable difference between the models in absolute value at particle sizes below ~2 to 3 mm. ORDEM 3.0 utilizes the Space Shuttle impact data to estimate the flux at the small particle sizes. ORDEM2000, while also using some early *in situ* shuttle data, is largely based upon examination of the Long Duration Exposure Facility (LDEF), so there is some difference between the basic data sets. But how they

extrapolate their respective data sets to higher altitudes causes the large difference for JPSS (discussed in greater detail later). An additional source of difference between the models is that ORDEM 3.0 also includes the effects of the FY-1C anti-satellite test, the Iridium-33/Cosmos-2251 collision, and other debris generating events since 2000.

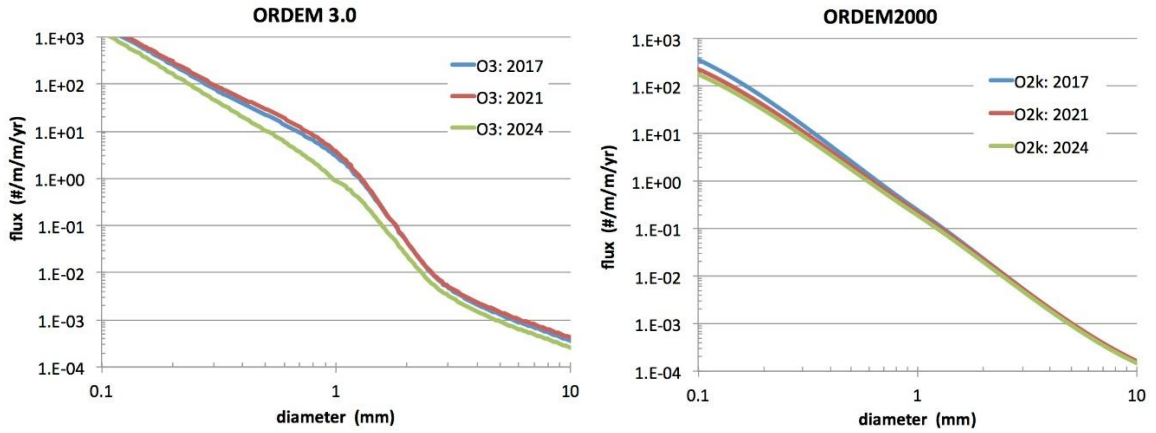

Figure 6.1-11. ORDEM 3.0 and ORDEM2000 Orbital Debris Flux for JPSS Orbit at Beginning, Middle, and End of Expected Mission

Figure 6.1-12 shows the flux versus size profile for ADEPT and MASTER-2009 for 2017, 2021, and 2024. As with the ORDEM models, there is small difference between the ADEPT and MASTER profiles for the different years of the JPSS mission. ADEPT is currently a fragmentation model and relies on collisions and explosions for its particle generation. ADEPT models particle sizes down to 1 cm and then uses data from large collision events (like the Iridium-33/Cosmos 2251 collision) along with catalog data to extrapolate downward to 1 mm. Improvements to ADEPT to accurately model collision and explosions to sub-mm sizes are currently being worked, but were unavailable for this assessment. Additional improvements to incorporate other sources of small particle generation are also being planned. Both the FY-1C and Iridium/Cosmos events were included in ADEPT.

MASTER-2009 does not model the Iridium/Cosmos event, but does include the FY-1C test. MASTER-2009 is built as a source-dependent model with individual physical models for each source. That is, MASTER-2009 models the individual sources of the particles and then checks the source parameters for particles sizes 3 mm and larger against the radar and other empirical data. For sizes smaller than 3 mm, the sources are checked against retrieved *in situ* data from LDEF, Hubble Space Telescope (HST) solar arrays retrieved during service missions 1 and 3, and the European Retrievable Carrier (EuReCa).

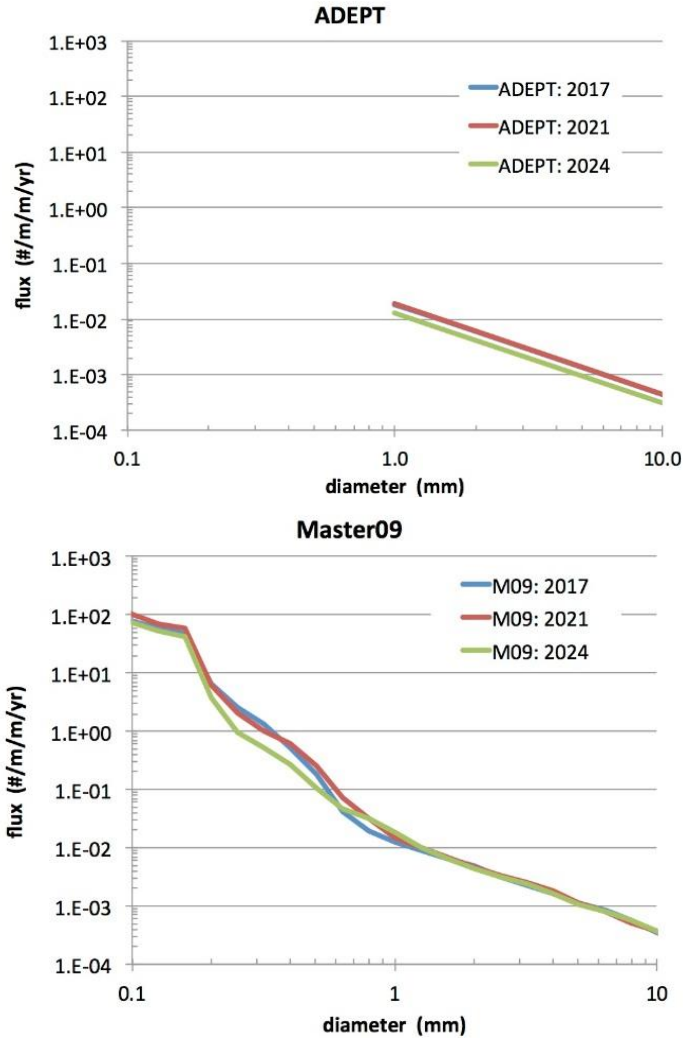

Figure 6.1-12. ADEPT and MASTER-2009 Orbital Debris Flux for JPSS Orbit

As MASTER builds its flux profiles based on models of individual sources, it also allows for the output of the flux for each of those sources. The MASTER sources are: collisions, explosions, intact (launched) objects, NaK droplets, aluminum dust and slag from solid rocket motor (SRM) firings, paint flakes, MLI, and ejecta. It also allows for the independent addition of large on-orbit collision/explosive events. The FY-1C test is currently being modeled in MASTER-2009 in this way. Naturally occurring micrometeoroids and annual meteoroid streams are also available as options, but were not included in the flux comparison to facilitate an apples-to-apples (i.e., orbital debris only) comparison of the models. The flux breakdown is shown in Figure 6.1-13 by source for particles less than 10 cm in size. The dominant sources above ~0.6 mm are fragments from historical explosions and collisions while the dominant sources

between 0.2 and 0.6 mm are ejecta (from small particle impacts) and aluminum SRM slag. The dominant sources below 0.2 mm are ejecta and paint flakes.

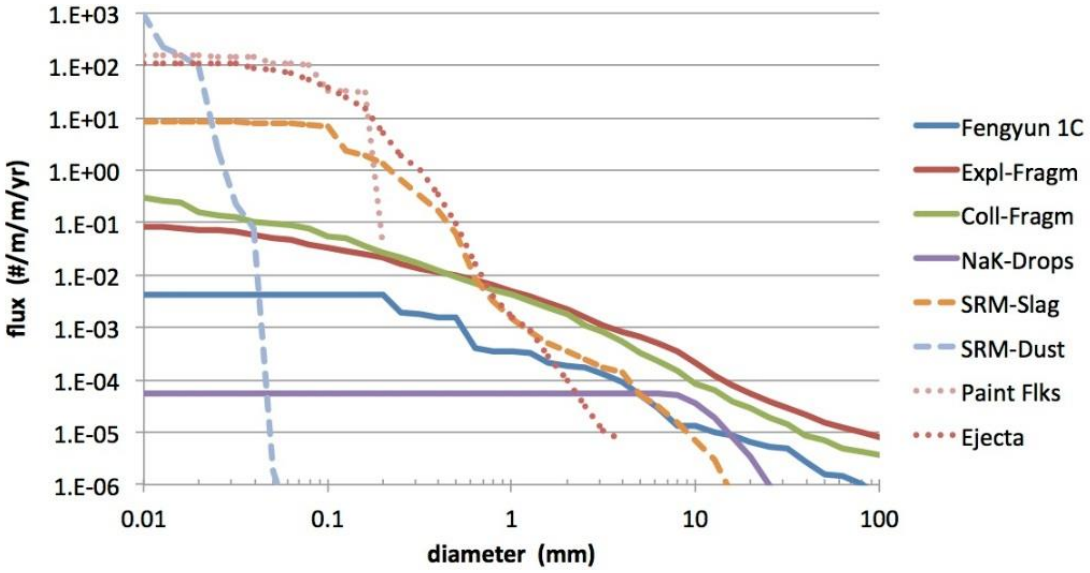

Figure 6.1-13. MASTER-2009 Orbital Debris Flux in 2017 Broken Down by Source

ORDEM 3.0 also breaks the flux down by source, but it breaks the sources down in a manner different from MASTER-2009. The categories for ORDEM 3.0 are: high density (e.g., stainless steel), medium density (e.g., aluminum), low density (plastic), NaK droplets, and intact objects. Figure 6.1-14 shows the flux as a function of size for the three largest categories (the intacts and the NaK droplets do not appear on this scale). The low density particle contribution is less than the medium density particles at all depicted sizes and is below the higher density particles for sizes smaller than ~2.5 mm, and so will not be further considered. The higher density flux is below the medium density flux at all depicted size ranges except at approximately 1 mm, where it slightly exceeds the medium density flux. This is precisely where the risk analysis for most space vehicles, including JPSS, indicates the greatest susceptibility to small particle damage. These 1 mm high density particles generate the majority of the risk that JPSS faces.

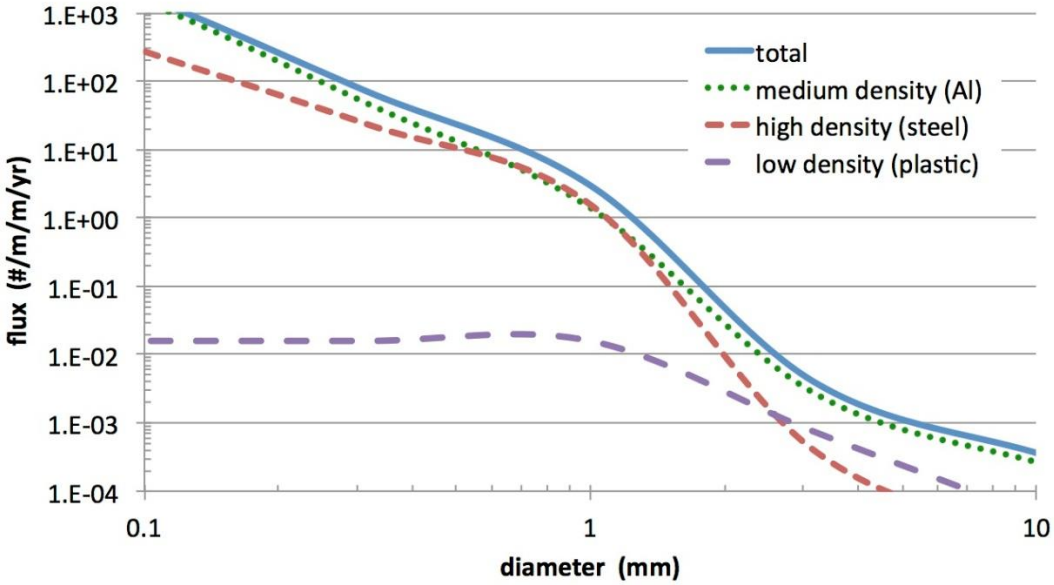

Figure 6.1-14. ORDEM 3.0 Orbital Debris Flux in 2017 for the JPSS-1 Orbit, Broken Down by Source

Figure 6.1-15 shows the 2017 fluxes from all the available models for the JPSS orbit altitude. In addition to MASTER-2009, the two previous versions of MASTER, MASTER01 and MASTER05, are included to give an idea of the variability in the MASTER predictions (MASTER05, like ADEPT, does not yield results below 1 mm). Also, the MEMR2 flux is depicted to show that, at this size range and orbit, the micrometeoroid flux is less than or equal to any of the models. At the size range for which radar measurements are available (>3 mm), the models are in fairly good agreement with each other, and at 1 mm, MASTER05, MASTER-2009, and ADEPT are still in fairly good agreement. However, at sizes below 1 mm, the differences between the models are substantial. ORDEM 3.0 shows the largest flux at 1 mm, ~13 times the value of ORDEM2000 and ~400 times the values of MASTER-2009 and ADEPT.

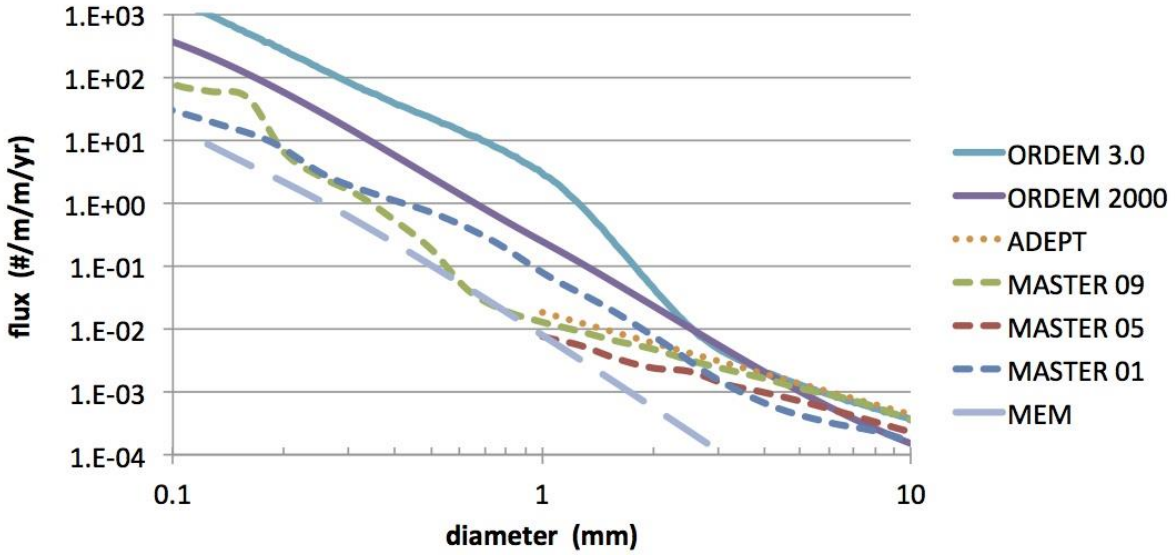

Figure 6.1-15. Comparison of Flux at JPSS Altitude for Year 2017 including all Models

The orbital debris environment that a satellite will face depends strongly on the altitude of the orbit. Large objects create the small particles and therefore it follows that the initial small particle debris environment will reflect the large object distribution. Figure 6.1-16 shows the fluxes for the 1 mm, 1 cm, and 10 cm particles sizes as a function of altitude for the various models. Given the difference in fluxes at the 1 mm size, ORDEM2000 and ORDEM 3.0 are shown in plots separate from ADEPT and MASTER-2009. Also note that ORDEM2000 does not model altitudes above 2000 km. Even so, the shape of the various curves is similar. The peak values at all sizes and for all four models occur at approximately 750 to 850 km altitude. This is where the highest concentration of satellites reside (Sun-synchronous orbits) and so it follows that this is where most debris will also be created. There is a secondary peak at 1400 to1500 km; the Globalstar, Strela-1, and Strela-3 constellations reside at this altitude. (Strela-1 is an inoperative Soviet constellation of small military communications satellites; there are 369 of them in orbit in this altitude range with another 143 Strela-3 satellites). ORDEM2000 shows an unexpected large trough at ~875 km altitude for the 1 mm particles; the reason for this is unknown, but is likely due to the assumptions made as to the source of the small particles in the ORDEM2000 model. Further examination of the ORDEM2000 results indicates that this trough is not present at either the 1 cm (shown) or 0.1 mm (not shown) particle sizes. At ISS altitude, the flux is orders of magnitude less than at higher altitudes in all the models. Decay accounts for this. As the altitude decreases, the atmospheric drag increases and the particles, regardless of size, have a shorter lifetime. As the particles generated at higher altitudes decay, they speed up their descent so that the flux at lower altitudes becomes less.

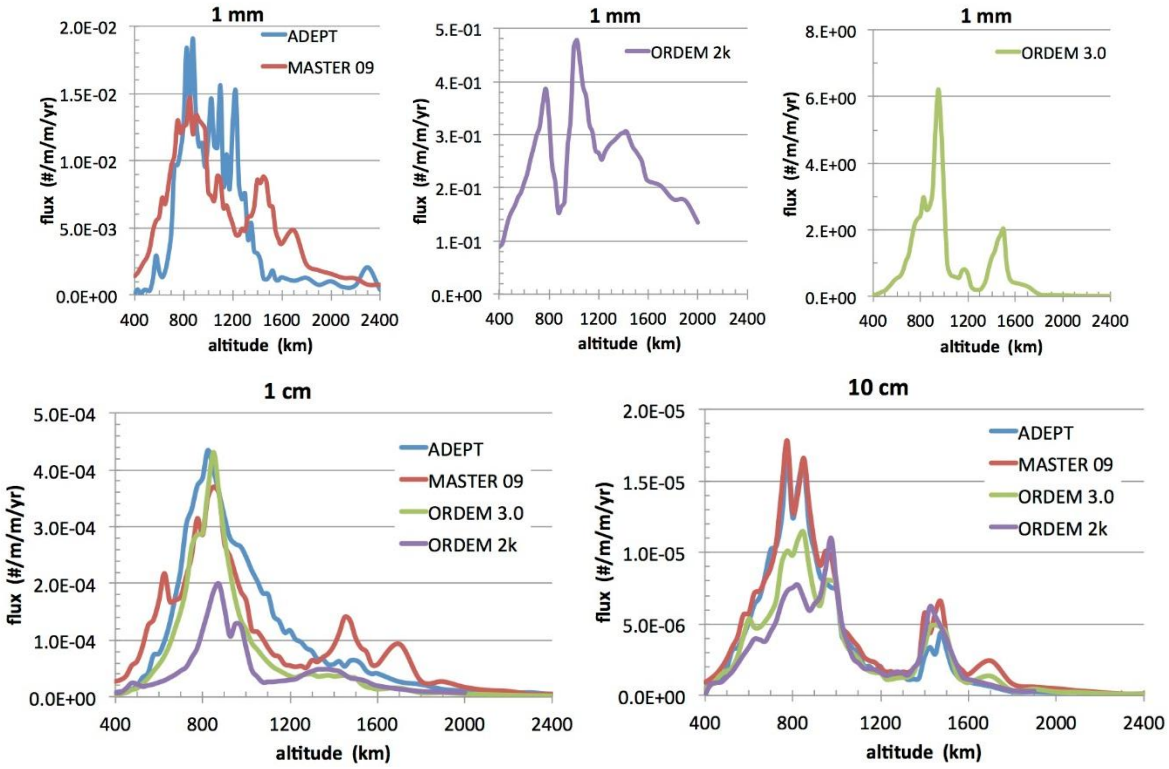

Figure 6.1-16. Variation of Orbital Debris Flux in 2017 as a Function of Altitude (Linear Scale)

Figure 6.1-17 shows the same 1 mm fluxes as depicted in the top row of the plots in Figure 6.1-16, but is on a log scale to facilitate comparison between the models. At the lower ISS/Space Shuttle altitudes (400 to 600 km), ORDEM2000 and ORDEM 3.0 agree fairly well. They are both based on the shuttle data so their agreement is not unexpected (noting that ORDEM 3.0 is based on a larger amount of shuttle data and includes particle density information from spectrographic analysis of crater damage). It is when those models are extrapolated to higher altitudes that they diverge. At JPSS altitude (824 km), ORDEM 3.0 is approximately a factor of 13 higher than ORDEM2000. Even though both models are starting from roughly the same point, the differences in how the extrapolation occurs results in a substantial difference in the fluxes at higher altitudes.

ORDEM 3.0 uses a surface degradation model for the production of small particles that is based on balancing the observed flux corresponding to the shuttle data with the decay of small particles created at higher altitudes. The particles are assumed to come off all large intact orbiting objects at a uniform rate; the particle production for each individual object is solely dependent on the surface area of that object. The particles are then propagated to decay to ISS/Space Shuttle altitude where the flux is computed. The rate at which the particles leave the surface of the intact objects is adjusted to balance the observed Space Shuttle flux. Since all intact objects are producing small particles, most of the small particles are starting off in near-circular (i.e., low

eccentricity) orbits. ORDEM2000 also uses a surface degradation model for all intact objects, but applies magnification factors to populations of small particles coming off objects predominantly in highly eccentric orbits. Given the highly eccentric orbits, many ORDEM2000 small particles are beginning their life in orbits crossing ISS/Space Shuttle altitude, rather than having to decay to get to ISS/Space Shuttle altitude. As a consequence, fewer small particles are produced in ORDEM2000 than in ORDEM 3.0. In addition, the highly eccentric small particles of ORDEM2000 will impact higher altitude LEO satellites much less than the near-circular small particles slowly decaying through those altitudes in ORDEM 3.0.

Neither ADEPT nor MASTER are based on the shuttle data. Instead, both models are based on the empirical data with a lower limit of ~3 mm, and then ADEPT extrapolates downward to 1 mm while MASTER uses source models. As a consequence, their fluxes at ISS/Space Shuttle altitude are much lower than the ORDEM models. At JPSS altitude, ORDEM 3.0 flux is ~400 times larger than either ADEPT or MASTER. MASTER, being based on source models, and ADEPT, being a fragmentation and extrapolated catalog model, do not use a surface degradation model to extrapolate upwards.

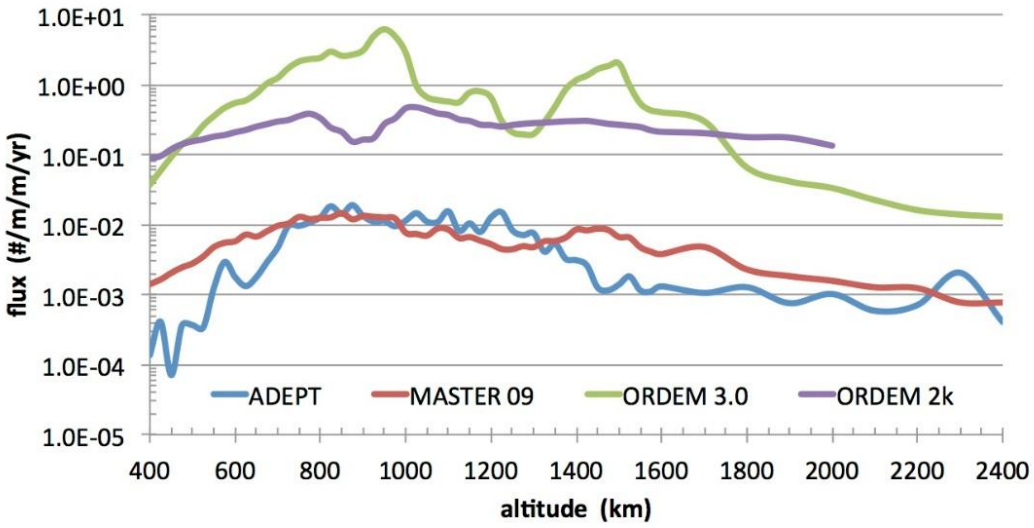

Figure 6.1-17. Variation of 1 mm Orbital Debris Flux with Altitude for 2017 (log scale)

Figure 6.1-18 shows the 1 mm ORDEM 3.0 flux broken down by source (high density and medium density) as a function of altitude. While all the models show an expected increase from ISS/Space Shuttle altitude up to ~700-800 km, ORDEM 3.0 shows a sharp peak, especially of the steel particles, at 950 km, which is not present in the other models. This is caused by the assumption in the degradation model that particles are coming off the surface of all large intact objects at the same rate into near-circular orbits. The aluminum particles that are also being created by the surface degradation model decay more rapidly so the steel particles reside longer at 950 km. Most (~90 percent by mass) of the objects at that 950 km altitude are either old Soviet satellites utilizing the Kaur-1 bus or the SL-8 upper stage rocket bodies that placed them

into orbit. Information on the material composition of the Kaur-1 bus was not available, but it is thought that the Karu-1 bus is covered with solar cells. However, it is known that the SL-8 rocket bodies are made predominantly of aluminum and only have small amounts of steel. Therefore, it is unlikely that the SL-8s are a significant source of the steel particles. More research is needed to determine if the Kaur-1 bus contains stainless steel that could produce the predicted particles, but at this point in time, it is also thought to be unlikely.

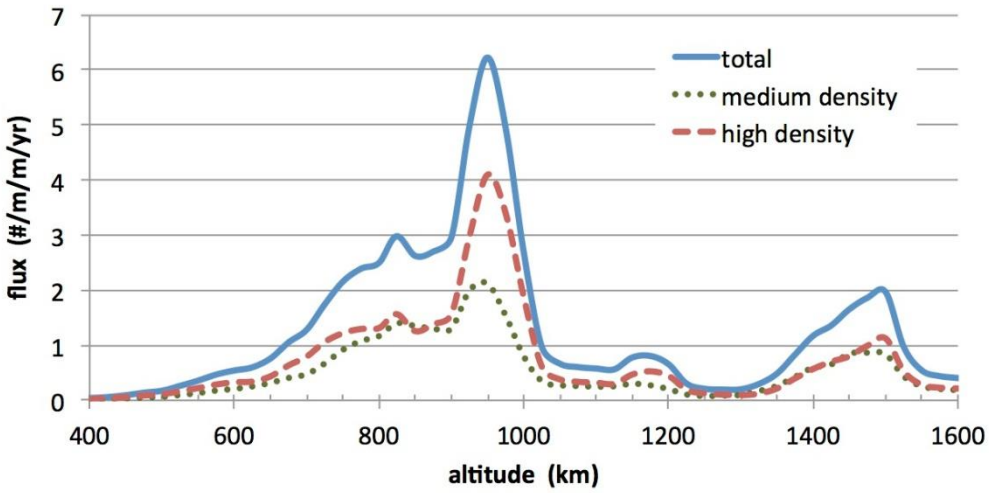

Figure 6.1-18. ORDEM 3.0 1 mm Orbital Debris Flux as a Function of Altitude by Particle Type

Each of the models allows for the computation of the flux over a range of times. The version of ADEPT used for this study has a starting epoch of 2012 and extends for 200 years. The version of MASTER-2009 used for this study begins in 1957 and ends in 2055. ORDEM 3.0 is based on data from the late 1990s until approximately 2011, but the software code allows for the selection of years from 2010 to 2035. By contrast, the previous version, ORDEM2000, covers the years 1991 to 2030. The expected JPSS-1 mission is from 2017 to 2024, and all the models cover this period. Figure 6.1-19 shows the flux by year for 1 mm, 1 cm, and 10 cm particles for ADEPT, MASTER-2009, and ORDEM 3.0 for the JPSS-1 orbit. There is little change over the timeframe of the JPSS mission for each model (on the order of a few tens of percent, which is small when compared to the orders of magnitude difference between the models), and for the larger 1 and 10 cm particles, the models agree to within a factor of 50 percent. Over the JPSS mission, the flux values are not expected to change enough to have a significant effect on the penetration results presented in the next section of this report. Therefore, the 2017 values will be used in that analysis. The full nominal mission timeframe was used for the assessment ultimately reported to OSMA.

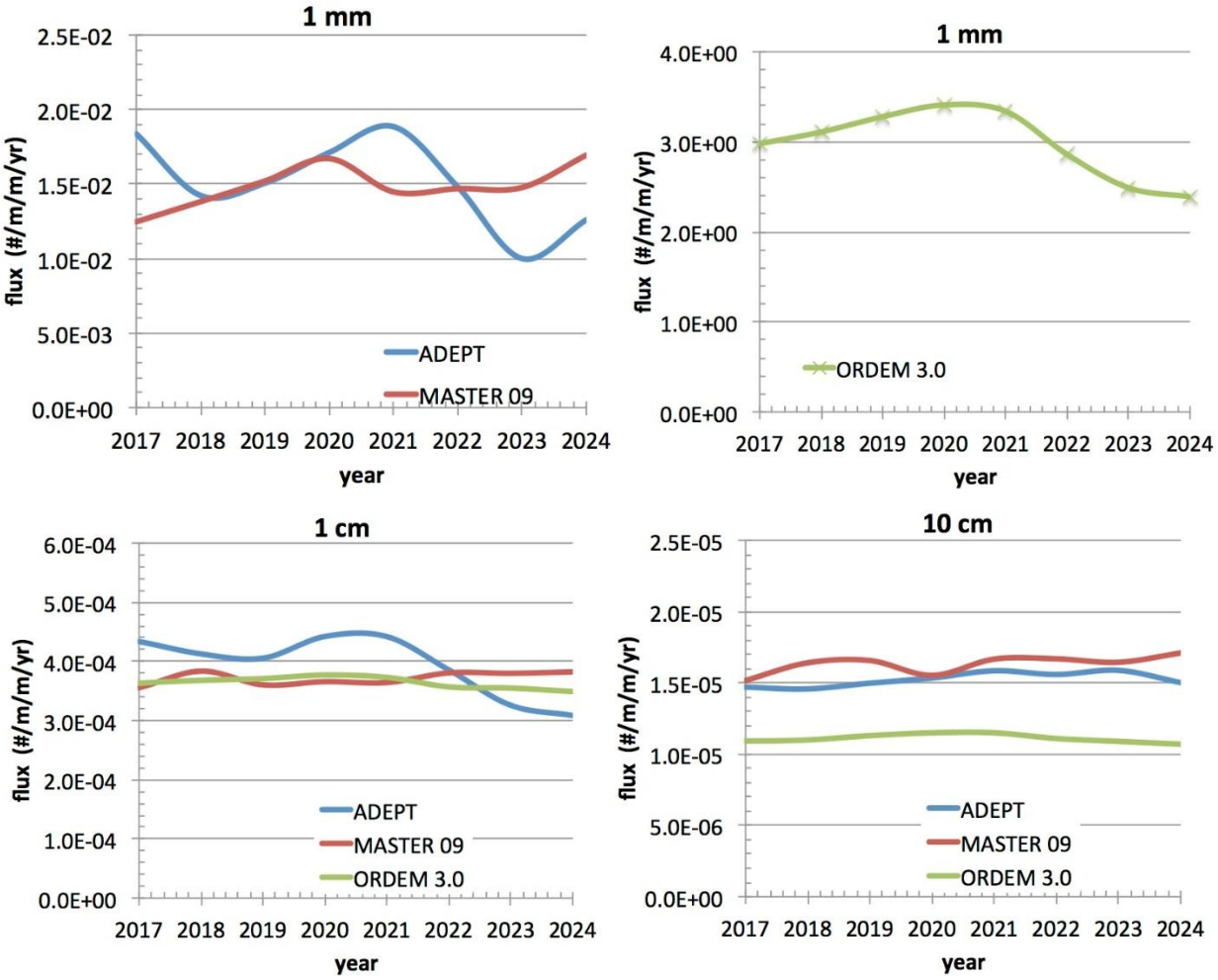

Figure 6.1-19. Variation of Orbital Debris Flux as a Function of Time during JPSS-1 Mission (2017-2024)

Within each of the models, the flux has a dependency on the inclination of the primary object's (i.e., satellites) orbit. Figure 6.1-20 shows the 1 mm, 1 cm, and 10 cm fluxes as a function of inclination for ADEPT, MASTER-2009, and ORDEM 3.0 at JPSS altitude (824 km). The peak flux occurs for primary objects that are in near polar (Sun-synchronous) orbits. Most of the debris in LEO is in near-polar orbits and as the primary object has the opportunity to counter-rotate against the debris, the flux increases since the primary object and the debris are more likely to approach each other head-on, resulting in a high average relative velocity at impact. Conversely, for near-equatorial orbits with inclinations near 0°, the primary object is encountering most of the debris at a substantial wedge angle which lowers the average relative velocity. For near-equatorial orbits with inclinations near 180°, the flux is similarly low, but slightly higher than the flux for inclinations near 0°. This is due to a smaller amount of debris with inclinations near 180°. Therefore, primary objects in these inclinations will see more

counter-rotating debris than the near-0° orbits. However, the difference between the peak and valley values of the flux indicates that the inclination dependency, regardless of model, is on the order of a factor of 2.

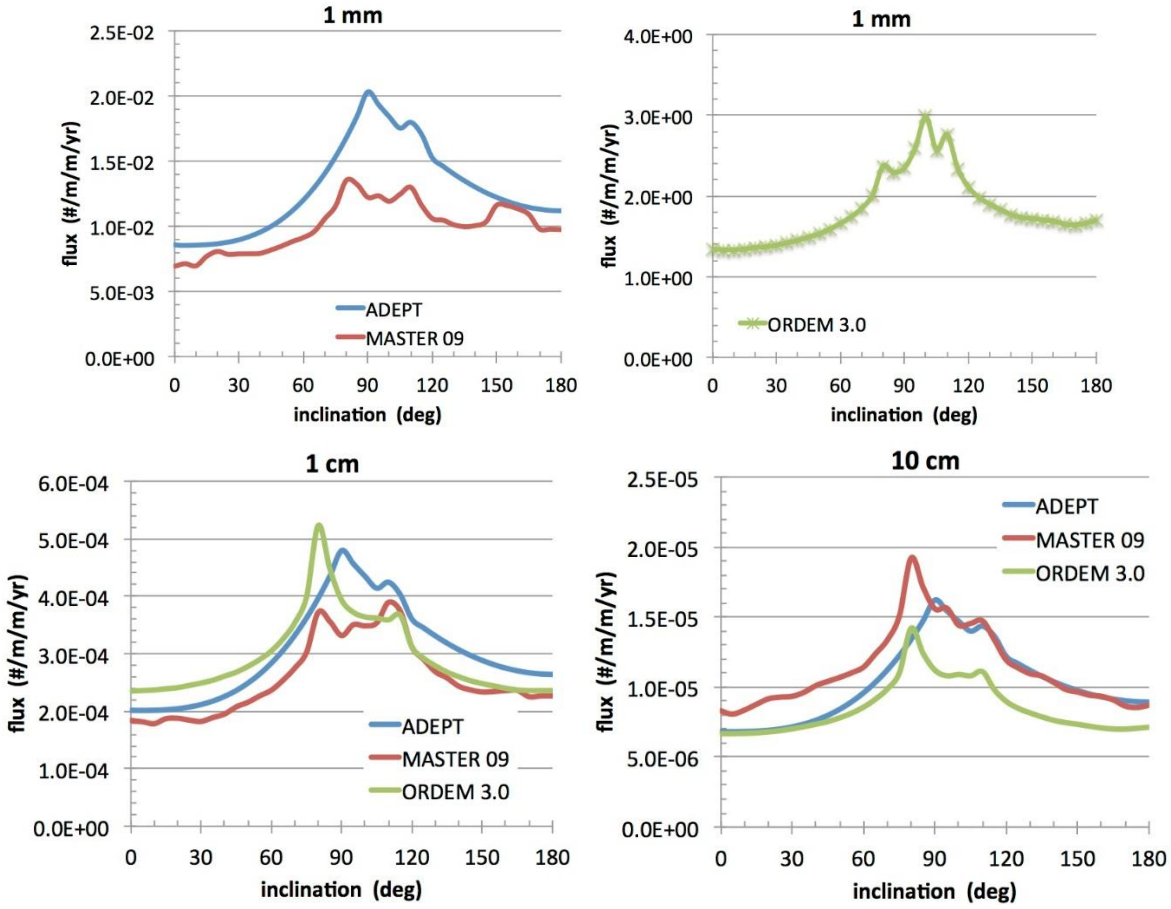

Figure 6.1-20. Variation of Orbital Debris Flux with Inclination at JPSS Altitude (824 km)

In summary, ORDEM 3.0 is predicting much higher fluxes in the 1 mm size range at JPSS altitude than any of the other models (~13x ORDEM2000, ~400x ADEPT and MASTER-2009). A large portion of these particles is assumed to be steel based on spectroscopic examination of the shuttle data. The physical source of these steel particles is currently unknown, but ORDEM 3.0 assumes a surface degradation model involving a constant production rate per unit area of all intact orbiting objects to produce them that results in the higher flux at JPSS altitude. This effect is exacerbated by the slower decay of high density particles relative to medium density particles. The effect that the higher flux has on a sample cubic shape at JPSS- altitude will be discussed in the following section.

The following findings were identified based on the results of this section:

F-3. The four models that were compared (ORDEM 3.0, ORDEM2000, MASTER-2009, and the current version of ADEPT) agree within a factor of ~2 for most debris sizes larger than 3 mm, where ground radar has provided data describing the environment over a large range of altitudes (i.e., from LEO-to-GEO).

F-4. The models disagree significantly for particles < 3 mm, which is also the size that poses the highest penetration risk to most spacecraft.

F-5. A higher 1 mm particle flux and assumptions behind the source of those particles constitute the primary drivers for the differences in flux between ORDEM 3.0 and ORDEM2000.

F-6. There are four factors contributing to the divergence of flux values between ORDEM2000 and ORDEM 3.0 from 400 to 600 km and the JPSS orbital altitude:

1. In ORDEM2000, high-eccentricity intact objects were assumed to have a significantly higher particle production rate relative to low-eccentricity intact objects. ORDEM 3.0 does not make a distinction between the rate of production from high-eccentricity and low-eccentricity intact objects, so its 1 mm population has a higher relative contribution from circular orbits than does ORDEM2000.
2. The impact data used to generate ORDEM 3.0 identify a higher proportion of particles as high density particles (stainless steel) at the higher altitudes, the source of which is assumed to come from intact objects (e.g., spacecraft and rocket bodies) in low eccentricity/high inclination orbits.
3. ORDEM 3.0 includes high density particles, which are not included in ORDEM2000. The higher density particles, with a lower area to mass ratio, will decay less rapidly than medium density particles assumed for ORDEM2000, contributing to a greater total flux at higher altitudes.
4. Surface degradation model particle emanation rates in ORDEM2000 and ORDEM 3.0 are significantly different.

F-7. The greater JPSS MMOD risk using ORDEM 3.0 compared to ORDEM2000 is due to two factors:

1. ORDEM 3.0 has a ~13x higher particle flux than ORDEM2000 at the JPSS orbital altitude.
2. ORDEM 3.0 contains high density particles. Smaller high density particles cause the same amount of damage as larger medium density particles and are more numerous. ORDEM2000 does not model high density particles.

F-8. Because all the orbital debris models are consistent at all altitudes for debris fluxes of particles ~3 mm and larger, designing spacecraft to withstand impacts by particles up to 3 mm in diameter will provide the least uncertainty in orbital debris risk.

F-9. The orbital debris risk for JPSS-1 would be reduced if the orbital altitude were <800 km or >1000 km.

- The results of the orbital debris model comparisons showed the highest flux between 800 and 1000 km for all of the orbital debris models analyzed.

6.1.3 Orbital Debris Damage Fluence Comparisons

In this section, predictions of damage fluence on a generic cube using the various orbital debris models are presented and compared to better study the combined effects of flux and density on the comprehensive penetration risk assessment. Damage was defined as penetration into the cube. The cube was selected to remove most JPSS-specific aspects of the problem, thereby broadening the applicability of the results. The length of the edges of the cube was one meter, thereby establishing an area on each face of 1 m^2. The bus was assumed to be fixed in the rotating local vertical local horizontal (LVLH) frame. One face had a normal vector always pointing in the "north" direction (parallel to orbital angular momentum vector). A second face had a normal vector always pointing in the "south" direction (i.e., opposite of north).

The cube did retain some JPSS aspects to maintain relevance. It was assumed to fly in the JPSS-1 orbit, and the mission duration was assumed to be 7 years (2017 to 2024). The bus was rotated about pitch by 15° from the LVLH frame. This represented the tilt of the surface on which the command and telemetry unit (CTU) box is mounted. A dual wall model was assumed for the cube surfaces, and the model parameters were the same as those used for the CTU box by the Bumper analysis cited by this study [ref. 6]. An aluminum inner wall represented the CTU box surface and had a thickness of 0.152 cm. An aluminum outer wall represented the MLI and had a thickness of 0.034 cm. It had the same mass per unit area as the MLI. Both the inner and outer walls had a density of 2.7 g/cm^3 and a yield strength of 40 ksi. The spacing between the inner and outer walls was 5.08 cm. The dual wall model parameters (type of aluminum, wall thicknesses, and spacing) were supplied by the HVIT [ref. 6]. Note that this model of the CTU was later updated for JPSS assessments to reflect additional information and design changes.

6.1.3.1 Meteoroid and Orbital Debris Risk Assessment (MODRA)

The Aerospace MODRA code was used to compute damage fluence for each face of the representative cube. MODRA performs a computation similar to that of Bumper. MODRA sweeps through all surface elements in a finite element model of a spacecraft. Each surface element is defined by orientation, area, and parameters needed by a damage model. In this case, each bus face is a surface element, and damage is defined as penetration of the inner wall behind the MLI.

For each surface element, MODRA sweeps through all particle flux components. Flux components are defined by bins characterized by impact velocity, azimuth, and elevation in the LVLH frame. Flux components are also defined by populations. As discussed in Section 6.0, ORDEM 3.0 produces five populations: low density particles (e.g., paint flakes), medium density particles (e.g., aluminum), high density particles (e.g., stainless steel), NaK droplets, and intact objects. For MASTER-2009 runs, density bins specified in an input file were used as MODRA population bins. ADEPT runs were made using the flux components (hence population bins) from either ORDEM 3.0 or MASTER-2009.

For each flux component, MODRA uses a damage model to determine critical particle diameter or mass that can penetrate the surface element. The code determines penetrating flux at the critical particle diameter or mass from the environmental flux versus diameter/mass file provided by the debris environment model. The flux at the critical diameter or mass is interpolated between size/mass points in the environmental flux file via linear interpolation in log-log space. MODRA multiplies the resulting penetrating flux by the projected area of the surface element, by the impact probability of the flux component (determined from the environmental model velocity and direction distributions), and by the mission duration to obtain the damage fluence for the flux component. MODRA then sums the damage fluences from all flux components and surface elements to obtain the total damage fluence.

6.1.3.2 Results Using ORDEM 3.0 with the Baseline New Non-optimum (NNO) BLE

The damage model was a dual-wall BLE. The baseline BLE used for the analysis was the NNO equation (also known as the Whipple bumper equation). This is the same BLE that was used in the Bumper analysis cited for this study [ref. 6]. The actual implementation in MODRA is the ESA Space Environment Information System (SPENVIS) [ref. 7] formulation with "NASA ISS" parameters modified to make it consistent with the NNO BLE implementation in Bumper [ref. 8]. One of the modifications was implementation of a 65° impact angle limit (i.e., for impact angles greater than 65°), the critical diameter corresponding to an angle of 65° is used. This angle limit was motivated by observations that for impact angles greater than 65°, most inner wall damage is caused by outer wall fragments (not by impactor fragments) and therefore the damage does not drop off as rapidly as for lower impact angles [ref. 9]. A second modification is that the high velocity region boundary of the NNO BLE was made to be dependent on impactor density (i.e., the velocity boundary was 7 km/s for impactor density less than or equal to 7 g/cm^3, and 9.1 km/s for impactor density > 7 g/cm^3) (to model stainless steel impactors). A third modification is that the normal component of impact velocity (not the full impact velocity magnitude, as in SPENVIS) is compared to the low velocity region and high velocity region boundaries.

The first set of results to be shown are those resulting from using ORDEM 3.0 with the baseline NNO BLE. Figure 6.1-21 shows the environmental flux versus impactor size for each of the ORDEM 3.0 populations. The curve of total flux versus size is from the SIZEFLUX_SC.OUT file generated by ORDEM 3.0. The data for the individual populations were extracted from the IGLOOFLUX_SC.OUT file. Two points per size decade are available from this file. The flux

values shown were obtained by summing fluxes from all igloo bins defined by azimuth, elevation, and velocity. The plot shows that the high density flux points are lower than the medium density flux points for most of the size range, with the exception of the vicinity near 1 mm, where high density and medium density fluxes are comparable. Therefore, for most sizes the medium density population dominates the environmental flux. However, it will be seen that the medium density population does not dominate the damage fluence.

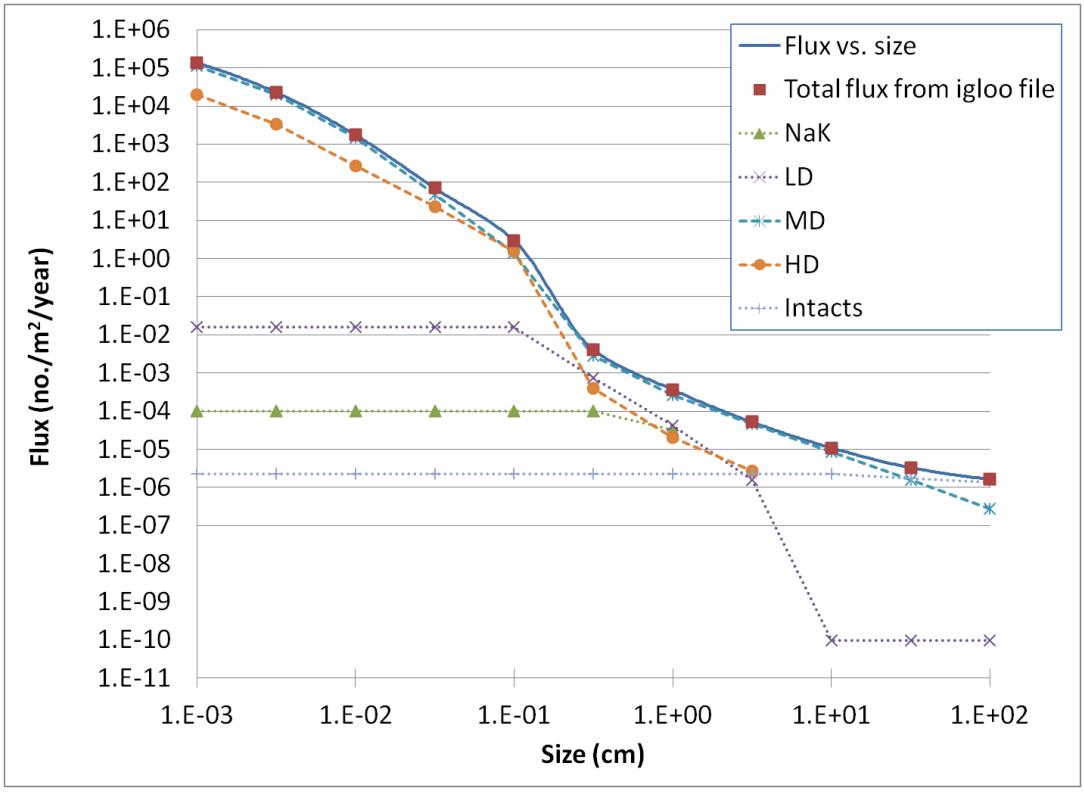

Figure 6.1-21. ORDEM 3.0 Environmental Flux versus Impactor Size

Table 6.1-1 shows the resulting damage fluence on each cube face from each of the populations. The table also shows the percentage of the total damage fluence that is contributed by the high density population. Overall, the high density population contributes 91 percent of the damage fluence for this shielding scenario. Since the high density environmental flux is approximately the same as the medium density environmental flux at a common size near 1 mm, but is less for all other sizes, the dominance of the high density population on the damage fluence must be due to the more damaging nature of the high density impactors.

Table 6.1-1. Cube Damage Fluence Resulting from use of ORDEM 3.0 with the NNO BLE

Cube face	Damage fluence							HD percent of total
	NaK	LD	MD	HD	Intacts	Total across populations	Total without HD	
Ram	1.11E-04	8.81E-04	2.45E-01	2.65E+00	4.20E-07	2.90E+00	2.46E-01	91.5%
Trail	0.00E+00	1.73E-06	6.62E-06	3.87E-05	1.52E-09	4.70E-05	8.35E-06	82.2%
South	7.37E-05	7.22E-04	9.21E-02	8.08E-01	1.60E-07	9.01E-01	9.29E-02	89.7%
North	7.37E-05	7.22E-04	9.21E-02	8.08E-01	1.60E-07	9.01E-01	9.29E-02	89.7%
Nadir	0.00E+00	1.98E-06	6.98E-06	5.10E-05	2.53E-09	5.99E-05	8.96E-06	85.0%
Zenith	7.85E-05	8.93E-04	6.45E-03	2.42E-01	3.45E-08	2.50E-01	7.42E-03	97.0%
Total across faces	3.37E-04	3.22E-03	4.36E-01	4.51E+00	7.79E-07	4.95E+00	4.40E-01	91.1%

As a check on the setup of the MODRA cube run, a CTU run was performed for comparison to previous Bumper results. The cube dimensions were scaled down to those of the CTU box, and percentage of view blocked for each face was visually estimated from a spacecraft computer-aided design (CAD) image. Table 6.1-2 shows the results for each CTU face alongside the corresponding Bumper results from reference 6. The nadir face is not included since it is mounted to the spacecraft bus. Agreement of the damage fluences is very good for faces with 10 percent blockage, as well as for the total.

Table 6.1-2. CTU Damage Fluence Resulting from use of ORDEM 3.0 with the NNO BLE

Surface Name	MODRA		BUMPER
	Assumed percent field of view blocked	Average number of penetrations	Average number of penetrations
CTU - Top Face	10%	1.60E-02	1.62E-02
CTU - Outboard Face	90%	8.61E-03	8.49E-04
CTU - Ram Face	90%	1.66E-02	5.84E-02
CTU - Inboard Face	50%	4.31E-02	1.67E-02
CTU - Anti-Ram Face	40%	2.72E-04	1.09E-06
Thermal Fin - CTU Low Standoff	10%	5.88E-03	6.00E-03
Thermal Fin - CTU Mid Standoff	10%	3.36E-03	3.40E-03
Total		9.37E-02	1.02E-01

Figure 6.1-22 illustrates the distribution of the cube damage fluence over impactor size. The plot is a histogram with the x-axis (impactor diameter) in log space. The bin width is 1/100th of a decade (determined by the SIZEFLUX_SC.OUT file produced by ORDEM 3.0). Damage fluences on all the cube faces are combined. From this plot, it is seen that debris impactors in the size range 0.6 to 3 mm dominate the damage fluence. Below an impactor size of 1.2 mm, the damage fluence is determined by the high density population because medium density impactors smaller than 1.2 mm are not able to penetrate the MLI and inner wall. Above an impactor size of 1.2 mm, both the medium density and high density populations contribute to the damage fluence. Larger debris particles impact too infrequently to dominate risk, and smaller particles cannot penetrate the MLI and inner wall of the cube faces.

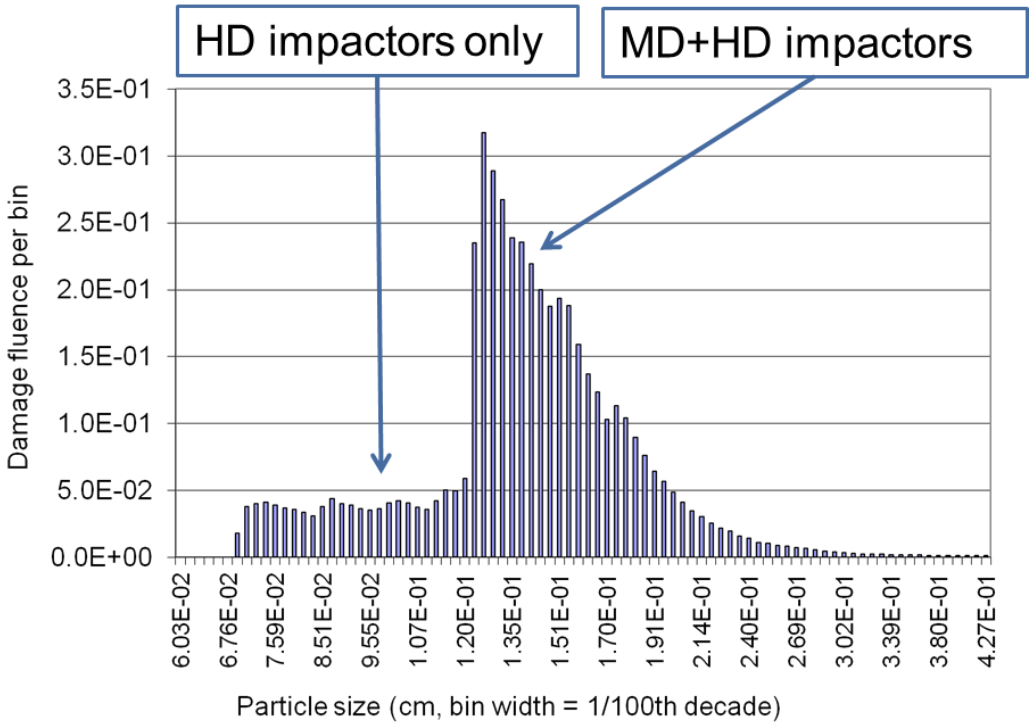

Figure 6.1-22. Distribution of Damage Fluence Over Impactor Size

Figure 6.1-23 shows the distribution of damage fluence over impact velocity. Damage fluences on all the cube faces are combined. The plot is a histogram with an x-axis (impact velocity) bin width of 1 km/s. From this plot it is seen that surface penetration velocity varies from 1 to 18 km/s. The most likely values (peak in the histogram) are in the 14 to 15 km/s bin. However, a significant fraction of the total damage fluence occurs at lower velocities.

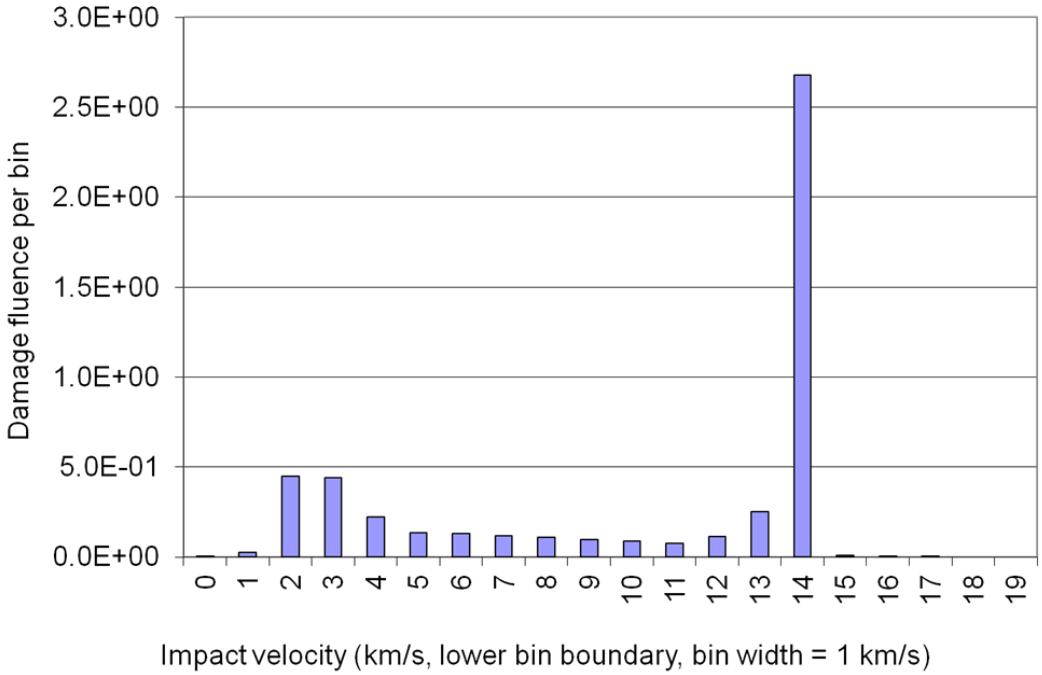

Figure 6.1-23. Distribution of Damage Fluence over Impact Velocity

Figure 6.1-24 shows the distribution of damage fluence over impact angle. Damage fluences on all the cube faces are combined. The plot is a histogram with an x-axis (impact angle) bin width of 5°. From this plot it is seen that surface penetration impact angle varies from 0 to 85°. The most likely values (peak in the histogram) are between 0 and 35°. However, a significant fraction of the total damage fluence occurs at higher impact angles. The resulting distribution is determined by both the fixed orientation of the cube in the LVLH frame as well as the orbital distributions of the five populations in ORDEM 3.0.

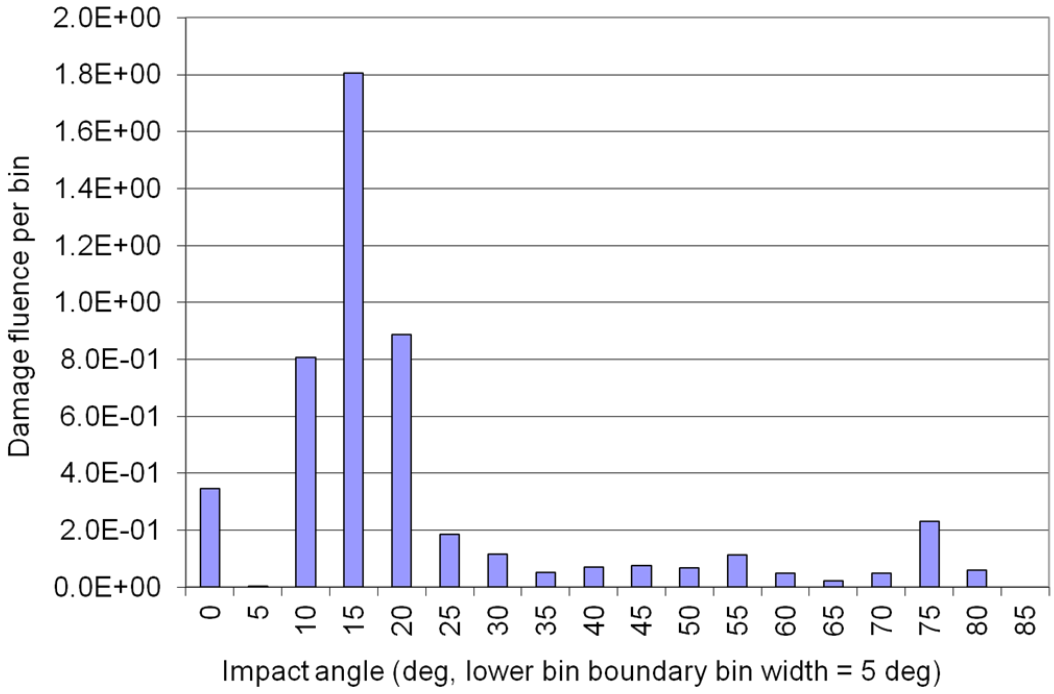

Figure 6.1-24. Distribution of Damage Fluence over Impact Angle

A MODRA run was executed with the variation that the impact angle limit of 65° was replaced with a value of 85°. Table 6.1-3 shows the resulting damage fluence on each cube face from each of the populations. In this case, the total damage fluence was 4.62. In comparison, the damage fluence for the case with the impact angle limit set to 65° was 4.95. The high density population still contributes the same percentage (91 percent) of the damage fluence. Using a higher impact angle limit reduced the total damage fluence, but the reduction was very small since the most common penetrating impacts occur at angles between 0 and 35°.

Table 6.1-3. Cube Damage Fluence Resulting from use of ORDEM 3.0 with the NNO BLE; Impact Angle Limit Changed to 85°

Cube face	Damage fluence							HD percent of total
	NaK	LD	MD	HD	Intacts	Total across populations	Total without HD	
Ram	1.09E-04	8.45E-04	2.45E-01	2.64E+00	4.04E-07	2.89E+00	2.46E-01	91.5%
Trail	0.00E+00	1.30E-06	5.33E-06	3.63E-05	1.26E-09	4.29E-05	6.63E-06	84.6%
South	6.36E-05	5.98E-04	9.14E-02	7.67E-01	5.71E-07	8.59E-01	9.21E-02	89.3%
North	6.36E-05	5.98E-04	9.14E-02	7.67E-01	5.71E-07	8.59E-01	9.21E-02	89.3%
Nadir	0.00E+00	8.63E-07	3.97E-06	1.61E-05	2.31E-09	2.09E-05	4.84E-06	76.9%
Zenith	2.90E-05	3.09E-04	2.37E-03	1.61E-02	2.07E-06	1.88E-02	2.71E-03	85.6%
Total across faces	2.65E-04	2.35E-03	4.30E-01	4.19E+00	3.62E-06	4.62E+00	4.33E-01	90.6%

6.1.3.3 Results Using ORDEM2000 with the Baseline NNO BLE

A MODRA run to determine cube damage fluence was executed with the variation that the ORDEM2000 debris environment was used in place of the ORDEM 3.0 debris environment. The baseline NNO BLE and a 65° angle limit was used for this run.

Since ORDEM2000 assumes that all debris particles are aluminum, a single population bin with impactor density of 2.8 g/cm^3 was implemented.

Figure 6.1-25 shows the environmental flux versus impactor size at the JPSS orbit from ORDEM2000 along with the total flux versus size curve from ORDEM 3.0 (summed over the different populations). The ORDEM2000 curve is from the flt.dat file. There are 20 points per size decade. The plot shows that the ORDEM2000 flux is lower for all sizes with the exception of the ranges from approximately 2.8 to 4 mm and above 18 cm.

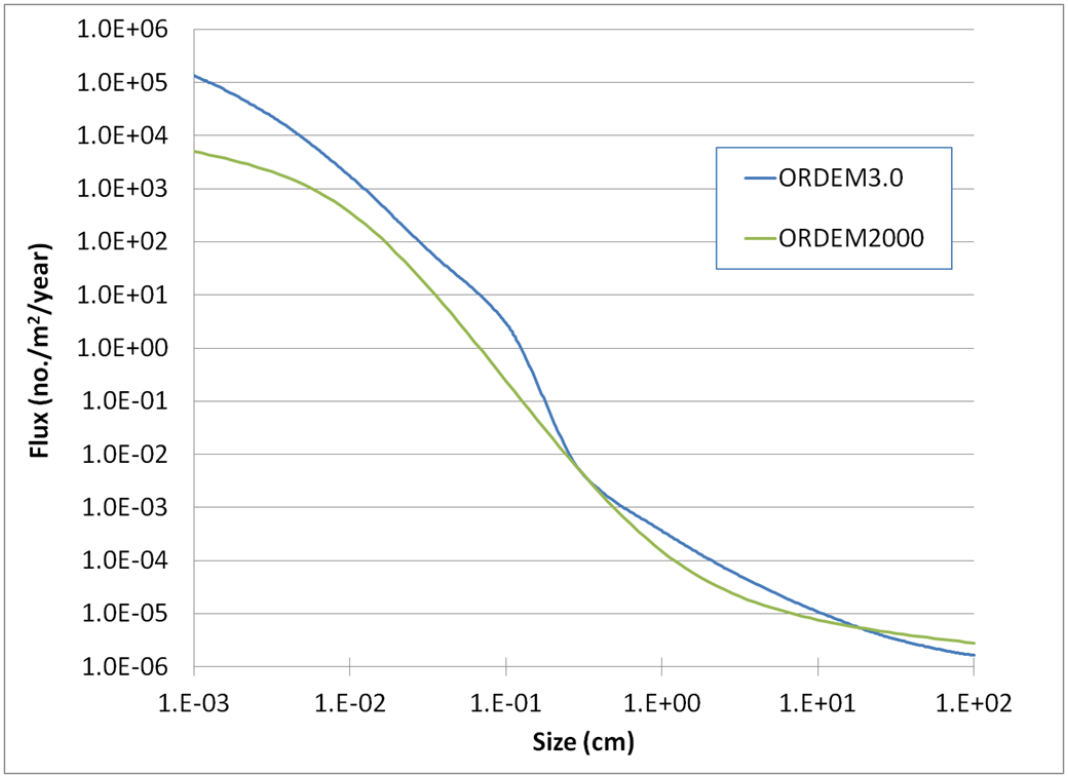

Figure 6.1-25. ORDEM2000 and ORDEM 3.0 Environmental Flux versus Impactor Size

Table 6.1-4 shows the damage fluence on each cube face when the ORDEM2000 debris environment is used with the baseline NNO BLE in MODRA. In this case, the total damage fluence is 0.169, which is ~29 times lower than the damage fluence of 4.95 using ORDEM 3.0. Note that the contribution to the total ORDEM 3.0 damage fluence by the medium density population, which has the same density as aluminum, is 0.436 (Table 6.1-1).

Table 6.1-4. Cube Damage Fluence Resulting from Use of ORDEM2000 with the Baseline NNO BLE

Face	Damage fluence
Ram	1.06E-01
Trail	4.36E-06
South	2.59E-02
North	2.60E-02
Nadir	9.71E-07
Zenith	1.08E-02
Total across faces	1.69E-01

Figure 6.1-26 illustrates the distribution of the cube damage fluence over impactor size resulting from using ORDEM2000 with the baseline NNO BLE. Damage fluences on all the cube faces are combined. This plot does not have the bi-modal pattern that is present in the same plot for ORDEM 3.0 due to the dominance of both medium density and high density particles (Figure. 6.1-22). The lowest size contributing damage fluence is 1 mm, which is higher than the lowest size contributing damage fluence from ORDEM 3.0 (0.676 mm).

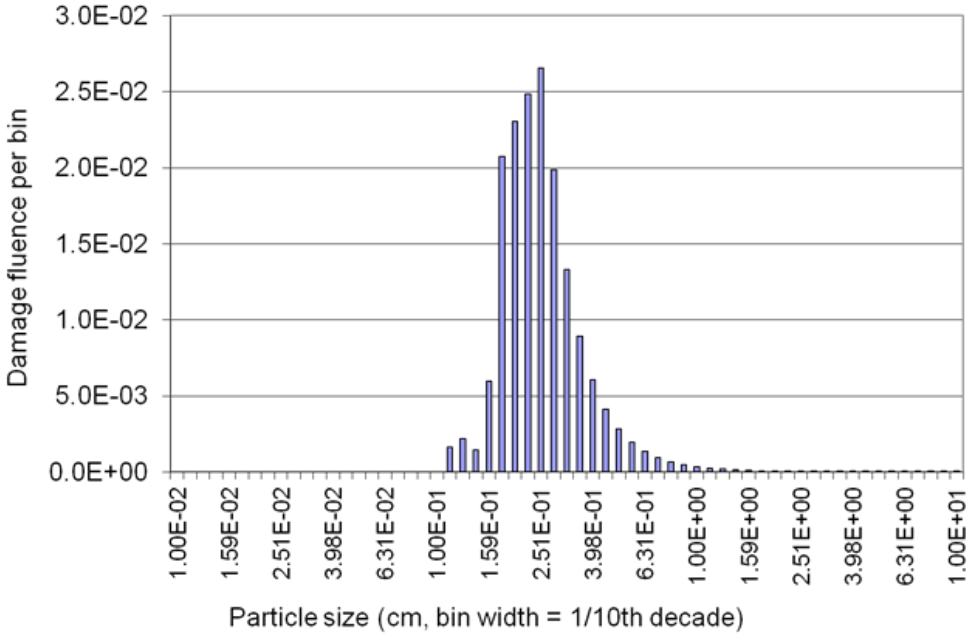

Figure 6.1-26. Distribution of Damage Fluence over Impactor Size; Results from All Cube Faces using ORDEM2000 with the Baseline NNO BLE

Figure 6.1-27 shows the distribution of damage fluence over impact velocity resulting from using ORDEM2000 with the baseline NNO BLE. Damage fluences on all the cube faces are combined. From this plot it is seen that the velocity range of penetrating particles is slightly broader than it was in the same plot for ORDEM 3.0 (Figure. 6.1-23). This may be due to the higher weighting factors on debris populations on highly eccentric orbits used by ORDEM2000. The peak in the low velocity range is not as high relative to the rest of the distribution as it is in the ORDEM 3.0 plot.

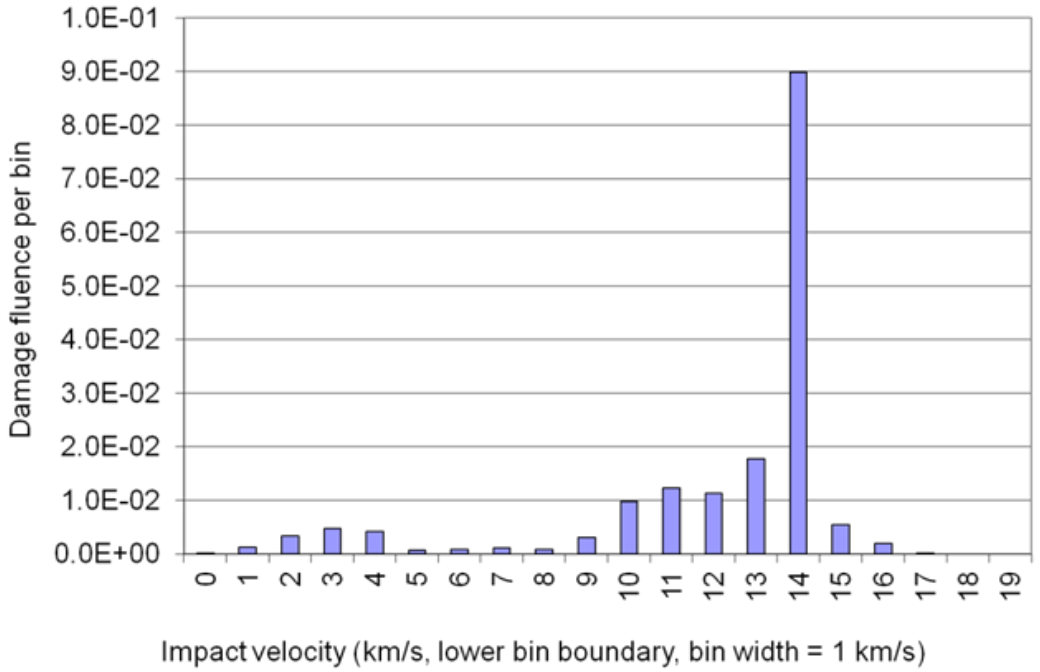

Figure 6.1-27. Distribution of Damage Fluence over Impact Velocity. Results from all Cube Faces using ORDEM2000 with the Baseline NNO BLE

Figure 6.1-28 shows the distribution of damage fluence over impact angle resulting from using ORDEM2000 with the baseline NNO BLE. Damage fluences on all the cube faces are combined. From this plot it is seen that the distribution is more uniform than in the same plot for ORDEM 3.0 (Figure 6.1-24). This may be due to the higher weighting factors on debris populations on highly eccentric orbits used by ORDEM2000.

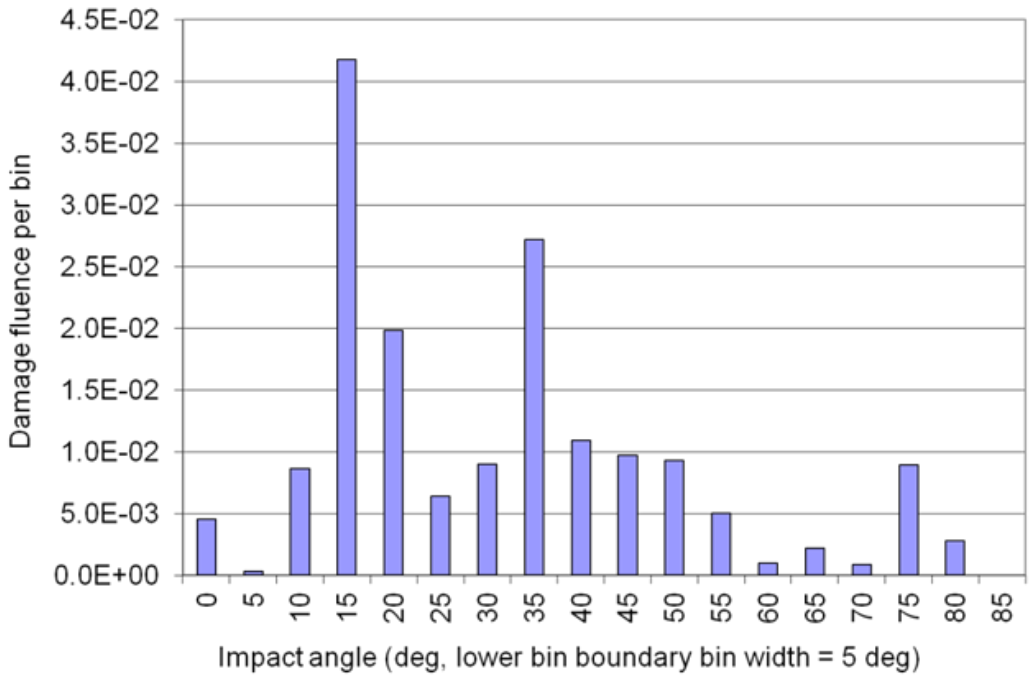

Figure 6.1-28. Distribution of Damage Fluence over Impact Angle; Results from all Cube Faces using ORDEM2000 with the Baseline NNO BLE

6.1.3.4 Results Using MASTER-2009 with the Baseline NNO BLE

A MODRA run to determine cube damage fluence was executed with the variation that the MASTER-2009 debris environment was used in place of the ORDEM 3.0 debris environment. The baseline NNO BLE with the 65° angle limit was used for this run.

MASTER-2009 reconstructs the current debris environment by modeling historical events and processes. Populations include explosion fragments, collision fragments, solid rocket motor slag and dust, ejecta from meteoroid impacts, paint flakes from surface degradation, multi-layer insulation pieces, launch-related operational debris, and NaK droplets. A debris population for the FY-1C collision is included, but there is no debris population for the Iridium 33/Cosmos 2251 collision. MASTER-2009 also contains a meteoroid population, but this was not used in this analysis to facilitate comparison with ORDEM 3.0 results. MASTER-2009 output files include flux versus size files (*c.dia) and standard environment interface (SEI) files (*.sei) for each population. The SEI files contain information similar to that of the ORDEM 3.0 igloo flux file. Flux is broken down by velocity, direction, size, and density bins. For this analysis, a preprocessor was developed to convert the SEI files into the flux component distribution file used by MODRA.

Figure 6.1-29 shows the environmental flux versus impactor size for each of the MASTER-2009 density bins. The curve of total flux versus size is from the *c.dia file generated by MASTER-

2009. The data for the individual density bins is extracted from the *.sei files for all populations, except meteoroids, and summed together. Two points per size decade are shown. The flux values shown were obtained by summing fluxes from all bins defined by azimuth, elevation, and velocity. Note that particles with density from 0.5 to 1.5 g/cm³ dominate the total flux at given size from 1 mm to 10 cm. The aluminum density bin (2.5 to 3 g/cm³) dominates in the size range 0.1 to 1 mm. The flux from 4.5 to 5 g/cm³ particles is comparable to the aluminum particle flux in the size range from 10 to 100 µm. For this orbit, MASTER-2009 outputs zero flux for particles with density > 5 g/cm³.

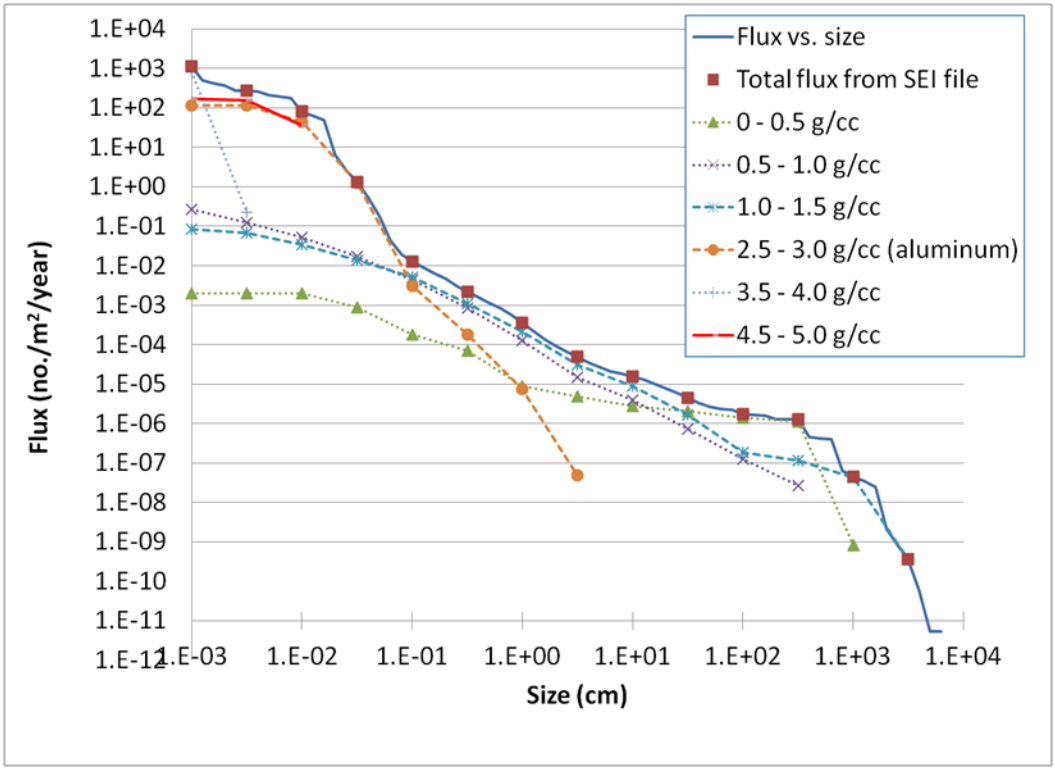

Figure 6.1-29. MASTER-2009 Environmental Flux versus Impactor Size

Table 6.1-5 shows the damage fluence on each cube face from each of the density bins when the MASTER-2009 debris environment is used with the baseline NNO BLE in MODRA. In this case, the total damage fluence is 0.03, which is a factor of 165 lower than the damage fluence of 4.95 using ORDEM 3.0. Particles with density from 0.5 to 3 g/cm³ all contribute in similar proportions to the total damage fluence.

Particles with density above 3 g/cm³ (i.e., above aluminum density of 2.8 g/ cm³) do not contribute to the damage fluence (i.e., there are no high density particles in the size range that could penetrate the sample cube).

Table 6.1-5. Cube Damage Fluence Resulting from use of MASTER-2009 with the Baseline NNO BLE

Cube face	Damage fluence						
	0 - 0.5 g/cc	0.5 - 1.0 g/cc	1.0 - 1.5 g/cc	2.5 - 3.0 g/cc (aluminum)	3.5 - 4.0 g/cc	4.5 - 5.0 g/cc	Total across populations
Ram	2.13E-04	4.95E-03	7.06E-03	6.32E-03	0.00E+00	0.00E+00	1.85E-02
Trail	2.16E-07	1.86E-06	7.63E-07	8.32E-06	0.00E+00	0.00E+00	1.12E-05
South	5.32E-05	1.16E-03	1.65E-03	1.32E-03	0.00E+00	0.00E+00	4.19E-03
North	4.88E-05	9.18E-04	1.73E-03	1.27E-03	0.00E+00	0.00E+00	3.97E-03
Nadir	3.09E-08	3.14E-06	6.07E-06	1.05E-05	0.00E+00	0.00E+00	1.98E-05
Zenith	3.71E-05	8.26E-04	1.38E-03	1.01E-03	0.00E+00	0.00E+00	3.26E-03
Total across faces	3.52E-04	7.86E-03	1.18E-02	9.95E-03	0.00E+00	0.00E+00	3.00E-02

Figure 6.1-30 illustrates the distribution of the cube damage fluence over impactor size resulting from using MASTER-2009 with the baseline NNO BLE. Damage fluences on all the cube faces are combined. This plot does not have the bi-modal pattern that is present in the same plot for ORDEM 3.0 due to the dominance of both medium density and high density particles (Figure 6.1-22). The lowest size contributing damage fluence is 1 mm, which is higher than the lowest size contributing damage fluence from ORDEM 3.0 (0.676 mm).

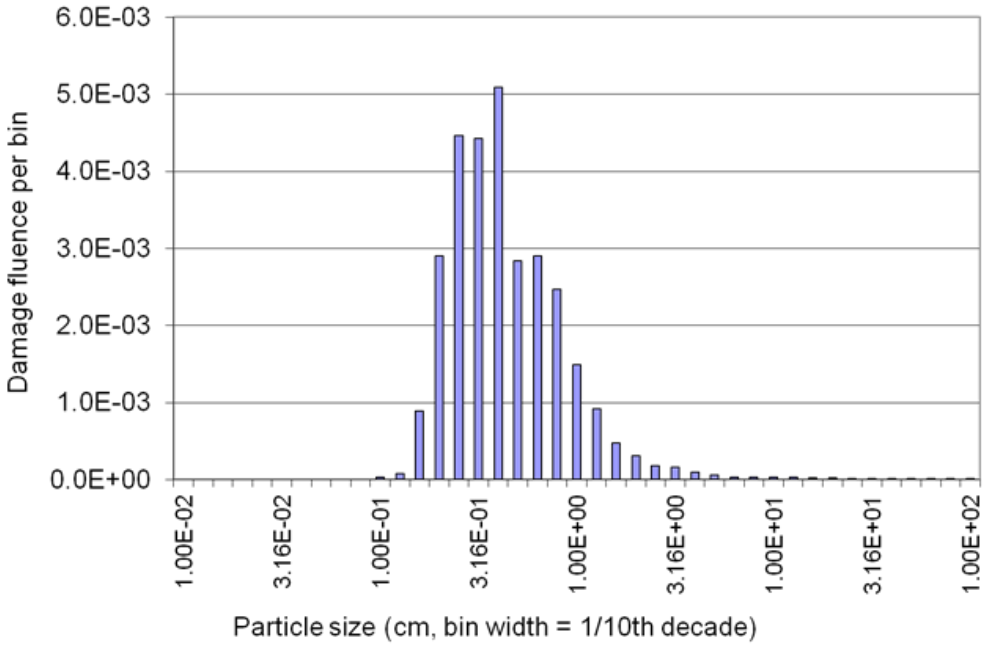

Figure 6.1-30. Distribution of Damage Fluence over Impactor Size; Results from all Cube Faces using MASTER-2009 with the Baseline NNO BLE

Figure 6.1-31 shows the distribution of damage fluence over impact velocity resulting from using MASTER-2009 with the baseline NNO BLE. Damage fluences on all the cube faces are combined. From this plot it is seen that the velocity range of penetrating particles is slightly

broader than it was in the same plot for ORDEM 3.0 (Figure 6.1-23). This may be due to a greater fraction of total flux attributable to debris populations on highly eccentric orbits. The peak in the low velocity range is not as high relative to the rest of the distribution as it is in the ORDEM 3.0 plot.

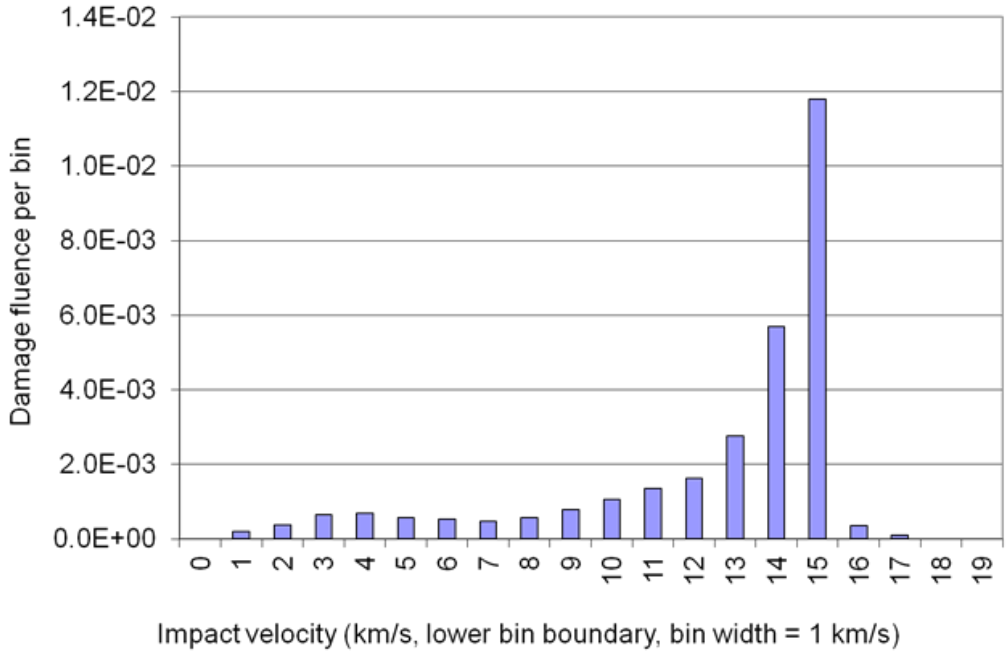

Figure 6.1-31. Distribution of Damage Fluence over Impact Velocity; Results from all Cube Faces using MASTER-2009 with the Baseline NNO BLE

Figure 6.1-32 shows the distribution of damage fluence over impact angle resulting from using MASTER-2009 with the baseline NNO BLE. Damage fluences on all the cube faces are combined. From this plot it is seen that the distribution is more uniform than in the same plot for ORDEM 3.0 (Figure 6.1-24). This may be due to a greater fraction of total flux attributable to debris populations on highly eccentric orbits.

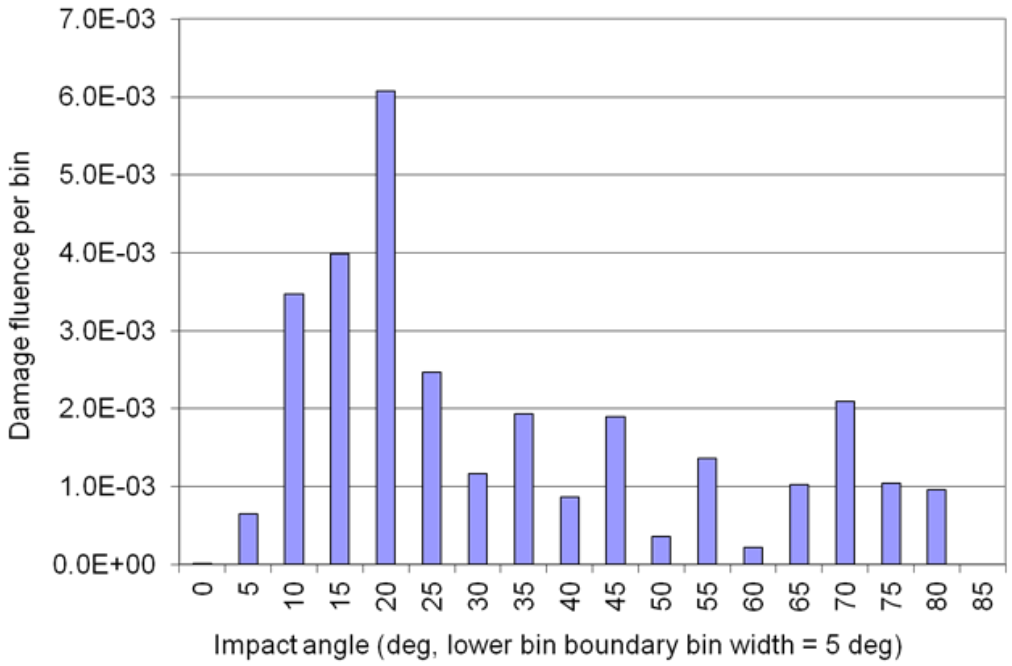

Figure 6.1-32. Distribution of Damage Fluence over Impact Angle; results from all cube faces using MASTER-2009 with the Baseline NNO BLE

6.1.3.5 Results Using ADEPT with the Baseline NNO BLE

A MODRA run to determine cube damage fluence was executed with the variation that the ADEPT debris environment was used in place of the ORDEM 3.0 debris environment. The baseline NNO BLE and a 65° angle limit was used for this run.

The current version of ADEPT was designed with emphasis placed on projecting the future debris environment down to 1 cm from future launch traffic, explosions and collisions [ref. 10]. The initial population consists of the following sub-populations:

- Unclassified catalog objects.
- A statistical population to represent the difference between the number of objects in the unclassified catalog and the total unclassified number cited by the United States Strategic Command's (USSTRATCOM) Space Control and Space Surveillance ("Unknown population") website.
- A population of untracked debris (10 cm down to 1 cm) determined by power law extrapolation ("small population"). The long term plan is to replace this population with a reconstruction of the current environment from historical events and processes (similar to the approach in MASTER-2009).

- Debris down to 1 cm from the FY-1C and Iridium 33/Cosmos 2251 collisions as modeled by the Aerospace breakup modeling code IMPACT ("FYCIC population").

To generate a flux versus size curve for MODRA analysis, the ADEPT initial population flux was further extrapolated down to 0.1 mm. Hence, the base for the extrapolation includes the Unknown, Small, and FY-1C populations.

Impact velocity and direction distributions for MODRA analysis can eventually be extracted from the ADEPT populations, but the tools to accomplish this were not yet available for this analysis. To circumvent this limitation, two MODRA runs were made. In the first run, the ADEPT flux versus size curve and the MASTER-2009 normalized velocity and direction distribution were used as inputs for MODRA. In the second run, the ADEPT flux versus size curve and the ORDEM 3.0 normalized velocity and direction distribution were used as inputs to MODRA.

Density information is available for the FYCIC population generated by IMPACT, but the tools to extract this information for MODRA were not yet available for this analysis. Therefore, it was assumed that all impactors have density of aluminum (consistent with ORDEM2000) (i.e., a single population bin with impactor density of 2.8 g/cm^3 was implemented).

Table 6.1-6 shows the damage fluence on each cube face when the ADEPT debris environment is used with the MASTER-2009 velocity/direction distribution and the baseline NNO BLE in MODRA. In this case, the total damage fluence is 0.0566. Table 6.1-7 shows the damage fluence on each cube face when the ADEPT debris environment is used with the ORDEM 3.0 velocity/direction distribution and the baseline NNO BLE in MODRA. In this case, the total damage fluence is 0.0575. Swapping the velocity/direction distribution had minimal effect on the total damage fluence, which is a factor of ~86 lower than the damage fluence of 4.95 using ORDEM 3.0.

Table 6.1-6. Cube Damage Fluence Resulting from use of ADEPT with the MASTER-2009 Velocity/Direction Distribution and the Baseline NNO BLE

Face	Damage fluence
Ram	3.57E-02
Trail	2.09E-05
South	7.85E-03
North	7.37E-03
Nadir	3.97E-05
Zenith	5.67E-03
Total across faces	5.66E-02

Table 6.1-7. Cube Damage Fluence Resulting from use of ADEPT with the ORDEM 3.0 Velocity/Direction Distribution and the Baseline NNO BLE

Face	Damage fluence
Ram	3.88E-02
Trail	8.33E-06
South	6.38E-03
North	6.38E-03
Nadir	9.40E-06
Zenith	5.93E-03
Total across faces	5.75E-02

Figure 6.1-33 illustrates the distribution of the cube damage fluence over impactor size resulting from using ADEPT with the MASTER-2009 velocity/direction distribution and the baseline NNO BLE. Figure 6.1-34 illustrates the distribution of the cube damage fluence over impactor size resulting from using ADEPT with the ORDEM 3.0 velocity/direction distribution and the baseline NNO BLE. Damage fluences on all the cube faces are combined. These plots do not have the bi-modal pattern that is present in the same plot for ORDEM 3.0 due to the dominance of both medium density and high density particles (Figure 6.1-22). The lowest size contributing damage fluence is 1 mm, which is higher than the lowest size contributing damage fluence from ORDEM 3.0 (0.676 mm).

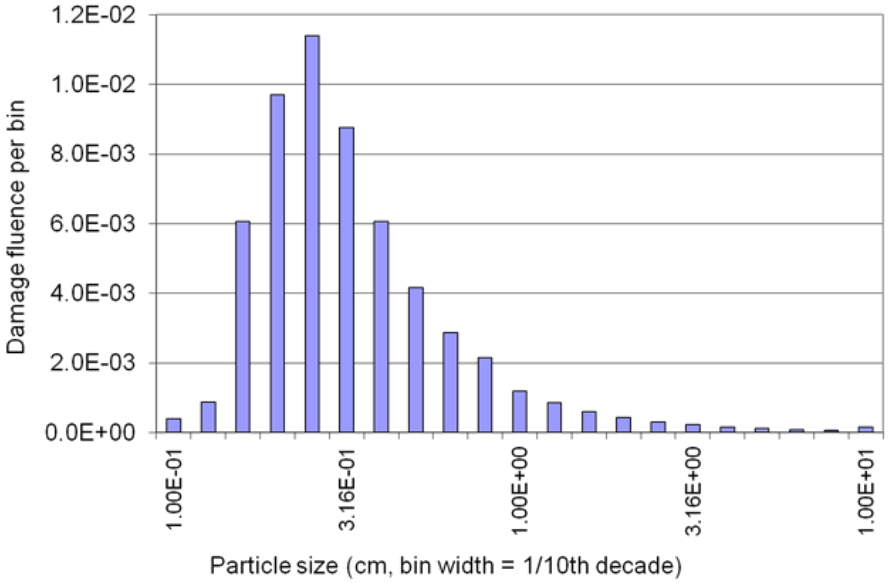

Figure 6.1-33. Distribution of Damage Fluence over Impactor Size; Results from all Cube Faces using ADEPT with the MASTER-2009 Velocity/Direction Distribution and the Baseline NNO BLE

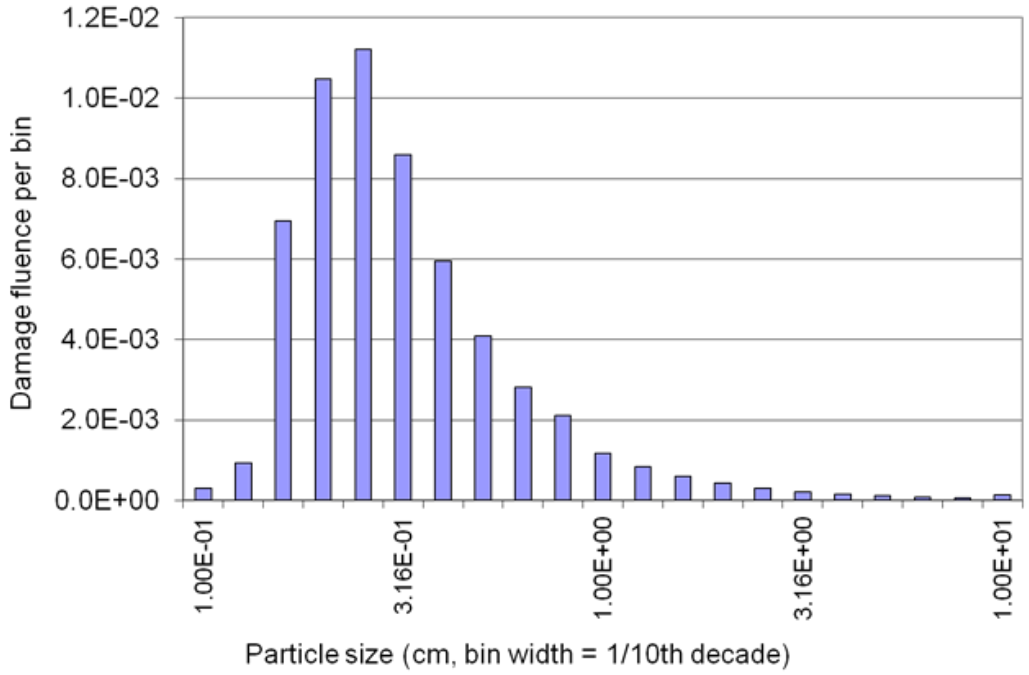

Figure 6.1-34. Distribution of Damage Fluence over Impactor Size; Results from All Cube Faces using ADEPT with the ORDEM 3.0 Velocity/Direction Distribution and the Baseline NNO BLE

Figure 6.1-35 shows the distribution of damage fluence over impact velocity resulting from using ADEPT with the MASTER-2009 velocity/direction distribution and the baseline NNO BLE. Damage fluences on all the cube faces are combined. The shape of the distribution is similar to that from the MASTER-2009 run (Figure 6.1-31). Figure 6.1-36 shows the distribution of damage fluence over impact velocity resulting from using ADEPT with the ORDEM 3.0 velocity/direction distribution and the baseline NNO BLE. In this case, the shape of the distribution at high velocities is similar to that from the ORDEM 3.0 run (Figure 6.1-23). The peak at lower velocities is not as high relative to the rest of the distribution as in the velocity distribution from the ORDEM 3.0 run.

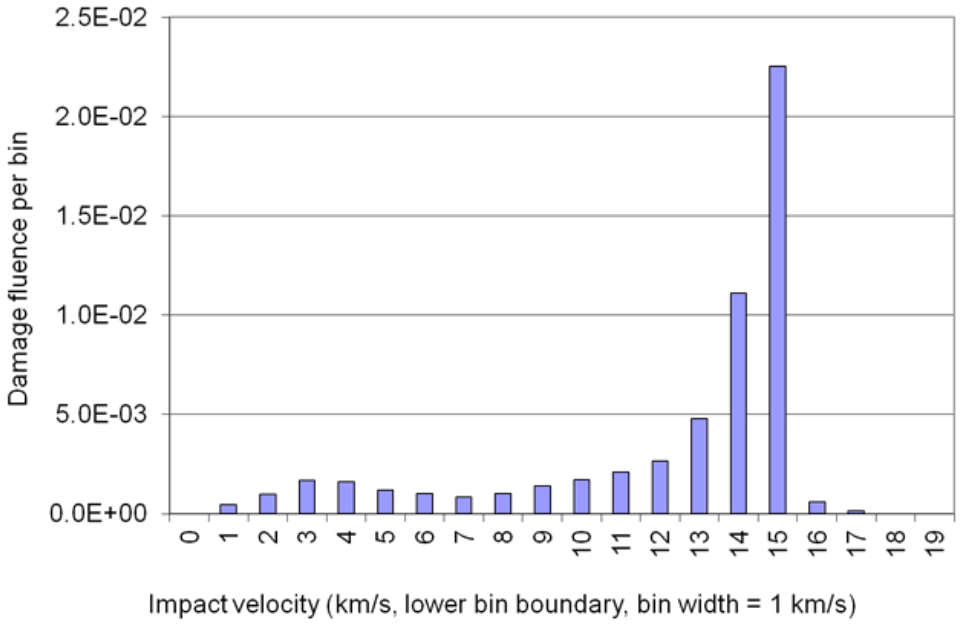

Figure 6.1-35. Distribution of Damage Fluence over Impact Velocity; Results from All Cube Faces using ADEPT with the MASTER-2009 Velocity/Direction Distribution and the Baseline NNO BLE

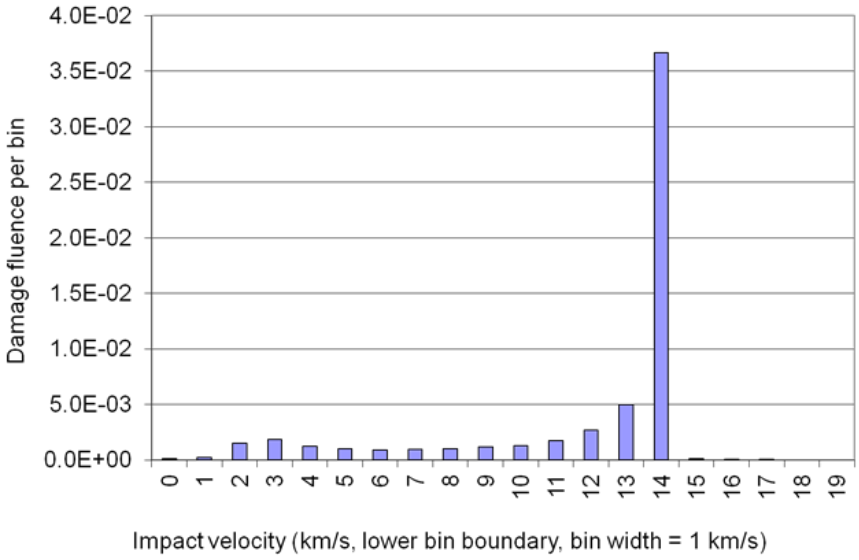

Figure 6.1-36. Distribution of Damage Fluence over Impact Velocity; Results from all Cube Faces using ADEPT with the ORDEM 3.0 Velocity/Direction Distribution and the Baseline NNO BLE

Figure 6.1-37 shows the distribution of damage fluence over impact angle resulting from using ADEPT with the MASTER-2009 velocity/direction distribution and the baseline NNO BLE.

Damage fluences on all the cube faces are combined. The shape of the distribution is similar to that from the MASTER-2009 run (Figure 6.1-32). Figure 6.1-38 shows the distribution of damage fluence over impact angle resulting from using ADEPT with the ORDEM 3.0 velocity/direction distribution and the baseline NNO BLE. The shape of the distribution is similar to that from the ORDEM 3.0 run (Figure 6.1-24).

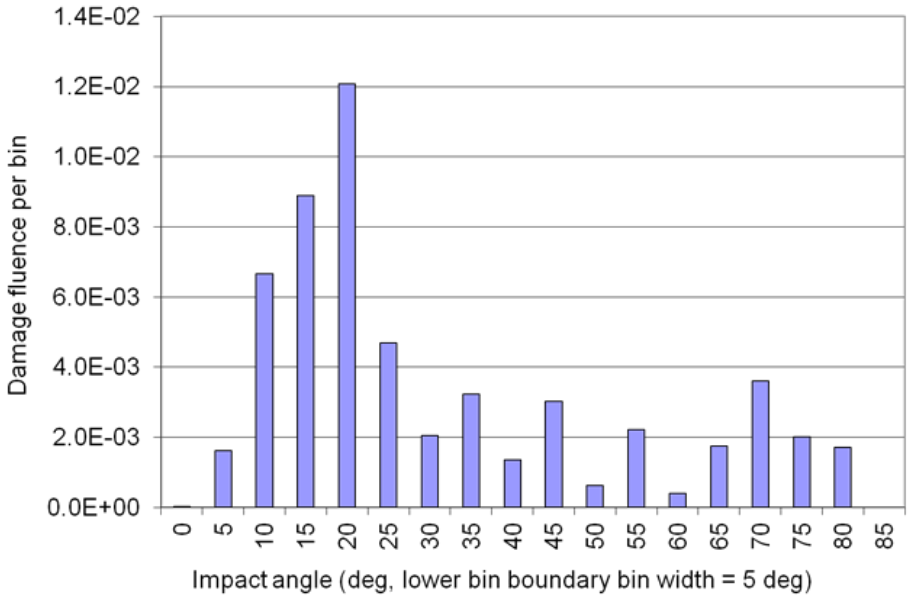

Figure 6.1-37. Distribution of Damage Fluence over Impact Angle; Results from all Cube Faces using ADEPT with the MASTER-2009 Velocity/Direction Distribution and the Baseline NNO BLE

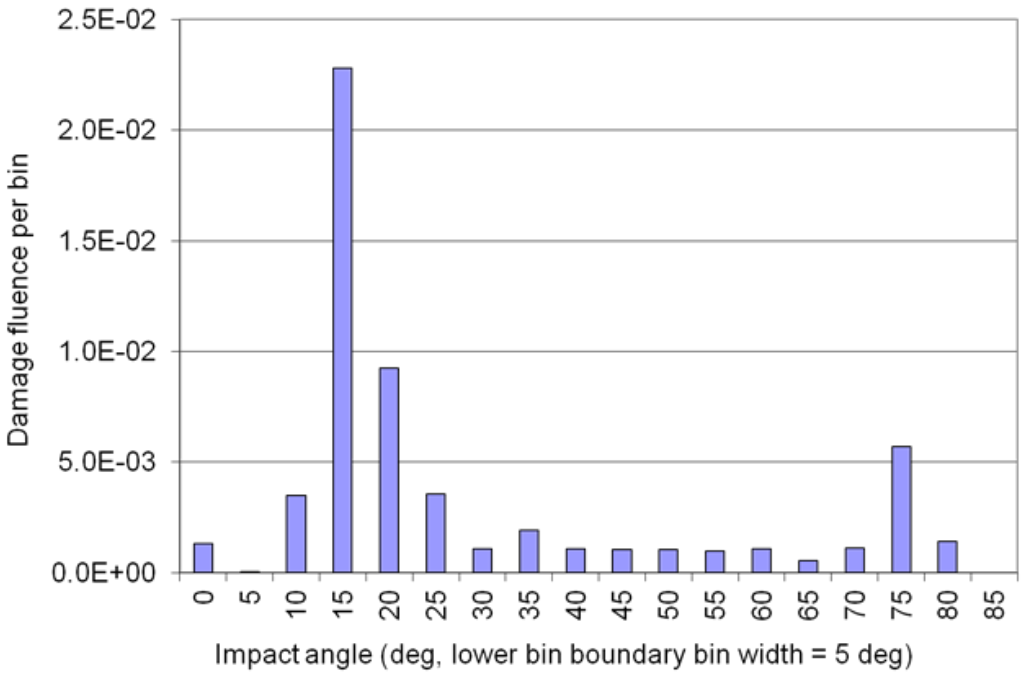

Figure 6.1-38. Distribution of Damage Fluence over Impact Angle; Results from all Cube Faces using ADEPT with the ORDEM 3.0 Velocity/Direction Distribution and the Baseline NNO BLE

6.1.3.6 Conclusions

Damage fluence on a generic cube was determined for various orbital debris models and variations of damage equations. The Aerospace MODRA code was used to compute damage fluence for each bus face. The baseline results were for the combination of ORDEM 3.0 with the NNO BLE. A test run on the JPSS CTU box produced results that compared well with corresponding Bumper results. Results for the cube showed that the high density particle (i.e., stainless steel) population accounts for ~90 percent of the total damage fluence. The total damage fluence on all cube faces was 4.95. Debris particles in the size range 0.6 mm to 3 mm dominate the damage fluence. Results also show that high velocity impacts dominate total damage fluence, although low velocity impacts also contribute a noticeable fraction of the total damage fluence. When the impact angle limit in the NNO BLE is changed from 65 to 85°, the total damage fluence is reduced slightly to 4.62.

MODRA runs were performed using the ORDEM2000, MASTER-2009, and ADEPT debris models with the NNO BLE. The ORDEM2000 and ADEPT runs assumed that all impactors are aluminum. MASTER-2009 only produced fluxes for particles with density of 5 g/cm^{3}or less. In all cases, the resulting cube damage fluence was lower than the damage fluence resulting from use of ORDEM 3.0. The MASTER-2009 and ADEPT damage fluence values were similar, but less than the ORDEM2000 damage fluence value. It was noted that the ORDEM2000 damage fluence was much closer to the ORDEM 3.0 damage fluence contributed by just the medium

density population (aluminum) than to the total ORDEM 3.0 damage fluence including the high density particle population.

6.1.4 Conclusions Regarding ORDEM 3.0

6.1.4.1 ORDEM 3.0 versus other Models

In many ways, ORDEM 3.0 does not predict a significantly different hazard than ORDEM2000. For example, a spacecraft at 400 km altitude can expect a **lower** hazard prediction from ORDEM 3.0 than by ORDEM2000, depending on its regions of spacecraft vulnerability, as shown in Figure 6.1-9, where the ORDEM 3.0 flux is compared to the ORDEM2000 flux. This is the result of ORDEM2000 using less *in situ* data with larger uncertainties from a different (and shorter) time span than ORDEM 3.0. As a result, the newer model was fit with a curve that required fewer source assumptions. At higher altitudes, the ORDEM 3.0 flux represents a significantly higher hazard, but only if the spacecraft is vulnerable to debris sizes less than 3 mm, as shown in Figure 6.1-10.

The shuttle impact data set when ORDEM2000 was developed had about 1/3 the exposure time as the shuttle data used in ORDEM 3.0. As a result, impacts as large as 1 mm were not included in the ORDEM2000 data, with the largest impacts being from debris of about 0.5 mm. At smaller sizes, most of the data revealed paint and aluminum oxide as the dominant debris type. However, the major data source used for ORDEM2000's small debris population was LDEF [ref. 11]. Because LDEF had a fixed orientation relative to the orbital velocity vector, the distribution of craters around LDEF's surfaces were used to conclude that most of the impacts were from objects in highly elliptical orbits. For example, especially noticeable were aluminum oxide impacts on LDEF's rear surface that could come only from high eccentricity orbits with inclinations similar to the orbital inclination of LDEF. This may be still be true of medium density and low density debris, and perhaps ORDEM 3.0 should have been modeled using this assumption for the LD debris; however, it would have reduced the ORDEM 3.0 hazard from the less than 3 mm population by only about 10 percent.

Another characteristic to note concerning ORDEM2000 is that it does not contain the debris populations modeled from the major collision events including the FY-1C test and the Iridium/Cosmos collision.

ORDEM 3.0 is burdened with the same limitations as all existing orbital debris models resulting from the absence of any *in situ* debris penetration data beyond 400-600 km altitude. All debris models have a level of uncertainty due to this reality. However, when compared to the other models, ORDEM 3.0 makes the greatest use of available *in situ* data for the development of the model. Indeed, MASTER-2009 and ADEPT poorly predict the flux at 400-600 km altitude that would be necessary to reproduce the observed Space Shuttle impact data. The NESC team understands the assumptions made and processes used to develop the ORDEM 3.0 debris population for regimes where no *in situ* or radar data exist, but it is still a concern that there is (as of yet) no source identified to explain the 1 mm steel particle population. Overall, the NESC team recommends ORDEM 3.0 as the best option for use in JPSS-1 MMOD risk assessments.

The NESC team considered the possibility of using ORDEM 3.0 minus the high density debris component, but decided that it was not appropriate to use only portions of the model when not designed to do so. For an alternate opinion on this subject, see Section 9.0.

F-10. In spite of the identified uncertainties, ORDEM 3.0 possesses several advantages over ORDEM2000, MASTER-2009 and the current version of ADEPT:

1. ORDEM 3.0 incorporates the most extensive use of Space Shuttle impact data, including residue chemical analysis. As a result of safety concerns about the orbiters, radiator and window surfaces represent the most complete, thoroughly examined returned spacecraft surfaces.
2. MASTER-2009 and ADEPT do not predict the 1 mm particle flux reflected by the Space Shuttle impact data.
3. ORDEM 3.0 contains high density particles that are not included in the other models, but are present in the Space Shuttle impact data.
4. ORDEM 3.0 includes an updated large-object catalog, including contributions from the FY-1C event, the Iridium-Cosmos collision, and other recent debris-producing events. ORDEM2000 includes none of these, MASTER-2009 includes only the FY-1C debris, and ADEPT includes FY-1C and Iridium-Cosmos debris.

6.1.4.2 Possible Sources of 1 mm Population

Although the ODPO did not identify a source for the 1 mm high density debris, the NESC team did speculate and research possible sources. To determine a source, one must first identify potential sources from the metals used in their construction, and then identify a mechanism that would generate a debris population consisting of mostly 1 mm debris.

Two spacecraft structure types were identified as containing stainless steel: propellant tanks used in upper stage rockets and liquid rocket engines. Aerospace identified that the propellant tanks in Delta I 2nd stages, Delta II 2nd stages, and Centaur upper stages were made of stainless steel, and that over 200 of these upper stages are still in orbit [ref. 12]. No attempt has been made to identify the materials used in Russian upper stages or spacecraft although anecdotal information obtained through the Inter-Agency Debris Coordination Committee (IADC) states that most, if not all, Russian/Soviet upper stages used aluminum propellant tanks. Informal contacts with individuals involved with testing liquid rocket engines provided mixed reports, with one saying that no erosion of the stainless steel surfaces was observed during testing and another saying that it is common.

However, what can be concluded with certainty is that upper stages with stainless steel tanks have exploded at high LEO altitudes, producing a possible reservoir of stainless steel debris, some exploding in orbits as high as 1500 km. In another analysis by Aerospace [Appendix C, ref. 13], it was concluded that these explosions alone are insufficient to be the only source of stainless steel debris. At most, these explosions represent a reservoir that is declining now that

their operation includes depleting excess fuel to prevent future explosions. But both explosions and collisions are capable of generating small fragments, with most of the expected collision events unlikely to produce a detectable change in the upper stage. One can confidently predict that existing debris fragments between 3 mm and a few cm are both numerous enough and massive enough to cause non-catastrophic debris-producing events with upper stage rockets as well as payloads. In addition, if the 1 mm debris population is as large as predicted in ORDEM 3.0, then that population would also contribute to an increasing 1 mm debris population and has the potential to become self-generating. What is missing is any experimental data to predict the amount of debris generated, as well as a model analysis to determine if the rate of generation is consistent with the Space Shuttle impact data.

Another possible explanation for the abundance of 1 mm particles may be a function of the LEGEND evolutionary model. The debris population model in LEGEND does not include ejecta from impacts from particles from 1-10 cm, nor a ground-tested non-catastrophic collision model that may apply to upper stages.

The following finding is related to the 1 mm steel particle source.

F-11. No source for 1 to 3 mm steel debris particles in ORDEM 3.0 has been definitively identified. Possible contributors include:

- Surface degradation (e.g., collisions with MMOD) of stainless steel rocket stages with thicknesses near 1 mm.
- Explosions of non-passivated stages.
- Ejecta from non-catastrophic collisions. The debris population model in LEGEND does not include ejecta from impacts from particles from 1 to 10 cm, nor a ground-tested non-catastrophic collision model that may apply to upper stages.

6.1.5 NASA-STD-7009 Evaluation Credibility Assessment

To gain a different perspective of ORDEM 3.0, the NESC team performed an informal credibility assessment based on NASA-STD-7009, *Standard for Models and Simulations.* The credibility assessment scale (CAS) was created to use a standardized process and nomenclature to inform NASA decision-makers about the credibility of model and simulation results. Since credibility is subjective, the CAS does not purport to determine credibility, but merely assesses on a graduated scale, key factors that contribute to a decision-maker's assessment of credibility [ref. 14]. The CAS is divided into eight factors, which are described later in this section. There are five levels numbered 0 to 4 with which to grade each factor. A higher level indicates greater confidence in establishing credibility as it relates to the factor evaluated. The values can be rolled into a combined credibility score and compared to target values set by the project.

For this assessment, the credibility factors and levels were used to give a qualitative assessment of ORDEM 3.0 and how NESC recommendations in this report could improve credibility as represented in the CAS. Figures 6.1-39 and 6.1-40 show the results of the credibility assessment. ORDEM 3.0 was treated as two separate models: one for orbital debris particles

>3 mm diameter, and one for particles <3 mm diameter. For the >3 mm regime, there is a higher confidence in the model results because there are radar measurements to ground and validate the model. Conversely, only for the 400 to 600 km altitude range, for which there is Space Shuttle impact data, are there any direct measurements available for particles <3 mm. This assessment was also directed to the modeled environment at the JPSS-1 orbital altitude, so any advantage gained at the 400 to 600 km altitude does not apply in this case. The disparity in confidence between the two model size regimes is reflected in the CAS matrices for the two cases (Figures 6.1-39 and 6.1-40). In the figures, the magenta line represents the current evaluation level for each factor. Some factors also have a blue line, placed higher than the magenta, which represents the level to which the factor might be improved if improvements outlined in the recommendations for this assessment are implemented.

Credibility Assessment for Particles Greater than ~3 mm

The results from the credibility assessment for ORDEM 3.0 for particles >3 mm can be seen in Figure 6.1-39. How the NESC team rated each factor is discussed in Figure 6.1-39.

	M&S Development		M&S Operations			Supporting Evidence		
	Verification	**Validation**	**Input Pedigree**	**Results Uncertainty**	**Results Robustness**	**Use History**	**M&S Mgt**	**People Qualifications**
4	Numerical errors small for all important features	Results agree with real-world data	Input data agree with real-world data	Non-deterministic & numerical analysis	Sensitivity known for most parameters; key sensitivities identified	De facto standard	Continual process improvement	Extensive experience in and use of recommended practices for this particular M&S
3	Formal numerical error estimation	Results agree with experimental data for problems of interest	Input data agree with experimental data for problems of interest	Non-deterministic analysis	Sensitivity known for many parameters	Previous predictions were later validated by mission data	Predictable process	Advanced degree or extensive M&S experience, and recommended practice knowledge
2	Unit and regression testing of key features	Results agree with experimental data or other M&S on unit problems	Input data traceable to formal documentation	Deterministic analysis or expert opinion	Sensitivity known for a few parameters	Used before for critical decisions	Established process	Formal M&S training and experience, and recommended practice training
1	Conceptual and mathematical models verified	Conceptual and mathematical models agree with simple referents	Input data traceable to informal documentation	Qualitative estimates	Qualitative estimates	Passes simple tests	Managed process	Engineering or science degree
0	Insufficient evidence	Insufficient evidence	Insufficient evidence	Insufficient evidence	Insufficient evidence	Insufficient evidence	Insufficient evidence	Insufficient evidence

Figure 6.1-39. NASA-STD-7009 Credibility Assessment for ORDEM 3.0 >3 mm Particle Size Regime

M&S Development

Verification: Level 3/*Formal numerical error estimation* – Verification is the process of determining that the application accurately represents the underlying mathematical model and its solution from the perspective of the intended uses of the M&S [ref. 14]. It confirms that the model is coded correctly and does not contain errors. The ODPO development process for ORDEM 3.0 was judged to be adequate for verifying the model.

Validation: Level 4/*Results agree with real-world data* – Validation is the process of determining the degree to which a model presents an accurate representation of the real world. Validation requires a source of data to which results from the model or simulation can be compared. ORDEM 3.0 was validated against the large radar measurement dataset available for particles >3 mm in diameter. A limitation was that the data source used to develop the model was in some cases the same as that used for validation.

M&S Operations

Input Pedigree: Level 4/*Input data agree with real-world data* – Input Pedigree evaluates the degree to which input data compares favorably with measured real-world data. Radar data was used as input data for ORDEM 3.0 in this size regime. While it still has uncertainties, radar measurements are a mature and well-understood process for obtaining direct measurements of the larger orbital debris particles.

Results Uncertainty: Level 2→3/*Deterministic analysis or expert opinion→ Nondeterministic analysis* – Results Uncertainty indicates the degree to which uncertainties are quantified and are based on nondeterministic analysis. Uncertainty in ORDEM 3.0 has not been quantified to any significant extent and is based primarily on expert opinions. While the nature of the environment being modeled is such that there will be large uncertainties, efforts to perform nondeterministic uncertainty analysis may be possible and could result in an improvement to Level 3 for this factor.

Results Robustness: Level 1→3/*Qualitative estimates→Sensitivity known for many parameters* – Results Robustness is the degree of how well the sensitivities of the model are known. Very limited sensitivity studies were performed for ORDEM 3.0, resulting in a Level 1 rating, which could be improved to as high as a Level 3 if more extensive sensitivity studies were performed.

Supporting Evidence

Use History: Level 2/*Used before for critical decisions* – Use History assesses the heritage of the model by evaluating how extensively it has been used for similar applications in the past. ORDEM 3.0 is gradually being adopted by spaceflight projects

for critical decisions, and its predecessors have been in use for many years. Independent mission data, aside from radar data used in the model, are not available to validate predictions.

M&S Management: Level 3/*Predictable process* – M&S Management determines how well the model's processes are managed. This would include assessing product management, process definition, continuous improvement, and configuration management. ORDEM 3.0 has a predictable and understandable process, and ODPO is working to continuously improve the model. One weakness noted is the lack of documentation describing ORDEM 3.0's validation and verification. There is a user's guide, which is useful, but it does not contain details on the model's best uses and limitations.

People Qualifications: Level 3.5/*Extensive experience and use of recommended practices for this particular M&S* – People Qualifications assesses the qualifications of the personnel developing, using, and interpreting the results from the model. The personnel who control ORDEM 3.0 possess a very high level of expertise and experience. The only consideration that prevented this factor rating a 4 was the fact that ODPO is understaffed and many of the team recommendations have not already been accomplished only because of a lack of resources.

Credibility Assessment for Particles Less than ~3 mm

The results from the credibility assessment for ORDEM 3.0 for particles <3 mm can be seen in Figure 6.1-40. Overall, the results are seen to exhibit a lower level of confidence in the model for this size regime because of the absence of any direct measurements in the JPSS orbit altitude. How the NESC team rated each factor is discussed in Figure 6.1-40.

	M&S Development		M&S Operations			Supporting Evidence		
	Verification	**Validation**	**Input Pedigree**	**Results Uncertainty**	**Results Robustness**	**Use History**	**M&S Mgt**	**People Qualifications**
4	Numerical errors small for all important features	Results agree with real-world data	Input data agree with real-world data	Non-deterministic & numerical analysis	Sensitivity known for most parameters; key sensitivities identified	De facto standard	Continual process improvement	Extensive experience in and use of recommended practices for this particular M&S
3	Formal numerical error estimation	Results agree with experimental data for problems of interest	Input data agree with experimental data for problems of interest	Non-deterministic analysis	Sensitivity known for many parameters	Previous predictions were later validated by mission data	Predictable process	Advanced degree or extensive M&S experience, and recommended practice knowledge
2	Unit and regression testing of key features	Results agree with experimental data or other M&S on unit problems	Input data traceable to formal documentation	Deterministic analysis or expert opinion	Sensitivity known for a few parameters	Used before for critical decisions	Established process	Formal M&S training and experience, and recommended practice training
1	Conceptual and mathematical models verified	Conceptual and mathematical models agree with simple referents	Input data traceable to informal documentation	Qualitative estimates	Qualitative estimates	Passes simple tests	Managed process	Engineering or science degree
0	Insufficient evidence	Insufficient evidence	Insufficient evidence	Insufficient evidence	Insufficient evidence	Insufficient evidence	Insufficient evidence	Insufficient evidence

Figure 6.1-40. NASA-STD-7009 Credibility Assessment for ORDEM 3.0 <3 mm Particle Size Regime

M&S Development

Verification: Level 3/*Formal numerical error estimation* – The ODPO development process for ORDEM 3.0 was judged to be adequate for verifying the model. Verification of the application is independent of the particle size regime so this matches the level for the >3 mm regime.

Validation: Level 1→2/*Conceptual and mathematical models agree with simple referents/Results agree with experimental data or other M&S on unit properties* – Real world data are not available to validate the model, highlighting one of the primary weaknesses of ORDEM 3.0. Some impact data that are available may be employed to help validate the model at 400-600 km, which may in turn have an effect on the results for the higher altitudes.

M&S Operations

Input Pedigree: Level 1→4/*Input data traceable to informal documentation/Input data agree with real-world data* – The only input data available used are Space Shuttle impact data. *In situ* impact measurements at altitudes higher than 600 km, for which there currently are no plans, would benefit the input pedigree a great deal.

Results Uncertainty: Level 1→3/*Qualitative estimates/Non-deterministic analysis* – Only qualitative estimates on uncertainty have been performed for ORDEM 3.0. The NESC team recommended that the uncertainty be quantified, which would raise this factor to a level 3.

Results Robustness: Level 1→3/*Qualitative estimates→Sensitivity known for many parameters* – As is the case for the model in the >3 mm size regime, sensitivity studies would increase the level in this factor to 3.

Supporting Evidence

Use History: Level 1/*Passes simple tests* – ORDEM 3.0 in the <3 mm size regime passes simple tests. ORDEM 3.0 for this smaller size regime does not give the same level of confidence as the >3 mm model.

M&S Management: Level 3/*Predictable process* and **People Qualifications**: Level 3.5/*Extensive experience and use of recommended practices for this particular M&S* – These categories are strengths for ORDEM 3.0 for both size regimes. The rationale given for the >3 mm model applies for the <3 mm model.

The following findings and observations are related to the credibility assessment.

F-12. ORDEM 3.0 has no technical documentation describing the validation and verification or user guide information detailing the best uses and limitations.

- Data for this assessment was provided to the NESC team by ODPO in the form of presentations, spreadsheets, and verbal exchanges.

O-4. The credibility assessment methodology in NASA-STD-7009 (*NASA Standard for Models and Simulations)* was useful in providing a high-level evaluation of ORDEM 3.0, highlighting opportunities for overall improvement and building confidence in the model. This was especially the case for orbital debris particle regimes <3 mm, where focus areas include validation, input pedigree, results uncertainty, results robustness, and model and simulation management. OSMA has determined that this standard is not mandatory for ORDEM 3.0, and an evaluation of this decision was outside the scope of this assessment.

6.2 Meteoroid Models

6.2.1 Description

NASA's meteoroid environment model is the MEM maintained by the MEO located at MSFC. MEM provides only the meteoroid environment and is independent from ORDEM, which supplies only the orbital debris environment. This is unlike MASTER-2009, which combines a meteoroid environment model and an orbital debris environment model. MASTER-2009 integrates the Divine-Staubach meteoroid model with its orbital debris model into one application. ESA also has another meteoroid model called the Interplanetary Meteoroid Engineering Model (IMEM). The model IMEM is based on modeling and limited *in situ* measurements, but is undergoing an extensive rework and is currently not used by ESA for predicting the meteoroid environment. Divine-Staubach is also under review by ESA.

MEM and the next generation, MEMR2, compute the meteoroid flux on a spacecraft along a user-provided trajectory. In addition to providing the overall flux of microgram-or-larger meteoroids, MEM reports the meteoroid flux directionality and speed distribution. MEM improved on prior models by using a physics-based model that yields accurate meteoroid fluxes between 0.2 and 2 au[4] from Earth. MEM results have been validated against observations (in particular, meteor observations from the Canadian Meteor Orbit Radar) and against other models, such as the Grün meteoroid flux model.

MEM generates a customized meteoroid environment, pulling data from four sporadic meteoroid source distributions in order to calculate the number, direction, and speed of meteoroids incident on a spacecraft traveling along an input trajectory, which can be input as a series of Cartesian state vectors or two-line elements. MEM takes the spacecraft's motion into account and reports meteoroid directionality and speed relative to the spacecraft. MEM has three sub-models for spacecraft in near-Earth, lunar, and interplanetary space. If the user chooses the Earth or lunar sub-models, MEM calculates the meteoroid flux taking the planet or Moon's gravitational focusing and shielding into account. The flux is calculated for each state vector or two-line element provided; MEM provides the user with the average flux and the standard deviation of the flux over the spacecraft's trajectory. The software provides supplementary output files that break this flux down by direction (equal-angle bins and quasi-equal area threat igloos) and by speed interval. At the completion of a run, the software presents the user with the main results and with a graph of the meteoroid speed distribution.

MEM is designed to work in conjunction with other engineering software tools and offers the user several options for customization. For instance, the input trajectories can be easily generated using Systems Tool Kit (STK), and the output files can be used with the Bumper threat assessment software. The user can choose the limiting mass, one of three spacecraft orientations (one stationary and two rotating), one of two output coordinate frames, and one of three output resolutions. The user has the option to analyze every input state vector or to choose a random

[4] au = astronomical unit = 149698 km, which is the average distance from the Earth to the Sun

sub-sample; the user can also choose whether or not to save a detailed flux output file for each state vector and whether to calculate the standard deviation of the flux along the trajectory. Thus, MEM can be customized to provide both low-resolution estimates of the meteoroid flux along the trajectory as a whole along with high-resolution descriptions of the flux at each point along the trajectory, depending on the needs of the user. The current version of MEM is MEMR2.

6.2.2 Model Comparison

MASTER-2009 integrates the Divine-Staubach meteoroid model with its orbital debris model into one application. As was done for the orbital debris models in Section 6.1.2, the flux of the meteoroid component of MASTER-2009 was compared to MEMR2, along with older versions of MASTER: MASTER-2005 and MASTER-2001. The results are displayed in Figure 6.2-1 plotted as flux as a function of diameter. MEMR2 produces values as a function of mass, so MEMR2 results were converted to mm assuming spherical particles with a density of 1 g/cm³.

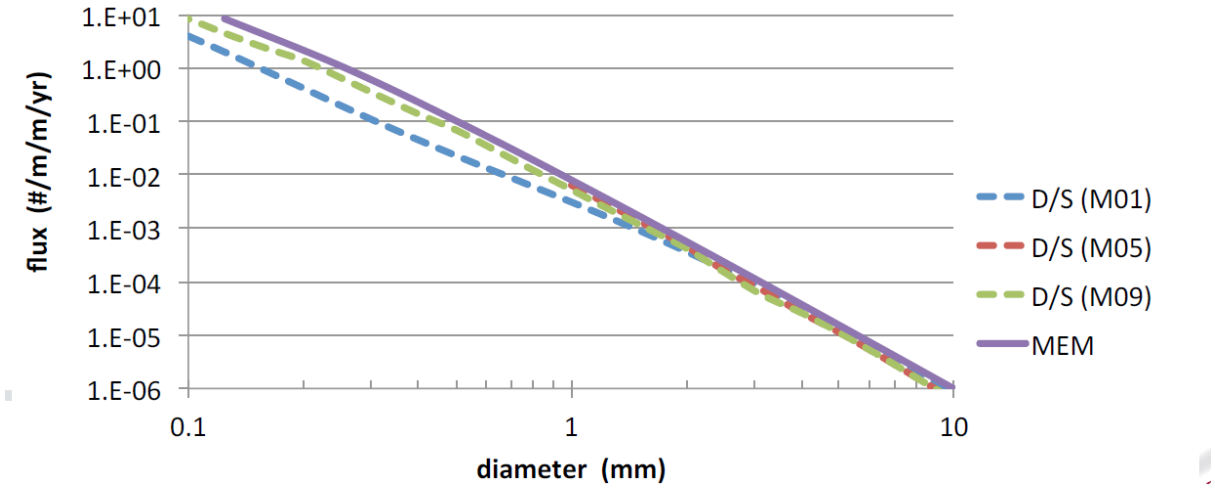

Figure 6.2-1. Meteoroid Flux Comparison for JPSS Orbit (D/S = Divine-Staubach)

As illustrated in Figure 6.2-1, the meteoroid models show close correlations for the size regimes analyzed, unlike the comparison of the orbital debris models.

The flux is also less for meteoroids than for orbital debris at most altitudes (see Section 6.1.2 and Figure 6.1-15). When the meteoroid and orbital debris components of the JPSS-1 component risk assessments are separated, it is clear that the relative contribution to the overall risk is greater for orbital debris than micrometeoroids. This is the case for both the current and the older environment models. This can be seen in Table 6.2-1, which displays the number of penetrations predicted from Bumper for a 7-year mission due to either micrometeoroids or orbital debris using the environment model indicated. The SSP 30425 meteoroid model results are shown for comparison to ORDEM2000 since that model is used by DAS and was used for initial Bumper assessments. The values are for components prior to any extra shielding or modifications to decrease MMOD risk.

Table 6.2-1. JPSS-1 Orbital Debris Risk versus Meteoroid Risk

Component	ORDEM3 # of penetrations	MEM # of penetrations	Ratio of OD:M	ORDEM2000 # of penetrations	SSP 30425 # of penetrations	Ratio of OD:M
Propellant Lines	6.66E-01	2.06E-02	32	2.92E-02	3.81E-03	8
Propellant Tank	2.95E-01	5.58E-03	53	1.00E-02	8.94E-04	11
Battery #1	5.24E-01	1.45E-03	361	1.14E-02	8.52E-04	13
Battery #2	5.67E-01	1.48E-03	383	1.20E-02	8.54E-04	14
CTU	1.02E-01	2.52E-04	405	4.61E-03	1.16E-04	40
PCDU #1	2.92E-03	3.64E-05	80	8.09E-04	1.74E-05	46
PCDU #2	3.32E-03	3.51E-05	95	8.56E-04	1.67E-05	51
SCP #1	1.56E-01	1.77E-04	881	6.52E-03	1.19E-04	55
SCP #2	2.93E-02	1.27E-04	231	1.84E-03	5.26E-05	35
Avg			**280**			**30**

It is clear from the table that the orbital debris risk is at least an order of magnitude greater than the micrometeoroid risk and is driving the total JPSS MMOD risk.

6.2.3 Previous NESC MEM Assessment

In 2009, the NESC performed an independent review of the Constellation Program's MMOD risk analysis process [ref. 15]. In the course of that earlier assessment, the NESC team evaluated MEM, the predecessor to MEMR2. The differences between MEM and MEMR2 are primarily in the user interface, so the conclusions drawn from the 2009 activity that applied to MEM apply to MEMR2. The 2009 report did not discover any deficiencies with MEM that would recommend not using it for MMOD risk assessments. The 2009 NESC team found that exclusion of some higher speed meteoroid particles and the global meteoroid density assumption of 1 g/cm³ would most likely lead to an under-prediction of risk. In other words, the actual micrometeoroid risk to spacecraft may actually be higher than indicated. The 2009 NESC team also recommended that uncertainties be derived for MEM, something in which the MEO is in the process of implementing.

The following findings and observations are related to the meteoroid environment models.

F-13. The assessed risk associated with meteoroids for individual JPSS components is roughly two orders of magnitude smaller on average than the assessed risk from orbital debris when using ORDEM 3.0 and MEMR2. The difference is roughly one order of magnitude when using ORDEM2000 and SSP 30425.

F-14. The meteoroid flux for 0.1 to 10 mm diameter sizes given by MEMR2 is within an order of magnitude of that produced by the Divine-Staubach model, which is used by MASTER-2009.

F-15. MEM was reviewed by the NESC in 2009 [ref. 15] and found to be appropriate for use in MMOD risk assessments. MEMR2 differs from MEM primarily in the graphical user interface. Neither MEM nor MEMR2 assess uncertainties, which was discussed in the 2009 NESC report.

O-5. MEMR2 is calibrated to ground-based radar observations and the data from which the Grün flux was derived.

O-6. ESA's iMEM model is based on modeling and limited *in situ* measurements. ESA has recently concluded that iMEM is not representing the meteoroid environment adequately and is initiating an extensive rework of the model. The Divine-Staubach model (used in MASTER-2009) is also no longer used by ESA.

7.0 Elements of JPSS MMOD Risk Assessment

The fundamental components of any MMOD risk assessment are MMOD environment models, damage response predictor equations (BLEs, etc.), and failure criteria. The MMOD environment is discussed in detail in Section 6.0. This section will discuss and assess the response predictor equations (specifically, BLEs) and the failure criteria used by the JPSS Project.

7.1 JPSS BLEs

BLE modifications discussed and reviewed include the adaption of a BLE used most often to characterize the response of aluminum structures to high speed impacts by aluminum projectiles to: 1) impacts by steel projectiles, and 2) non-aluminum bumper materials.

The predictions of this BLE in the case of very high velocity impacts are also studied and compared against those of alternative equations that might be more applicable to the types of structural elements used in the JPSS satellites.

7.1.1 BLE Description

A response predictor equation, such as a BLE, is developed to characterize the performance of a hypervelocity impact shield. Such an equation defines the threshold particle size that causes, for example, perforation or detached spall from the inner wall of a multi-wall system as a function of velocity, impact angle, particle density, shield and inner wall thicknesses, and particle shape. BLEs are typically drawn as lines of demarcation between regions of inner-wall failure and no failure in two-dimensional projectile diameter-impact velocity space. When graphically represented they are referred to as BLCs.

The high-speed impact testing that provides data for the development of BLEs and BLCs typically use spherical projectiles fired in light gas guns at impact velocities between 3 and 7 km/s (although some can reach velocities up to 10 km/s now). These data are then fitted with scaled single-wall equations below approximately 3 km/s, and with theoretical momentum and/or energy-based penetration relationships above approximately 7 km/s to obtain three-part BLCs that cover the full range of impact velocity from approximately 0.5 to 16 km/s. The transitional

velocity region (from approximately 3 to 7 km/s for normal aluminum-on-aluminum impacts) takes the form of a linear interpolation between the low and high velocity regions.

Figure 7.1-1 shows a typical BLC for a dual-wall system (i.e., Whipple shield) under normal projectile impact. In Region I, the projectile is deformed following its impact on and passage through the outer (i.e., bumper) plate, but remains mainly intact as it travels towards and eventually strikes the inner wall of the dual-wall system. For aluminum projectiles impacting aluminum bumpers, Region I is typically impact velocities below 3 km/s. In Region I, the form of the BLC is analogous to that of a single-wall curve. In Region II, the projectile is fragmented and the energy of the impacting projectile and ejected shield material is dispersed over an increasingly larger area of the inner wall. As a result, the ability of the dual-wall system to resist inner-wall failure (whether defined as a perforation or detached rear-side spall) increases as reflected in the curve. This gives rise to the bucket shape of the BLC for a dual-wall system. In Region III (which typically starts at 7 km/s for aluminum-on-aluminum impacts), the projectile is completely melted and the impulse delivered to the rear wall is increasingly more difficult to resist.

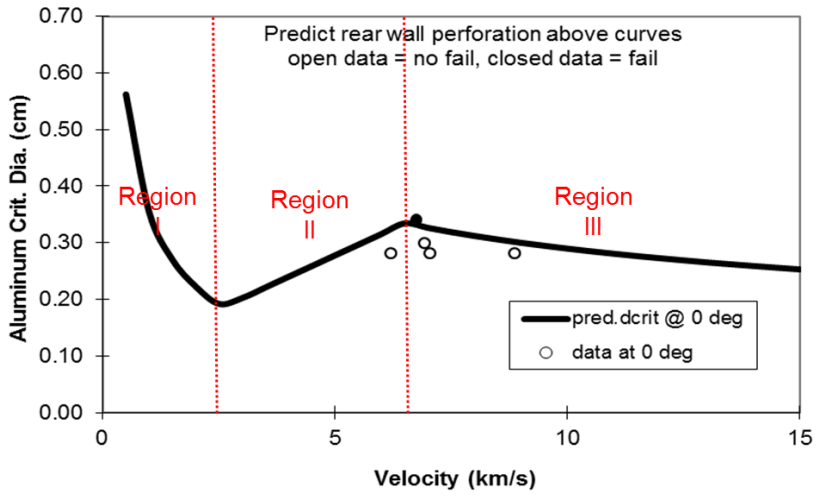

Figure 7.1-1. Typical BLC for a Dual-wall System under Normal Projectile Impact

F-16. Over 90 percent of the orbital debris impacting the JPSS-1 spacecraft have a velocity above 7 km/s, with an average velocity over 12 km/s. Because of this, the BLE Region III curve requires critical understanding.

7.1.2 Applications and Modifications

Initial risk assessments for JPSS-1 were performed using ORDEM2000 and a modified version of what is frequently referred to as the NNO BLE [ref. 16]. The NNO BLE was developed primarily for aluminum-on-aluminum impacts and for configurations with bumpers or shields that are sufficiently thick so as to cause significant fragmentation of an incoming projectile. This BLE has been applied to the various components and wall materials of JPSS-1 by equivalencing

JPSS-1 materials and wall thicknesses to aluminum on a mass density basis. For example, in the event of a non-aluminum bumper on JPSS-1 of a specified thickness and having a certain density (ρ), the thickness (t) of an equivalent aluminum shield has been calculated as follows:

$$\rho_{aluminim} t_{equiv\ alum}^{bumper} = \rho_{matl\ denisity}^{JPSS\ bumper} t_{JPSS\ matl}^{bumper} \quad (1)$$

so that

$$t_{equiv\ alum}^{bumper} = t_{JPSS\ matl}^{bumper} (\rho_{matl\ density}^{JPSS\ bumper} / \rho_{aluminim}) \quad (2)$$

Equations (1) and (2) are usually applied to lightweight multilayer thermal blankets and other heavier materials to allow wall configurations with those materials to be part of a risk assessment exercise performed by Bumper. The exception is the case of a Kevlar® MMOD blanket for which NASA has developed a more complicated equivalencing procedure [ref. 17]. However, even in this case, the procedure appears to be ad-hoc and is without proper documentation or source referencing. Interestingly enough, other than these ad-hoc equivalencing procedures, there are no written guidelines in existence for how to apply the NNO BLE (or any other BLE) in situations that lie outside of the materials and/or geometries for which it was developed. This approach is similar to that used for DAS assessments, where shielding layer inputs are limited to areal density (density multiplied by thickness).

To make the original 1993 version of the NNO BLE applicable to the MMOD environment description as given in ORDEM 3.0, it was modified to include a higher high-end transition velocity (i.e., transition from Region II to Region III) option that would engage if a risk assessment run ever called for a calculation involving the impact of a high density particle, such as steel. This so-called high-end transition velocity in the BLE for a dual-wall system is the impact velocity beyond which the projectile is believed to be substantially melted. As mentioned previously, for normal aluminum-on-aluminum impacts, this transition velocity is approximately 7 km/s. However, for non-aluminum projectiles impacting aluminum plates, this value can be expected to be something other than 7 km/s. Since ORDEM2000 assumed all particles to be made of aluminum, this new feature of the NNO BLE was never used in risk assessments performed for JPSS-1 using ORDEM2000; only risk assessments performed using ORDEM 3.0 made use of this new capability.

Initial attempts at modifying the high-end transition velocity for dual-wall BLEs subjected to high density projectile impact were undertaken in the 2003-2004 time period [ref. 18]. Based on an analysis of data from tests involving steel projectiles impacting traditional Whipple shields and stuffed Whipple shields, a high-end transition velocity of 9.5 km/s was proposed. The modification to the NNO BLE to include a higher high-end transition velocity for high density particles was incorporated using the results of a previous NESC study [ref. 19]. In this assessment, it was determined that a value of 9.1 km/s would be an appropriate high-end transition velocity for steel (or particles with a material density close to steel) particles impacting aluminum plates [ref. 20]. This value was obtained using the SESAME tabular equation of state

(EOS) to determine the impact pressure (and then the corresponding impact velocity) that would be required for an iron projectile to be substantially melted on impact on an aluminum plate.

In this current study, the Mie-Gruneisen EOS was used as part of an analytical 1-D shock physics-based calculation to determine the fractions of solid, molten, and vaporous material remaining in steel and aluminum projectiles impacting thin aluminum plates (%S, %L, and %V, respectively). The results of these calculations are presented in Table 7.1-1.

Table 7.1-1. Fractions of Solid, Molten, and Vaporous Material

%S-%L-%V For Projectile Material						
Velocity	Aluminum on Aluminum			Steel on Aluminum		
(km/s)	%S	%L	%V	%S	%L	%V
4.0	100.0	0.0	0.0			
5.0	100.0	0.0	0.0			
5.5	99.5	0.5	0.0			
6.5	28.3	71.7	0.0			
6.8	5.1	94.9	0.0			
7.0	0.0	100.0	0.0	100.0	0.0	0.0
8.0				36.7	63.3	0.0
8.3				8.2	91.8	0.0
9.0				0.0	100.0	0.0

For aluminum-on-aluminum impact, projectile melt begins at impact velocities near 5.5 km/s with the projectile being completely melted at approximately 6.9-7.0 km/s. These values agree with the information also published in JSC 66619 [ref. 20]. For steel-on-aluminum impacts, projectile melt likely begins at impact speeds between 7.0 and 7.5 km/s, with the projectile being substantially melted at an impact velocity of approximately 8.5 km/s. The difference between this value and the value calculated in reference 20 is likely due to the use of the Mie-Gruneisen EOS in scenarios involving impact velocities and pressures that push the limits of its applicability.

In reference 18, the NESC team also found mention of different low-end transition velocities for non-aluminum projectiles. The low-end transition velocity is the impact speed at which the projectile begins to shatter or fragment (i.e., Region I to Region II transition). For aluminum-on-aluminum impacts, this occurs at approximately 3 km/s. Much like there being a different high-end transition velocity for non-aluminum projectiles impacting aluminum plates, it is logical to conclude that there would be a different low-end transition velocity under similar impact conditions. However, the current modifications to aluminum projectile-based BLEs to render them applicable to steel projectile impacts do not include any changes to the low-end transition velocity. It would appear that having alternate low-end transition velocities for the materials or material classes in ORDEM 3.0 would more accurately reflect the response of spacecraft wall systems to high speed impacts by projectiles made of those types of materials.

The effects of incorporating the 9.1 km/s high-end transition velocity in an aluminum projectile-based BLE to render it applicable to steel projectile impacts are shown in Figures 7.1-2 and 7.1-3. In these figures, the NNO BLE is plotted for steel projectiles impact aluminum bumper plates. Figure 7.1-2 presents a 0° (normal) impact, while Figure 7.1-3 presents a 45° (oblique) impact.

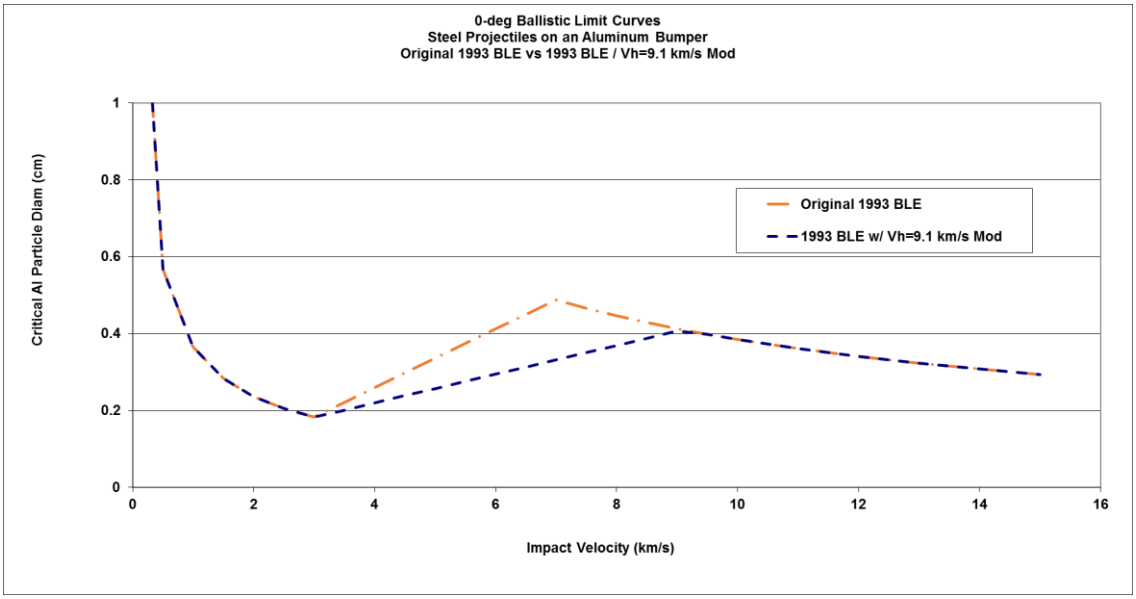

Figure 7.1-2. Comparison of Steel-on-Al BLEs without and with the High-End Transition Velocity Modification for 0° Impacts

It is interesting to note that the use of a higher high-end transition velocity results in a smaller critical particle diameter at that new transition velocity value. This reduced critical diameter is an outcome of the increased high-end transition velocity value, not an imposed value.

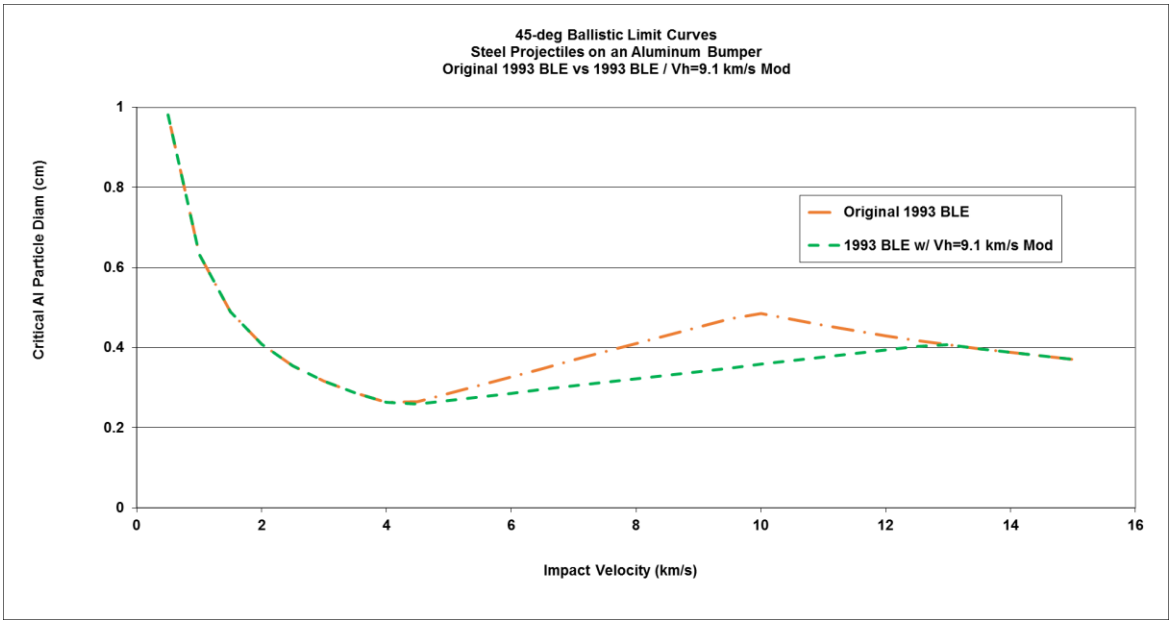

Figure 7.1-3. Comparison of Steel-on-Al BLEs without and with the High-End Transition Velocity Modification for 45° Impacts

In both of these figures, the regions between the two curves are those projectile diameter-impact velocity combinations that the original NNO predicts would not cause inner wall failure (because they lie below the curve). However, the modified NNO BLE (with its new high-end transition velocity – for normal impacts – of 9.1 km/s) predicts that those projectile diameter-impact velocity combinations *would* cause failure to the inner wall of a dual-wall system (because they now lie above the BLE). Not having been completely melted by the impact on the lower density aluminum plate, these higher density steel projectiles still possess enough energy (as well as momentum) to inflict serious damage on the inner wall plate.

F-17. The choice of 9.1 km/s as the Region II to Region III transition velocity for steel-on-aluminum uses valid reasoning and assumptions and realistically models the phenomenology associated with the HVI of a steel projectile on a thin aluminum plate. However, this value may not be an appropriate choice for other bumper materials (e.g., MLI).

When ORDEM 3.0 was used instead of ORDEM2000, the higher high-end transition velocity in the modified version of the NNO BLE was used in Bumper III because ORDEM 3.0 had the capability to include variable particle densities and provided debris flux information for high density particles such as steel. The NESC team believes that it was the use of the new ORDEM version together with the use of the higher high-end transition velocity in the modified NNO BLE that was a primary contributor to the high increase in assessed risk for JPSS when using ORDEM 3.0 as opposed to ORDEM2000.

At the time of this assessment, there were no BLEs available that were developed specifically for the various structural elements of JPSS-1. As a result, risk assessments were being performed using equations that were not developed for the materials or wall configurations on JPSS-1. Where necessary and because no other option was available, the modified version of the NNO BLE was used with non-aluminum materials equivalenced to aluminum on a mass density basis using the process described previously. As such, the NESC team investigated whether using the modified version of the NNO BLE is appropriate for the JPSS wall configurations in the case of high density projectile impacts. In other words, how close are the predictions of the modified NNO BLE equations to the actual response characteristics of those materials/wall configurations under high density projectile impacts?

In 2013, NASA developed a new BLE that would be applicable to the case of high density projectiles impacting a very specific and specialized wall configuration, namely, that of the Soyuz orbital module (OM). This wall configuration can be, ostensibly, considered as a dual-wall configuration. If the array of the Soyuz OM bumper materials is equivalenced to a single aluminum wall, then the modified NNO BLE could, in theory, also be used to predict the response of the Soyuz OM wall system to high density projectile impact. The Soyuz OM wall system can therefore be used to see how well the modified NNO BLE predicts the response of a dual-wall system for which it was not developed, but can nonetheless be used following appropriate equivalencing of the original system's configuration parameters.

A study was conducted to compare the predictions of the NNO BLE (modified to be applicable to high density projectile impacts) for the Soyuz OM wall configuration against those of the new Soyuz OM steel-projectile-based BLE. If the predictions of the two BLEs were found to be relatively close, that would give some confidence to the practice of using modified NNO BLEs in situations involving high density projectiles impacting wall configurations for which BLEs do not currently exist. This confidence could be increased further with some tests using steel projectiles and comparing results against the predictions of the revised NNO BLEs for high density projectile impact. However, if the predictions were found to be not very close, some testing would certainly be called for to assess the validity of this equivalencing approach and/or its continued use.

Figures 7.1-4 and 7.1-5 compare the recently developed steel projectile BLE for the Soyuz OM and the NNO BLE with the revised high-end transition velocity for the geometric parameters of the Soyuz OM wall configuration. Figure 7.1-4 presents the 30° impacts while Figure 7.1-5 presents the 45° impacts.

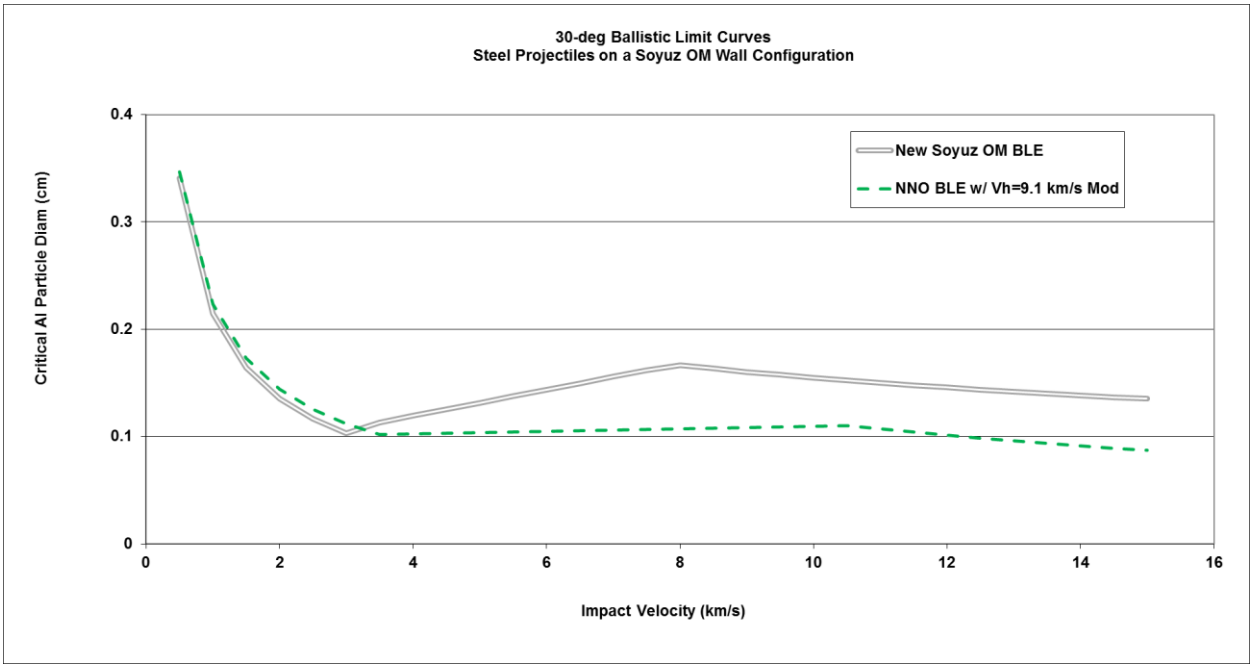

Figure 7.1-4. Comparison of New Soyuz OM BLE and NNO BLE with the High-End Transition Velocity Modification for 30° Impacts

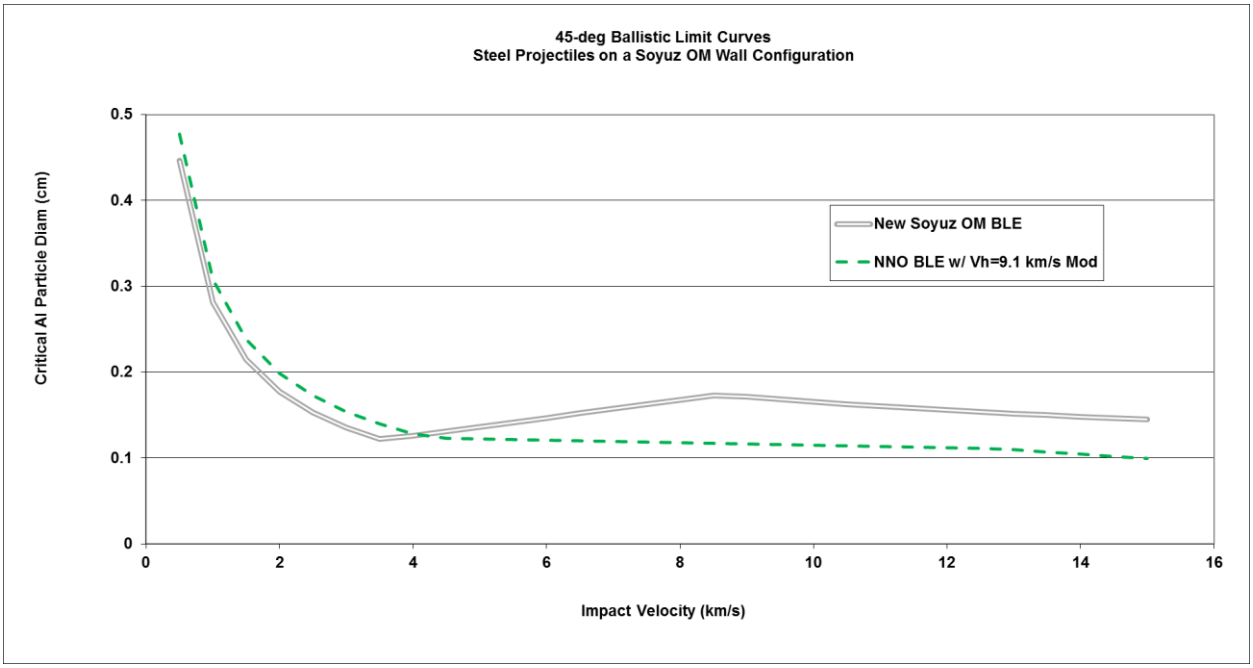

Figure 7.1-5. Comparison of New Soyuz OM BLE and NNO BLE with the High-End Transition Velocity Modification for 45° Impacts

To be able to apply the revised NNO BLE to the Soyuz OM wall system, the multi-material Soyuz OM bumper was first equivalenced to a monolithic aluminum bumper on a mass density basis. Specifically,

$$\rho_{aluminim} t_{equiv\ alum}^{bumper} = \rho_{areal\ density}^{Soyuz\ OM\ bmpr} \quad (3)$$

so that

$$t_{equiv\ alum}^{bumper} = \rho_{areal\ density}^{Soyuz\ OM\ bmpr} / \rho_{aluminim} \quad (4)$$

All other geometric parameters (inner wall thickness and stand-off distance) were kept the same as in the Soyuz OM wall system.

Figures 7.1-4 and 7.1-5 show the modified NNO BLE and the new Soyuz OM BLE are fairly close until the low-end transition velocity (approximately 3 km/s for 30°impacts, and 3.5 km/s for 45°impacts). However, above the low-end transition velocity the two curves diverge – the new Soyuz BLE has the canonical "bucket" shape while the modified NNO BLE more resembles the BLE of a single wall, not a dual-wall, system.

In fact, above 9 -10 km/s, the critical projectile diameters predicted by the new Soyuz OM BLE can exceed that of the modified NNO BLE by as much as 50 percent of the modified NNO BLE values. Thus, using the modified NNO BLE in this particular case would contribute to a more conservative value of assessed risk. If the same trends hold true for the JPSS wall configurations, then it is also possible that using modified NNO BLEs in a JPSS risk assessment might result in more conservative (i.e., higher) values of assessed risk.

It is also important to note that this divergence between the new Soyuz OM BLE and the modified NNO BLE is not due to the introduction of the higher high-end transition velocity. Very little difference was found to exist between the original and modified NNO BLEs for a Soyuz OM wall configuration. It was found that both the original and modified NNO BLEs are relatively flat beyond an impact velocity of approximately 3 km/s, and both resemble a single wall BLE. Hence, moving the higher-end transition velocity from 7 km/s to 9.1 km/s had very little effect on the NNO BLE for this particular wall configuration.

This is in stark contrast to the plots in Figures 7.1-2 and 7.1-3, which showed quite a bit of difference between the original and modified NNO BLEs for a space station module wall configuration. In this particular case, the modified NNO BLE retained the 'bucket' shape of the original NNO BLE following the modification in the high-end transition velocity. As a result, the differences between the original and modified NNO BLEs were quite significant in those figures.

F-18. There are no BLEs available that were developed specifically for the JPSS-1 structural elements. As a result, risk assessments are being performed using equations that were not developed for the materials or wall configurations used on

JPSS-1. Using the modified NNO, adjusted for materials used by JPSS, may be predicting smaller critical diameters (i.e., increased assessed risk) than would BLEs purposely developed for actual JPSS-1 configurations.

7.1.3 BLE Comparisons

This section considers alternative damage models (i.e., BLEs) to the NNO BLE, which was used initially by JPSS for their MMOD risk assessments. The two BLEs discussed are the Modified Wilkinson BLE and the Remeirdes BLE. Damage fluence comparisons were performed for these BLEs using the same generic cube described for the orbital debris model damage fluence comparisons in Section 6.1.3. Each MODRA run uses ORDEM 3.0 as the orbital debris model, and the results are compared to the MODRA run using the baseline NNO BLE/ORDEM 3.0 discussed in Section 6.1.3.2.

7.1.3.1 Modified Wilkinson BLE

Damage Fluence Results Using ORDEM 3.0 with the Modified Wilkinson BLE

A MODRA run was executed with the variation that the Modified Wilkinson BLE was used in place of the NNO BLE in the high velocity range. The original Wilkinson BLE is described in reference 21. The modified version applies a factor of 0.8 (20 percent reduction) to the critical diameter computed using the original Wilkinson BLE. A reduction in critical diameter was suggested separately by Elfer and Bjorkman [ref. 21]. Elfer proposed it to account for lower impactor debris cloud dispersion angles observed in hydrocode runs of impacts at velocities of 7 and 13 km/s. Wilkinson's analysis was done at higher, meteoroid impact velocities, which resulted in higher vaporization of aluminum impactors, and an associated higher dispersion angle. A lower impactor debris cloud dispersion angle results in higher momentum loading on the inner wall and hence smaller impactors can penetrate. Bjorkman proposed the 0.8 factor based on the potential for elastic rebound, which could increase the momentum loading.

The modified Wilkinson formulation applies for normal impact velocities higher than the high velocity region boundary (Region III, see Section 7.1.1 and Figure 7.1-1). For normal impact velocities in Region I, the low velocity NNO formulation for critical diameter was used. For normal impact velocities in Region II, the critical diameter was interpolated. The same velocity boundaries were used as in the NNO formulation, including the modification for high density impactors. The same 65° impact angle limit was also used.

The original Wilkinson equations contain a failure factor $c_2\left(\xi/c_2\right)_a$, where c_2 is the speed of sound in the inner wall. Reference 21 states that a value for the factor $\left(\xi/c_2\right)_a = 0.27$ km/s was used in early Bumper codes. Setting $c_2 = 5.1$ km/s (the value for aluminum), the resulting failure factor value used in this analysis was $c_2\left(\xi/c_2\right)_a$ =1.377.

Figure 7.1-6 shows a plot of critical diameter versus impact velocity for a stainless steel particle with an impact angle of 0° (normal incidence). Curves are shown for both the NNO BLE and the Modified Wilkinson BLE. The plot shows that for impact velocities greater than the low

velocity region boundary at 3 km/s, the critical diameter computed using the Modified Wilkinson BLE is higher than the critical diameter computed from the NNO BLE. The difference increases as impact velocity increases. Figure 7.1-7 shows the same plot, but for an impact angle of 45°. The boundary velocities are shifted to the right because they are the full impact velocities and not the normal components of impact velocity.

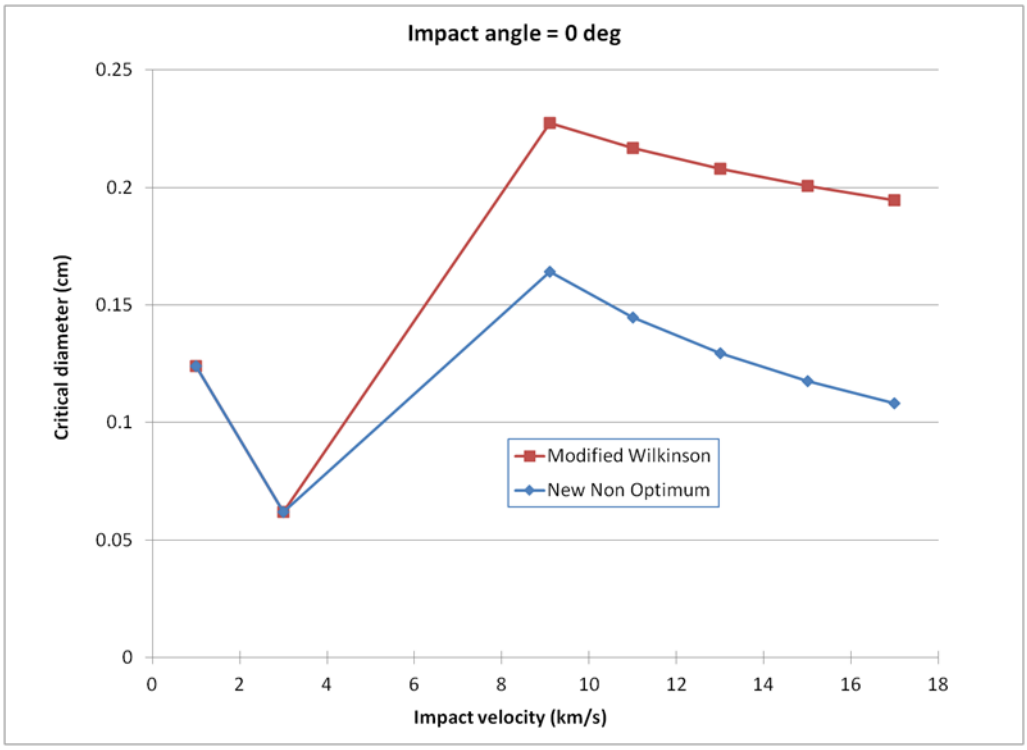

Figure 7.1-6. Critical Diameter versus Impact Velocity for a Stainless Steel Particle with Impact Angle of 0°

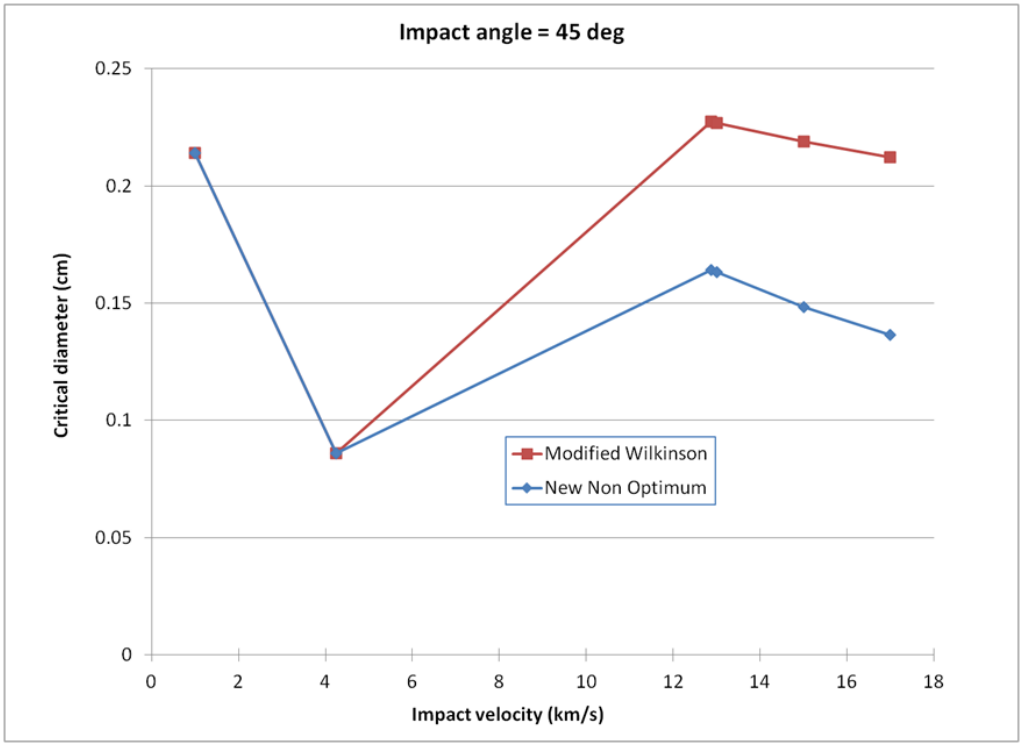

Figure 7.1-7. Critical Diameter versus Impact Velocity for a Stainless Steel Particle with Impact Angle of 45°

Table 7.1-2 shows the damage fluence on each cube face from each of the populations when the Modified Wilkinson BLE is used. In this case, the total damage fluence was 1.45, whereas in comparison, the damage fluence using the NNO BLE was 4.95. The reduction in damage fluence corresponds to the higher critical diameter shown in Figures 7.1-6 and 7.1-7. Overall, the high density population contributes 89 percent of the damage fluence (versus 91 percent when using the NNO BLE). It is noted that on the ram face, where impacts at low incidence angles with high normal velocity components dominate, the damage fluence from the modified Wilkinson BLE (0.196) is much lower than from the NNO BLE (2.9). On the South and North faces, where impacts at high incidence angles with low normal velocity components dominate, the difference in damage fluence is smaller (0.584 from modified Wilkinson versus. 0.901 from NNO).

Table 7.1-2. Cube Damage Fluence Resulting from use of ORDEM 3.0 with the Modified Wilkinson BLE

Cube face	Damage fluence							HD percent of total
	NaK	LD	MD	HD	Intacts	Total across populations	Total without HD	
Ram	1.29E-04	1.44E-03	1.18E-02	1.83E-01	8.52E-06	1.96E-01	1.33E-02	93.2%
Trail	0.00E+00	1.73E-06	6.62E-06	3.87E-05	1.52E-09	4.70E-05	8.35E-06	82.2%
South	4.25E-05	3.76E-04	7.03E-02	5.13E-01	1.65E-06	5.84E-01	7.07E-02	87.9%
North	4.25E-05	3.76E-04	7.03E-02	5.13E-01	1.65E-06	5.84E-01	7.07E-02	87.9%
Nadir	0.00E+00	1.96E-06	6.75E-06	4.28E-05	2.55E-09	5.15E-05	8.71E-06	83.1%
Zenith	3.58E-05	3.85E-04	2.99E-03	8.38E-02	1.91E-06	8.73E-02	3.41E-03	96.1%
Total across faces	2.50E-04	2.58E-03	1.55E-01	1.29E+00	1.37E-05	1.45E+00	1.58E-01	89.1%

Figure 7.1-8 illustrates the distribution of the cube damage fluence over impactor size resulting from use of the Modified Wilkinson BLE. Damage fluences on all the cube faces are combined. From this plot it is seen that the sharp rise observed in the distribution from the NNO BLE at 1.2 mm has been significantly reduced.

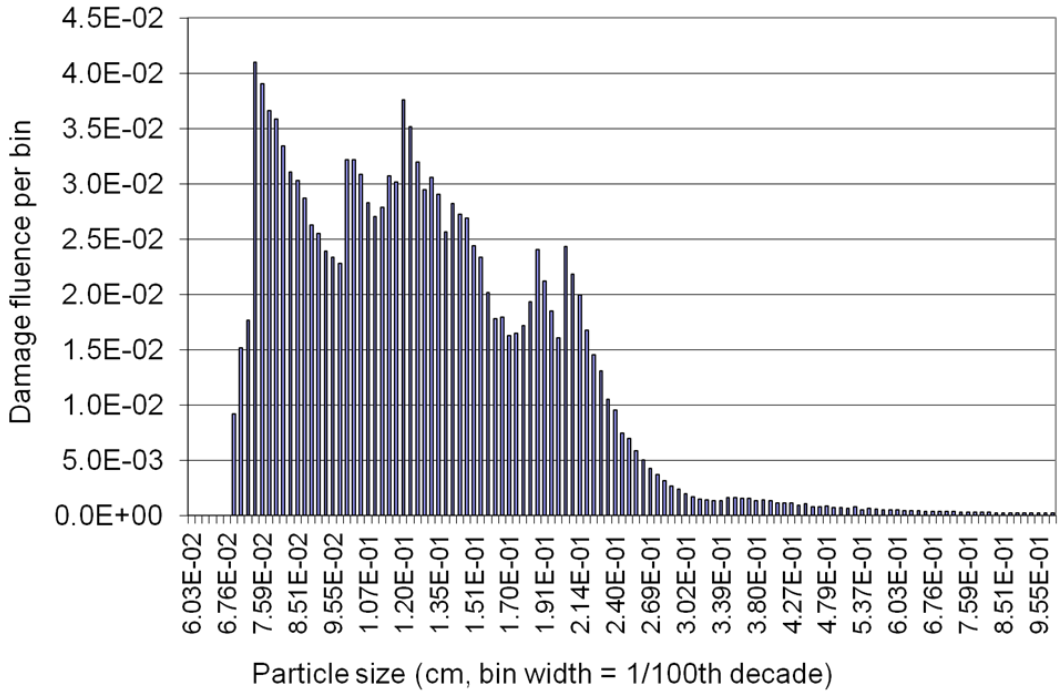

Figure 7.1-8. Distribution of Damage Fluence over Impactor Size; Results from all Cube Faces using the Modified Wilkinson BLE

Figure 7.1-9 shows the distribution of damage fluence over impact velocity resulting from use of the Modified Wilkinson BLE. Damage fluences on all the cube faces are combined. From this plot it is seen that damage fluence in the high velocity region has been reduced significantly compared to results from the NNO BLE. This is consistent with the large reduction on the ram

face. Damage fluence is only slightly reduced in the low velocity region, where the NNO formulation dominates.

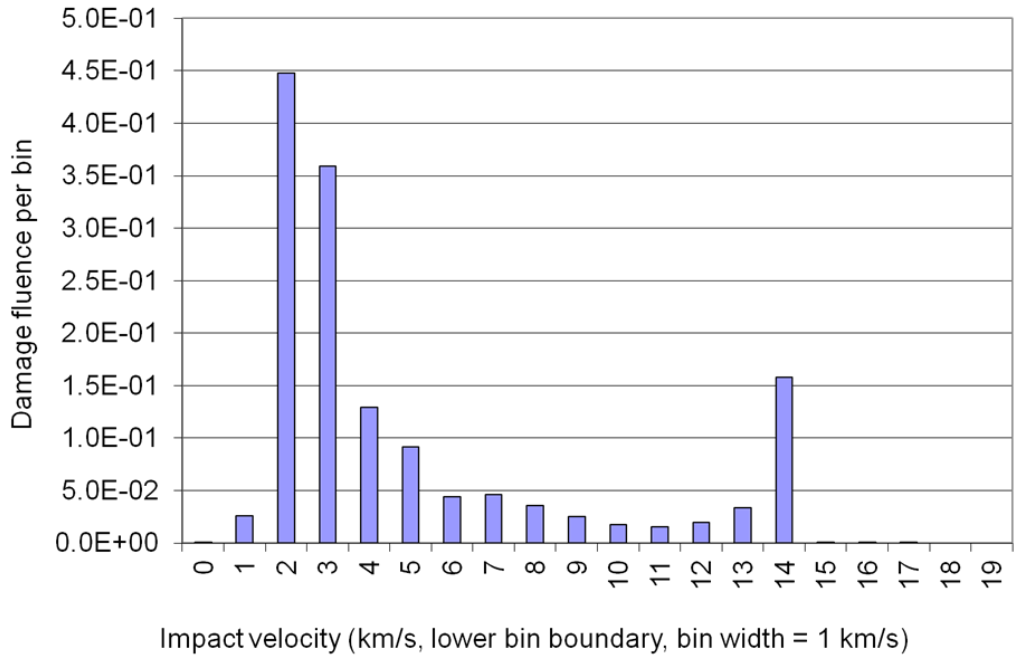

Figure 7.1-9. Distribution of Damage Fluence over Impact Velocity; Results from all Cube Faces using the Modified Wilkinson BLE

Figure 7.1-10 shows the distribution of damage fluence over impact velocity for only the South and North faces resulting from use of the Modified Wilkinson BLE. Damage fluences from the North and South faces are combined. From this plot it is seen that damage fluence is concentrated in the low velocity region, where the NNO formulation dominates. The peak of the distribution is near the low velocity region boundary of 3 km/s, where critical diameter is lowest.

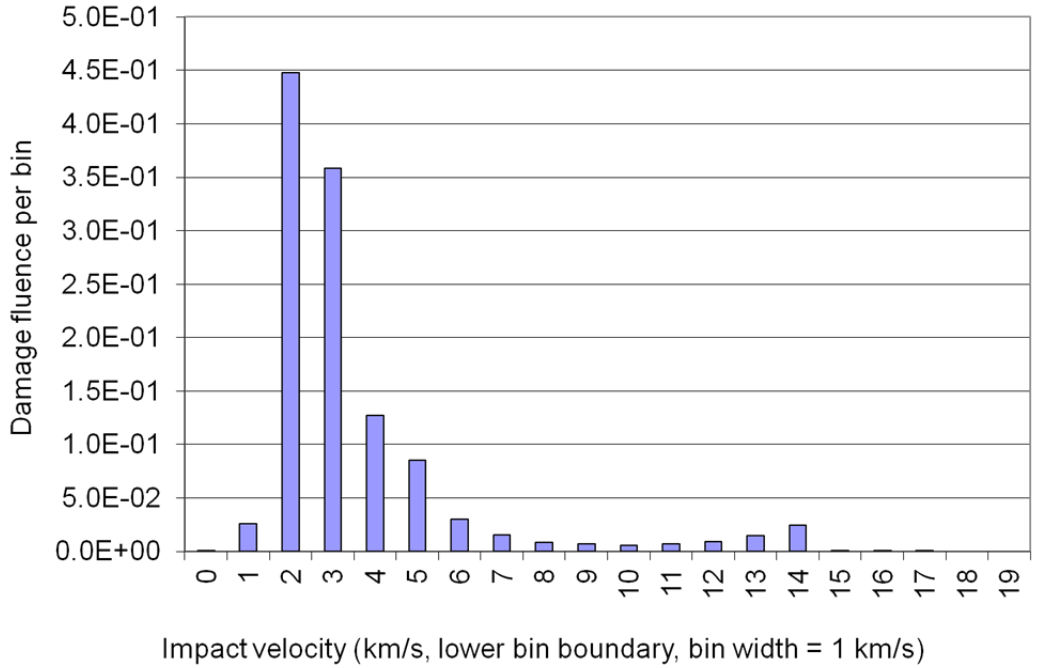

Figure 7.1-10. Distribution of Damage Fluence over Impact Velocity; Results from only the South and North Faces using the Modified Wilkinson BLE

Figure 7.1-11 shows the distribution of damage fluence over impact angle resulting from use of the Modified Wilkinson BLE. Damage fluences on all the cube faces are combined. The distribution is similar to that from use of the NNO BLE (Figure 7.1-5).

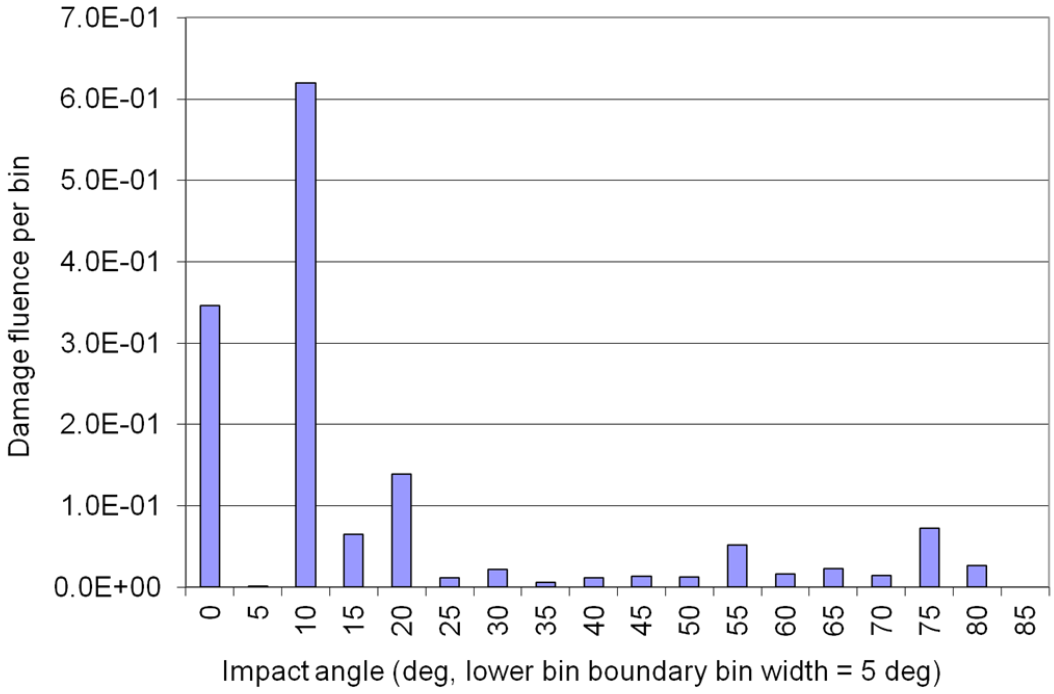

Figure 7.1-11. Distribution of Damage Fluence over Impact Angle; Results from all Cube Faces using the Modified Wilkinson BLE

Figure 7.1-12 shows the distribution of damage fluence over impact angle for only the South and North faces resulting from use of the Modified Wilkinson BLE. Damage fluences from the North and South faces are combined. While impacts at high incidence angles are more frequent on the South and North faces, few of these impactors actually penetrate the inner wall.

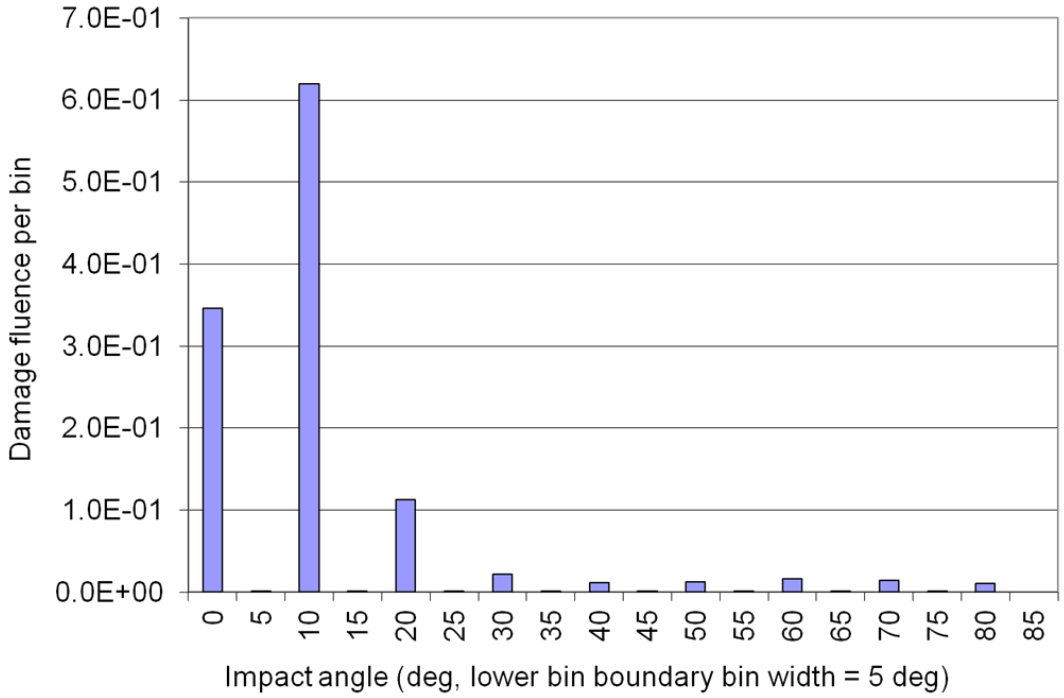

Figure 7.1-12. Distribution of Damage Fluence over Impact Angle; Results from only the South and North Faces using the Modified Wilkinson BLE

7.1.3.2 Reimerdes BLE

The most recent risk assessments performed by JPSS now use modifications to the NNO BLE as proposed in Reference 22. These modifications address several of the main issues associated with the NNO BLE. The first is that bumper thickness is included as a parameter only in the Region I and Region II formulations of the NNO BLE – it is completely absent from the Region III formulation. Figure 7.1-13 shows a series of plots of the NNO BLEs for a particular dual-wall system with changing bumper thickness.

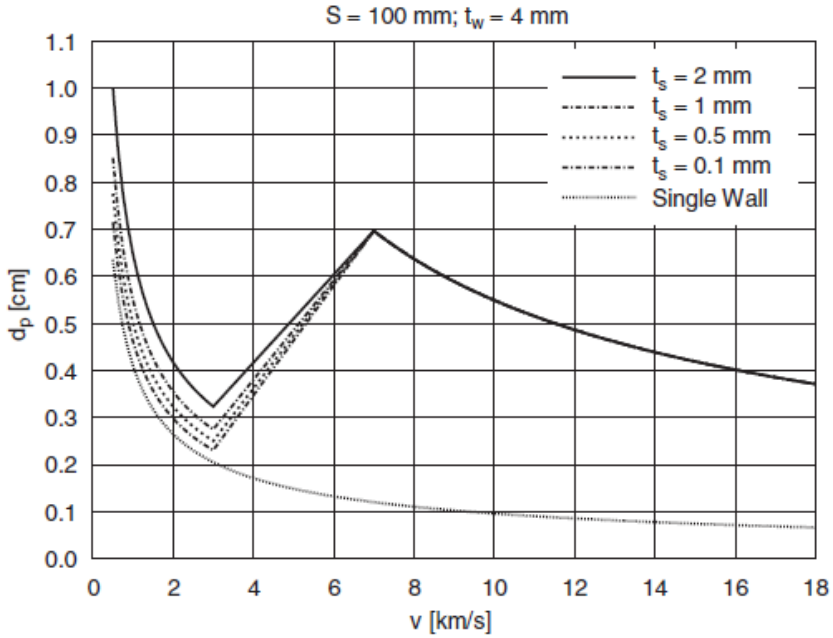

Figure 7.1-13. Effect of Changing Bumper Thickness on NNO BLE Predictions [Ref. 22]

In Figure 7.1-13, the effects of changing the bumper thickness are seen to occur only in Regions I and II of the NNO BLE. Figure 7.1-14 shows a series of plots for the same dual-wall system and the same bumper thickness variations, but this time using the Reimerdes BLE.

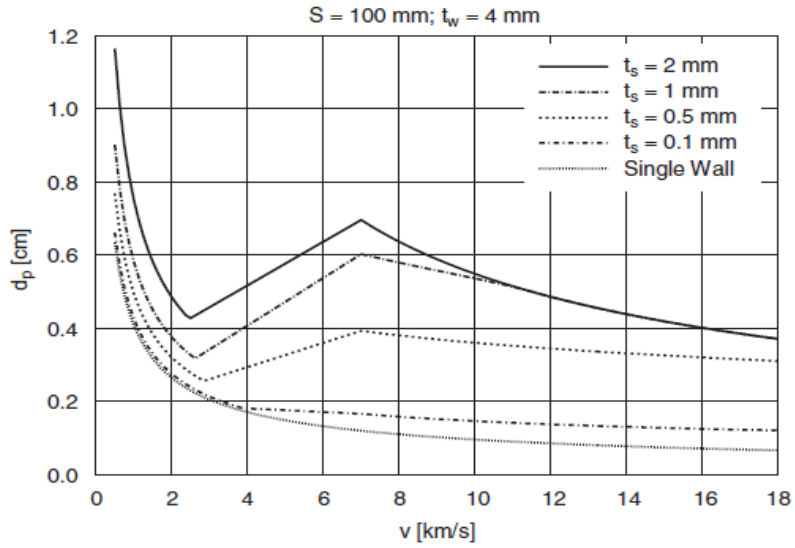

Figure 7.1-14. Effect of Changing Bumper Thickness on Reimerdes BLE Predictions [Ref. 22]

It is important to note that not only does the Reimerdes BLE take into account variations in bumper thickness in all three regions of the BLE, but the Reimerdes BLE also exhibits the appropriate behavior as the bumper thickness becomes increasingly small (a feature also missing from the NNO BLE). Namely, as bumper thickness approaches 0, the dual-wall Reimerdes BLE approaches a standard single-wall BLE for the inner wall of the dual-wall system. This is to be expected because as the thickness of the bumper becomes exceedingly small, its usefulness in breaking up impacting projectiles does likewise, leaving only the inner wall to act as a single-wall in responding to the impact projectiles. Also, as expected, the Reimerdes BLE is identical to the NNO BLE for sufficiently thick bumper plates.

The modifications to the NNO BLE were first proposed in 1993 in an effort to render the NNO BLE applicable to dual- and triple-wall systems with very thin or very lightweight bumper plates (i.e., t_s/d_p < ~0.20, the lower limit of applicability for the NNO BLE). In this manner, the modified version of the NNO BLE (i.e., the Reimerdes BLE) was applicable to the design and development of the ESA's ISS Columbus module. The Reimerdes BLE was subsequently used in an optimization study that included the mass of the spacers that would be needed in a dual-wall design configuration [ref. 22].

Initial experimental validation of the Reimerdes BLE was presented in reference 22. In that study, eight tests were performed using two dual-wall configurations with different bumper thicknesses. In both cases, the Reimerdes BLE showed a substantial improvement in the predictions of ballistic limits when compared against those of the NNO BLE. However, it is important to note that all eight tests were performed at normal impact trajectories – the predictions of the Reimerdes BLE have yet to be compared against empirical data obtained from oblique impact tests. Reference 22 also cited the need to perform some testing nearer to the lower end of impact velocity spectrum to assess the performance of the Reimerdes BLE at those impact speeds.

Most recently, the Reimerdes BLE was presented in NASA's Handbook for Designing MMOD Protection [ref. 23] and the SHIELD computer program's user's manual [ref. 24] as an option for use in the case of exceedingly thin or lightweight bumpers. The Reimerdes BLE was first encoded in Bumper in 2008 with several updates and code corrections through 2012. Bumper encodes the Reimerdes BLE as a set of formulas that ultimately require the solution of an implicit equation for critical projectile diameter given an impact velocity and the geometry of the dual-wall configuration.

The NNO BLE in Region III assumes that the impactor is completely shattered, regardless of shield thickness. Therefore, it is expected to under-predict risk posed by larger impactors. Reference 22 presents hypervelocity test results confirming that the NNO failed to predict penetrations for sufficiently large impactors (Figures 8 and 9 of reference 22). The Reimerdes formulation introduces a factor, F_2^*, that transitions from the NNO dual wall BLE in Region III to a single wall BLE as the ratio of shield thickness to particle size t_s/d_p decreases. The F_2^* factor is applied to the inner wall thickness required to stop an impactor (referred to here as the

"critical wall thickness") of a given size as computed from the NNO formulation in the high velocity region. The factor is not a regression fit to data, but is rather a quadratic expression in terms of t_s/d_p that is derived from three-end point conditions. The first condition is that, when there is no shielding ($t_s/d_p = 0$), the critical wall thickness is equal to that from a single wall BLE, i.e., $F_2^* = r_{S/D}$, where $r_{S/D}$ is the ratio of critical wall thickness from the single wall BLE to that from the NNO formulation. The second condition is that the critical wall thickness is equal to that from the NNO when t_s/d_p is equal to the critical value required to completely shatter the impactor (i.e., $F_2^* = 1$. This critical value $(t_s/d_p)_c$ is specified by the NNO formulation). The third condition is that the slope of the quadratic expression is zero when $t_s/d_p = (t_s/d_p)_c$, i.e., $dF_2^*/d(t_s/d_p) = 0$. The resulting expression for F_2^* is

$$F_2^* = r_{S/D} - 2\frac{t_s/d_p}{(t_s/d_p)_c}(r_{S/D} - 1) + \left[\frac{t_s/d_p}{(t_s/d_p)_c}\right]^2 (r_{S/D} - 1) \text{ when } t_s/d_p < (t_s/d_p)_c \quad (3)$$

$$F_2^* = 1 \text{ when } t_s/d_p \geq (t_s/d_p)_c \quad (4)$$

As part of this analysis, the mathematical derivation of the expression for F_2^* was reconstructed and verified. This expression for F_2^*, which is also shown in reference 9, is more generalized than the expression in reference 22, and was coded in MODRA. Note: Reference 9 appears to incorrectly apply the F_2^* factor to critical particle diameter. Reference 6 shows that it is applied to critical wall thickness and the mathematical derivation is consistent with that approach.

O-7. NASA TM-2009-214789 [ref. 24] appears to apply the Reimerdes BLE dual wall-to-single wall transition factor, F_2^*, differently than specified by Reimerdes et al. [ref. 22] and verified mathematically by the NESC team. Reference 9 applies F_2^* to the critical particle diameter, while the prescribed method in reference 22 is to apply F_2^* to the critical wall thickness.

The Reimerdes formulation as specifically described in reference 21 also has two other features. One is that it replaces the NNO formulation in the low velocity region with the single wall equation of Frost [ref. 25]. The second feature is that it computes the low velocity region boundary as a function of t_s/d_p using a regression fit, whereas in the NNO formulation it was fixed to a value of 3 km/s.

The F_2^* factor is applied to the NNO high velocity region formulation for normal impact velocities in Region III, and the single wall BLE is used for normal impact velocities in Region I. For normal impact velocities between the low and high velocity region boundaries, critical wall thickness was interpolated. The same high velocity region boundary was used as in the NNO formulation, including the modification for high density impactors. The same 65° impact angle limit was also used.

To accommodate the implementation of the F_2^* factor, a modification was made to MODRA. Previous NNO results from MODRA were based on critical diameter computed directly using the BLE. Results presented in the following material from this approach are labeled "critical diameter method." Using this approach for the Reimerdes formulation would require implementation of an iteration to solve for the critical impactor diameter since it is not available in closed form as F_2^* is a function of impactor diameter. While the Bumper subroutine contains a routine that iterates to solve for critical diameter, this approach would not be efficient within the MODRA algorithmic structure. Instead, the NNO BLE was rearranged to compute critical wall thickness (wall thickness required to prevent an impactor from penetrating) at diameter values in the ORDEM 3.0 flux versus size data, and MODRA was modified to interpolate critical diameter at the actual wall thickness. Results presented in the following material from this approach are labeled "critical wall thickness method." Results presented in the following material show that the effect of interpolation error on the results is small. The same modification was made for the NNO-only implementation to provide for an apples-to-apples comparison between NNO results and Reimerdes formulation results.

A subroutine formulation of the Reimerdes formulation used for Bumper was provided in HVIT [ref. 26]. This was used to ensure that the equivalent formulation was coded into MODRA. Several observations on the descriptions in references 22 and 9 and the subroutine version motivated running several variations of the MODRA implementation.

In the subroutine, there are two formulations for F_2^* that apply to two different ranges of the shield spacing to impactor diameter ratio S/d_p. The formulation for the case when $S/d_p \geq 30$ has the value $\left(t_s/d_p\right)_c = c_s = 0.2$ (where c_s is a constant) substituted into the expression. The formulation for the case when $S/d_p < 30$ has the value $\left(t_s/d_p\right)_c = c_s = 0.25$ substituted into the expression. This formulation was implemented in one version of MODRA and the results presented in the following material are labeled "Bumper Reimerdes implementation."

According to reference 9 (Eq. 43) and reference 22 (Eqs. 4 and 5), $\left(t_s/d_p\right)_c = c_s \, \rho_p/\rho_s$, i.e., it depends on the ratio of particle density to shield density. This was implemented in another version of MODRA and the results presented in the following material are labeled "original Reimerdes formulation."

Additionally, it was observed that reference 22 may have an error in the algorithm for the parameter $r_{S/D}$ used to calculate F_2^*. References 22 and 9 state that this parameter is evaluated only at the high velocity region boundary. This algorithm is implemented in the Bumper subroutine. However, it was determined during this analysis that this approach causes the resulting critical wall thickness to exceed the value from the single wall BLE. A MODRA case was run with the parameter evaluated at the actual normal impact velocity of the flux component, and the results presented in the following material are labeled "Modified Reimerdes formulation."

Figure 7.1-15 shows critical wall thickness versus impactor diameter for the case of an aluminum particle impacting normally at 7 km/s for the cube dual wall parameters. Three curves are shown: one generated from the NNO BLE, one generated from the single wall Frost BLE, and one generated from the original Reimerdes formulation. The plot shows that for small impactor sizes, the original Reimerdes curve is the same as the NNO curve. When impactor diameter is large enough so that t_s/d_p falls below the critical value, the original Reimerdes curve separates from the NNO curve and asymptotically approaches the single wall curve as diameter increases.

Figure 7.1-16 shows a similar plot for the case of a stainless steel particle impacting normally at 14 km/s. In addition to the three curves mentioned for Figure 7.1-15, this plot also has curves generated from the Bumper Reimerdes implementation and the Modified Reimerdes formulation. The plot shows that the Bumper Reimerdes curve is lower than the original Reimerdes curve and will correspond to a lower damage fluence. In addition, as impactor diameter increases, the original Reimerdes curve exceeds the single wall curve, which is not a desired result. This result would mean that with larger impactors, the performance of the dual-wall system described by the original Reimerdes BLE would actually be worse than a single wall, which is not consistent with reality. This occurs because the $r_{S/D}$ parameter is evaluated only at the high velocity region boundary (9.1 km/s for a stainless steel impactor) in accordance with reference 22. The Modified Reimerdes curve, which is the result when $r_{S/D}$ is evaluated at the actual normal impact velocity of the flux component (in this case, 14 km/s), approaches, but does not exceed the single wall curve. Since this is the desired result, it appears that the specification in reference 22 to evaluate the $r_{S/D}$ parameter only at the high velocity region boundary is incorrect.

O-8. There appears to be an error in the algorithm that defines the ratio of critical wall thickness from the single wall BLE to that from the NNO BLE ($r_{S/D}$) in the Reimerdes BLE definition set forth by Reimerdes et al. in reference 22. The specification in reference 22 to evaluate the $r_{S/D}$ parameter only at the high velocity region boundary results in a BLE curve (impactor diameter versus critical wall thickness) that exceeds the single wall curve as the impactor diameter increases, instead of approaching the single wall curve asymptotically as would be

expected. Evaluating the $r_{S/D}$ parameter at the actual normal component of impact velocity appears to rectify the problem.

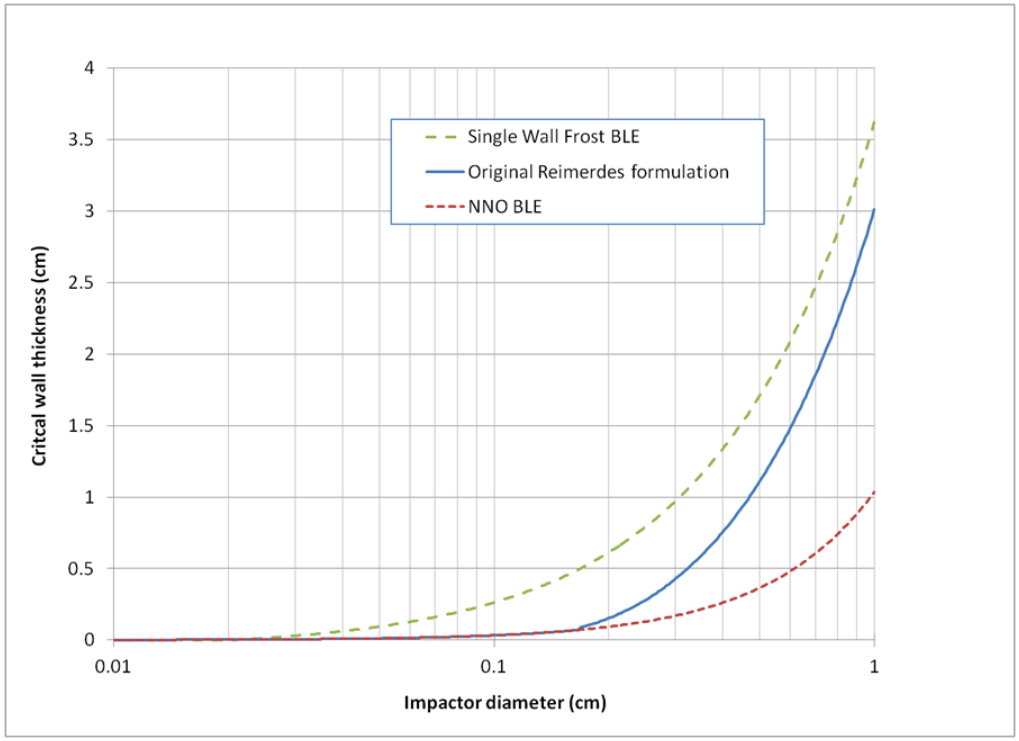

Figure 7.1-15. Critical Wall Thickness versus Impactor Diameter for the Case of an Aluminum Particle Impacting normally at 7 km/s

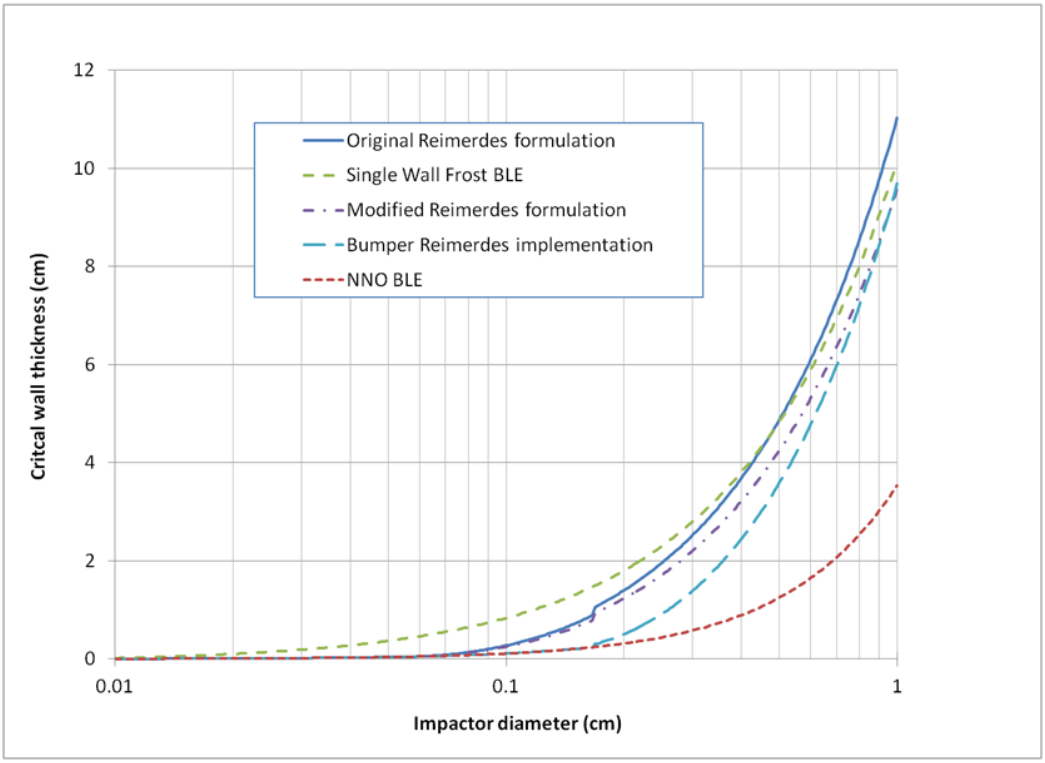

Figure 7.1-16. Critical Wall Thickness versus Impactor Diameter for the Case of a Stainless Steel Particle Impacting Normally at 14 km/s

Figure 7.1-17 shows critical wall thickness versus impact velocity for the case of a 1 mm-diameter aluminum particle impacting normally for the cube dual wall parameters. Three curves are shown: one generated from the NNO BLE, one generated from the single wall Frost BLE, and one generated from the original Reimerdes formulation. The plot shows that the original Reimerdes formulation has a lower boundary for the low velocity region than the NNO low velocity region boundary. In the low velocity and interpolation regions, the original Reimerdes curve is lower than the NNO curve. In effect, the NNO curve is higher than the single wall curve. In the high velocity region, the original Reimerdes curve is the same as the NNO curve. This occurs because a 1 mm-diameter aluminum particle is small enough to be completely shattered by the shield (MLI).

Figure 7.1-18 shows a similar plot for the case of a 1-mm diameter stainless steel particle. In addition to the three curves mentioned for Figure 7.1-17, this plot also has curves generated from the Bumper Reimerdes implementation and the Modified Reimerdes formulation. In the high velocity region, the original and Modified Reimerdes curves are higher than the NNO and Bumper Reimerdes implementation curves, which are the same. The reason for this result is that a 1 mm-diameter stainless steel particle is only partially shattered in the original and Modified Reimerdes formulations, which account for the higher density of stainless steel. In the NNO

formulation and the Bumper Reimerdes BLE implementation, the particle is completely shattered.

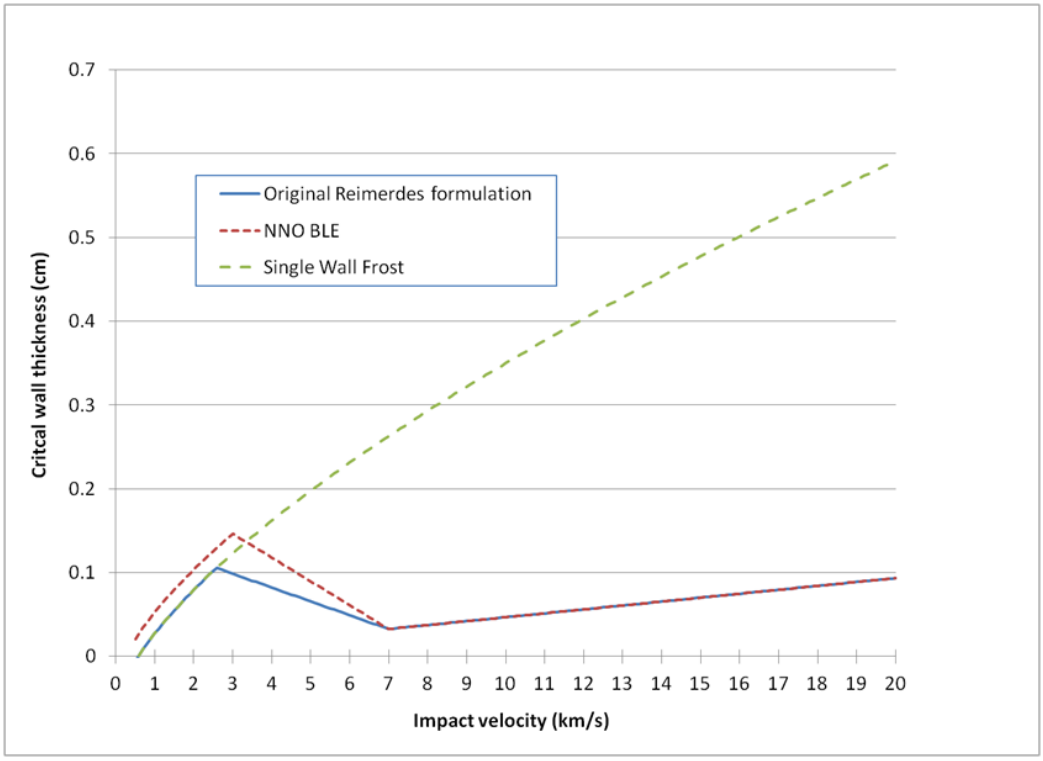

Figure 7.1-17. Critical Wall Thickness versus Impact Velocity for the Case of a 1 mm-Diameter Aluminum Particle Impacting Normally

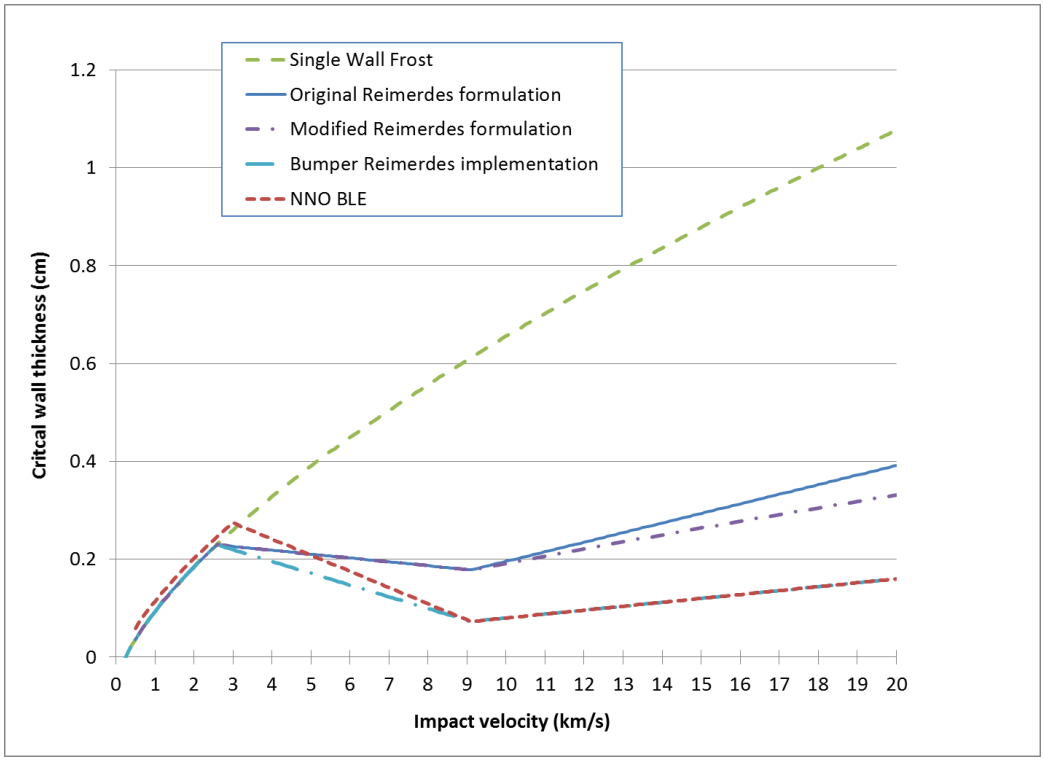

Figure 7.1-18. Critical Wall Thickness versus Impact Velocity for the Case of a 1 mm-diameter Stainless Steel Particle Impacting Normally

In Figure 7.1-14, it can be seen that the Reimerdes BLE is below the NNO BLE for dual-wall systems with thin or lightweight bumpers. The region between the NNO BLE and the corresponding Reimerdes BLE are those projectile diameter-impact velocity combinations that the NNO predicts would not cause inner wall failure (because they lie below the curve) in such dual-wall configurations. However, because they lie above the Reimerdes BLE, that BLE predicts that those projectile diameter-impact velocity combinations *would* cause failure to the inner wall of a dual-wall system because of the presence of a thin or light-weight bumper. Not having been completely disrupted by the thin bumper, the Reimerdes BLE predicts those projectiles to still possess enough energy (as well as momentum) to inflict serious damage on the inner wall plate. As a result, using the Reimerdes BLE in such cases (i.e., for wall configurations with exceedingly light or thin bumpers, such as those where a MLI blanket is acting as a bumper) would contribute to a more conservative (i.e., higher) value of assessed risk.

Damage Fluence Using ORDEM 3.0 with the Reimerdes Modification to the NNO BLE
Another MODRA run was executed with the variation that the Reimerdes modification to the NNO BLE was used in place of the baseline NNO BLE. A description of this formulation is presented in reference 22.

Table 7.1-3 shows the damage fluence on each cube face from each of the populations when the NNO BLE is used in the version of MODRA that interpolates critical diameter ("critical wall thickness method"). In this case, the total damage fluence was 5.60. The damage fluence obtained using the version of MODRA that directly computes critical diameter ("critical diameter method") was 4.95. The difference was due to the interpolation in the "critical wall thickness" method is relatively small compared to the effect of other uncertainties.

Table 7.1-3. Cube Damage Fluence Resulting from use of ORDEM 3.0 with the NNO BLE using the "Critical Wall Thickness Method"

Cube face	Damage fluence							HD percent of total
	NaK	LD	MD	HD	Intacts	Total across populations	Total without HD	
Ram	1.12E-04	8.82E-04	2.46E-01	2.71E+00	4.22E-07	2.95E+00	2.47E-01	91.6%
Trail	0.00E+00	1.73E-06	6.62E-06	3.87E-05	1.52E-09	4.70E-05	8.35E-06	82.2%
South	6.63E-05	7.91E-04	1.33E-01	1.06E+00	2.39E-07	1.20E+00	1.33E-01	88.9%
North	6.63E-05	7.91E-04	1.33E-01	1.06E+00	2.39E-07	1.20E+00	1.33E-01	88.9%
Nadir	0.00E+00	1.98E-06	6.99E-06	5.11E-05	2.53E-09	6.01E-05	8.97E-06	85.1%
Zenith	7.83E-05	8.91E-04	6.51E-03	2.44E-01	3.46E-08	2.52E-01	7.48E-03	97.0%
Total across faces	3.23E-04	3.36E-03	5.18E-01	5.08E+00	9.38E-07	5.60E+00	5.21E-01	90.7%

Table 7.1-4 shows the damage fluence on each cube face from each of the populations when the original Reimerdes formulation is used. In this case, the total damage fluence is 17.4, which is higher than the damage fluence of 5.60 using the NNO BLE. The damage fluence has been increased because larger high density particles are not shattered by the MLI.

Table 7.1-4. Cube Damage Fluence Resulting from use of ORDEM 3.0 with the Original Reimerdes Formulation

Cube face	Damage fluence							HD percent of total
	NaK	LD	MD	HD	Intacts	Total across populations	Total without HD	
Ram	7.64E-05	7.05E-04	4.57E-01	1.04E+01	7.15E-07	1.08E+01	4.57E-01	95.8%
Trail	0.00E+00	2.84E-06	1.68E-05	1.41E-04	5.68E-10	1.60E-04	1.96E-05	87.8%
South	3.66E-05	1.50E-04	1.00E-01	1.87E+00	2.30E-07	1.97E+00	1.01E-01	94.9%
North	3.66E-05	1.50E-04	1.00E-01	1.87E+00	2.30E-07	1.97E+00	1.01E-01	94.9%
Nadir	0.00E+00	2.91E-06	6.09E-05	4.64E-04	1.29E-09	5.27E-04	6.38E-05	87.9%
Zenith	4.13E-07	1.41E-04	1.08E-01	2.50E+00	1.87E-07	2.61E+00	1.08E-01	95.9%
Total across faces	1.50E-04	1.15E-03	7.66E-01	1.66E+01	1.36E-06	1.74E+01	7.67E-01	95.6%

Table 7.1-5 shows the damage fluence on each cube face from each of the populations when the Modified Reimerdes formulation is used. In this case, the total damage fluence is 16.8, which is slightly lower than the damage fluence of 17.4 using the original Reimerdes formulation. The damage fluence has been decreased to a small amount because critical wall thickness does not exceed the value from the single wall BLE at larger sizes.

Table 7.1-5. Cube Damage Fluence Resulting from use of ORDEM 3.0 with the Modified Reimerdes Formulation

Cube face	Damage fluence							HD percent of total
	NaK	LD	MD	HD	Intacts	Total across populations	Total without HD	
Ram	7.64E-05	7.05E-04	4.51E-01	9.79E+00	7.06E-07	1.02E+01	4.52E-01	95.6%
Trail	0.00E+00	2.84E-06	1.68E-05	1.41E-04	5.68E-10	1.60E-04	1.96E-05	87.8%
South	3.66E-05	1.50E-04	1.00E-01	1.87E+00	2.29E-07	1.97E+00	1.00E-01	94.9%
North	3.66E-05	1.50E-04	1.00E-01	1.87E+00	2.29E-07	1.97E+00	1.00E-01	94.9%
Nadir	0.00E+00	2.91E-06	6.09E-05	4.64E-04	1.29E-09	5.27E-04	6.38E-05	87.9%
Zenith	4.13E-07	1.41E-04	1.08E-01	2.50E+00	1.87E-07	2.61E+00	1.08E-01	95.9%
Total across faces	1.50E-04	1.15E-03	7.60E-01	1.60E+01	1.35E-06	1.68E+01	7.61E-01	95.5%

Table 7.1-6 shows the damage fluence on each cube face from each of the populations when the Bumper Reimerdes implementation is used in MODRA. In this case, the total damage fluence is 8.97, which is lower than the damage fluence of 16.8 using the Modified Reimerdes formulation. The damage fluence from the Modified Reimerdes formulation is higher because more stainless steel particles can penetrate the shield (MLI) without being completely shattered.

Table 7.1-6. Cube Damage Fluence Resulting from use of ORDEM 3.0 with the Bumper Reimerdes Implementation

Cube face	Damage fluence							HD percent of total
	NaK	LD	MD	HD	Intacts	Total across populations	Total without HD	
Ram	8.58E-06	2.55E-03	4.49E-01	3.28E+00	7.02E-07	3.73E+00	4.52E-01	87.9%
Trail	0.00E+00	2.84E-06	1.68E-05	1.41E-04	5.68E-10	1.60E-04	1.96E-05	87.8%
South	9.06E-07	2.78E-04	9.66E-02	1.45E+00	2.22E-07	1.55E+00	9.69E-02	93.7%
North	9.06E-07	2.78E-04	9.66E-02	1.45E+00	2.22E-07	1.55E+00	9.69E-02	93.7%
Nadir	0.00E+00	2.91E-06	6.09E-05	4.38E-04	1.29E-09	5.02E-04	6.38E-05	87.3%
Zenith	9.30E-07	3.00E-04	1.02E-01	2.04E+00	1.78E-07	2.14E+00	1.02E-01	95.2%
Total across faces	1.13E-05	3.41E-03	7.44E-01	8.22E+00	1.33E-06	8.97E+00	7.48E-01	91.7%

Figure 7.1-19 illustrates the distribution of the cube damage fluence over impactor size resulting from use of the Modified Reimerdes formulation. Damage fluences on all the cube faces are combined. From this plot it is seen that fewer particles at the low end of the size range are penetrating compared to the NNO case (Figure 7.1-2) and more particles in the middle of the size range are penetrating.

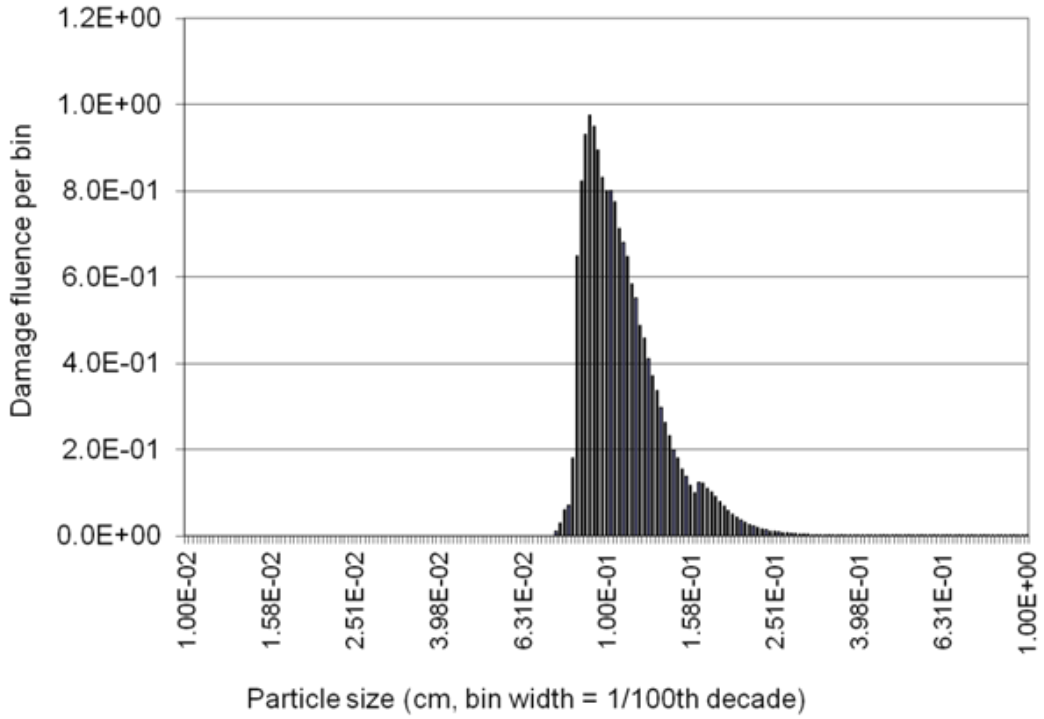

Figure 7.1-19. Distribution of Damage Fluence over Impactor Size; Results from all Cube Faces using the Modified Reimerdes Formulation

Figure 7.1-20 shows the distribution of damage fluence over impact velocity resulting from use of the Modified Reimerdes formulation. Damage fluences on all the cube faces are combined. From this plot it is seen that fewer low velocity particles are penetrating compared to the NNO case (Figure 7.1-3) and more high velocity particles are penetrating.

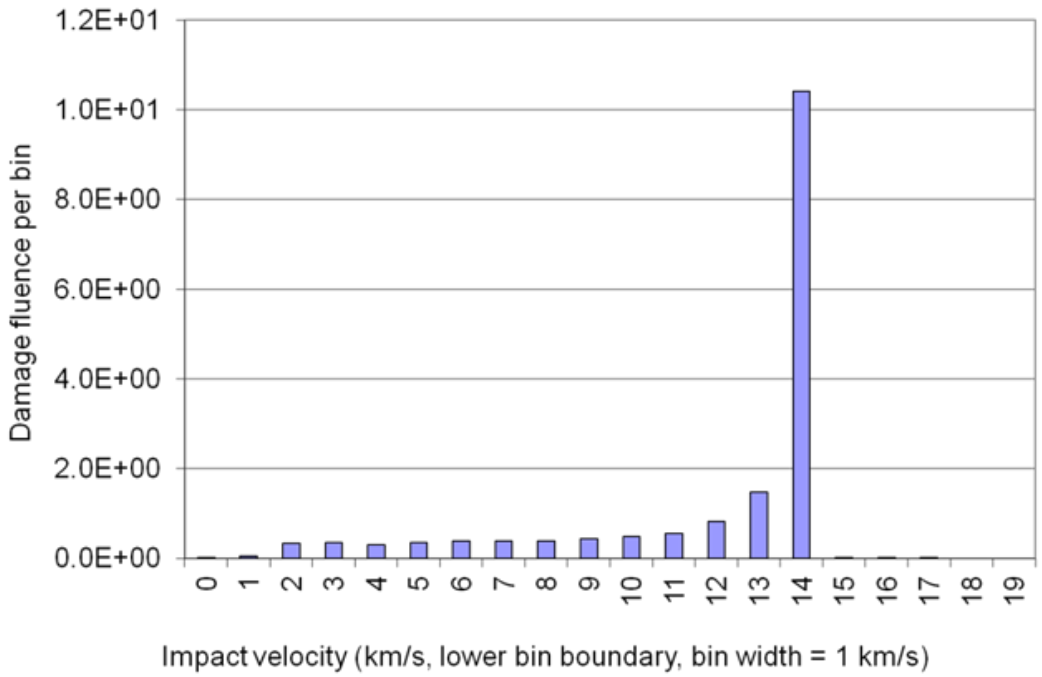

Figure 7.1-20. Distribution of Damage Fluence over Impact Velocity; Results from all Cube Faces using the Modified Reimerdes Formulation

Figure 7.1-21 shows the distribution of damage fluence over impact angle resulting from use of the Modified Reimerdes formulation. Damage fluences on all the cube faces are combined. From this plot it is seen that more particles are penetrating at most angles compared to the NNO case (Figure 7.1-4).

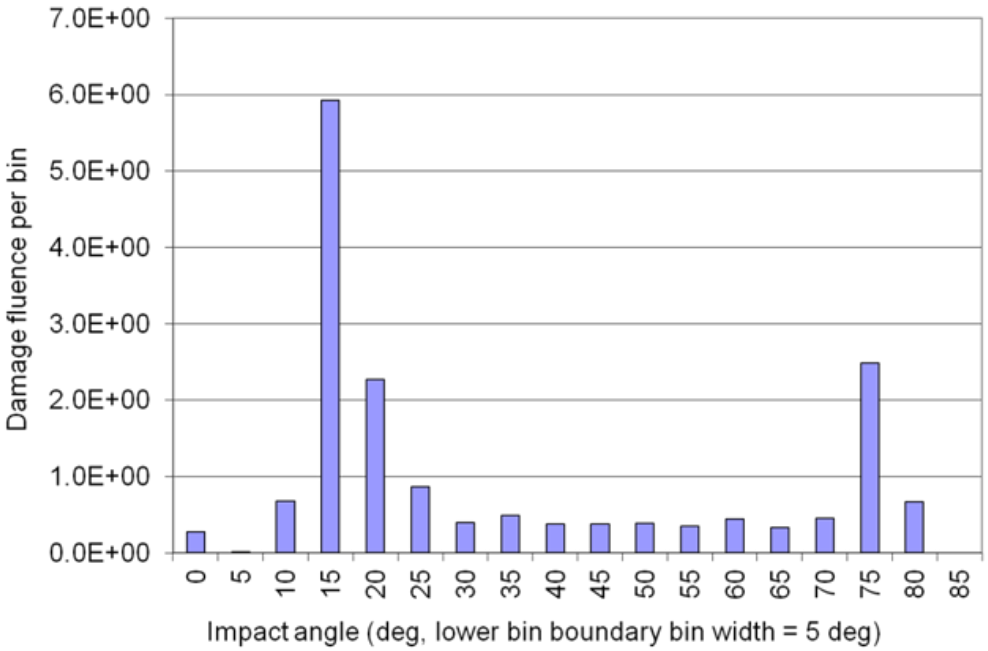

Figure 7.1-21. Distribution of Damage Fluence over Impact Angle; Results from all Cube Faces using the Modified Reimerdes Formulation

7.1.3.2 Over-Prediction of Small Particle Penetrations by the NNO BLE

The use of the Reimerdes formulation addresses the reduced effectiveness of the shield at shattering impactors as impactor size increases. At the opposite size extreme, as impactor size decreases, the shield should reduce the energy and momentum of the impactor material before it reaches the inner wall. In other words, the critical diameter should increase, and the critical inner wall thickness should decrease. The NNO equation for critical diameter in the high velocity regime, which assumes that the impactor is completely shattered, is [ref. 9].

$$d_c = 3.918 F_2^* \frac{t_w^{2/3} S^{1/3} (\sigma/70)^{1/3}}{\rho_p^{1/3} \rho_s^{1/9} (V \cos\theta)^{2/3}}$$

where t_w is the inner wall thickness, S is the spacing between the inner and outer walls, σ is the inner wall yield strength, ρ_p is the density of the impacting particle, ρ_s is the density of the shield, V is the impact velocity, and θ is the impact angle. Note that the formula does not contain the shield thickness t_s (i.e., there is no dependence of critical diameter on shield thickness). The formula assumes that the shield thickness has been set to the critical (minimum) value needed to shatter an impactor of a specific size, i.e.:

$$t_s = d_p (t_s/d_p)_c = d_p c_s \rho_p/\rho_s .$$

This is because the NNO equation is originally intended for designing inner wall and shield thicknesses to stop penetration by impactors of a specific size.

In reality, the shield thickness is fixed and does not vary with impactor diameter. Therefore, the NNO in the high velocity regime does not model the impeding effect of a shield thickness that is higher than the critical value. This means that the NNO BLE may under-estimate critical diameter (or equivalently, over-estimate critical wall thickness) for smaller, more numerous impacts when shield thickness is higher than the critical value. In other words, use of the NNO BLE in a situation with fixed shield thickness and a range of impactor diameters (as specified by an environment model like ORDEM 3.0) will result in an over-prediction of damage fluence by smaller impactors. Finding a way to modify the NNO BLE to account for the impeding effect of shield thickness larger than the critical value may reduce the conservatism in the estimation of penetration risk.

7.1.3.3 Conclusions

When the Modified Wilkinson BLE is used in place of the NNO BLE, the total damage fluence is reduced to 1.45, approximately one-third of the equivalent NNO result. Damage fluence is reduced primarily in the high velocity region, where the Modified Wilkinson formulation replaces the NNO formulation. Damage fluence is only slightly reduced in the low velocity region, where the NNO formulation is not modified.

A MODRA run was performed using ORDEM 3.0 with the Reimerdes formulation of the NNO BLE. The Reimerdes formulation introduces a transition from the NNO BLE to the single wall BLE as impactor size increases and is less shattered by shielding (in this case, MLI). It was found that the source reference on the Reimerdes formulation [ref. 22] may have an error in the algorithm. The reference 22 version with the error is implemented in the Bumper subroutine [ref. 26]. A modification was identified that resolves the error. The resulting cube damage fluence using the Modified Reimerdes formulation was 16.8. The damage fluence from the Modified Reimerdes formulation is higher than the damage fluence from the NNO BLE because there are high density particles in the size range that contributes to the damage fluence, which are not shattered by the MLI layer.

It was also observed that the NNO BLE may over-estimate the damage fluence in penetration risk analyses that consider a range of particle sizes but involve a fixed shield (MLI) thickness. This is because the NNO formulation in the high velocity region does not have any dependence on shield thickness. It assumes the shield thickness is at the critical value to shatter a given size particle. For smaller particles with higher fluxes, the critical thickness assumed by the NNO BLE is smaller than the actual shield thickness, and therefore the shield impedance faced by these particles is not modeled. The Reimerdes formulation does not address this issue since it models the reduced shattering of larger particles by the shielding.

The following findings and observations are related to the BLE comparison.

F-19. The BLEs used for JPSS were developed for manned spacecraft and take a conservative approach to model spacecraft penetrations beyond a 7 km/s normal impact velocity.

- HVI test results suggest that the actual Region III BLE may provide higher performance and yield less assessed risk than currently assumed in the modified NNO BLE.
- Using a modified Wilkinson BLE (80 percent of original Wilkinson BLE, as recommended by Elfer and Bjorkman) resulted in a factor of ~3.4 lower probability of penetration for a 1 meter cube at the JPSS orbit than the NNO BLE.

F-20. Use of the NNO BLE for fixed shield thickness and a range of impactor diameters, as specified by an environment model like ORDEM 3.0, will result in an over-prediction of damage fluence (i.e., increased conservatism) by smaller impactors.

7.2 Avionics Box Failure Criteria Assessment

This section presents the results of an examination of the risk of orbital debris penetration and failure of critical CTU internal components. The objective was to determine whether redefining failure criteria to include failure of critical internal CTU components -- not just failure of the outer shell of the box -- would correspond to a decrease in calculated orbital debris critical failure risk. Updated information from the vendor showed that for the CTU, the majority of internal components are critical. Therefore, the analysis presented in this section is notional and illustrates possibilities for refining avionics failure criteria by considering damage to internal components and not solely using the assumption of a box penetration as the defined failure criterion.

Figure 7.2-1 shows the position and construction of the CTU as part of JPSS-1. On the port side next to the CTU is the spacecraft's radiator, on the starboard side are cables, on the zenith side is MLI, on the front and aft are avionics boxes, and the bottom is covered by the spacecraft structure. Preliminary risk assessments of the CTU in May 2014 indicated that it was one of the largest remaining contributors to orbital debris critical failure risk since many of its internal components were required to safely reenter at the end of the JPSS-1 mission (JSC calculated a 9.7 percent risk of MMOD penetrating the CTU box). Unlike most other reentry-critical components on JPSS-1, the CTU employs redundancy internally: redundant cards within one box, as opposed to separate boxes.

The NESC team's objectives in examining the CTU were to:

- Examine the internal/external CTU structure, Bumper risk assessment, and failure criteria.
- Identify critical internal functions and components of the CTU.
- Perform hydrocode assessments of orbital debris penetration through external MLI and CTU elements to determine particle sizes and velocities that caused internal critical

element failure.

- Perform independent risk assessments of orbital debris failure risk using ORDEM 3.0 particle sizes and velocities.
- Compare results to those derived from Bumper by HVIT.
- Suggest alternative failure criteria (risk criteria, penetration equations, etc.) for future NASA orbital debris risk assessments of CTU and other critical JPSS elements.

Through a query of the JPSS-1 vendor, Ball Aerospace, the NESC team learned that the HVIT-derived risk for the CTU was based on an incorrect conception of the CTU design. The actual MLI was only about one-third the areal density initially reported to HVIT.

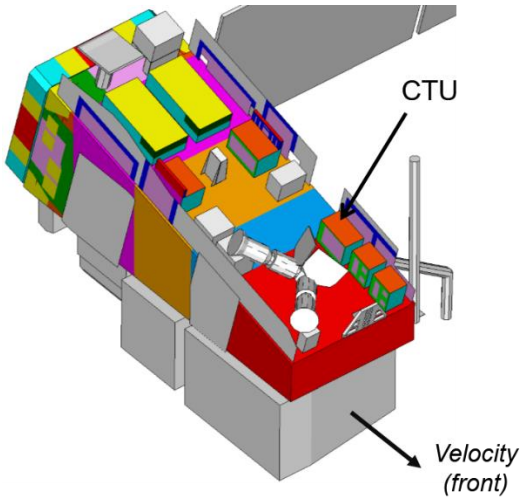

Figure 7.2-1. JPSS-1 CTU Location and Orientation

F-21. The JPSS configuration used to perform the MMOD risk assessment resulted in a 9.7 percent failure risk for the CTU contained configuration inaccuracies. These deviations tended to underestimate the assessed risk:

1. The risk assessment assumed a 5 cm (2-inch) stand-off between the MLI blanket and the CTU, while the actual stand-off varies, and is less than 5 cm in some locations.
2. The risk assessment used an MLI density of 0.091 g/cm2, while the actual blanket has a density of 0.034 g/cm2.

Figure 7.2-2 shows the internal structure of the CTU box. Originally, the NESC team was told that only the gray areas within the box power supply and command cards were critical (Case 1). Subsequently, the NESC team was informed that the sun sensor at the front of the box (red area) was also critical (Case 2).

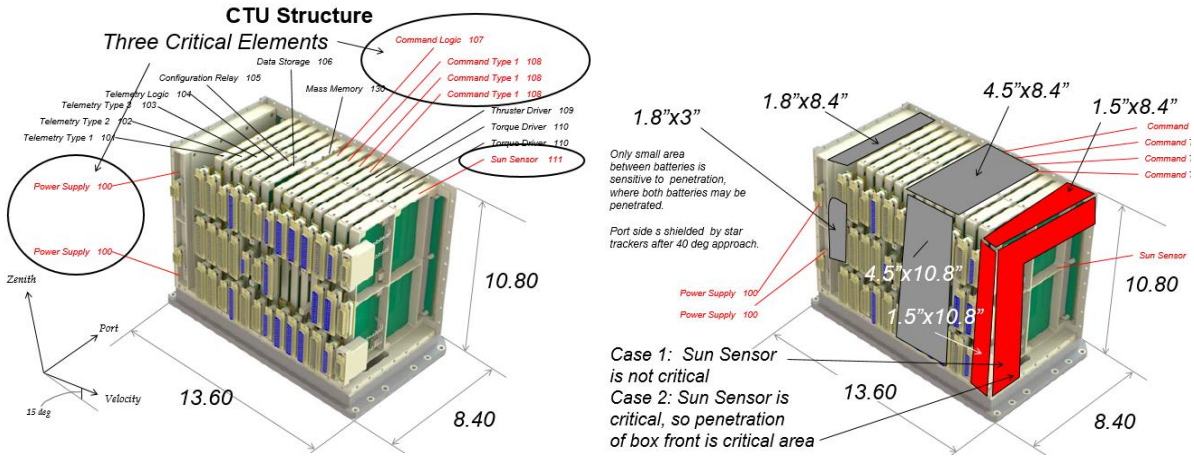

Figure 7.2-2. JPSS-1 Internal Critical Element Locations

Based on this information, the NESC team performed assessments at MSFC using the smooth particle hydrodynamic (SPH) in C (SPHC) hydrocode that established the size and velocity of orbital debris particles that would penetrate the MLI, outer CTU box, and inner card protective layers, exposing the critical internal cards to debris cloud spray from the penetration process. Figure 7.2-3 shows a representative sample of the types of hydrocode evaluations performed. Note that the orbital debris impacts occur at a very high velocity (14.61 km/sec) and obliquity (75°) when approaching the front and top surfaces of the CTU (in the red area shown in Figure 7.2-2). The hydrocode impact evaluation not only established the size and velocity that would penetrate the box, but where it would penetrate and whether structures under the debris cloud were impacted.

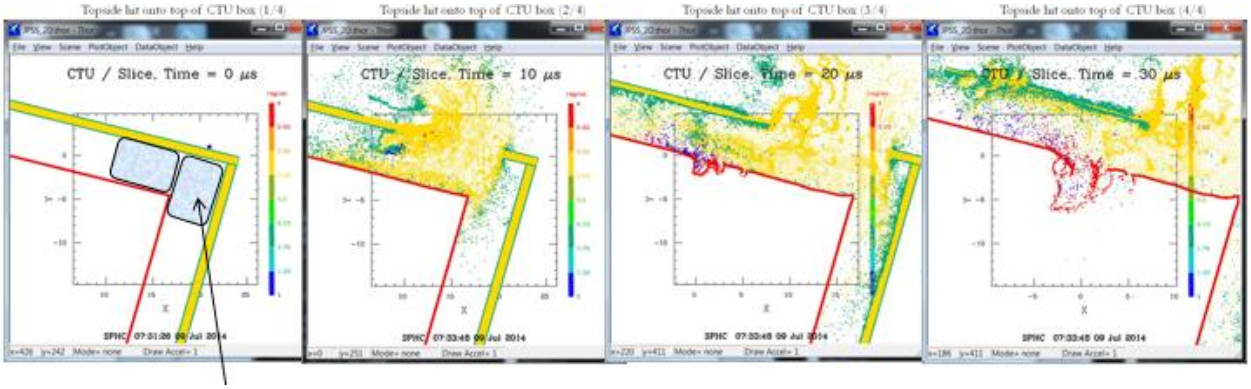

Figure 7.2-3. Sample NESC-Sponsored Hydrocode Assessments

Following the establishment of the size, velocity, and location of aluminum and steel orbital debris particles that penetrate the box and reach critical internal elements (for both Cases 1 and

2), the NESC team used the ORDEM 3.0 orbital debris environment to evaluate the likelihood of penetrating critical internal element cards. Table 7.2-1 shows the results of this assessment. The effect of including the MLI layer can be seen by comparing the single wall only risk of 8.791 to the MLI+Single Wall risk of 0.06195. Note that when the sun sensor is considered noncritical (Case 1), a large reduction from a risk of 0.06195 (assuming MLI and a single wall of the CTU shell) to 0.011299 (a factor of 5.5) in orbital debris risk is possible. This is because the number of critical internal elements are fewer, and no internal elements are located in the area of the box most likely to be penetrated (the red, forward area of the box shown in Figure 7.1-2). However, when the sun sensor is considered critical (Case 2), nearly every penetration is critical and the probability of critical failure decreases by ~20 percent (i.e., from 0.06195 to 0.04997). The risk assessment from HVIT is also shown for reference.

Table 7.2-1. Results of NESC Risk Assessments for Two Internal CTU Configurations

	Risk Assessment Performed				
Surface	**Single Wall**	**MLI + Single Wall**	**Sun Sensor Critical Reduced Area (Case 2)**	**Sun Sensor not Critical Reduced Area (Case 1)**	**HVIT**
Top (Cards)	0.8394	0.00667	0.00400	0.00300	
Top (Cables)	0.2798	0.0022	0.00133	0.00100	
Top (Power Supplies)	0.4029	0.00336	0.00168	0.00160	
Top Total	**1.522**	**0.01229**	**0.00217**	**0.0056**	**0.0162**
Port (Cards)	0.0002	0.00027	0.000160	0.000123	
Port (Cables)	0.00006	0.00008	0.000014	0.0000141	
Port Total	**0.0002**	**0.00036**	**0.00018**	**0.000137**	**0.0008**
Stbrd (Cables)	2.7819	0.00679	0.00246	0.001845	
Stbrd (Power Supplies)	1.0015	0.00244	0.00021	0.000205	
Stbrd Total	**3.7833**	**0.00923**	**0.00267**	**0.00205**	**0.0167**
Front (Cards)	2.0409	0.024995	0.024995	0	
Front (Power Supplies)	0.9797	0.011600	0.011600	0	
Front Total	**3.0705**	**0.0366**	**0.036597**	**0**	**0.0584**
Total Risk	**8.3791**	**0.06195**	**0.04997**	**0.011299**	**0.0921**

Conclusions

The NESC team's objective for this task was to determine whether redefining failure criteria to include failure of critical internal CTU components (not just failure of the outer shell of the box) would allow a significant decrease in calculated orbital debris critical failure risk. Initial indications (with few critical internal CTU components) indicated substantial improvement in assessed risk was possible. However, a later assessment showed that the number of critical CTU components were numerous and, most importantly, covered internal areas that were most likely to be penetrated by orbital debris. In the end, although the NESC team demonstrated that such an assessment could readily be performed, there was little reason to pursue this strategy in this case. Doing so would also require establishing the capability of internal components to resist impact-generated contamination after box penetration—not worth the effort for the expected reduction in critical risk for the CTU.
Additional details for this assessment are included as Appendix D.

F-22. Higher fidelity analyses of the internal structure and expected failure modes for critical electronics box interior elements aboard JPSS-1 (i.e., examining the resistance of interior critical elements to penetration within each box) may result in a lower MMOD assessed risk for those boxes (compared to assuming any box penetration is a failure).

- This examination must be balanced with long-term concerns over interior box element contamination from penetrations.
- This is a first-order assessment and thorough risk evaluation would require HVI testing to verify hydrocode results.

7.3 Wire Bundle Risk Assessment

This section presents the results of two hypervelocity impact failure risk assessments for JPSS-1 critical (i.e., necessary for controlled reentry) wire bundles exposed to the ORDEM 3.0 orbital debris environment at its 824 km, 98.8° inclination orbit. The first "generic" approach predicted the number of wires broken by orbital debris ejecta emerging from normal impact with MLI covering 36-, 18-, and 6-strand wire bundles at a 5 cm standoff using SPH hydrocode. This approach also included a mathematical approach for computing the probability that redundant wires were severed within the bundle. Based in part on the high computed risk of a critical wire bundle failure from the generic approach, an enhanced orbital debris protection design was implemented, consisting of betacloth-reinforced MLI suspended at a 5 cm standoff over a seven layer betacloth and Kevlar® blanket, draped over the exposed wire bundles. A second SPH-based risk assessment was conducted that also included the beneficial effects from the high obliquity (75°) of orbital debris impact and shadowing by other spacecraft components and resulted in a considerably reduced likelihood of critical wire bundle failure compared to the original baseline design. This second approach is consistent with earlier wire failure assessments for the James Webb Space Telescope [ref. 27] and other spacecraft such as the Advanced X-ray Astrophysics Facility [ref. 28], which assumed that any penetration of the shield over the wire bundle caused failure of the bundle.

F-23. Exterior wire bundles, especially those on the most-exposed zenith side, on JPSS-1 have not been considered in the risk assessment, and their inclusion in future risk assessments can be expected to increase the assessed MMOD risk.

Task 1: Generic Risk Assessment of Baseline MLI over Wire Bundles

The NESC team performed SPHC hydrocode assessments of orbital debris penetration through a typical wire harness with baseline MLI blanket protection, as shown in Figure 7.3-1. The SPHC hydrocode is a C language implementation developed by Stellingwerf (1985-95). The present incarnation of SPHC, V12.8, runs up to one million particle problems on Windows personal computers or work stations having 1.5 Gb of memory. In smooth particle hydrodynamics, the "particle" is the analog of the mesh point in a traditional hydrocode. A SPH particle consists of a fixed mass of material at a given position in space, together with a smoothing function, or "kernel," that defines the particle's extent.

Figure 7.3-1. JPSS-1 Showing Wire Bundles

As shown in Figure 7.3-2, a typical cable is assumed to consist of 36 wires (18 redundant wire pairs) where every wire pair is considered critical to the function of the cable. The wires were placed in a hexagonal pattern in order to scale the damage seen in 36 wires to smaller wire bundles (18- and 6- wire bundles). It is noted that the actual hexagonal patterns undergoing hydrocode assessment were of 37, 19, and 7 wires, with the damage to the last (deepest) wire neglected in the risk results for the 36, 18, and 6 wire strands. The risk assessment considered a one-year exposure to the ORDEM 3.0 environment with a zenith/nadir wire orientation. A 5 cm standoff of baseline MLI-to-wire harness was included in the hydrocode run.

Figures 7.3-2 and 7.3-3 show typical results from the SPH analyses for a predicting the number of wires cut considering a variety of orbital debris impact materials, velocities, and diameters. Note that the expected number of penetrated wires increases with velocity, diameter, and density of the projectile. Figure 7.3-4 shows the likelihood of an entire cable failing based on the number of redundant wire failures. As shown, once more than half of the wires (i.e., 19 wires) are penetrated in a 36-wire bundle, there is a 100 percent chance that two redundant wires have been hit, thus disabling the critical instrument that the wire is feeding. The likelihood of critical instrument failure increases with the number of wires penetrated until 100 percent is reached when penetrating more than half the wires.

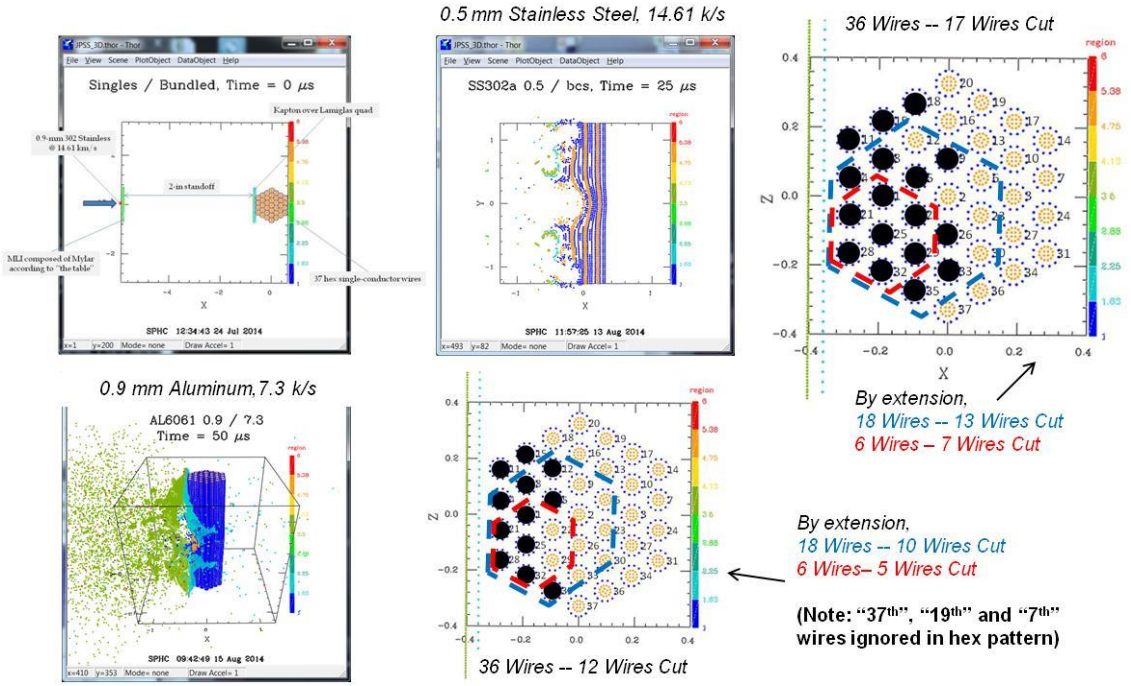

Figure 7.3-2. Typical SPH Hydrocode Predictions for Steel and Aluminum Orbital Debris Impacts

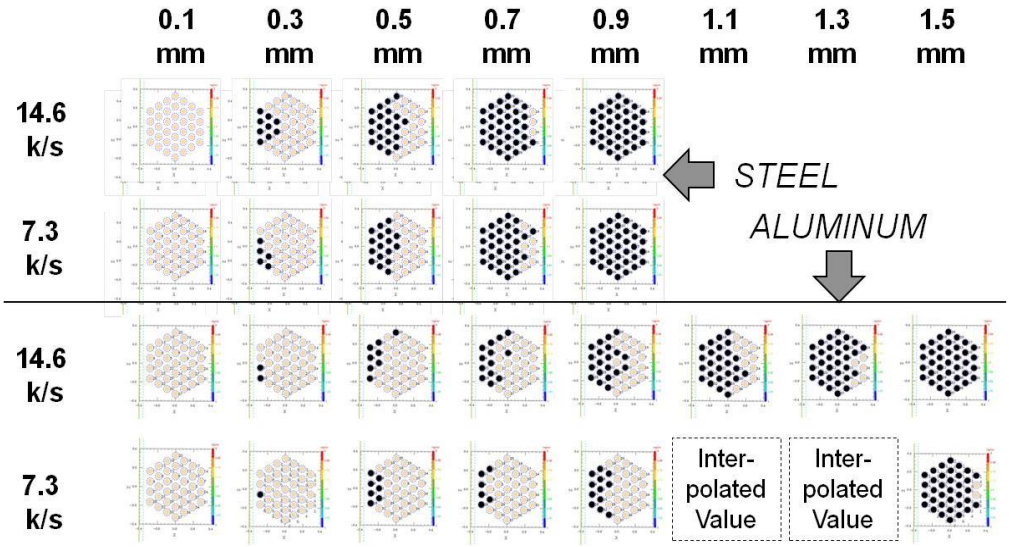

Figure 7.3-3. Number of Wires Cut in 36-wire Bundle for Given Combinations of Orbital Debris Densities, Diameters, and Velocities

Once the number of penetrated wires are predicted through SPH hydrocode assessment and associated with a probability of cable failure, the analyst can determine the probability of those conditions occurring on orbit using ORDEM 3.0 [ref. 29]. In this case, an Excel spreadsheet was developed that interpolates the size and velocity of steel and aluminum particles causing from 1 to 36 wire failures based on the hydrocode results, then calculates the likelihood of those particle combinations impacting the cables for a 1-foot length of cable in a year.

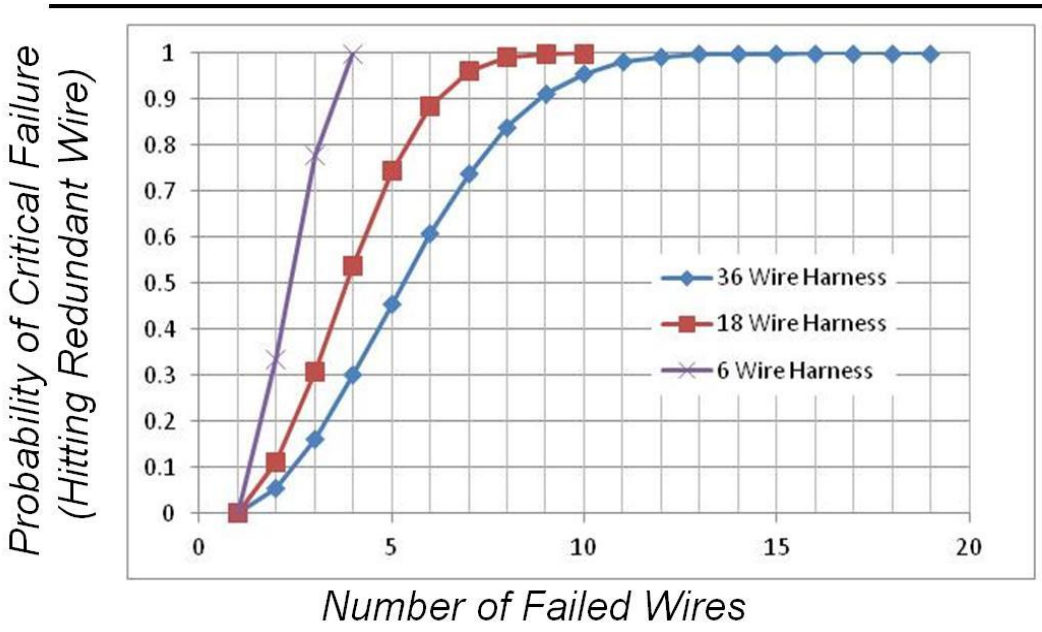

Figure 7.3-4. Probability of Critical Failure versus Wire Harness Size Given Randomly Placed Redundant Wire Failure

Figure 7.3-5 shows the expected probability of orbital debris-induced cable failure for a 1-year exposure of a 1-foot length of 6-, 18-, and 36-strand cables, where every strand within a cable carries a critical function and has a redundant strand somewhere in the cable carrying the same critical function. However, real spacecraft cables are often bundled together, shadowing one another, and located in orientations and locations where other spacecraft components shadow them. They also often carry more than just critical functions. As shown in Table 7.3-1, the baseline number of fails determined from the analysis is multiplied by factors that represent shadowing from different perspectives relative to the cable and a factor that takes into account wire redundancy in each cable. The result is an estimated number of fails that is a factor of ~20 less than the baseline.

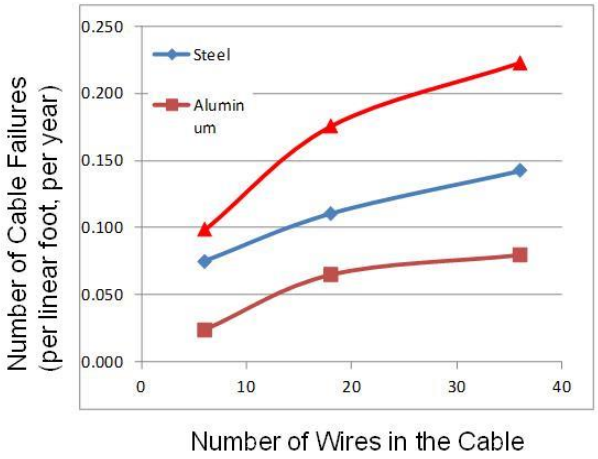

Bundle Size	Steel	Aluminum	Total
6	0.075	0.024	0.099
18	0.111	0.065	0.176
36	0.143	0.080	0.223

Figure 7.3-5. Cumulative Number of Cable Failures for Three Cable Sizes (1-Foot Length, Zentih/Nadir Orientation, 1 Year Exposure)

Table 7.3-1. Effect of Shadowing and Reduced Criticality on a Typical 8-Foot Cable

Cable #	Length (ft)	Baseline no. of fails	Shadowing Factors: Portside	Front (0°)	45°	Bundle	Criticality Factor (assumes redundant wires)	Adjusted no. of fails
1	2	0.446	0.5	0.46	0.84	1	0.5	0.043
2	2	0.446	0.5	0.46	0.84	0	0.5	0
3	2	0.446	0.5	0.46	0.84	1	0.5	0.043
4	2	0.446	0.5	0.46	0.84	0	0.5	0
Total		1.784					**Total**	0.086
Fails per Foot		0.223					**Fails per Foot**	0.011
		Ratio of baseline no. of fails to adjusted no. of fails						20.7

O-9. Assessing exposed wire bundle MMOD risk is complex, encompassing hard-to-quantify failure contributions associated with variables such as wire redundancy, bundle size, criticality, and failure modes. This results in a high level of uncertainty for the critical failure probability prediction due to MMOD for JPSS-1.

Task 2: Evaluating an Enhanced MMOD Blanket Over Zenith Deck Wires

Based in part on the high computed risk of a critical wire bundle failure from the generic approach (Task 1), JPSS decided to implement an enhanced MMOD protection design consisting of betacloth-reinforced MLI suspended at a 5 cm standoff over a seven layer betacloth and Kevlar® blanket, draped over the exposed wire bundles, as shown in Figure 7.3-6. It is noteworthy that 99.5 percent of orbital debris approaches from within the X-Y (orbital) plane,

and that orbital debris approaching from the Y-axis (from the "front" as viewed by the spacecraft or ram direction) makes up nearly 50 percent of this flux. The impact velocity would be 14.6 km/sec and impact the blanket at 75° obliquity relative to the exposed wires on the zenith deck. The ultimate objective was to develop a design that prevented penetration of 3 mm aluminum spheres from the worst-case impact conditions shown in Figure 7.3-7.

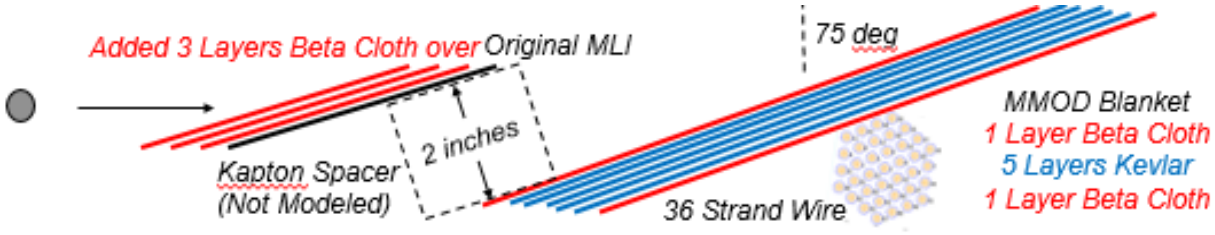

Figure 7.3-6. Enhanced Shield Configuration for Defeat of 3mm Aluminum Orbital Debris Particles

As shown in Figure 7.3-7, SPHC analyses showed that the enhanced shield was capable of preventing penetration of a 3 mm aluminum and 2.12 mm stainless steel orbital debris particle at the stated conditions.

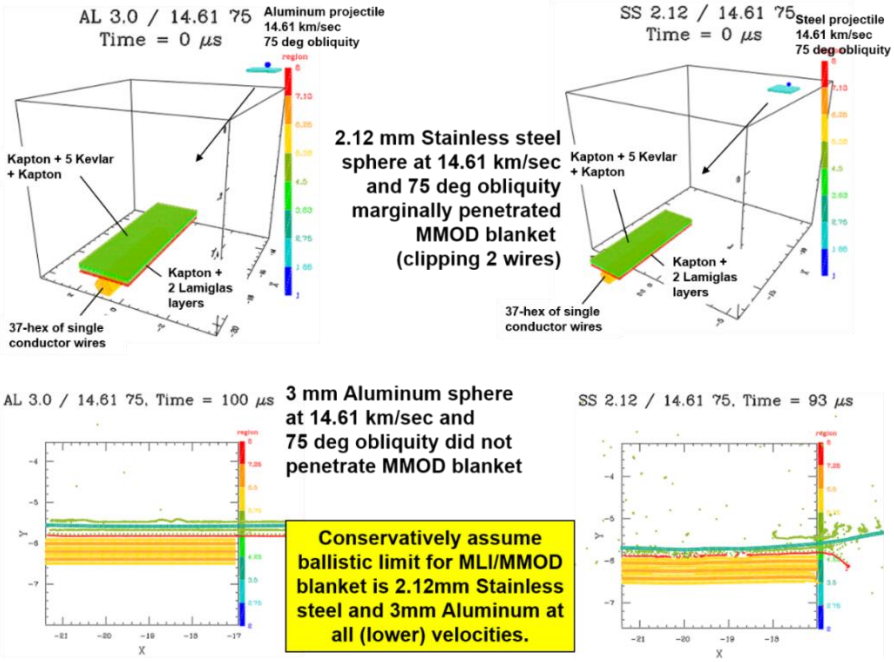

Figure7.3-7. Hydrocode Evaluation of Enhanced MMOD Shield for Steel and Aluminum Orbital Debris

Once the ballistic limit for the worst-case orientation (and highest orbital debris flux) was determined using SPHC, the exposed area for the blanket (and wiring beneath it) was calculated using the configuration shown in Figure 7.3-8. This area includes all regions where a wiring harness might be present, not just the critical harness bundles themselves, which could not be estimated reliably at the time of this assessment. As shown, the JPSS-1 spacecraft features radiators on the sides of the spacecraft that block much of the orbital debris from approaching the spacecraft from angles at 15° or more from the velocity vector.

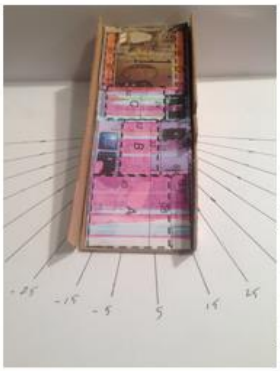

Orbital Debris Approach Angles

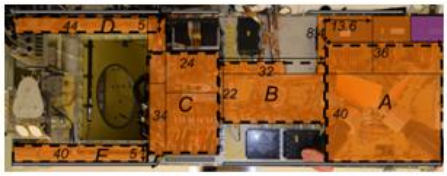

Example: 25 Degree Approach Angle

		Exposed Area Including Shadowing by Approach Direction (m^2)									
Region	Surface Area	0 deg	5	15	25	35	45	55	65	75	85
A	0.930	0.241	0.239603	0.233331	0.219177	0.098527	0.042508	0.013805	0.005134	0.000639	0.000218
B	0.454	0.118	0.117139	0.114073	0.053577	0	0	0	0	0	0
C	0.527	0.137	0.135775	0.105777	0	0	0	0	0	0	0
D	0.142	0.037	0.036606	0.035648	0	0	0	0	0	0	0
E	0.129	0.033	0.033278	0	0	0	0	0	0	0	0
	Obliquity	75	75.1	75.5	76.4	77.8	79.5	81.5	83.7	86.1	88.7
	Total Area	0.57	0.56	0.49	0.27	0.10	0.04	0.01	0.01	0.00	0.00

Exposed areas of wire harnesses by approach angle

Figure 7.3-8. Calculation of Exposed Areas for Wiring Harnesses by Approach Angle

Table 7.3-2 shows that for steel orbital debris particles, there is a 4.3 percent probability that one or more orbital debris penetrations of the enhanced shield over the zenith deck wiring will occur in the expected 7-year operation of the JPSS-1 spacecraft. Similarly, there is a 1.0 percent risk for aluminum particles, resulting in a combined risk of 5.3 percent. Most of this risk results from penetration by stainless steel particles due to their lower ballistic limit and higher flux on the enhanced wiring shield.

Table 7.3-2. Orbital Debris Penetration Risk for Enhanced Wiring Shield (Ppen = Probability of Penetration)

	Steel Projectiles (Ballistic Limit = 2.12 mm)				Aluminum Projectiles (Ballistic Limit = 3.00 mm)		
Approach Angle (deg.)	Penetration Flux (pens./m²-yr)	Area (m²)	Number of Penetrations in 7 years		Penetration Flux (pens./m²-yr)	Area (m²)	Number of Penetrations in 7 years
5	0.003448	0.562	0.0136		0.000678	0.562	0.0027
15	0.001757	0.488	0.0060		0.000505	0.488	0.0017
25	0.000942	0.272	0.0018		0.000259	0.272	0.0005
35	0.000688	0.098	0.00047		0.000184	0.098	0.000126
45	0.000549	0.042	0.00016		0.000149	0.042	4.38E-05
55	0.000484	0.013	4.4E-05		0.000129	0.013	1.17E-05
65	0.000462	0.005	1.62E-05		0.000116	0.005	4.06E-06
75	0.000471	0.0006	2.0E-06		0.000114	0.0006	4.8E-07
85	0.0000955	0.0002	1.34E-07		6.57E-05	0.0002	9.2E-08
		Total Port	**0.0221**			**Total Port**	**0.0051**
		Total Starboard	**0.0221**			**Total Starboard**	**0.0051**
		Total Number of Penetrations	**0.0431**			**Total Number of Penetrations**	**0.0101**

Conclusions

Two approaches were pursued to evaluate the risk from orbital debris penetration of exposed JPSS-1 wiring. In the first case, a generic approach considering normal impact of the baseline MLI over wires resulted in an evaluation of wire damage that was very conservative in that it did not consider the effects of obliquity and shadowing by other spacecraft components and adjoining wiring, and could not be sufficiently refined to account for the exact wiring bundle design, including redundancy.

In the second case, an enhanced orbital debris shield was evaluated to provide less than a 5.3 percent probability of penetration in 7 years when placed over the exposed wires. However, shield penetration should not be equated to critical wire failure; the figure of 5.3 percent "risk" of shield penetration is an upper bound for critical wire failure risk for the following reasons:

- Actual wire coverage is less than the coverage of the MMOD blanket (lowering critical wire risk).
- There is a higher ballistic limit of the shield at other approach angles since that debris approaches at a lower velocity.
- Shield penetration does not necessarily imply wire damage or failure.

- There are inadequate impact test data for wiring harnesses available to correlate the hydrocode simulations to actual performance.
- Not every wire is critical, and many wires are redundant.
- Many of the critical wires are placed below other wires, so more shadowing is likely than was accounted for in this assessment.

Considering these factors, the probability of critical wire failure on the zenith deck may be less than 1 percent.

Additional details for this assessment are included as Appendix E.

O-10. Preliminary NESC orbital debris risk assessments for representative wire bundles leading from reentry-critical elements on the zenith surface of the JPSS-1 covered only by baseline MLI predicted that a critical failure penetration per year might be expected for every 100 feet of exposed cables, considering blockage from other JPSS-1 wiring and equipment. This first order analysis was intended to give an estimate of the order of magnitude risk for the wire bundles. This baseline risk could be reduced through heavier MLI blanket/shielding protection over these zenith bundles.

7.4 Debris Shape Assumptions

Prior NESC assessments of MMOD risk for the Constellation Program [ref. 30] and ISS [ref. 31] noted that NASA risk assessments make the assumption that all orbital debris is spherical, with the same outer dimension as the characteristic length called out in ORDEM 3.0 and previous models. In reality, most orbital debris particles are not spherical. The characteristic length is a description of the average of three major dimensions of any shape particle, and the use of a spherical debris particle results in particles that are much heavier than the average particles (which are also more representative of fragments from upper stage explosions or breakups). NASA's own Standard Breakup Model (SBM) is used to determine orbital debris reentry life, and arguments have been made to include it or other models in future debris penetration risk assessments (see charts from reference 30 in Figures 7.4-1 and 7.4-2). These prior studies, considering such disparate structural designs as aluminum single walls, Whipple shields, and thermal protection systems, indicate that the use of spherical debris assumptions is overly conservative, arriving at orbital debris risk assessments that are higher by a factor of ~2 compared to SPH-based models.

Fragment Shapes from Impact Experiments

NASA fired particles into satellites (on ground), & correlated debris radar cross sections to characteristic length (Lc).

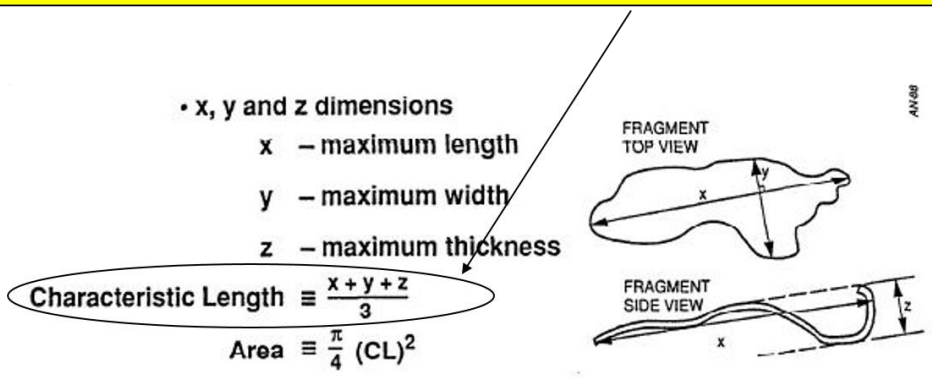

Results showed small Lc particles were chunky; larger Lc particles were more like flakes.

Based these and other tests, NASA proposed a particle that changes shape from cubes (small fragments) to flakes (for larger fragments) for use in their Standard Breakup Model (SBM).

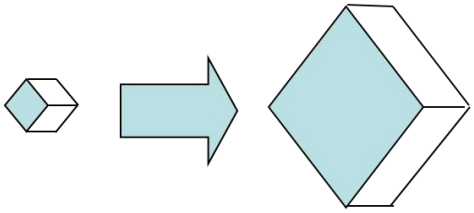

Lc = 1 mm **Lc = 5 mm**

Figure 7.4-1. Fragment Shapes from Impact Experiments [ref. 30]

Standard Breakup Model (SBM) "Flake" Compared to (Current) Sphere Debris Shape Assumption

Spheres are More Massive than SBM Fragments of the Same Lc

For the same Lc (characteristic length), spheres are heavier than cubes (nuggets), and cubes are generally heavier than flakes—thus, they strike with a higher energy at the same velocity, overpredicting risk.

	Sphere, Lc = D	Cubes		SBM-Based Debris Flakes		
Lc (mm)	m (g)	L (mm)	m (g)	L (mm)	T (mm)	m (g)
1.00	0.0015	0.6	0.0006	0.60	0.60	0.0006
1.50	0.005	0.9	0.002	0.90	0.90	0.002
1.66	0.007	1	0.003	1.00	1.00	0.003
2.00	0.012	1.20	0.005	1.29	1.07	0.005
2.50	0.023	1.50	0.009	1.75	1.16	0.010
3.00	0.04	1.80	0.016	2.22	1.23	0.017
3.50	0.063	2.10	0.026	2.71	1.30	0.027
4.00	0.094	2.40	0.039	3.20	1.35	0.039
4.50	0.134	2.70	0.055	3.70	1.41	0.054
5.00	0.183	3.00	0.076	4.20	1.45	0.072
5.50	0.244	3.30	0.101	4.69	1.49	0.092
6.00	0.317	3.60	0.131	5.19	1.53	0.116
6.50	0.403	3.90	0.166	5.70	1.57	0.143
7.00	0.503	4.20	0.208	6.20	1.61	0.173
7.50	0.619	4.50	0.255	6.71	1.64	0.207
8.00	0.751	4.80	0.31	7.22	1.67	0.244
8.50	0.900	5.10	0.372	7.73	1.70	0.285
9.00	1.069	5.40	0.441	8.24	1.73	0.329
9.50	1.257	5.70	0.519	8.75	1.76	0.377
10.00	1.466	6.00	0.606	9.27	1.78	0.429

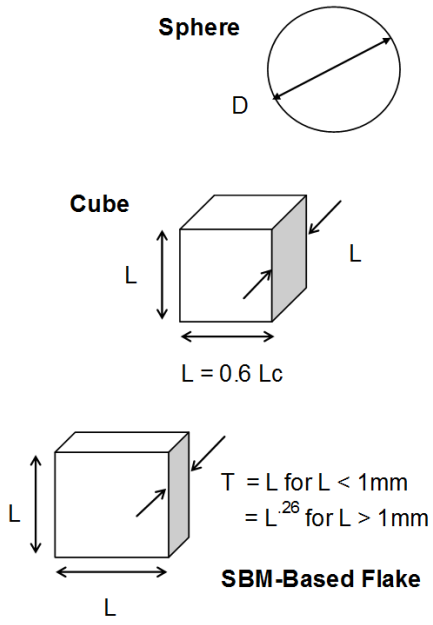

Figure 7.4-2. SBM "Flake" Compared to Sphere Debris Shape Assumption (Current Assumption)

The following finding and observation are related to orbital debris shape.

F-24. Assuming a spherical debris shape is a source of uncertainty in the MMOD risk assessment, some studies suggest assuming a spherical shape (versus cubes or flat plates of the same critical length) may overestimate risk by a factor of ~2. However, not all potential debris shapes have been examined for their effect on risk.

O-11. The ORDEM 3.0 environment does not explicitly describe the expected shape, or range of shapes possible in the orbital debris environment. It accounts for non-spherical particles when determining debris populations from the radar sources, while assuming spherical particles when associating particle sizes with crater sizes (*in situ* environment).

7.5 Pressure Vessel Failure Criteria

When the NNO BLE is applied to pressurized elements of the JPSS-1 (e.g., the propellant tank), the wall thickness of the tank, which is the inner wall of a dual-wall (i.e., Whipple) shield, is assumed to be 50 percent of its actual thickness based on the following argument:

1. Inner wall "failure" as used in development of the NNO BLE is defined as detached rear-side spall, even without an actual through-hole or perforation of the inner wall.
2. According to reference 32, to avoid rear-side detached spall, the thickness of a thin plate must be between 1.8 and 2.2 times the maximum expected crater depth in the thin plate.
3. If an average value of 2.0 is used, this means that implicit in the NNO BLE is a maximum allowable crater penetration depth of 50 percent before inner wall failure is said to occur.
4. According to reference 33, to prevent pressurized tank failure, maximum crater penetration depth cannot exceed 25 percent of the tank wall thickness.
5. Therefore, in order for the NNO BLE to be used in the prediction of the failure response of a pressurized tank, only 50 percent of the actual rear wall thickness is to be used as an input value.

The implementation of this "25 percent thickness rule" is illustrated in Figure 7.5-1. This figure also shows the difference between the initial design parameters of the JPSS-1 tank and those used in the initial Bumper runs. First, the MLI blanket, with an areal density of 0.32 g/cm², has been equivalenced to a thin aluminum bumper, and then the thickness of the titanium wall has been reduced by 50 percent (although the wall material, in this particular case, was kept as titanium and not equivalenced to aluminum).

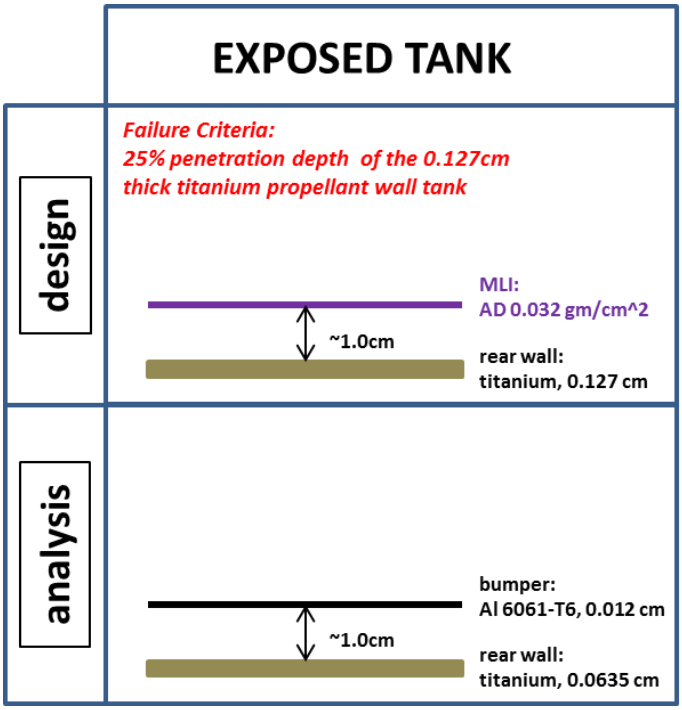

Figure 7.5-1. Application of the "25 Percent Thickness Rule" for the Exposed Portion of the JPSS Propellant Tank

While the above argument regarding the "25 percent thickness rule" appears to be self-consistent, several important points must be taken into consideration if the NNO BLE is to be applied to pressurized structural elements in this fashion.

1) The actual allowable thickness rule or criterion in [ref. 33] consists of two parts:

    a. *"The concentrated damage area should not exceed 1 inch in diameter.*
    b. *The reduction in cross-sectional area (crater and spall) must not exceed 25 percent of the wall thickness."*

At present, it is not clear as to whether or not the first part of the criterion has been discussed or checked to determine if it has been met for the geometries and impact conditions of interest on JPSS-1. Furthermore, the wording in the second part may be confusing as written. This second part of the criterion speaks to a reduction in cross-sectional area, not a reduction in cross-sectional thickness (although the allowable reduction in area is related to a fraction of the initial wall thickness). First of all, area cannot be reduced by a length. Secondly, unless one bounds the edges of a region, how can initial and final cross-sectional areas be compared?

2) The allowable thickness rule in reference 33 was based on a series of seven tests, all performed under the following nearly identical conditions:

> *"... 0.32-cm-diameter glass spheres were impacted on shielded tanks at 7.0 km/sec. The tanks were made of type 6Al-4V titanium alloy and were pressurized with alcohol to 960 lb/in^2 to develop a hoop stress of 90,000 lb/in^2. Aluminum shields were placed 1 inch from the tank walls. In seven tests, no tanks were ever ruptured, and there was no spallation inside the tank. The front-surface cratering was nominal, and the total reduction in cross-sectional area was less than 25 percent. Concentrated damage was confined to a 1/2-inch circular area."*

No documentation has been found indicating that in the 45 years since this rule first appeared, it has ever been checked for applicability to materials and impact conditions other than those from which it was developed. Further, these seven tests resulted in no spallation or rupture. So they represent conservative acceptance criteria, not necessarily a definition of a failure condition.

Although mentioned briefly in Section 4.2.3.2 of NASA-SP-8042 (Space Vehicle Design Criteria: Meteoroid Damage Assessment), a review of more current NASA standards reveals that neither NSS 1740.14, nor NASA-STD 8719.14A, nor NPR 8715.6A, nor the DAS 2.0 User's Guide offer any information on the subject of how to design pressurized volumes intended to operate in the MMOD environment.

To determine what modification DAS 2.0.2 performs regarding allowable penetration depth for pressure vessels, several runs were performed using DAS 2.0.2 and a generic pressure vessel. The orbit was not considered to be a contributor, so simple default parameters of 500 km circular, 28.5° inclination, 1 year, 100 kg, and 0.01 m^2/kg were used in the Mission Editor. A post-mission disposal maneuver was specified to limit the assessment period to 1 year in all cases. The generic tank used had a 4 g/cm^2 areal density and a 1 m^2 critical surface area, with no additional shielding. This baseline tank was initially specified as pressurized. DAS was then run again using parameters and tanks identical to this first run tank, except in subsequent runs (1) the tanks were not pressurized, and (2) a variety of areal densities were used to simulate different allowable penetration depths. All tank critical surfaces in all of the runs were oriented directly into the ram direction to maximize the risk result (and therefore to better highlight any differences). The MMOD risk for each case was calculated by DAS and is shown in Table 7.5-1.

Table 7.5-1. MMOD Risk Assessment Results Calculated by DAS for a Generic Pressure Vessel

Critical Surface	Areal Density (g/cm²)	Surface Area (m²)	Pressurized? (yes/no)	DAS 2.0.2 Calculated MMOD Risk
Tank - Full Thickness	**4**	**1**	**yes**	**0.018997**
Tank - 1/2 Thickness	2	1	no	0.001599
Tank - 1/4 Thickness	1	1	no	0.009470
Tank - 1/8 Thickness	0.5	1	no	0.075316
Tank - 1/5 Thickness	**0.8**	**1**	**no**	**0.018977**

As shown in Table 7.5-1, the reported risk for the initial baseline case (with a 4 g/cm^2 areal density) was 0.018997 (~1.9 percent). Furthermore, the results for the case where the tank was unpressurized and where its wall thickness was simulated as one-fifth as thick as the baseline wall thickness (or put another way, for the case where the maximum allowable penetration depth was 20 percent of the original wall thickness) exactly matched the baseline case. This indicates that when a component is specified as pressurized, DAS 2.0.2 multiplies the areal density by 0.20 (and not 0.25), effectively dividing the tank wall thickness by a factor of five (i.e., allowing a penetration depth of only 20 percent of the original wall thickness). By adding an identical MLI layer to all cases and running DAS again, it was confirmed that this compensation factor applies only to the pressurized vessel wall itself. This was confirmed by examination of the actual DAS program, which revealed the following lines of code:

```
      IF (PRESS) THEN                    !ONLY NEED TO PENETRATE 20% OF
         SIGMATOT=0.2D0*SIGMABW          !PRESSURE WALL TO CAUSE
FAILURE
      ELSE
         SIGMATOT=SIGMABW
      ENDIF
```

Since (1) areal density is equal to material bulk density multiplied by the wall thickness, and (2) DAS considers wall failure to occur when the rear side of a wall is breeched (that is, DAS considers a penetration depth of 100 percent of the wall thickness to be a failure, and not just a 50 percent penetration depth as does Bumper), this reduction by DAS in the areal density and, by implication, a corresponding reduction in the thickness, of a pressurized tank wall to 20 percent = one-fifth of its original value would be equivalent to specifying a maximum

allowable penetration depth of 40 percent in Bumper (instead of the currently assumed and used value of 50 percent in Bumper).

This use of a 20 percent reduction factor (instead of 25 percent, which would correspond to a maximum allowable penetration depth of 50 percent in Bumper) may be an attempt to add an additional layer of conservatism to the DAS calculation process.

F-25. Apollo-era failure criteria for pressure vessels are being applied to modern era spacecraft without tests or analysis to confirm their applicability.

7.6 Updated JPSS Risk Assessment

As the JPSS design evolved during the course of this NESC activity, members of the NESC team participated in telecons among NASA and contractor JPSS personnel to give real time recommendations to improve MMOD shielding and assessed risk posture. These recommendations played a part in improving the component-level MMOD risk assessments, along with improvements already underway. The critical component risk assessments as of the conclusion of this activity (October 2014) are shown in Table 7.6-1 for comparison to the risk numbers at the beginning of this activity (March 2014). Each of the components saw varying degrees of improvement in values for assessed risk. Most of the components received additional MMOD protection from the addition of either layers to MLI or MMOD blankets. A protective cover was added to the propulsion tank. The results of these modifications combined with a better understanding of the configuration and operational conditions is displayed in Table 7.6-1. JPSS did not perform risk assessments for those components that were not part of the reentry package (e.g., the science instruments). Consequently, the NESC team did not consider how MMOD risk would affect mission success.

Table 7.6-1. Risk Assessments for JPSS-1 Critical Components for Designs as of May 2014 compared to October 2014

Component	Probability of Penetration		
	ORDEM2000/ SSP 30425 (May 2014)	**ORDEM 3.0/ MEMR2 (May 2014)**	**ORDEM 3.0/ MEMR2 (Oct. 2014)**
Propellant Tank	1.1%	26.0%	0.22%
Propellant Lines	3.2%	49.7%	included with Propellant Tank
Battery #1 (Stbd)	1.2%	40.9%	0.84%
Battery #2 (Port)	1.3%	43.4%	0.64%
Command and Telemetry Unit (CTU)	0.5%	9.7%	0.3%
PCDU #1 (Stbd)	0.1%	0.3%	0.21%
PCDU #2 (Port)	0.1%	0.3%	not assessed
SCP #1 (Forward)	0.7%	14.5%	0.81%
SCP #2 (Aft)	0.2%	2.9%	0.29%

The following observations are related to the JPSS-1 risk assessment process.

O-12. Preliminary assessments of risk are most often characterized by a conservative initial approach, including use of the minimum standoff and density of shielding, minimum thickness of rear wall material, and use of the lowest applicable ballistic limit relationship. The JPSS Project has followed this practice for JPSS-1, refined subsequently by program inputs in locations where the MMOD risk was seen to be a driver (e.g., the propulsion tank). Continued refinement of shielding characteristics and failure criteria could lead to a reduction in assessed risk.

O-13. The fidelity of the penetration risk modeling improved throughout the assessment as more details became available and analysts refined the model.

- The spacecraft construction is complex, and representing the applicable details of the construction in the model accurately is difficult.

O-14. The required MMOD risk assessment for safe reentry has been performed, but risk assessment for mission success has not.

- There is no NASA requirement to perform MMOD risk assessment for mission success.

7.7 Correlation of MMOD Environment Models to Failure History

The NESC team considered the possibility of using historical data from satellite failures to evaluate the orbital debris models. In other words, how close do any of the orbital debris models come to predicting either actual failures or observed penetrations?

The first element of a comparison is to determine what type of data is available. *In situ* data exists only for spacecraft components that have been returned to Earth. The Space Shuttle orbiter window and radiator impact data were used to develop ORDEM2000 and ORDEM 3.0. So, as expected, the MMOD risk assessments produced using these models agree relatively well with the impact damage. LDEF was used for ORDEM2000 and was considered too old to be useful for ORDEM 3.0. Other impact data were similarly rejected for being out of date including solar array panels from the HST (one recovered in 1993 and one in 2002), Solar Max hardware flown from 1980-1984, the EuReCa from 1993, and other MIR and ISS witness plates. All of these sources represent exposure at altitudes from 400 to 600 km because they flew at an altitude that allowed recovery via the Space Shuttle and therefore they would not provide any *in situ* information for the altitudes of greatest interest where the models are predicting higher orbital debris fluxes (e.g., JPSS-1's 824 km altitude).

MMOD impacts may also present themselves as anomalies occurring in operational satellites. There are several challenges in using these data to "validate" orbital debris models. Much of the data on satellite failures that has been collected is unavailable due to reluctance on the part of satellite owners and operators to sharing data relative to failures. These data are sometimes considered proprietary information, or the operators are concerned about maintaining reputation. Information on DoD assets is also usually unavailable due to national security concerns. For failure data that do exist, it can be difficult to pinpoint the root cause for a given failure as one due to an MMOD impact. Satellite operators typically place a higher priority on returning the spacecraft to active service over troubleshooting the root cause. Also, there may not be enough information to identify whether a specific anomaly was caused by an MMOD impact. This places a high level of uncertainty on establishing an MMOD-related failure rate for a given satellite population.

If a failure rate is obtained, there are further challenges to correlating that rate to the environment models. There is sometimes a misconception that the MMOD environment models directly result in a risk of penetration. In reality, the environment models are only one of several contributors to an MMOD risk assessment, which is produced using a software application such as DAS or Bumper. Any perceived disconnect between the calculated MMOD-related satellite anomaly rate and MMOD risk assessment is due to other factors along with the MMOD environment models. These other factors include the failure criteria, the fidelity of the risk assessment, and the BLEs chosen. In addition, very few detailed MMOD risk assessments have been performed for robotic spacecraft, limiting the efficacy of a statistically significant correlation. JPSS-1 may present a unique opportunity to gain some insight into its risk predictions. The predecessor to JPSS-1 in the JPSS constellation, S-NPP, uses the same general design as JPSS-1, with some reorientation of components and a few different subsystem designs.

JPSS-1 has undergone a detailed MMOD risk assessment that could be assumed to apply to S-NPP, with some modification (the S-NPP assessment performed before launch was not as detailed or as rigorous as the JPSS-1 assessment). For over 3 years, S-NPP has been in the same orbit as JPSS-1. Comparing the anomaly record of S-NPP to the risk for JPSS-1 may provide some useful insight into the risk assessment process for JPSS-1. The NESC team considered applying Bayesian statistical analysis to the S-NPP anomaly history to quantify uncertainty in ORDEM 3.0, but determined that the uncertainties in the analysis were too great to achieve confidence (See Section 9.0 for an alternate viewpoint). In addition, the S-NPP mission reported anecdotally that no on-orbit anomalies had occurred to that time that could be attributed to MMOD strikes.

The following finding and observation are related to comparisons of satellite historical data to MMOD risk assessments for the purpose of risk assessment validation.

F-26. It is difficult to correlate recorded spacecraft failure rates with those predicted by MMOD models. Reasons for this include:

1. Spacecraft operators are either reluctant to share failure data or unable to discern the cause of failures so it is problematic to obtain MMOD-induced failure rates for operational spacecraft.
2. Failure criteria may drive the risk assessment for MMOD as much, if not more, than variations in the environment model.
3. Most operational spacecraft have not undergone MMOD risk assessments to predict the expected failure rate.

O-15. S-NPP has a similar design and operates in the same orbit as JPSS-1. The risk of MMOD-induced damage on JPSS-1 can, to some extent, be compared to the performance of S-NPP. However, that comparison may become statistically meaningful only after a long period with no failures or after experiencing many failures.

8.0 Findings, Observations, and NESC Recommendations

8.1 Findings

The following findings were identified:

F-1. The degree of uncertainty present in the prediction of the 3 mm orbital debris flux by any orbital debris model at altitudes higher than 600 km has not been characterized, but is expected to be large because of the lack of direct measurements of orbital debris particles smaller than 3 mm at altitudes higher than where the Space Shuttle orbiter operated.

F-2. For the flux for particles < 3 mm, orbital debris model validation for altitudes above 600 km is most effective using *in situ* data.

F-3. The four models that were compared (ORDEM 3.0, ORDEM2000, MASTER-2009, and the current version of ADEPT) agree within a factor of ~2 for most debris sizes larger

than 3 mm, where ground radar has provided data describing the environment over a large range of altitudes.

F-4. The models disagree significantly for particles < 3 mm, which is also the size that poses the highest penetration risk to most spacecraft.

F-5. A higher 1 mm particle flux and assumptions behind the source of those particles constitute the primary drivers for the differences in flux between ORDEM 3.0 and ORDEM2000.

F-6. There are four factors contributing to the divergence of flux values between ORDEM2000 and ORDEM 3.0 from 400 to 600 km up to the JPSS orbital altitude:

1. In ORDEM2000, high-eccentricity intact objects were assumed to have a significantly higher particle production rate relative to low eccentricity intact objects. ORDEM 3.0 does not make a distinction between the rate of production from high-eccentricity and low-eccentricity intact objects, so its 1 mm population has a higher relative contribution from circular orbits than does ORDEM2000.
2. The impact data for ORDEM 3.0 identify a higher proportion of particles as stainless steel/high density at the higher altitudes, the source of which is assumed to come from intact objects (e.g., spacecraft and rocket bodies) in low eccentricity/high inclination orbits.
3. ORDEM 3.0 includes high density particles, which are not included in ORDEM2000. The higher density particles, with a lower area to mass ratio, will decay less rapidly than medium density particles assumed for ORDEM2000, contributing to a greater total flux at higher altitudes.
4. Surface degradation model particle emanation rates in ORDEM2000 and ORDEM 3.0 are significantly different.

F-7. The greater JPSS MMOD risk using ORDEM 3.0 compared to ORDEM2000 is due to two factors:

1. ORDEM 3.0 has a ~13x higher particle flux than ORDEM2000 at the JPSS orbital altitude.
2. ORDEM 3.0 contains high density particles. Smaller high density particles cause the same amount of damage as larger medium density particles and are more numerous. ORDEM2000 does not model high density particles.

F-8. Because all the orbital debris models are consistent at all altitudes for debris fluxes of particles ~3 mm and larger, designing spacecraft to withstand impacts by particles up to 3 mm in diameter will provide the least uncertainty in orbital debris risk.

F-9. The orbital debris risk for JPSS-1 would be reduced if the orbital altitude were <800 or >1000 km.

- The results of the orbital debris model comparisons showed the highest flux between 800 and 1000 km for all of the orbital debris models analyzed.

F-10. In spite of the identified uncertainties, ORDEM 3.0 possesses several advantages over ORDEM2000, MASTER-2009 and the current version of ADEPT:

1. ORDEM 3.0 incorporates the most extensive use of Space Shuttle impact data, including residue chemical analysis. As a result of safety concerns about the orbiters, radiator and window surfaces represent the most complete, thoroughly examined returned spacecraft surfaces.
2. MASTER-2009 and ADEPT do not predict the 1 mm particle flux reflected by the Space Shuttle impact data.
3. ORDEM 3.0 contains high density particles that are not included in the other models, but are present in the Space Shuttle impact data.
4. ORDEM 3.0 includes an updated large-object catalog, including contributions from the FY-1C event, the Iridium-Cosmos collision, and other recent debris-producing events. ORDEM2000 includes none of these, MASTER-2009 includes only the FY-1C debris, and ADEPT includes FY-1C and Iridium-Cosmos debris.

F-11. No source for 1 to 3 mm steel debris particles in ORDEM 3.0 has been definitively identified. Possible contributors include:

1. Surface degradation (e.g., collisions with MMOD) of stainless steel rocket stages with thicknesses near 1 mm.
2. Explosions of non-passivated stages.
3. Ejecta from non-catastrophic collisions. The debris population model in LEGEND does not include ejecta from impacts from particles from 1 to 10 cm, nor a ground-tested non-catastrophic collision model that may apply to upper stages.

F-12. ORDEM 3.0 has no technical documentation describing the validation and verification or user guide information detailing the best uses and limitations.

1. Data for this assessment was provided to the NESC team by ODPO in the form of presentations, spreadsheets, and verbal exchanges.

F-13. The assessed risk associated with meteoroids for individual JPSS components is roughly two orders of magnitude smaller on average than the assessed risk from orbital debris when using ORDEM 3.0 and MEMR2. The difference is roughly one order of magnitude when using ORDEM2000 and SSP 30425.

F-14. The meteoroid flux for 0.1 to 10 mm diameter sizes given by MEMR2 is within an order of magnitude of that produced by the Divine-Staubach model, which is used by MASTER-2009.

F-15. MEM was reviewed by the NESC in 2009 [ref. 15] and found to be appropriate for use in MMOD risk assessments. MEMR2 differs from MEM primarily in the graphical user interface. Neither MEM nor MEMR2 assess uncertainties, which was discussed in the 2009 NESC report.

F-16. Over 90 percent of the orbital debris impacting the JPSS-1 spacecraft have a velocity above 7 km/s, with an average velocity over 12 km/s. Because of this, the BLE Region III curve requires critical understanding.

F-17. The choice of 9.1 km/s as the Region II to Region III transition velocity for steel-on-aluminum uses valid reasoning and assumptions and realistically models the phenomenology associated with the HVI of a steel projectile on a thin aluminum plate. However, this value may not be an appropriate choice for other bumper materials (e.g., MLI).

F-18. There are no BLEs available that were developed specifically for the JPSS-1 structural elements. As a result, risk assessments are being performed using equations that were not developed for the materials or wall configurations used on JPSS-1. Using the modified NNO, adjusted for materials used by JPSS, may be predicting smaller critical diameters (i.e., increased assessed risk) than would BLEs purposely developed for actual JPSS-1 configurations.

F-19. The BLEs used for JPSS were developed for manned spacecraft and take a conservative approach to model spacecraft penetrations beyond a 7 km/s normal impact velocity.

1. HVI test results suggest that the actual Region III BLE may provide higher performance and yield less assessed risk than currently assumed in the modified NNO BLE.
2. Using a modified Wilkinson BLE (80 percent of original Wilkinson BLE, as recommended by Elfer and Bjorkman) resulted in a factor of ~3.4 lower probability of penetration for a 1 meter cube at the JPSS orbit than the NNO BLE.

F-20. Use of the NNO BLE for fixed shield thickness and a range of impactor diameters, as specified by an environment model like ORDEM 3.0, will result in an over-prediction of damage fluence (i.e., increased conservatism) by smaller impactors.

F-21. The JPSS configuration used to perform the MMOD risk assessment resulted in a 9.7 percent failure risk for the CTU contained configuration inaccuracies. These deviations tended to underestimate the assessed risk:

1. The risk assessment assumed a 5 cm (2-inch) stand-off between the MLI blanket and the CTU, while the actual stand-off varies and is less than 5 cm in some locations.
2. The risk assessment used a MLI density of 0.091 g/cm^2, while the actual blanket has a density of 0.034 g/cm^2.

F-22. Higher fidelity analyses of the internal structure and expected failure modes for critical electronics box interior elements aboard JPSS-1 (i.e., examining the resistance of interior critical elements to penetration within each box) may result in a lower MMOD assessed risk for those boxes (compared to assuming any box penetration is a failure).

1. This examination must be balanced with long-term concerns over interior box element contamination from penetrations.
2. This is a first-order assessment and thorough risk evaluation would require HVI testing to verify hydrocode results.

F-23. Exterior wire bundles, especially those on the most-exposed zenith side, on JPSS-1 have not been considered in the risk assessment, and their inclusion in future risk assessments can be expected to increase the assessed MMOD risk.

F-24. Assuming a spherical debris shape is a source of uncertainty in the MMOD risk assessment, some studies suggest assuming a spherical shape (versus cubes or flat plates of the same critical length) may overestimate risk by a factor of ~2. However, not all potential debris shapes have been examined for their effect on risk.

F-25. Apollo-era failure criteria for pressure vessels are being applied to modern era spacecraft without tests or analysis to confirm their applicability.

F-26. It is difficult to correlate recorded spacecraft failure rates with those predicted by MMOD models. Reasons for this include:

1. Spacecraft operators are either reluctant to share failure data or unable to discern the cause of failures, so it is problematic to obtain MMOD-induced failure rates for operational spacecraft.
2. Failure criteria may drive the risk assessment for MMOD as much, if not more, than variations in the environment model.
3. Most operational spacecraft have not undergone MMOD risk assessments to predict the expected failure rate.

8.2 Observations

The following observations were identified:

O-1. The NASA standard break-up model used by LEGEND does not account for the 1 mm population observed in Space Shuttle impact data.

O-2. The surface degradation model in ORDEM 3.0 dominates the population particles smaller than 3 mm.

1. This is based on a default assumption that intact object surface-degradation generates particles that caused the Space Shuttle impacts.
2. Because of the orbital distribution of the source intact objects, most debris-producing surfaces are located in near-circular orbits between 700 and 1000 km altitude.

O-3. The generation of 1 mm stainless steel debris via surface degradation in ORDEM 3.0 is assumed to continue into the future beyond the dates of Space Shuttle impact data.

O-4. The credibility assessment methodology in NASA-STD-7009 (*NASA Standard for Models and Simulations)* was useful in providing a high-level evaluation of ORDEM 3.0, highlighting opportunities for overall improvement and confidence building in the model. This was especially the case for orbital debris particle regimes <3 mm, where focus areas include validation, input pedigree, results uncertainty, results robustness, and model and simulation management. OSMA has determined that this standard is not mandatory for ORDEM 3.0, and an evaluation of this decision was outside the scope of this assessment.

O-5. MEMR2 is calibrated to ground-based radar observations and the data from which the Grun flux was derived.

O-6. ESA's iMEM model is based on modeling and limited *in situ* measurements. ESA has recently concluded that iMEM is not representing the meteoroid environment adequately and is initiating an extensive rework of the model. The Divine-Staubach model (used in MASTER-2009) is also no longer used by ESA.

O-7. NASA TM-2009-214789 (Ref 24) appears to apply the Reimerdes BLE dual wall-to-single wall transition factor, F_2^*, differently than specified by Reimerdes et al. [ref. 22] and verified mathematically by the NESC team. Reference 9 applies F_2^* to the critical particle diameter, while the prescribed method in reference 22 is to apply F_2^* to the critical wall thickness.

O-8. There appears to be an error in the algorithm that defines the ratio of critical wall thickness from the single wall BLE to that from the NNO BLE ($r_{S/D}$) in the Reimerdes BLE definition set forth by Reimerdes et al. in reference 22. The specification in reference 22 to evaluate the $r_{S/D}$ parameter only at the high velocity region boundary results in a BLE curve (impactor diameter versus critical wall thickness) that exceeds the single wall curve as the impactor diameter increases, instead of approaching the single wall curve asymptotically as would be expected. Evaluating the $r_{S/D}$ parameter at the actual normal component of impact velocity appears to rectify the problem.

O-9. Assessing exposed wire bundle MMOD risk is complex, encompassing hard-to-quantify failure contributions associated with variables, such as wire redundancy, bundle size, criticality, and failure modes. This results in a high level of uncertainty for the critical failure probability prediction due to MMOD for JPSS-1.

O-10. Preliminary NESC orbital debris risk assessments for representative wire bundles leading from reentry-critical elements on the zenith surface of the JPSS-1 covered only by baseline MLI predicted that a critical failure penetration per year might be expected for every 100 feet of exposed cables, considering blockage from other JPSS-1 wiring and equipment. This first order analysis was intended to give an estimate of the order of

magnitude risk for the wire bundles. This baseline risk could be reduced through heavier MLI blanket/shielding protection over these zenith bundles.

O-11. The ORDEM 3.0 environment does not explicitly describe the expected shape, or range of shapes possible in the orbital debris environment. It accounts for non-spherical particles when determining debris populations from the radar sources, while assuming spherical particles when associating particle sizes with crater sizes (*in situ* environment).

O-12. Preliminary assessments of risk are most often characterized by a conservative initial approach, including use of the minimum standoff and density of shielding, minimum thickness of rear wall material, and use of the lowest applicable ballistic limit relationship. The JPSS Project has followed this practice for JPSS-1, refined subsequently by program inputs in locations where the MMOD risk was seen to be a driver (e.g., the propulsion tank). Continued refinement of shielding characteristics and failure criteria could lead to a reduction in assessed risk.

O-13. The fidelity of the penetration risk modeling improved throughout the assessment as more details became available and analysts refined the model.

1. The spacecraft construction is complex, and representing the details of the construction in the model accurately is difficult.

O-14. The required MMOD risk assessment for safe reentry has been performed, but risk assessment of mission success has not.

1. There is no NASA requirement to perform MMOD risk assessment for mission success.

O-15. S-NPP has a similar design and operates in the same orbit as JPSS-1. The risk of MMOD-induced damage on JPSS-1 can, to some extent, be compared to the performance of S-NPP. However, that comparison may become statistically meaningful only after a long period with no failures or after experiencing many failures.

8.3 NESC Recommendations

The following NESC recommendations were identified and directed towards the JPSS, ODPO, HVIT, MEO, and NASA/OSMA unless otherwise identified:

Directed to JPSS

R-1. Use MEMR2 as the meteoroid model in JPSS-1 MMOD risk assessments. ***(F-15)***

R-2. Use ORDEM 3.0 as the orbital debris model in JPSS-1 MMOD risk assessments, recognizing that there are large uncertainties associated with the unknown source of stainless steel particles. ***(F-10)***

R-3. Assess the MMOD risk for JPSS-1 wire bundles, include in the overall JPSS-1 risk assessment, and add additional protection if necessary. ***(F-23, O-9, O-10, O-14)***

R-4. Develop BLEs using materials (especially MLI) that are specific to JPSS-1. ***(F-18, F-19, F-17)***

R-5. Conduct trades to determine MLI thickness, spacing, and other elements (e.g., Kevlar® blankets) that will optimize penetration risk for electronics boxes such as the CTU, SCP, and PCDU. ***(F-22, O-15)***

R-6. Add spacers to maintain the desired stand-off between the MLI and critical elements (e.g., CTU). ***(F-22, F-18, O-15)***

R-7. Explore methods to modify the NNO BLE to account for the impeding effect of shield thickness larger than the critical value. ***(F-18, F-19, F-20)***

Directed to ODPO/HVIT

R-8. Concentrate efforts toward characterizing and reducing the uncertainty in ORDEM 3.0. ***(F-1, F-3)***

1. Recommendations R-9, R-10, R-11, and R-19 will help to bound and define the uncertainty.
2. Sensitivity studies that vary assumptions and contributors will also help to bound the model uncertainty.
3. Allowing for periodic updates to the model for solar flux intensity will help to reduce uncertainty.

R-9. Work to identify the source of 1 mm stainless steel particles. This includes creating a comprehensive database of satellite/rocket body material composition and investigating rocket engine firings as a possible source. ***(F-1, F-3, F-4, F-5, F-6, F-11, O-2, O-3)***

R-10. Pursue ground testing to improve break-up models, which would include explosion/HVI testing of complex surfaces representing spacecraft and rocket body structures. ***(F-1, F-3, F-4, F-5, F-6, O-1)***

R-11. Use available *in situ* impact data to help validate ORDEM 3.0 at 400-600 km. ***(F-1)***

1. Impact data from the HST Wide Field Planetary Camera is a possible data source. These impact data have just been received by the ODPO and still need to be formatted for use.
2. Two HST solar arrays have been returned and examined by ESA for impacts. To date, the raw data have not been available.
3. Materials ISS Experiment data may be a data source.
4. These data sources may not include chemical analyses to identify impactor material composition.
5. Look for variations in the data based on altitude.

R-12. Document the data analysis and modeling in ORDEM 3.0 and its validation and verification. Incorporate in the user's guide information detailing best uses and limitations of the model. ***(F-12)***

R-13. Perform HVI testing (especially in Region III) to produce and refine BLEs for steel and aluminum projectiles on typical materials and configurations used by robotic satellites. ***(F-18, F-19, F-17, F-16, O-15)***

R-14. Perform HVI testing to interrogate effect of shape (e.g., cube and flake-shaped particles) on the orbital debris model and penetration risk. ***(F-24, O-11)***

R-15. Update pressure vessel HVI failure criteria for structural materials and impact conditions that metallic spacecraft pressurized elements will likely encounter based on existing data and HVI testing. Use the Apollo-era maximum allowable pressure vessel penetration depth criterion of 25 percent of the pressure shell thickness until the updated assessments are available. ***(F-25)***

R-16. Document guidelines for selection and use of BLEs and failure criteria (e.g., limits for stand-offs, obliquity cut-off, and non-aluminum materials). ***(F-18, F-19, F-17, F-16, F-25)***

R-17. Include internal component configuration inside electrical boxes when assessing MMOD failure criteria, which includes consideration of post-penetration contamination. ***(F-22)***

Directed to MEO

R-18. Incorporate uncertainties in MEMR2 revisions. ***(F-15)***

Directed to NASA/OSMA

R-19. Increase efforts to directly characterize the debris environment, especially at altitudes above 600 km for which there is currently no *in situ* data. ***(F-1, F-2, F-4, F-5, F-6, F-7***)

- Note: Possible ways in which this could be accomplished include examining impact craters on spacecraft at higher altitudes using advanced telescopic imaging, or dedicated missions to directly measure orbital debris at 600+ km altitudes (e.g., the Debris Resistive/Acoustic Grid Orbital Navy-NASA Sensor (DRAGONS) in development to detect MMOD impacts) -- including sample retrieval to analyze the impacts for material composition. As an example, the three Pegasus missions in the 1960's obtained direct *in situ* measurements of the meteoroid environment in LEO. Those measurements have provided an essential description of the meteoroid environment for the last 45 years.

R-20. Create a database of spacecraft anomalies to track and understand MMOD-induced failures. ***(F-25)***

R-21. Issue guidance regarding the conditions for incorporation of orbital debris models into MMOD risk assessments for both new and existing designs. ***(F-3, F-10)***

1. Specific guidance is needed for the use of the DAS assessment tool in the interim until ORDEM3.0 is incorporated into it. Guidance is also needed not only on when ORDEM3.0 is to be phased in, but also how it is to be used.

R-22. Ensure that independent and external peer reviews of technical content and software are performed prior to all new orbital debris model releases. ***(F-1, F-6, F-11, F-12)***

R-23. Use NASA-STD-7009 during the development of new orbital debris model releases to help focus on areas of weakness related to the model and its intended usage. ***(O-4)***

9.0 Alternate Viewpoints

Alternate Viewpoint #1
Alternate Opinion Relative to Observation 8 by Dr. William Vesely

Alternate Opinion to the Observation that Long Time Periods or Many Observed Failures May be needed to Provide Meaningful Statistical Estimates
Dr. William Vesely
Technical Risk Manager
Office of Safety and Mission Assurance
September 30, 2014

Overview

There are two important issues regarding the uncertainty in a risk prediction using ORDEM 3.0 that need to be addressed: 1) the characterization of the uncertainty in an MMOD risk prediction using ORDEM 3.0 to allow updating and revision of the predicted risk, and 2) the effective use of observational data to update and revise an MMOD risk prediction using ORDEM 3.0 or any other code. Having worked for many years in using data to update risk estimates, I want to provide an alternate opinion to the observation in the main body that indicates that a long time period or many failures are necessary to use observation data to update an MMOD risk prediction. Long time periods are not necessarily needed even if no events are observed if the uncertainty is appropriately characterized and effective statistical analysis techniques are used. This applies to effectively using S-NPP observational data to update and revise the MMOD risk prediction for JPSS-1. It more generally applies to using relevant observational data for any other spacecraft.

ORDEM 3.0 has a strong basis in its use of a comprehensive analysis of measured stainless steel debris impacts on the Space Shuttle. The measured impacts are then extrapolated to a postulated stainless steel flux contribution that gave rise to the impacts. The postulated flux contribution is assumed to still exist. The postulated flux contribution in turn results in a significant risk contribution particularly at higher altitudes, (e.g., greater than 600 km), which corresponds to the

altitude of the JPSS-1 mission. There is a potentially large uncertainty in the postulated flux contribution and associated risk contribution because the postulated flux contribution has not been measured nor validated. Also, none of the assumptions have been validated which are used to extrapolate the measured shuttle impacts to the postulated flux contribution.

In spite of these weaknesses, there is a strong motivation to use ORDEM 3.0 because of its strong shuttle analysis basis and because of the implications of the predicted increased flux and risk contribution. However, because of the potentially large uncertainty in the predicted risk the uncertainty needs to be bounded and be characterized in a necessary manner for risk informed decision making and for incorporation of observational data. Without appropriate characterization of the uncertainty, there is no information as to how conservative or non-conservative the predicted risk value may be. As importantly, by appropriately characterizing the uncertainty, observational data can be effectively used to update and revise the predicted risk value and associated uncertainty. This observational data includes data that can be collected not only in the long term, but data that are presently available and can be made available in the shorter term. It includes periods of no failure-causing MMOD hits as well as periods in which MMOD hits occurred. By appropriately characterizing the uncertainty and using appropriate statistical techniques, long observation times and large amounts of data are not needed to provide useable updates and revisions of the predicted risk and associated uncertainty. Approaches for the necessary characterization of the uncertainty in the predicted risk value using ORDEM 3.0, and for effectively using observational data are described in the following sections. These approaches are direct and follow NASA guidelines. Examples and references are given.

The Modeling Uncertainty in ORDEM 3.0

There are two basic uncertainty contributions in ORDEM 3.0 - the parameter uncertainty contribution and the model uncertainty contribution. The parameter uncertainty contribution involves the uncertainty in the measured parameters used in ORDEM 3.0, such as the density and composition of the stainless steel debris impacts analyzed on the Space Shuttle radiators. The model uncertainty contribution in ORDEM 3.0 involves the uncertainty in the modeling and extrapolations used to postulate a new stainless steel flux contribution giving rise to the measured debris impacts on the Space Shuttle. The dominant uncertainty contribution in an ORDEM 3.0 risk prediction is the modeling uncertainty contribution.

The important difference in ORDEM 3.0 from ORDEM2000 and other debris codes is the new, postulated flux contribution containing high density, stainless steel debris. This new flux contribution results in a high risk contribution at higher altitudes, which for the JPSS-1 mission results in the predicted MMOD risk being of the order of a factor of 10 higher than predicted using ORDEM2000. The postulated flux contribution used in ORDEM 3.0 is not unreasonable and is even plausible. However, the new flux contribution in ORDEM 3.0 has not been validated by observation and measurement. Also, the model used to postulate the flux contribution is based on specific assumptions which include the assumption of the stainless steel debris fluxes continuing after the Space Shuttle impacts occurred several years ago, the assumption of particular inclinations and eccentricities for the stainless steel debris flux that determine the flux

patterns and that cause high risks, and the assumption that the stainless steel debris is continually being emitted from surfaces of orbiting spacecraft containing stainless steel. None of these assumptions have been validated. Furthermore, a plausible mechanism by which the stainless steel debris is emitted has not been able to be identified.

Ways to Address the Modeling Uncertainty in ORDEM 3.0

The modeling uncertainty in ORDEM 3.0 due to the extrapolation of the Space Shuttle measurements to a postulated flux contribution is not itself a justification for not using ORDEM 3.0 since it has the strongest foundation in terms of being based on the most detailed analyses of Space Shuttle debris impacts. Furthermore, the implications of the new flux contribution and new risk contribution potentially existing are important enough that they cannot be dismissed. This does not mean, however, that the associated uncertainty in a predicted risk value using ORDEM 3.0 should be ignored since it can be large. Instead, it is critical that the uncertainties be addressed. There are three ways to do this: 1) take detailed *in situ* measurements of fluxes in relevant environments, 2) characterize the predicted risk uncertainty to provide a framework for risk-informed decision making and to allow observational data to be effectively used, and 3) use observational data to update and revise the predicted MMOD risk estimate and associated uncertainty. Taking *in situ* measurements has been addressed in the main body. The other two important ways are addressed in the following.

Characterization of the Uncertainty Range for a Risk Prediction Using ORDEM 3.0

To appropriately characterize the uncertainty associated with a predicted risk value, an uncertainty range and associated coverage probability need to be estimated. The coverage probability is the probability of the risk value lying in the range. In addition, a probability distribution needs to be associated with the uncertainty range. Important points are that only approximate values are needed and that methods have been developed that are standardly used in NASA probabilistic risk analysis and NASA risk-informed decision making (refs. WV-1, WV-2, WV-3, and WV-4). The other important point is that the uncertainty characterization is only an initial estimate which is subsequently updated and revised as additional observational data and knowledge are obtained. Methods and software for doing this for risk estimates are described in the NASA guidelines given in the references. The methods are straightforward and involve the use of probabilistic approaches to characterize uncertainties.

An example of the application of the guidelines to the characterization of the uncertainty in an MMOD risk estimate for JPSS is useful. It is not as thorough as it would be for an application, but it illustrates the basic processes and rationale used. As an initial assessment, it can be reasoned that because the predicted risk value for JPSS using ORDEM 3.0 differs by approximately a factor of 10 from that using ORDEM2000, therefore approximately a factor 10 uncertainty needs to be assigned to the predicted MMOD risk value using ORDEM 3.0. This treats the difference in the risk predicted value using ORDEM 3.0 as an uncertainty because of the present lack of validation for ORDEM 3.0. It also allows for the possibility that the predicted MMOD risk value using ORDEM2000 is applicable. A moderate coverage probability (i.e., a moderate confidence, such as 75 percent) is associated with the uncertainty range to reflect the

situation that there is not a high confidence in the range. To complete the uncertainty description, an uncertainty distribution is associated with the uncertainty range to allow for use in risk assessments and to allow updating and revision with observational data. A gamma distribution or log normal distribution is commonly used as risk uncertainty distributions in risk predictions. Each has its own features. Both could be used and differences be included in the final uncertainty characterization.

The above is only a preliminary assessment, but it provides a framework for refinement for an actual application. For refinement, a more consensual basis for the uncertainty characterization would be carried out. Also, a more analytical basis for estimating the uncertainty range could be carried out by evaluating variations in fluxes and risks that result from different extrapolations in ORDEM 3.0, such as by using different eccentricities and inclinations for the new flux. Plausibilities would be assigned the different fluxes based on expert knowledge and judgment. The focus again would be on general sizes and not precise values. Significant differences in the uncertainty sizes using different assumptions can be incorporated in the overall uncertainty assessment. The procedures and tools identified in the NASA references allow these evaluations to be efficiently carried out. This uncertainty characterization is as important as the prediction of a specific risk value and this work needs to be done.

Use of Observational Data to Update and Revise a Risk Prediction Using ORDEM 3.0

Observational data consists of observed numbers of MMOD hits on relevant exposed spacecraft surfaces in given time periods. The hits can be failure causing or non-failure causing. The observational data can also consist of periods of no hits or no failure hits. The relevant spacecraft are those that are exposed to potential MMOD hits at similar altitudes as the spacecraft whose risk is to be predicted. Differences in exposed areas are handled by appropriately proportioning the exposure probability by the exposed area. Difference in failure criteria can also be handled by appropriately weighting the events. These are common ways of modifying observed data to be applicable to the particular spacecraft of interest and are not the focus here. The focus here is how to systematically use observational data to update an MMOD risk prediction using ORDEM 3.0.

Consistent with NASA risk assessment guidelines, Bayes's rule is applied to update the predicted risk value using observational data. Bayes's rule is a basic probability relationship and its use in analyzing data is termed Bayesian statistical analysis. To apply Bayes's rule to updating an MMOD risk prediction let R be the MMOD predicted occurrence rate for failure (i.e., the occurrence rate due to an MMOD fatal hit). The occurrence rate R is in units of per time period such as per year. Let D be a set of observational data such as a number of MMOD occurrences, or no occurrence, in a given time period. Bayes's rule is used to give the updated probability of the MMOD occurrence rate having a specific value incorporating both the model prediction and observational data.

For updating an MMOD risk prediction, application of Bayes's rule gives:

$$P(R/D) = \frac{P(D/R)P(R)}{P(D)} \tag{1}$$

where

$P(R/D) =$ the updated probability that the MMOD occurrence rate has value R including the observed data D and the ORDEM 3.0 prediction (2)

$P(D/R) =$ the observational probability for the data D using an MMOD occurrence rate with value R (3)

$P(R) =$ the probability that the MMOD occurrence rate has value R based on the ORDEM 3.0 prediction (4)

and

$P(D) =$ the probability of the observed data over all possible values of the MMOD occurrence rate. (5)

$P(D)$ is a normalization factor and is the sum (or integral) of the numerator of Bayes's rule over all possible occurrence rate values.

The key factor in Bayes's rule is the uncertainty characterization $P(R)$, of the MMOD occurrence rate which is the probability of the predicted occurrence rata having a specific value. As indicated this probability is commonly represented as a gamma distribution or log normal distribution over the uncertainty range. The observational data probability $P(D/R)$ is the standard Poisson probability of observing a given number of MMOD occurrences or zero occurrences in a time period. This is the standard probability used for occurrences of discrete events and is used in ORDEM 3.0. Substitution of the probabilities for a particular MMOD prediction and for given observational data yields the applicable updated predicted probability. Examples are given in the next section.

Before the examples, it is useful to contrast the use of Bayes's rule with the use of a purely empirical statistical estimate, which is also termed a classical statistical estimate. The empirical statistical estimate only uses the Poisson observational data probability $P(D/R)$ and ignores the model prediction $P(R)$. The predicted model occurrence rate and associated uncertainty are thus not updated in any systematic manner. The observational probability alone is used to obtain a best estimate of the occurrence rate and bounds on the occurrence rate. When there is sparse data as there often is in a risk assessment then the best estimate and bounds obtained are not generally useable since the prediction from the model is not used to direct and constrain the estimate. This is illustrated in the next section. When there is a preponderance of data consisting of a large number of events then the model predicted occurrence rate and associated

bounds using only observational data will be essentially the same as those obtained using Bayes's rule. However, this will generally take a long time and in the meantime the empirical estimates obtained are not useable. This again is illustrated in the next section. The fact that the use of Bayes's rule provides the most information in a timely manner is why it is standardly used for updating a risk prediction in NASA probabilistic risk and reliability assessments.

Examples of Risk Prediction Updates When No MMOD Events Are Observed

Figure 1 illustrates the application of Bayes's rule to determine the factor reduction in the model predicted MMOD occurrence rate for failure when no such MMOD occurrences are observed for a given time period. The factor reduction is the model predicted occurrence rate divided by the updated predicted occurrence rate accounting for the observation of no occurrences. The predicted occurrence rate is taken to be the expected value. The factor reduction in the model predicted occurrence rate versus time period without any observed occurrences is plotted for a model predicted occurrence rate of 0.01 per year for different sizes of the characterized uncertainty. The characterized uncertainty in the model predicted occurrence rate is described by the coefficient of variation (CV) which is the standard deviation in the predicted occurrence rate divided by the expected value of the occurrence rate. The coefficient of variation is also commonly called the error factor. A gamma distribution is used here for the uncertainty distribution and a Poisson distribution is used for the observational probability.

As seen from Figure 1 the factor reduction is always greater than one for any non-zero observation time period since the updated predicted occurrence rate is less than the initial model predicted occurrence rate. For a large uncertainty in the prediction (e.g., for CV=5), the factor reduction is relatively large and hence there is a significant reduction in the model predicted value when there are no observed occurrences. This shows the importance of accounting for the uncertainty in the model predicted occurrence rate in effectively using observational data to update the prediction. As also observed, moderate differences in the uncertainty characterization do not cause large differences in the reduction factor for smaller observation time periods. Larger differences in the uncertainty characterization that cannot be resolved can be accommodated by using appropriate bounds on the reduction factor. Figure 2 shows similar plots for a model predicted occurrence rate of 0.1 per year. The factor reductions are now significantly larger for the same time period especially when the uncertainty in the predicted occurrence rate is large. This makes sense since smaller times without occurrences are needed to provide significant reduction when the model predicted occurrence rate is relatively large and has large uncertainty. More details of the evaluations used for Figures 1 and 2, which are meant to be illustrative, are given in Reference WV-5. Using the software described in the NASA guide given in Reference WV-1, similar updates can be efficiently evaluated for any number of observed occurrences for different characterizations of the uncertainty and using different uncertainty distributions.

Figure 1. Factor Reduction in the Predicted Occurrence Rate: Model Predicted Value=0.01

Figure 2. Factor Reduction in the Predicted Occurrence Rate: Model Predicted Value=0.1

In concluding this section, it is instructive to compare the informative results in Figures 1 and 2 with the purely empirical statistical estimates using only the Poisson observational probability and ignoring the model predicted value and uncertainty. Since no occurrences were observed in any of the time periods, the empirical best estimate for the occurrence rate is zero for any observational time period. The empirical 95 percent upper bound for the occurrence rate for any observational time period is 3.7 divided by the time period. This upper bound is generally not usable because of its large value. Even after 20 years with no observed occurrence there is little useful information obtained for updating the model predicted occurrence rate as long as it is below 3.7/20=.18 per year regardless of the size of uncertainty associated with the prediction. This lack of information from the empirical statistical estimates arises because the model predicted occurrence rate and associated uncertainty are not used to provide important information in the updating. This lack of information occurs for any observational data that does not encompass a long observation time or numerous occurrences; it is why Bayesian statistical analysis is standardly used in probabilistic risk and reliability predictions.

Summary

A long time observation time period is not necessary to effectively update and revise an MMOD risk prediction using ORDEM 3.0 if appropriate statistical analysis is used. The appropriate statistical analysis is Bayesian analysis and is standardly used in NASA probabilistic risk and reliability predictions. NASA guideline documents give methods and tools for carrying out this analysis. These methods involve probabilistically characterizing the uncertainty in the predicted risk so that observational data can be effectively used to update and revise the risk prediction. By using these methods relatively short observation time periods and presently available data can be used to update and revise the predicted risk using ORDEM 3.0. A risk prediction using ORDEM 3.0 has large uncertainty due to the lack of validation of the assumptions used. It is therefore important and necessary to probabilistically characterize the uncertainty to not only meaningfully bound the risk value, but to effectively use presently available observational data to update and revise the risk prediction. The other alternatives are to take *in situ* measurements which is direct but costly and longer term or to wait and observe for many years until there are numerous MMOD events on present spacecraft so that meaningful empirical statistical estimates can be obtained. There is a better way in the near term.

References

WV-1. Bayesian Inference for NASA Probabilistic Risk and Reliability Analysis, NASA/SP-2009-569, June 2009.

WV-2. NASA Risk-Informed Decision Making, NASA/SP-2010-576, April 2010.

WV-3. NASA Risk Management Handbook, NASA/SP-2011-3422, November 2011.

WV-4. Probabilistic Risk Assessment Procedures Guide for NASA Managers and Practitioners, NASA/SP-2011-3421, December 2011.

WV-5. Bill Vesely, Updating Factors for the Model Predicted Occurrence Rate from Observational Experience, NESC team paper, August 2014.

Alternate Viewpoint #2
Alternate Opinion Relative to Recommendation 2 by Scott Hull

There is incomplete agreement regarding Recommendation 2 (R-2), which recommends that JPSS use ORDEM 3.0 as the orbital debris model for MMOD assessments, recognizing (and accepting) the large uncertainties associated with the unknown source of high density particles (assumed to be stainless steel). Because this source is neither identified nor characterized over time or altitude (see Findings F-1 and F-11), inclusion of the assumed effects of this high density particle population is premature for orbits higher than 600 km altitude.

All physical data, which suggest the currently assumed surface degradation mechanism, have been collected from Space Shuttle missions between 400 km and 600 km and prior to 2012 (F-1). Slower decay of high density particles drives the model toward a higher flux of these particles at altitudes above those shuttle missions (see F-6), where no data exists. The ORDEM 3.0 model uses a default surface degradation assumption (see O-2) that generation of stainless steel particles will continue, and even increase, into the foreseeable future as additional launch vehicles accumulate (O-3). Three other potential stainless steel particle sources identified in F-11, though, would each result in different long-term evolution characteristics, potentially yielding far fewer stainless steel particles over time, especially at altitudes higher than 600 km. All of this results in uncertainty potentially as much as an order of magnitude for these higher altitude orbits (F-1).

If the effect of this high density population were to only marginally increase the assessed risk, then in the interests of conservatism the responsible course of action would be to accept this assumed additional risk, and modify hardware designs accordingly. For the JPSS example, though, the overall risk using ORDEM 3.0 is approximately 30 times higher than with the previous model, mostly driven by the introduction of the high density population (F-7). In fact, this new high density population accounts for approximately 90 percent of the risk in most spacecraft regions examined in detail, effectively increasing the assessed risk by an order of magnitude. At this time, the evidence for the assumed source of the high density stainless steel population is insufficient to justify inclusion of a mechanism with such a strong effect on the assessed risk.

ORDEM 3.0 includes several important advantages and advances over other orbital debris models, including previous versions of ORDEM (F-10). Since the high density population effects on the ORDEM 3.0 environment have greatest impact above the 400 km to 600 km region (F-5), it is recommended that ORDEM 3.0 be used as-is for missions with apogee below 600 km. However, until additional *in situ* information can be collected to characterize the high density population at higher altitudes, missions with apogee above 600 km (such as JPSS-1) should omit the high density particle contribution when using ORDEM 3.0 as the orbital debris model for MMOD risk assessments. This can be accomplished easily using the existing Bumper III risk assessment tool.

Efforts should continue to identify and characterize the source of the stainless steel particles observed on returned surfaces (R-4). Such information will reduce the uncertainty associated with the ORDEM 3.0 model in the 600 km to 2000 km region, and allow future versions of ORDEM to be used with greater confidence for missions operating in this region. Until that time, such missions should use ORDEM 3.0 without the high density contribution as the orbital debris environment model.

10.0 Other Deliverables

No unique hardware, software, or data packages, outside those contained in this report, were disseminated to other parties outside this assessment.

11.0 Lessons Learned

No applicable lessons learned were identified for entry into the NASA Lessons Learned Information System (LLIS) as a result of this assessment.

12.0 Recommendations for NASA Standards and Specifications

No recommendations for NASA standards and specifications were identified as a result of this assessment.

13.0 Definition of Terms

Corrective Actions	Changes to design processes, work instructions, workmanship practices, training, inspections, tests, procedures, specifications, drawings, tools, equipment, facilities, resources, or material that result in preventing, minimizing, or limiting the potential for recurrence of a problem.
Finding	A relevant factual conclusion and/or issue that is within the assessment scope and that the team has rigorously based on data from their independent analyses, tests, inspections, and/or reviews of technical documentation.
Lessons Learned	Knowledge, understanding, or conclusive insight gained by experience that may benefit other current or future NASA programs and projects. The experience may be positive, as in a successful test or mission, or negative, as in a mishap or failure.
Observation	A noteworthy fact, issue, and/or risk, which may not be directly within the assessment scope, but could generate a separate issue or concern if not addressed. Alternatively, an observation can be a positive acknowledgement of a Center/Program/Project/Organization's operational structure, tools, and/or support provided.
Problem	The subject of the independent technical assessment.

Proximate Cause	The event(s) that occurred, including any condition(s) that existed immediately before the undesired outcome, directly resulted in its occurrence and, if eliminated or modified, would have prevented the undesired outcome.
Recommendation	A proposed measurable stakeholder action directly supported by specific Finding(s) and/or Observation(s) that will correct or mitigate an identified issue or risk.
Root Cause	One of multiple factors (events, conditions, or organizational factors) that contributed to or created the proximate cause and subsequent undesired outcome and, if eliminated or modified, would have prevented the undesired outcome. Typically, multiple root causes contribute to an undesired outcome.
Supporting Narrative	A paragraph, or section, in an NESC final report that provides the detailed explanation of a succinctly worded finding or observation. For example, the logical deduction that led to a finding or observation; descriptions of assumptions, exceptions, clarifications, and boundary conditions. Avoid squeezing all of this information into a finding or observation

14.0 Acronyms List

ADEPT	Aerospace Debris Environment Projection Tool
BLC	Ballistic Limit Curve
BLE	Ballistic Limit Equation
CAD	Computer Aided Design
CAS	Credibility Assessment Scale
CORDS	Center for Orbital and Reentry Debris Studies
CTU	Command and Telemetry Unit
CV	Coefficient of Variation
DAS	Debris Assessment Software
DoD	Department of Defense
DRAGONS	Debris Resistive/Acoustic Grid Orbital Navy-NASA Sensor
EOS	Equation of State
ESA	European Space Agency
EuReCa	European Retrievable Carrier
FEM	Finite Element Model
FY-1C	Fengyun-1C
GSFC	Goddard Space Flight Center
HAX	Haystack Auxiliary Radar
HD	High Density
HST	Hubble Space Telescope
HVIT	Hypervelocity Impact Technology

IADC	Inter-Agency Debris Coordination Committee
IMEM	Interplanetary Meteoroid Engineering Model
ISS	International Space Station
JPSS	Joint Polar Satellite System
JSC	Lyndon B. Johnson Space Center
LaRC	Langley Research Center
LD	Low Density
LDEF	Long Duration Exposure Facility
LEGEND	LEO-to-GEO Environment Debris Model
LEO	Low Earth Orbit
LVLH	Local Vertical Local Horizontal
MASTER	Meteoroid and Space Debris Terrestrial Environment Reference
MD	Medium Density
MEM	Meteoroid Engineering Model
MEMR2	Meteoroid Engineering Model Release 2
MEO	Meteoroid Environment Office
MLI	Multi-layer Insulation
MMOD	Micrometeoroid and Orbital Debris
MSFC	George C. Marshall Space Flight Center
NaK	Sodium-potassium
NESC	NASA Engineering and Safety Center
LaRC	Langley Research Center
NNO	New Non-optimum [BLE]
NOAA	National Oceanographic and Atmospheric Administration
ODAR	Orbital Debris Assessment Report
ODPO	Orbital Debris Program Office
OM	Orbital Module
ORDEM	Orbital Debris Engineering Model
OSMA	Office of Safety and Mission Assurance
PCDU	Power Control and Distributor Unit
RBD	Reliability Block Diagram
RCS	Radar Cross-Section
RORSAT	Radar Ocean Reconnaissance Satellite
SBM	Standard Breakup Model
SCP	Spacecraft Control Processor
SEI	Standard Environment Interface
S-NPP	Suomi National Polar-orbiting Partnership
SPENVIS	ESA Space Environment Information System
SPH	Smooth Particle Hydrodynamic
SPHC	SPH in C
SRM	Solid Rocket Booster
SSN	Space Surveillance Network

SSP	Space Station Program
STK	Systems Tool Kit

15.0 References

1. E.G. Stansbery, C.C. Pitts, G. Bohannon, et al., *Size and Orbit Analysis of Orbital Debris Data Collected Using the Haystack Radar,* NASA JSC-25245, NASA Johnson Space Center, Houston, Texas, 1991.
2. R.P. Bernhard and M.E. Zolensky, NASA TM-104784, Analysis of Impactor Residues in Tray Clamps from the Long Duration Exposure Facility, Part 1: Clamps from Bay B, 1994.
3. Orbital Debris Program Office presentation, ORDEM 3, part of a review package, Aug, 2012.
4. Orbital Debris Program Office Excel data file, ShuttleImpaceDB_June14.xlsb.
5. Briefing by the ODPO at JSC, July 9-10, 2014.
6. JPSS – PID List – 8May2014_withComments.xlsx, spreadsheet supplied by Eric Christiansen via email, June 25, 2014.
7. Space Environment Information System (SPENVIS), European Space Agency, website operated by Belgian Institute for Space Aeronomy, https://www.spenvis.oma.be/help/background/metdeb/metdeb.html#MWBL
8. JPSS BLEs_BumperSubroutines.docx, word document supplied by Eric Christiansen via email, July 2, 2014.
9. Ryan, S., Christiansen, E.L., "Micrometeoroid and Orbital Debris (MMOD) Shield Ballistic Limit Analysis Program," NASA TM-2009-214789, February 2010.
10. Jenkin, A.B., Sorge, M.E., McVey, J.P., Peterson, G.E., Yoo, B.B., "MEO Debris Environment Projection Study," Proceedings of the Sixth European Conference on Space Debris, Darmstadt, Germany, April 22-25, 2013 (ESA SP-723, August 2013).
11. Jer-Chyi Liou, Mark J. Matney, Phillip D. Anz-Meador, Donald Kessler, Mark Jansen, Jeffery R. Theall, NASA/TP-210780, The New NASA Orbital Debris Engineering Modekl ORDEM2000, May 2002.
12. Alan B. Jenkin, Possible Sources of Stainless Steel Orbital Debris, Aerospace NESC JPSS MMOD Review, July 9, 2014.
13. Glenn E. Peterson, Consideration of Rocket Body Events as a Possible Source of High Density Particles in ORDEM 3.0, Released to NESC study group only, August 18, 2014.
14. *Standard for Models and Simulations*, NASA-STD-7009, July 11, 2008.

15. Squire, M. D, et al.: Independent Review of Constellation (Cx) Orion Vehicle Micrometeoroids and Orbital Debris (MMOD) Risk Analysis. NASA/TM-2009-215912, August 2009.
16. Christiansen, E.L., 1993. "Design and Performance Equations for Advanced Meteoroid and Debris Shields," Int. J. Impact Eng. Vol. 14, pp 145-156, 1993.
17. Bohl, W, et al, 2010. Orion Spacecraft MMOD Protection Design and Assessment," Hypervelocity Impact Symposium Paper, Freiburg, Germany, April 11-15, 2010.
18. Kalinski, M. (2004): "Hypervelocity Impact Analysis of International Space Station Whipple and Enhanced Stuffed Whipple Shields." Master's Thesis, Naval Post Graduate School, California.
19. Squire, M. D, et al.: Micrometeoroid and Orbital Debris (MMOD) Design and Analysis Improvements. NASA/TM−2014-218268/Volume I, May 2014.
20. Bjorkman, M.: Ballistic Limit Equation Updates for BUMPER Analyses Using the ORDEM 3.0 Orbital Debris Environment, JSC-66619, September 2013.
21. Elfer, N.C., "Structural Damage Prediction and Analysis for Hypervelocity Impacts – Handbook," NASA Contractor Report 4706, February, 1996.
22. Reimerdes, H.G., Nölke, D., Schäfer, F., "Modified Cour-Palais/Christiansen Damage Equations for Double-Wall Structures," International Journal of Impact Engineering 33 (2006) 645-654.
23. Christiansen, E. L.: Handbook for Designing MMOD Protection. NASA/TM–2009–214785, June 2009.
24. Ryan, S.; and Christiansen, E. L.: Micrometeoroid and Orbital Debris (MMOD) Shield Ballistic Limit Analysis Program. NASA/TM–2009-214789, February 2010.
25. Frost, V.C., "Meteoroid Damage Assessment," NASA SP-8042, 1970.
26. bleReimerdesNNOwithMLI – Copy_JSC_HVIT.docx, Word document supplied by Eric Christiansen via email, October 6, 2014.
27. NASA Engineering and Safety Panel, 2008. "James Webb Space Telescope (JWST) Integrated Science Module (ISIM) Electrical Cable Protection," NASA RP-08-59, June 8, 2008.
28. NASA Presentation, 2008, "AXAF Harness Meteoroid Protection," January 4, 2008.
29. Matney, et al, 2014. "Orbital Debris Environment Model, ORDEM 3.0," NASA John Space Center Presentation to NESC, March 2014.
30. Williamsen, J. et al, 2007. "A Comparison of NASA, DoD, and Hydrocode Ballistic Limit Predictions for Spherical and Non-spherical Shapes versus Single and Dual Wall Targets, and Their Effect on Orbital Debris Penetration Risk", Hypervelocity Impact Symposium Paper, Williamsburg, VA, September 23, 2007.

31. Williamsen, J. and Schonberg, W. "Effect of Orbital Debris Mass and Shape Variations on Crew Escape Vehicle Risk," Presentation to NESC, 7 November 2008.
32. Cour-Palais, B.: "Hypervelocity Impact Investigations and Meteoroid Shielding Experience Related to Apollo and Skylab." NASA Conference Publication 2360 (1982) page 247.
33. Cour-Palais, B.: "Meteoroid Protection by Multiwall Structures." AIAA Paper AIAA-69-372. *Presented at the Hypervelocity Impact Conference*, Cincinnati, Ohio, April 30-May 2, 1969.

16.0 Appendices

Appendix A. Evidence Network Evaluation
Appendix B. Examination of Possible Sources of High-Density 1-mm Particles
Appendix C. Delta and Atlas Centaur Tanks as Possible Sources of Stainless Steel Orbital Debris
Appendix D. CTU Risk Assessment
Appendix E. JPSS-1 Zenith Deck Orbital Debris Wire Harness Failure Assessment

Appendix A. Evidence Network Evaluation

An evidence network is a tool used by a wide variety of organizations to perform assurance assessments. In an evidence network, also referred to as a credibility assessment, several evidence sources can be identified and then integrated to give an overall level of assurance. Each individual source can be graded according to its identified level of importance, and even a lack of information can be addressed by assigning different support levels to different scenarios. The support levels are combined to give an overall assurance level with an associated uncertainty. Evidence networks are flexible. The number of levels of support can be as large and detailed as required, and levels of support may be expressed in quantitative or qualitative terms. Several software applications are available that produce evidence network evaluations. The charts in this appendix present an example of how an evidence network can be used to evaluate the basis for the 1-mm range stainless steel debris model in ORDEM 3. The example shown uses the AgenaRisk tool.

Using an Evidence Network to Provide a Representation of the Credibility of the High Density Flux Model in ORDEM3.0

Bill Vesely

September 18, 2014

1

Overview

- An evidence network combines the credibilities of different evidence sources to determine the credibility of an associated finding
- Evidence networks are used in a variety of applications including assurance assessments and safety case assessments (1-8)
- An evidence network is shown which identifies basic elements of the high density flux model in ORDEM3.0
- Each element is rated for its basis and credibility using NESC findings: three ratings are used: comprehensive, partial, or minimal
- The ratings are translated to degrees of credibility and are combined (summed) to give the overall degree of credibility of the flux model
- The overall credibility is shown in terms of relative weights for specific credibility intervals

2

Breakdown of the Elements of the High Density Flux Model

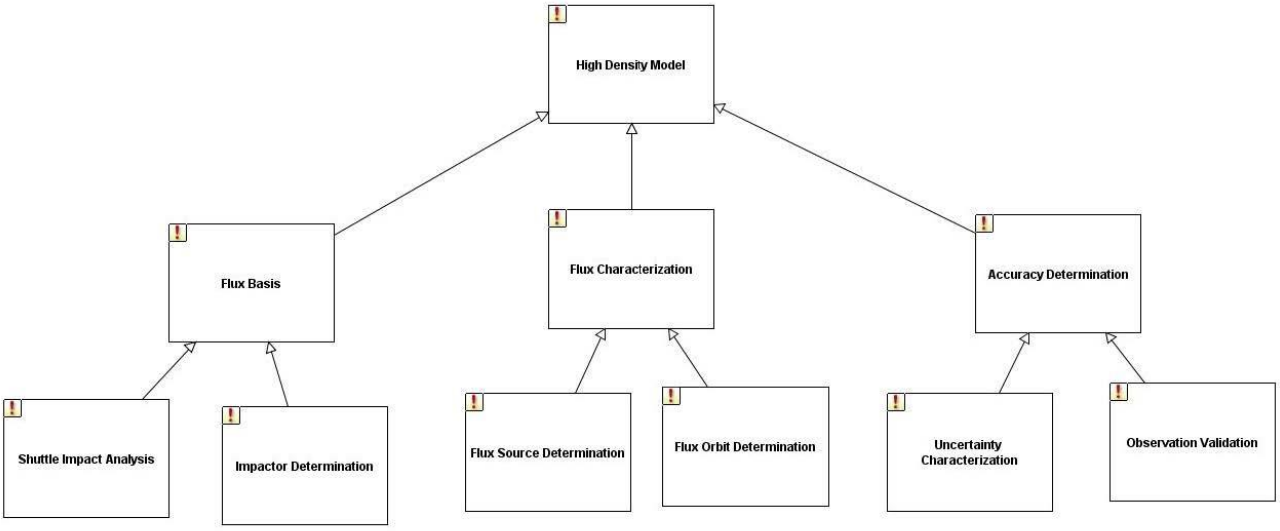

3

Rating Scale of Comprehensive, Partial, or Minimal Basis for Each of the Lowest Level Elements

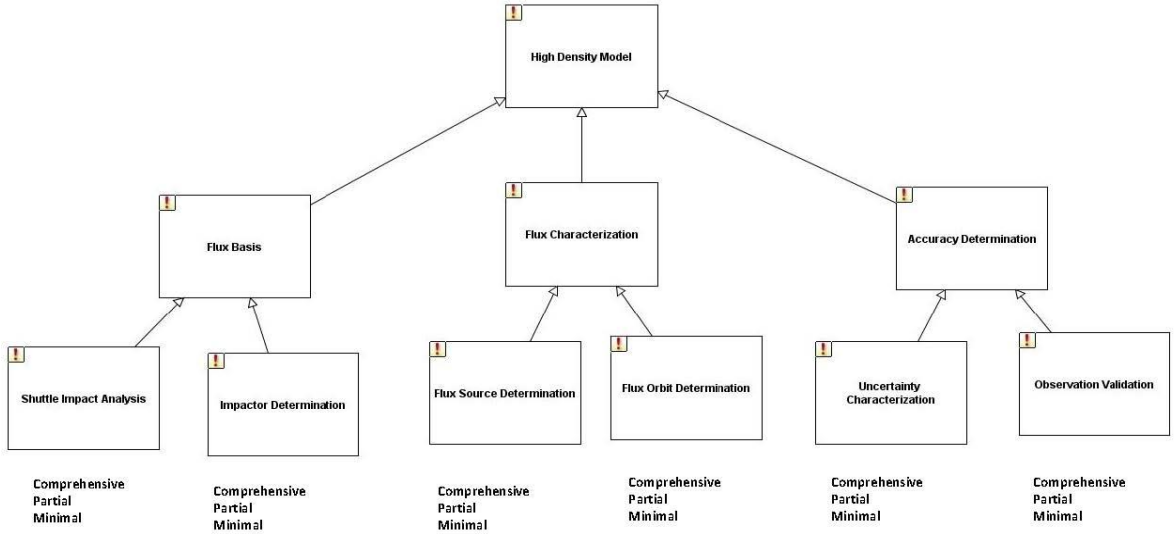

Rating Scale for Each Element

4

Overall Credibility Rating of the High Density Flux Model in ORDEM3.0 Based on Assessments of the Individual Elements

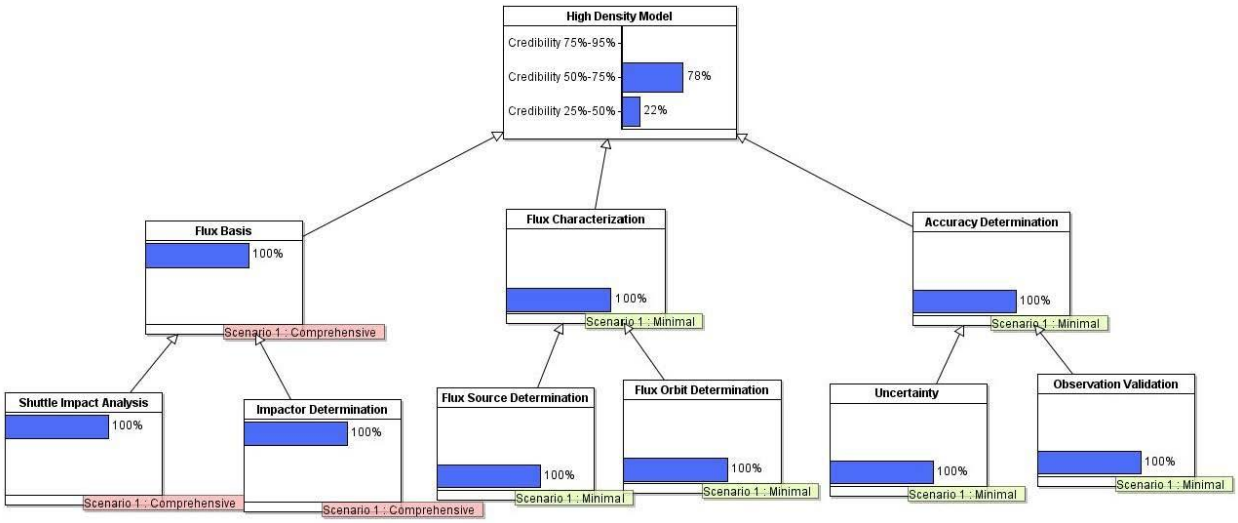

5

References

1. W. E. Vesely, Systematic Quantification of the Prior Risk Assurance of a New System Using Bayesian Evidence Analysis, International Journal of Performability Engineering, Vol. 9, No.6, Nov. 2013, pp. 689-699
2. Norman Fenton and Martin Neil, Risk Assessment and Decision Analysis with Bayesian Networks, CRC Press, 2013 (AgenaRisk® source)
3. R.G. Coswell, A.P. Dawid, S.C. Lauritzen, and D.J. Spiegelhalter, Probabilistic Networks and Expert Systems, Springer-Verlag, 2007
4. Ronald P.S. Mahler, Statistical Multisource-Multitarget Information Fusion, Artech House, 2007
5. Eloi Bosse, Jean Roy, and Steve Wark, Concepts, Models, and Tools for Information Fusion, Artech House, 2007.
6. T. Anderson, D. Schum, and W. Twining, Analysis of Evidence, Cambridge University Press, 2005
7. D. Schum and S. Starace, The Evidential Foundations of Probabilistic Reasoning, Northwestern University Press, 2001
8. R.G. Almond, Graphical Belief Modeling, Chapman and Hall, 1996

Appendix B. Examination of Possible Sources of High-Density 1-mm Particles

Introduction

ORDEM 3.0 is showing a large flux of high-density particles (i.e., steel) at 1 mm size. There are at least 3 possible physical sources of these 1-mm particles: 1) Surface degradation. This is assumed as the current model in ORDEM 3.0, and is likely a conservative assessment (i.e., maximum) given that it assumes all intact objects continually produce particles at a rate dependent on the on-orbit surface area; 2) Explosions. This is a temporally erratic source in the sense that historical explosions do not occur at a uniform rate; 3) Liquid engine firings. Given conversations with propulsion experts, this is not likely a significant source, but these might also produce small stainless steel particles per discussion with ULA regarding their tests of a new RCS thruster. Also, there is little knowledge regarding what foreign rocket engines would produce on-orbit. Residue from firings is likely conservative in the other direction (i.e., minimum) since, once an upper stage has deposited the payload, it will no longer fire and therefore will not contribute any further to the debris environment. In reality, the production of the high-density small particles is likely a combination of the three effects and possibly others.

Figure 1 shows the ORDEM 3.0 1-mm flux profile in the year 2010 as a function of altitude broken down into the high density (steel) and medium density (aluminum) components. High-density particles dominate in the 900-1000 km altitude range but are fairly comparable to the aluminum particles elsewhere. As these particles decay, they cross the higher altitude orbit of satellites such as JPSS and contribute extensively to the survivability risk results. Particles originating lower than ~850 km altitude do not last long enough on orbit to cause long-term issues for orbiting satellites at JPSS altitude.

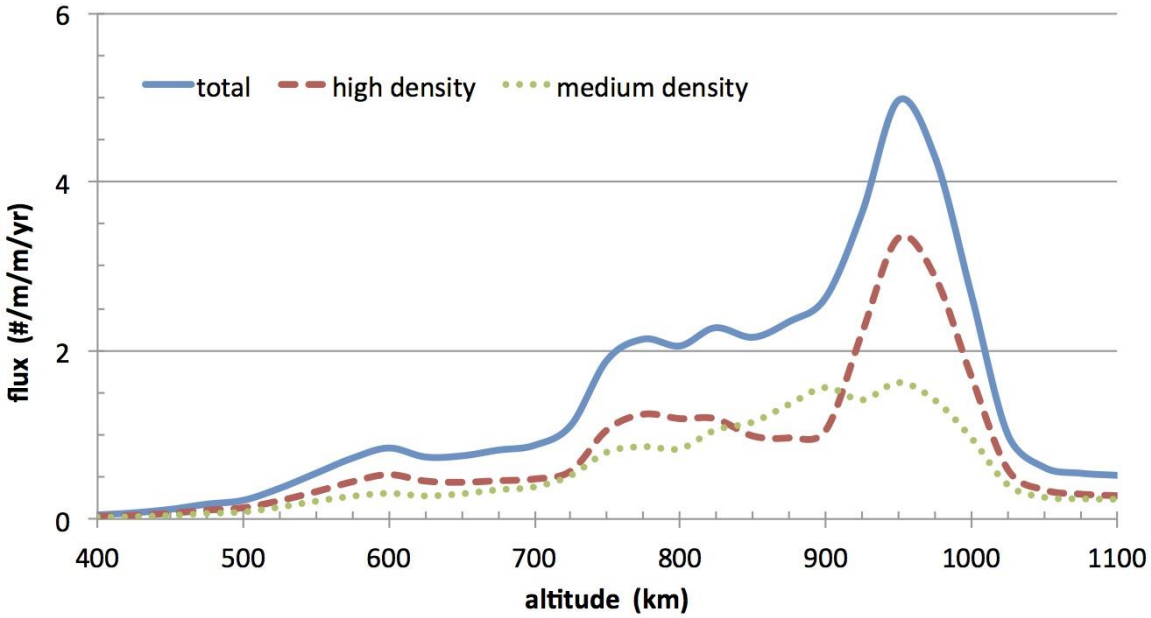

Figure 1: ORDEM 3.0 1-mm Flux as a Function of Altitude for Year 2010 by Source

Figure 2 shows the 1-mm ORDEM 3.0 flux at 950 km altitude as a function of time with the medium and high-density components called out explicitly. The high-density flux continues to grow with time over the ORDEM 3.0 model time span (2010-2035). This is consistent with a surface degradation model that is based on all intact objects emitting high-density particles. As more objects are launched, the overall surface area grows, and the more particles are released. The medium density flux does not grow with time due to decay counteracting the increased surface area, and actually shows a slight decrease during the next anticipated solar cycle maximum. In 2035, the high-density flux at 950 km averages about 41% higher than the value in 2011 (end of STS *in situ* data).

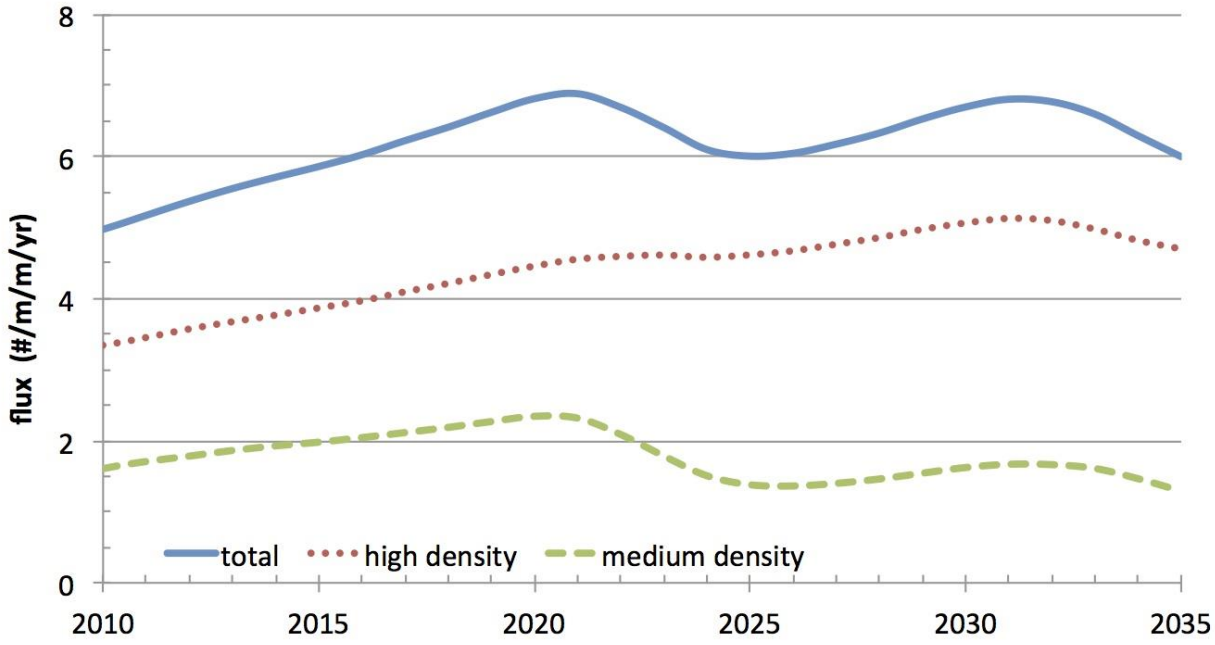

Figure 2: ORDEM 3.0 1-mm Flux at 950 km Altitude as a Function of Time

Surface Degradation

The source of the steel particles is unknown but is currently modeled to be coming from the degradation of exposed surface area of all intact orbiting objects, which implies that the small particles are starting their life in near-circular, high inclination orbits (commensurate with the on-orbit distribution of intact objects). This is a reasonable first estimate. However, there is little exposed steel in satellites and most rocket bodies use aluminum tanks. Atlas/Centaurs did (and still do) use stainless steel tanks, but Centaurs are mostly on high eccentricity, low inclination orbits (Figure 3). Older Delta 1 and Delta 2s also had steel tanks on their upper stages that were very similar to each other but, taken in totality, were split between different types of orbits: high eccentricity/low inclination, low eccentricity/low inclination, and low eccentricity/high inclination orbits. Given the material properties of the two types of tanks (Centaurs: ~355-640 kg in steel tanks depending on the configuration with 0.25-0.5 mm thickness[1]; Delta P/TR-201: ~230-250 kg of steel in main propellant tank, 1-2 mm thickness), then approximately 62% of the steel mass and 68% of the surface area from the Centaurs and Deltas is in high eccentricity/low inclination orbits and only 17% of the steel mass and 13% of the surface area is in low eccentricity/high inclination orbits. If the steel particles are coming from surface degradation off the Centaurs and Deltas, then the majority of these particles should be in high eccentricity/low inclination orbits.

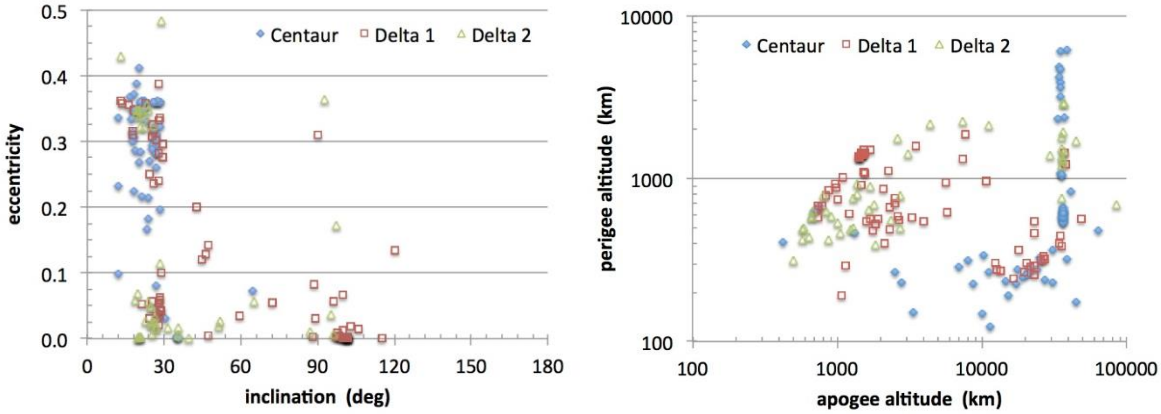

Figure 3: Centaur and Delta Upper Stage Orbit Element Distribution

Figure 4 shows the approximate rocket body mass of the various types of major upper stages beyond the Centaurs and Deltas. Information on the actual material composition of many foreign upper stages is difficult to come by. Therefore, the types of rocket bodies have been grouped by whether their tanks are known to be aluminum, are unknown (but likely aluminum), and known stainless steel. Three columns of data are shown for each upper stage: total mass launched, the current mass that is on-orbit, and the normalized on-orbit mass that passes through LEO (i.e., rocket bodies in GEO, like the Block DM-SL or the SL-12, would not show in this column). The largest contributor to the upper stage mass that is currently both on-orbit and crossing LEO comes from the SL-8 system. However, it is known that the SL-8s used aluminum tanks, not stainless steel. The known stainless steel tanks (Centaur and Delta) are a small part of the overall rocket body mass. This would indicate that, unless the unknowns are mostly steel, then aluminum particles should be produced at a much greater rate than stainless steel particles if surface degradation is the source mechanism.

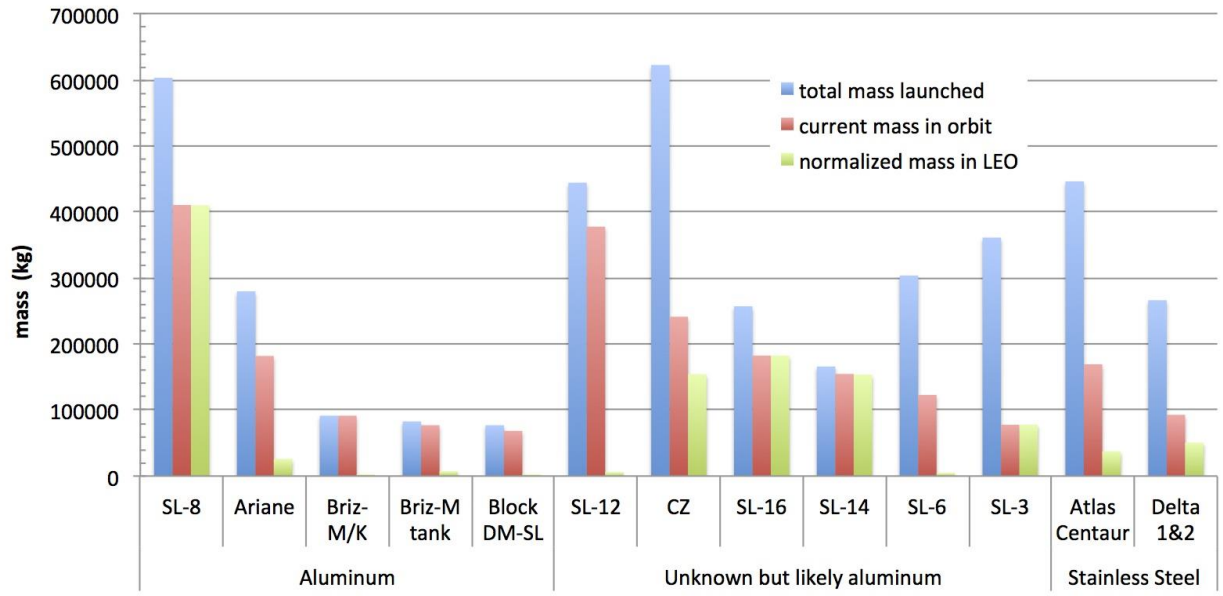

Figure 4: Approximate Mass of Rocket Bodies by Type and Likely Tank Material

Figure 5 shows estimates of the mass and surface area present in the currently orbiting rocket bodies as a function of altitude. The only stainless steel tanks known are those of the Centaur and Delta 1 & 2 upper stages, which do not reside in the 950 km regime therefore they cannot be the dominant source for the large reservoir seen in Figure A.1. There is little available information on engine material composition, but based on older RL-10 data, approximately 6-15% of empty stage weight would be high-density material if the tanks were not stainless steel (mostly in the thrust chamber). There is a large spike at ~950 km altitude corresponding to the peak observed in the ORDEM 3.0 flux plot. There are smaller peaks at lower Sun-synchronous altitude (many types of upper stages) and at ~775 km (mostly SL-8) and ~625 km (mostly SL-14).

Figure 5 also shows estimates of the mass and surface area present in the currently orbiting satellites as a function of altitude. The plots for the satellites are on the same scale as those for the rocket bodies to facilitate comparison. There is little available information on how much high density material is in satellites, but it is thought to be minimal (1-5% by mass) due to the dominance of lighter weight aluminum. As with the rocket bodies, there is a large spike at ~950 km altitude corresponding to the peak observed in the ORDEM 3.0 flux plot. There are also smaller peaks at lower Sun-synchronous altitude (many types of satellites), at ~775 km (Iridium) and at ~500-600 km (Soviet/Russian Tselina-D). The spike at ~900-1000 km is comparable in total mass, but smaller in surface area, for the satellites than the rocket bodies.

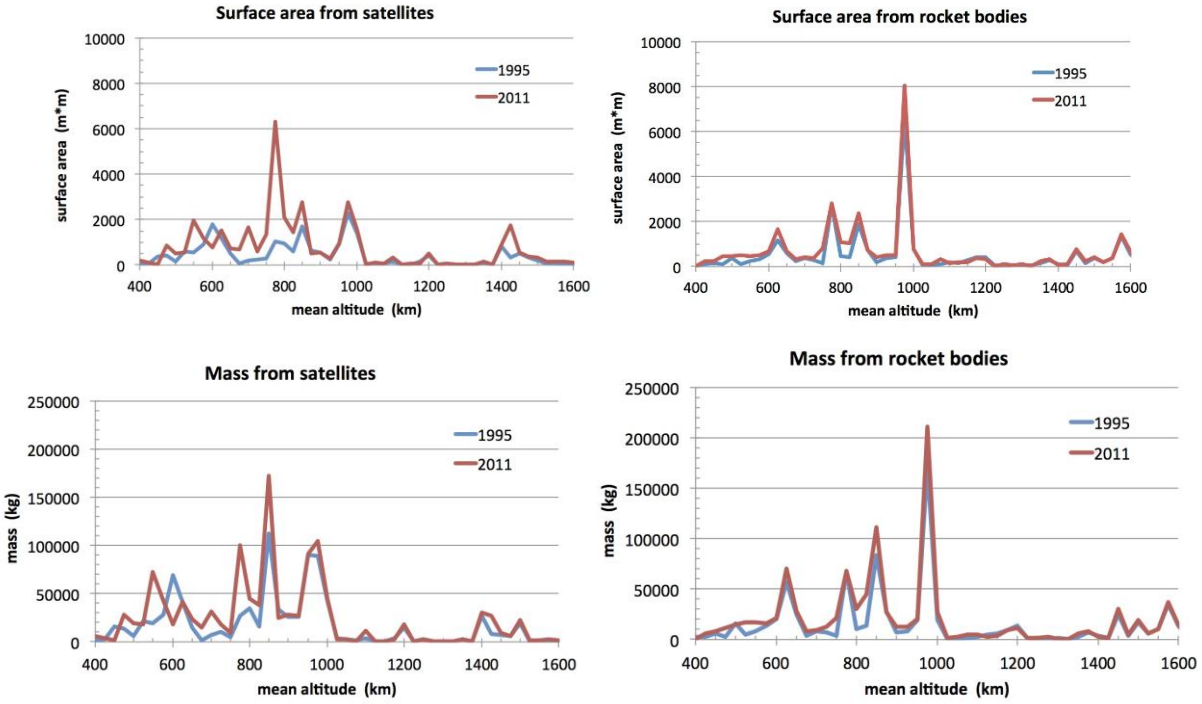

Figure 5: Mass and Surface Area of On-orbit Satellites and Rocket Bodies

The public catalog was then examined to determine what objects lie near 950 km, subject to the following conditions: semi-major axis altitude had to be between 900-1000 km (i.e., near-circular at the right mean altitude), the perigee altitude had to be above 800 km (or any small particles given off with zero relative velocity would decay too rapidly), and only intact satellites and rocket bodies were included (i.e., fragmentation debris was excluded). This left 421 objects (255 satellites, 182 rocket bodies) remaining. Figure 6 below shows the breakdown. The Kaur-1 bus (Soviet) dominates the satellites (145 out of 255), while the SL-8 upper stages (also Soviet) dominate the rocket bodies (165 out of 182).

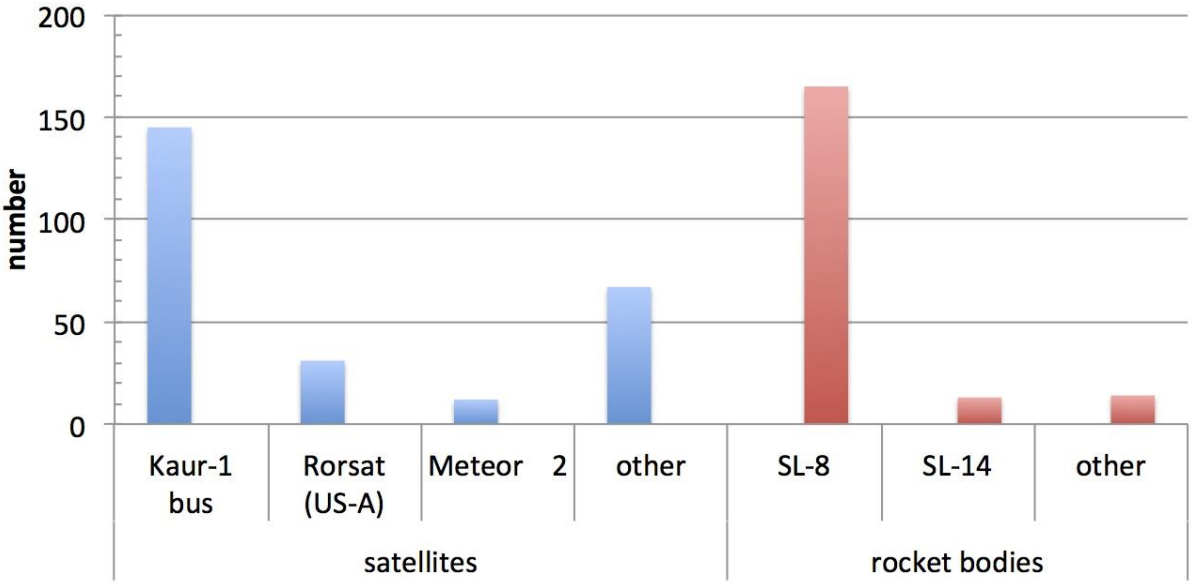

Figure 6: Number of Intact objects near 950 km Altitude by Type

Figure 7 shows the mass and exposed surface area for the examined objects. The SL-8 rocket bodies dominate both the mass and surface area in the reservoir region (47% of the total mass (91% of the rocket body mass) and 56% of the total surface area (87% of the rocket body surface area)). The Kaur-1 bus satellites were used widely on multiple constellations; the Parus, Nadezhda, Tsiklon, Tsikada, and Sfera satellites are all at ~900-1000 km. Other Kaur-1 bus satellites are the GEO-IK at 1500 km and Strela-2 at 785 km. The Kaur-1 bus is a cylindrically shaped satellite with solar cells attached to the body (no panels, except for GEO-IK); thermostatic temperature regulators are also on the surface. It is about 2 meters in length with a diameter of 1 meter and a 600-800 kg mass depending upon configuration and specific mission. By percent, the Kaur-1 bus dominates the satellite mass and surface area (27% of the total mass (58% of the satellite mass) and 25% of the total surface area (65% of the satellite surface area)). (As a side note: the RORSAT satellites are the source of the NaK population due to nuclear core ejections. A casing of stainless steel surrounded the pre-ejected core consisting of ~38 kg of steel per satellite. So, some small amount of steel could have been released by the RORSATs, but not nearly enough to account for the stainless steel particles predicted by ORDEM 3.0.). If the reservoir at 950 km exists and the SL-8s have aluminum tanks, then the Kaur-1 bus should be investigated as the most likely possible physical source of steel.

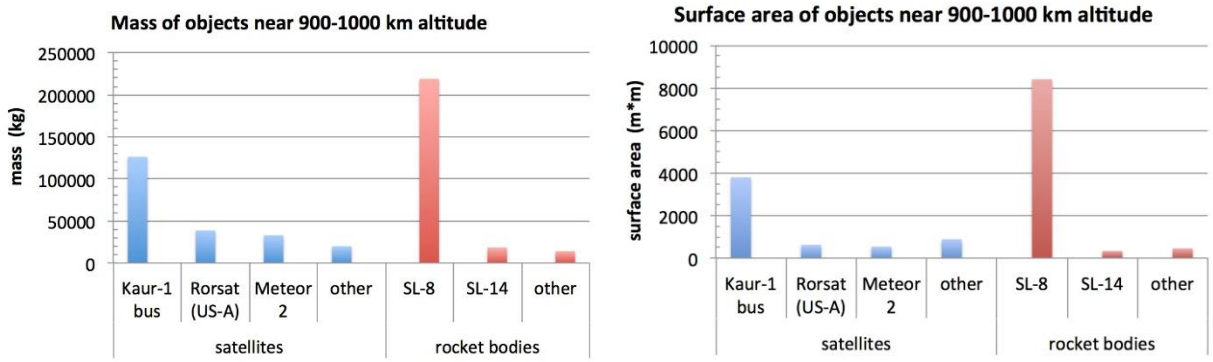

Figure 7: Mass and Surface Area of Intact Objects near 950 km Altitude

Figure 8 shows the number of SL-8/Kaur-1 launches to the ~950 km altitude as a function of time. The last SL-8 launch was in 2010 (to any altitude, not just ~950 km). Long-term models like ORDEM 3.0 and ADEPT assume a future launch model that mimics recent historical activity (2000-2009 time frame). However, if there have been no SL-8 launches to the 950 km regime since 2010, then assuming such activity in the future launch model is not appropriate, and the increase in the 950 km reservoir due to the existing surface degradation model should actually be a constant. It should be noted that the Chinese are placing satellite(s) at ~1100 km with the rocket body from the launch being left in an elliptical orbit crossing 950 km (about 1 per year since 2010).

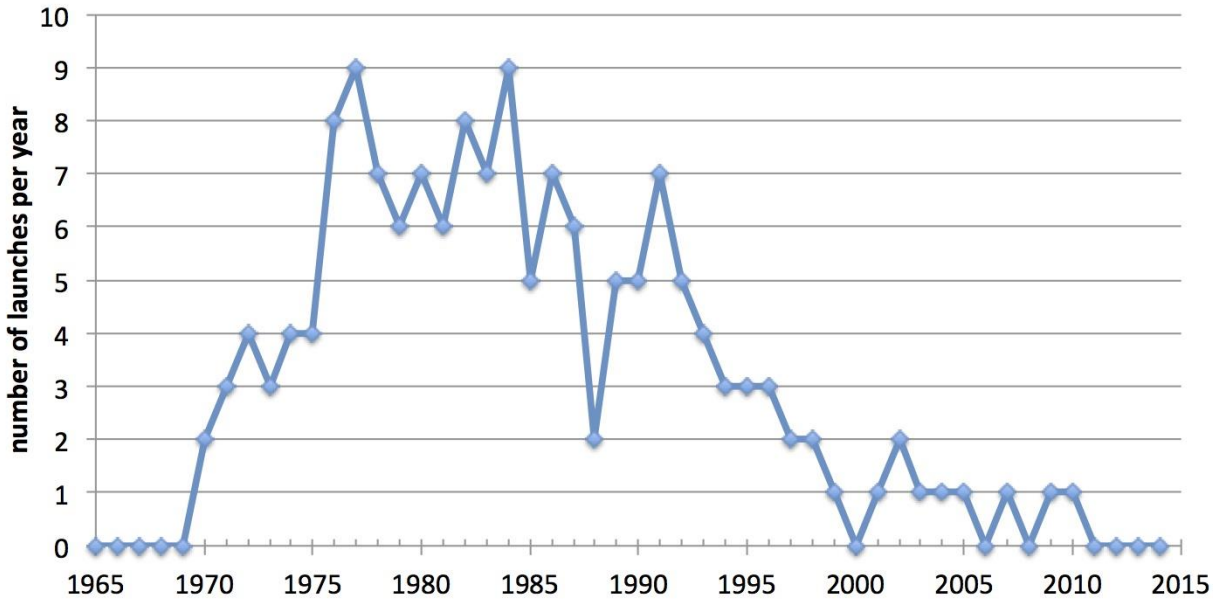

Figure 8: SL-8 Launches to 950 km Altitude

On-orbit Explosions

Another possible source of the 1-mm particles is on-orbit explosions of upper stages. While only some upper stages have steel propellant tanks, all have steel parts in their engines (mostly in the thrust chamber) so that the rocket engines may be composed of one-half high-density material by mass. While the thrust chambers are protected from surface degradation, explosions could release that material. The Atlas/Centaur upper stages have not had any known explosive debris producing events, but the older Deltas have experienced at least eight such events (7 in 1973-1981, 1 in 1991). A mass balancing is here performed to determine whether the upper stage explosions could have produced enough 1-mm particles to account for the observed *in situ* STS flux.

The mass balancing was performed in two parts. First, determine the high-density mass that is predicted to be on-orbit at the start of the JPSS mission (roughly the current status) based on the ORDEM 3.0 model. Then an estimate is made on how much high density mass has re-entered based on the ORDEM 3.0 model. These two mass values (currently on-orbit + re-entered) together will yield the total amount of high-density small-particle mass that would have been produced if the ORDEM 3.0 predictions were correct.

Then the problem is approached from the other direction. An estimate is made of the amount of high–density mass that would be available from the upper stage events. This estimate will be a conservative upper bound since it only looks at the mass capability of the upper stages and does not include time or only partial disintegration, but it does provide for a check on whether the events could possibly have contributed to the high-density environment. Finally, the temporal variation (decay) of the upper stage event particles is examined to determine if they could have been present at STS/ISS altitude during the 1995-2011 timeframe of the returned *in situ* data.

The computational process to determine the ORDEM predicted high-density mass consists of the following steps: 1) the input data (flux and median velocity) was determined from ORDEM 3.0 runs at 25 km intervals from 400-1600 km for 2017; 2) the spatial object density was computed from the flux and velocity; 3) the volume for each 25 km shell was computed; 4) the number of particles present in each shell is computed through the spatial object density times the volume of the shell; 5) the mass of a 1-mm particle is determined; 6) the total mass of high-density particles in each shell is computed as the number times the mass; 7) the cumulative mass is the sum of the individual shell masses. Three particle shapes will be examined: spheres (representing steel that melted during an explosion and then re-formed), cubes (representing chunks from a deteriorating thin (~1 mm) propellant tank skin), and octahedrons (representing nuggets of material that did not melt). All of these shapes are Platonic solids, which has the benefit that their area-to-mass ratios, for the same characteristic length (L_c), will differ only by a constant. For each of the three shapes, the mass for an individual particle was determined using a material density value of 8000 kg/m^3.

Figure 9 shows the amount of high-density mass as a function of altitude in 2017. The plot to the left shows the amount of mass in each of the 25 km shells (note the log scale for the y-axis). The amount of high-density mass at JPSS altitude ranges from 72 to 227 kg. The plot to the right shows the cumulative high density mass. Accumulation was performed from the bottom up (the values in the plot show the total mass at and below a given altitude). For example, the total mass of steel

1-mm particles at or below the JPSS altitude (824 km) ranges from 413 to 1297 kg. Approximately half of the mass is below 950 km, about half above. The total amount of high-density mass in LEO ranges from 1700 to 5200 kg.

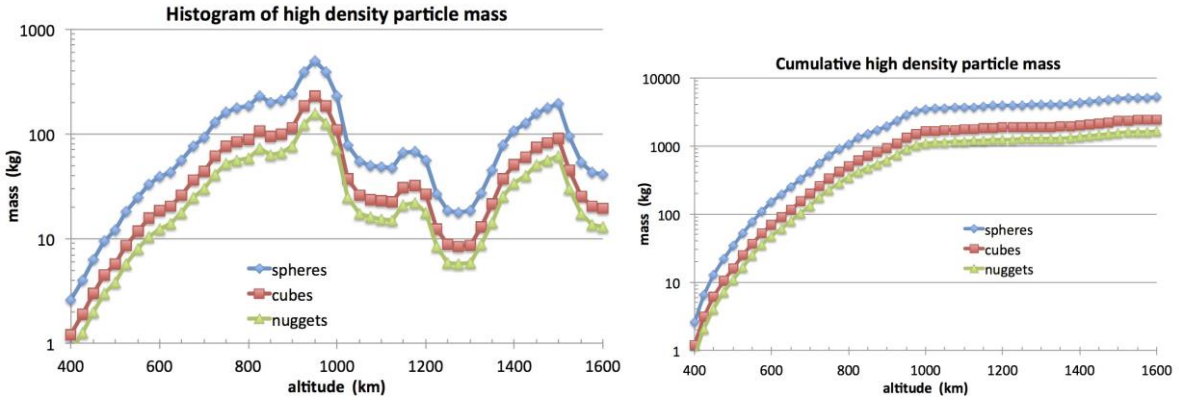

Figure 9: High-density Mass as a Function of Altitude Predicted from ORDEM 3.0

To compute the amount of particles that decay in each year, the 1-mm high-density ORDEM 3.0 flux is adjusted back to the time frame of the rocket body events (i.e., 1970, 1974, etc.). Then for each year, sample 1-mm particles are propagated to establish the altitude at which decay takes 1 year. The flux at and below this altitude gets removed for that year, and finally the mass equivalent to the flux that decayed is computed.

The ORDEM 3.0 model does not allow for the selection of years prior to 2010. To account for this, it is noted that the 1-mm high-density flux in the model assumes the small particles are produced as a function of on-orbit intact surface area. Therefore, when computing how much high-density mass has decayed since the upper stage explosions, the ORDEM 2010 flux was scaled by the historical time-varying surface area curve. For example, since the surface area in LEO in 1995 is approximately one-half of the current surface area, then the 1-mm high-density flux in 1995 is one-half of the current flux.

In any given year, the effect of decay will depend upon the level of atmospheric activity. The atmospheric activity profiles used are the historical values from Marshall Space Flight Center. Roughly speaking and noting that there is a slight difference between the three particle shapes, then for an average atmosphere, the maximum STS altitude of 600 km is where a 1-mm particle will have a lifetime of 1 year.

The resulting amount of 1-mm high-density mass that has decayed out of the environment will depend upon the level of atmospheric activity with annual values ranging from 14-256 kg per year (Figure 10). When summing over time, ~2200-4300 kg of high density mass should have re-entered between 1970 and 2017. When adding what is currently on orbit to what has decayed, the amount of high-density mass that ORDEM 3.0 predicts to have been created since 1970 is ~3900-9500 kg.

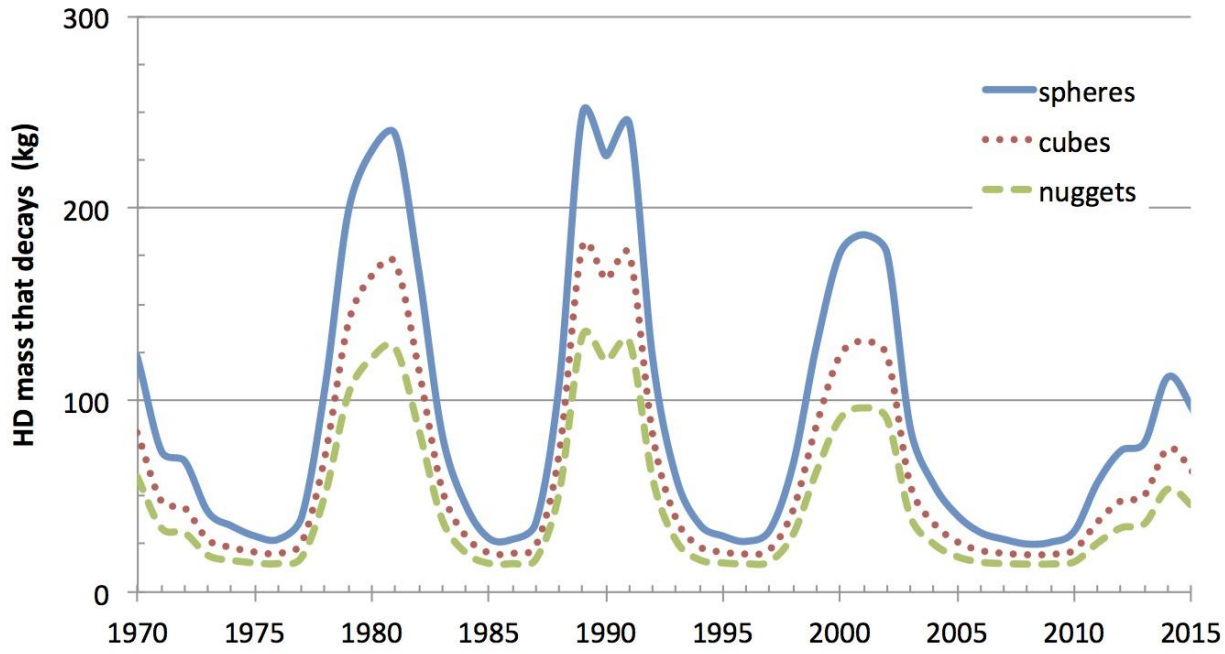

Figure 10: High-density Mass Loss due to Decay

The other side of the mass balance equation consists of the amount of mass that could have been generated by upper stage explosive events. To determine the amount of high-density mass, the most dominant events (i.e., those events that produced the most cataloged debris) were examined[2]. These events were included on the assumption that the events that produced the greatest amount of large tracked debris are also those that produced the greatest amount of small, untracked debris.

Table 1 shows the specific upper stage events that were examined along with an estimate of their possible high density mass. The largest contributors were the 8 Delta upper stages and the 2 SL-16s. Using a mass estimate for the Centaur RL-10 engine[3,4], it is estimated that approximately 1/2 of the mass for a rocket engine is high-density material with most of that in the thrust chamber (~1/3 of the mass) and the rest in mountings, cables, etc. From Table 1, the total amount of available high density mass is ~4800 kg, which is within the range of mass predicted by ORDEM (3900-9500 kg). However, this estimate assumes all the steel was available to create 1-mm particles (i.e., complete disintegration to the 1-mm size). This is highly unlikely and not born from the presence of many objects that are of tracked size (>10 cm), but it does provide a conservative upper bound on how much these events could have affected the environment and is at the lower end of the predicted mass range (3900-9500 kg).

Table 1: Examined Upper Stage Explosive Events

Upper stage	satellite	launch date	event date	num of objs	apo (km)	per (km)	inc (deg)	mass (kg)	engine type	engine mass (kg)	potential for high density mass (kg)
DELTA 1	Landsat 1	7/23/72	5/22/75	226	910	635	98.3	919	TR-201	113	306.5
DELTA 1	NOAA 3	11/673	12/28/73	197	1510	1500	102.1	919	TR-201	113	306.5
DELTA 1	Landsat 2	1/22/75	2/9/76	207	915	740	98.8	919	TR-201	113	306.5
DELTA 1	Nimbus 6	6/12/75	5/1/91	268	1105	1095	99.6	919	TR-201	113	306.5
DELTA 1	NOAA 5	7/29/76	12/24/77	162	1520	1505	102	919	TR-201	113	306.5
DELTA 1	Landsat 3	3/5/78	1/27/81	210	910	900	98.8	919	TR-201	113	306.5
DELTA 1	Himawari	7/14/77	7/14/77	172	2025	535	29	919	TR-201	113	306.5
DELTA 1	NOAA 4	11/15/74	8/20/75	146	1460	1445	101.7	919	TR-201	113	306.5
SL-16	Cosmos 2227	12/25/92	12/30/92	226	855	845	71	8300	RD-120 /RD-8	1505	752.5
SL-16	Cosmos 2237	3/26/93	3/28/93	84	850	840	71	8300	RD-120 /RD-8	1505	752.5
SL-8	Cosmos 61	3/15/65	3/15/65	147	1825	260	56.1	1407	11D49	185	92.5
SL-14	Cosmos 1703	11/22/85	5/4/06	50	640	610	82.5	1407	S5M/RD-861	123	61.5
SL-14	Meteor 2-16	8/18/87	2/15/98	83	960	940	82.6	1407	S5M/RD-861	123	61.5
PSLV	TES/Proba-1/Bird-2	10/22/01	12/19/01	346	675	550	97.9	920	PSLV-4	150	75.0
CZ-4	Fengyun 1B	9/3/90	10/4/90	84	895	880	98.9	1000	YF-40	120	60.0
CZ-4	CBERS-1/SACI-1	10/14/99	3/11/00	345	745	725	98.5	1000	YF-40	120	60.0
ARIANE 1	Spot 1 / Viking	2/22/86	11/13/86	489	835	805	98.7	1457	HM7-A	149	74.5
PEGASUS	STEP 2	5/19/94	6/3/96	713	820	585	82	176	Hercules	104	52.0
THORAD AGENA D	Nimubs 4	4/8/70	10/17/70	385	1085	1065	99.9	673	Bell 8096	132	66.0
THORAD AGENA D	OPS 7613	9/30/69	10/4/69	261	940	905	70	673	Bell 8096	132	66.0
THOR ABLESTAR	Transit 4a	6/29/61	6/29/61	296	995	880	66.8	450	AJ10-104	90	45.0
TITAN 3C TRANSTAGE	OV-2	10/15/65	10/15/65	473	520	210	48.4	1950	AJ10-138 (x2)	110	110.0

However, while the overall mass does balance to within acceptable limits, there is still an issue as to when the particles cross STS altitude and so could have impacted the STS windows and radiators. Many of the events listed in Table 1 occurred years before the beginning of the 1995-2011 *in situ* data; if the particles decayed before 1995, then they could not have been detected through STS impacts. To determine the amount of high-density mass that could have been present during the time and at the altitude of the STS *in situ* data, propagations were performed using a sample data set to represent the 1-mm particles that would have been created by each explosion. This starting population consisted of taking the tracked objects from the catalog for each event and assigning an area-to-mass ratio consistent with a 1-mm particle. Only cataloged objects that appeared within 1 year of each event were included to avoid objects that had already gone through significant decay. This population is hereafter called the "sample population." The goal then was to propagate the sample population forward using the historical solar cycle activity and determine how many of these objects were still in orbit in 1995 and in 2011 (start and end of STS data). Figure 11 gives a graphical description of the computational process.

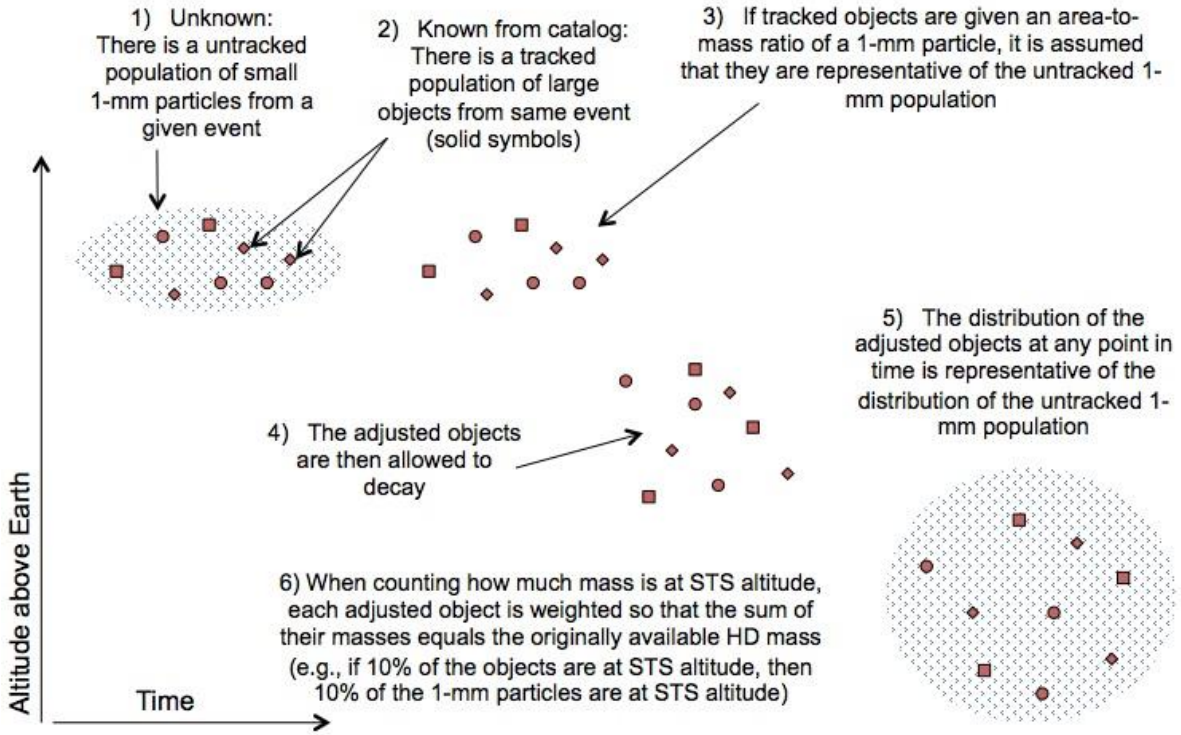

Figure 11: Graphical Description of Computational Process

The assumption here is that the cataloged object population is representative of the orbit element distribution of the 1-mm high-density particles. However, given the limited number of tracked objects from each of these events, the extreme tails of the 1-mm distribution would not be represented. To account for this, when summing to determine the high-density mass at STS altitude, each particle in a given event's sample population was weighted so that the sum of the

sample population's mass would be equivalent to the potential high-density mass for that event (Table 1). Examining the sample population during 1995 and 2011 will give an approximate idea as to how much of the event-created 1-mm population was still in orbit at those times.

Figure 12 shows the initial conditions of each of the Delta events used in the propagation. The plot on the left shows the number of cataloged objects available for analysis with a total sample population of 1289 objects. The plot on the right shows the spread in the perigee altitude for each event of the cataloged objects. It should be noted that six of the events had some objects with initial perigees in the STS range. These 1289 objects were given 1-mm area-to-mass ratios and propagated forward.

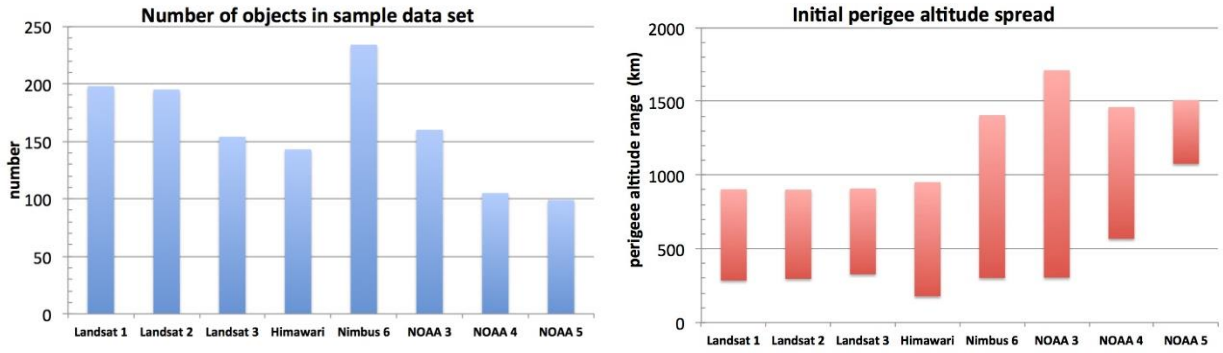

Figure 12: Initial Conditions of the Delta Sample Data Sets

Figure 13 shows the perigee histogram of the sample Delta particle population that was still on-orbit in 1995 and 2011 (dotted line shows the original spread). By 1995, that portion of the original population residing at lower altitudes was largely gone (largely the Landsat and Himawari Deltas). At higher altitudes (Nimbus and NOAA Deltas), little decay had occurred. By 1995, most of the Delta particles that were going to decay have, and those that were too high to experience decay by 1995 still had not decayed by 2011. Between 1995 and 2011, 54 sample particles passed through STS altitude out of the original 1289 (or only about 4%). The conclusion here is that the Delta events are unlikely to have contributed many steel particles to the observed STS flux during 1995-2011.

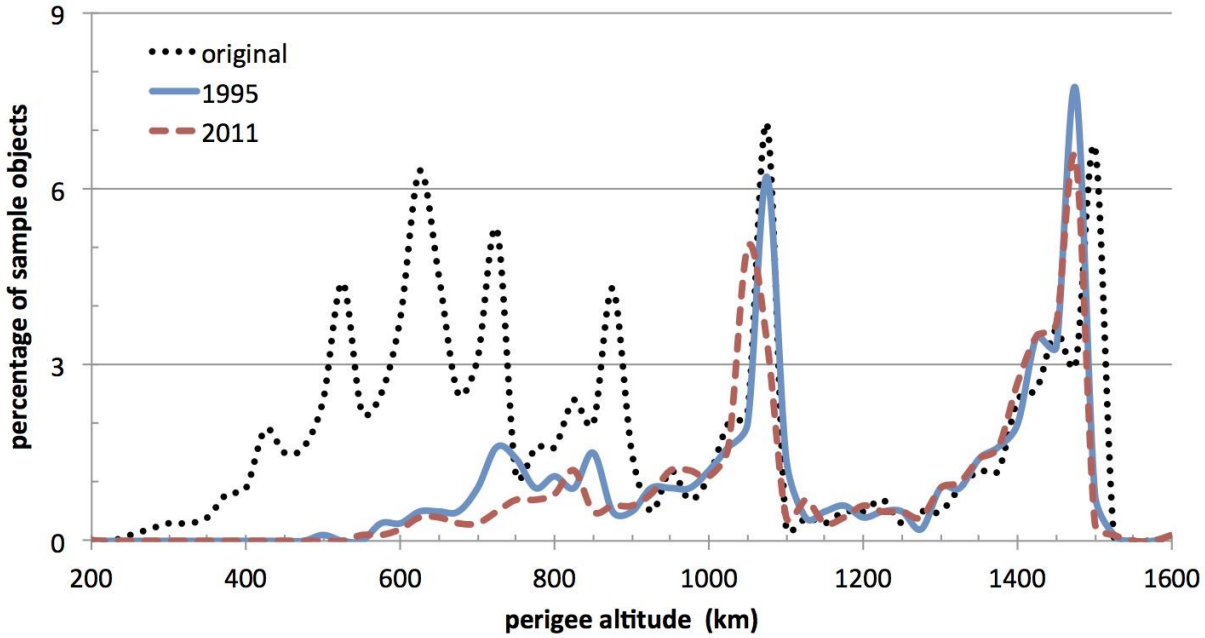

Figure 13: Perigee Altitude Histogram of Delta Sample Particles

Figure 14 shows the ratio of the high-density fluxes in the STS altitude (400-600 km) range for both all of the debris-producing events along with the few that contributed the most (Deltas, SL-16, and SL-14). The divisor of the ratio is the temporally adjusted high-density flux from ORDEM 3.0. The high-density small particle mass from the Deltas is largely gone by 1995, but the mass from the two SL-16 breakups would have been present at STS altitude from 1993-2002. During the years 2006-2010, the SL-14 breakup at ~635 km dominated the system. After ~2012, the sample particles are largely gone from the environment. The values here imply that while the Delta explosive events cannot account for the ORDEM 3.0 modeled flux, the SL-16 and SL-14 events could have contributed a noticeable fraction of the flux to at most a couple tens of percent (again, this assumes complete disintegration).

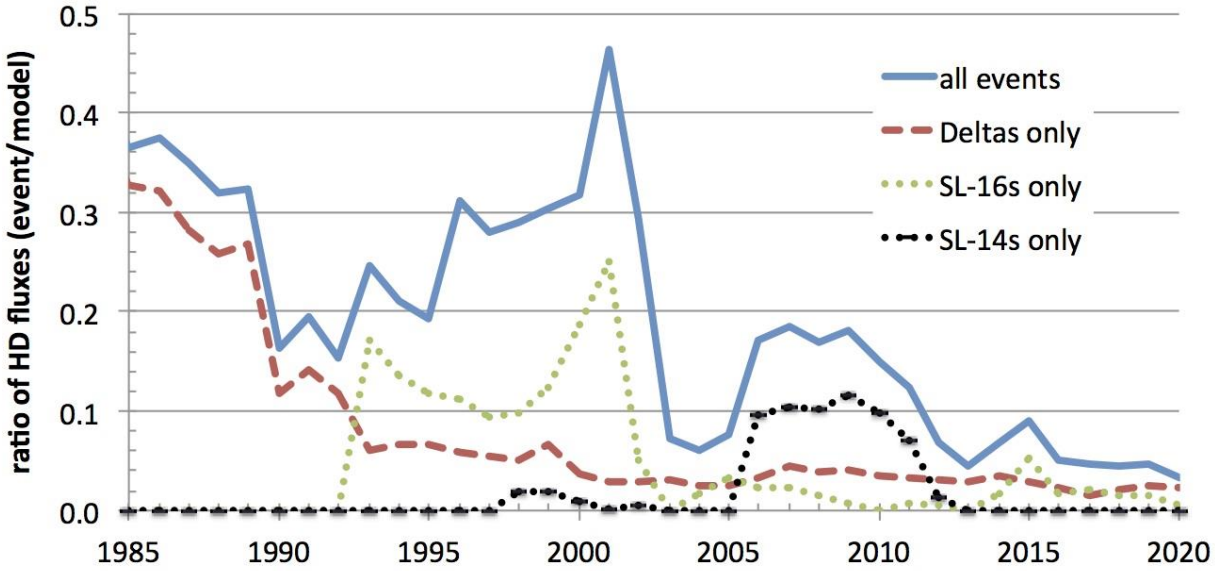

Figure 14: Ratio of High-density Fluxes in the 400-600 km Altitude Range

A comparison was then performed between the ODPO spreadsheet and the predicted high-density mass at STS altitude from the preceding analysis. The spreadsheet's raw steel impact counts were normalized by the number of days the STS was on-orbit for that year (yielding impacts per day). The results are shown in Figure 15. From 1990-1995, all the curves are low; from 95-02, all are high, from 05-11, all are middling. While the shapes of the curves match fairly well, the absolute values of the fluxes do not (Figure 14).

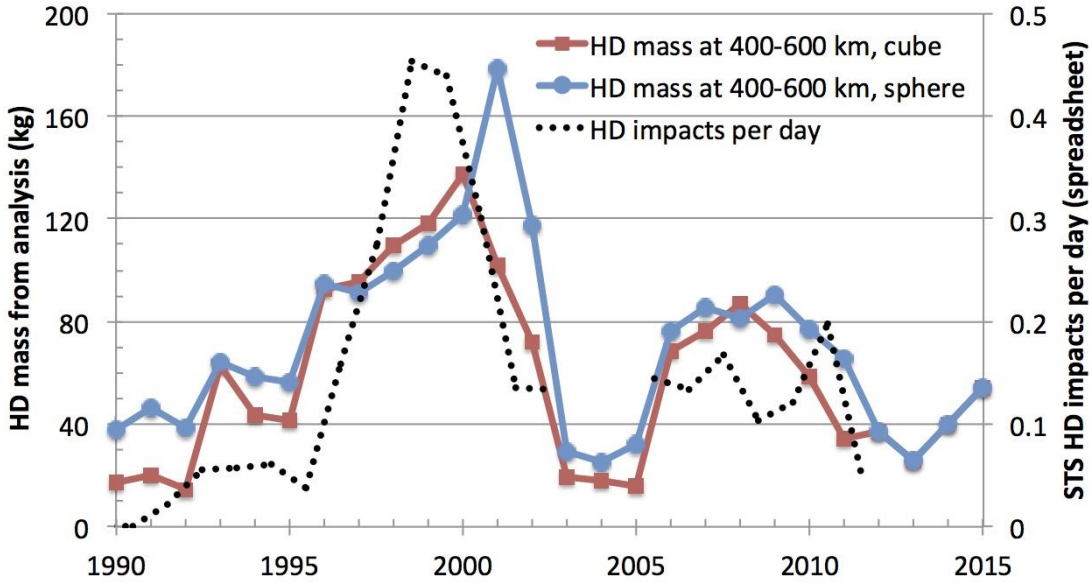

Figure 15: Results of Comparison with ODPO-provided Spreadsheet of STS Impacts

Liquid Rocket Engine Firings in the 950 km Reservoir

A third possible source of small steel particles is residue from liquid engine firings. This source is not likely, but given a lack of knowledge of how foreign engines work (i.e., the SL-8s at 950 km), comments by ULA that a new RCS engine may be emitting small steel particles during test firings, and solid rocket motors giving off aluminum slag and dust, the possibility should be considered.

If the source of the particles were liquid rocket engine firings, then once the upper stage has deposited its payload there would be no further particle production. Since there have been no launches to that regime since 2010 (Figure 8), the ~950 km reservoir should actually be decreasing as the particles decay. This in turn, would cause a general decrease in the amount of flux that spacecraft at lower altitudes would face in the future. To investigate the effect this would have on the reservoir, then for every SL-8 launch, a 1-mm particle was released with zero relative velocity and then followed through time as the particle decays. The issue then is: how long does it take for the particles to decay past either the 900 km point (out of the reservoir) or past JPSS altitude? The thought being that if the firings are the source of the high-density particles in the reservoir, then once they have decayed past 900 km, they are no longer part of the reservoir, and when they decay past 824 km, they are no longer a threat to satellites like JPSS. The base data set consisted of single 1-mm particles released from the actual post-mission parent SL-8 upper stage orbit right after launch. Two sets of area-to-mass ratios were examined: spheres and cubes. Since there were 155 SL-8 launches to ~950 km altitude, 155 sample particles were present in each of the two data sets.

Figure 16 shows the results of the propagation. There are three curves on each of the plots below. The first is the number of sample particles that are on-orbit in any given year, the second is the number of sample particles that are both on-orbit, AND have apogees higher than 800 km (potentially affecting a satellite at JPSS altitude), and the third is the number of sample particles that are both on-orbit, AND have apogees higher than 900 km (still in the reservoir). During the 2017-2024 time frame, only about 12.5% of the cubic particles and 34% of the spherical particles are still in the reservoir. Compare this to the ~33% increase in the flux as seen in Figure 2 averaged over that same time span.

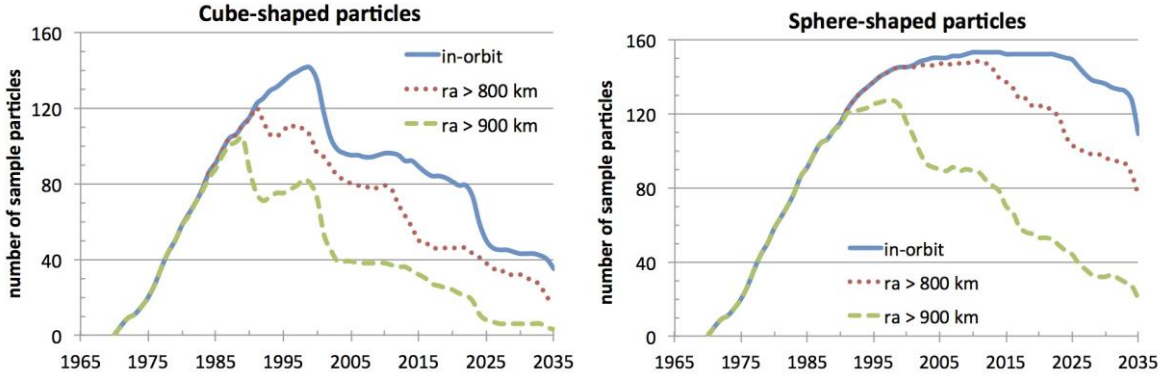

Figure 16: Projected Presence of Small Particles from Rocket Engine Firings

If the source of the high density particles at ~950 km are the SL-8/Kaur-1 objects, then that source is no longer being added to through new launches since the last SL-8 launch was in 2010. If production is due to SL-8/Kaur-1 surface degradation, then the new particles should be added at a constant rate since the SL-8/Kaur-1 surface area is constant. If production was due to SL-8 rocket engine firings, then no new particles are being added to the environment and once the particles decay past a given satellite's altitude, they are no longer a threat.

As a consequence, the ORDEM 3.0 future predictions of the 1-mm high-density flux at the reservoir altitude may be an over-prediction during the JPSS 2017-2024 time frame as compared to the 2011 reservoir flux. The current surface degradation model shows an increase in the high-density flux when going into the future (~33%), but no new launches to ~950 km implies a reservoir flux equal to the 2011 value. Rocket engine firings (spherical) imply that ~34% of the particles remain during the JPSS mission while rocket engine firings (cubic) imply that only ~12.5% of the particles remain. Correctly identifying the source of the high-density particles is crucial and viable source models could change future predictions by a large amount.

Conclusions

The total amount of >1-mm high-density mass predicted by ORDEM 3.0 to be on-orbit in LEO in 2017 ranges from 1700 to 5200 kg. Decay predictions imply that an additional ~2200-4300 kg of high density mass re-entered between 1970 and 2017. This gives a total amount of created high-density mass of 3900-9500 kg.

The total amount of high-density mass available from upper stage explosive events is ~4800 kg if complete disintegration to particles of 1-mm size occurred. Since it is known from the direct observation of tracked objects that complete disintegration did not occur, it is highly unlikely that upper stage explosions can account for all of the predicted steel particles. However, it is also possible that the events can account for a noticeable fraction of the steel. The shapes of the impacts/day curve from the STS data (sparse as the data may be) and the STS-altitude HD event-driven mass correspond fairly well.

SL-8/Kaur-1s are the most likely source of the reservoir of particles at 950 km, but there have been no SL-8 launches since 2010, and furthermore there have been no launches at all to ~950 km since the last SL-8 launch. Therefore, the 950 km reservoir should be either constant (no-new-SL-8 surface degradation model) or decreasing (engine firings) rather than increasing (current surface degradation model).

References

[1]Reusable Centaur Study, General Dynamics, 1974.
[2]History of On-orbit Satellite Fragmentations, 14th ed., NASA ODPO, June, 2008
[3]RL-10 Liquid Rocket Installation Handbook, Pratt & Whitney, 1966
[4]Design Report for RL10A-3-3 Rocket Engine, PWA FR-1769, Pratt & Whitney, 1966

Appendix C. Delta and Atlas Centaur Tanks as Possible Sources of Stainless Steel Orbital Debris

Introduction

Chemical analysis of impact craters on space shuttle windows and perforations on radiator surfaces indicate that some impacting particles contain stainless steel (ref. 1). Impacts by these particles as large as several millimeters were found. The source of these particles has not yet been determined.

A query about which historically launched upper stages and satellites contain stainless steel was submitted to Dr. Mike Weaver of the Fluid Mechanics Department at The Aerospace Corporation (Aerospace). Dr. Weaver has extensive experience performing atmospheric reentry survivability analyses for a wide range of satellites and upper stages. These analyses require detailed information on satellite or upper stage components, including material composition. Dr. Weaver provided the following list of objects that are definitively known to be made of stainless steel: Delta I and II second stage propellant tanks; and Centaur stage propellant tanks.

The objective of this analysis is to briefly investigate the possibility that the Delta I and II second stage propellant tanks and Centaur propellant tanks could be sources of the stainless steel debris that was observed on space shuttle surfaces. In particular, the number of meteoroid impacts that may have created stainless steel ejecta was estimated.

Catalog Information

The unclassified USSTRATCOM catalog of resident space objects (SATCAT) dated June 24, 2014, was examined for information on Delta I and II second stages and Centaur stages. Catalog data showed that as many as 157 Delta I second stages had been flown from 1960 to 1990. As many as 139 Delta II second stages had been flown from 1989 to 2011. As many as 138 Centaur upper stages had been flown on a variety of mostly Atlas and some Titan missions since 1963. Centaur upper stages continue to be flown on Atlas V missions.

A series of Delta I upper stages exploded through 1984. A total of 1882 debris objects had been correlated to Delta I upper stages as of June 24, 2014 (excluding yo-yo weights used for despinning). Of these, 1013 were still on orbit. Only 64 debris objects had been correlated to Delta II second stages, of which 28 were still on orbit. Only 22 debris objects had been correlated to Centaur upper stages, of which eight were still on orbit.

Mechanisms for Generating Stainless Steel Debris

Two possible mechanisms for release of stainless steel debris from intact propellant tanks were briefly considered.

- Generation during upper stage breakups.
- Gradual release of particles from intact tanks due to surface degradation.

Peterson modeled the orbital decay of hypothetical millimeter-sized stainless steel objects from the orbits of cataloged fragments from the Delta I second stages that exploded. Results showed that the majority of such particles would have either reentered before most of the impacts on the shuttle surfaces occurred or not have decayed into the shuttle altitude range by then (see appendix by Peterson).

There are several possible causes of surface degradation. Atomic oxygen and ultra violet radiation are known to cause deterioration of paint, plastics, etc. The likelihood that they could cause stainless steel particles to be released was not considered here. Thermal cycling is also known to cause material cracking, but again the likelihood that this could result in the release of stainless steel particles from stainless steel surfaces was not considered here.

Impacts by orbital debris and meteoroids can produce ejecta. The generation of ejecta due to impacts by meteoroids is considered in this analysis. Ejecta from impacts by other orbital debris particles is plausible but not considered in this analysis due to limited scope of the study.

Meteoroid Impact Analysis

The objective of the analysis was to determine the total number of meteoroid impacts on Delta I, II, and Centaur stainless steel tanks over time. Such impacts may have produced stainless steel ejecta that were observed by the shuttle and that may pose a risk to JPSS. To accomplish this analysis, an estimate of the total on-orbit tank area vs. time was generated. The area at each time was then multiplied by the meteoroid flux at several size levels. The resulting rate of impacts was then integrated over time.

The determination of total on-orbit tank area was performed as follows. In an analysis performed in late 2011 by Bernard Yoo of the Astrodynamics Department at Aerospace, orbital element time histories for intact objects (satellites and rocket bodies) in the SATCAT from end of 2010 were created from time series of two-line element sets obtained from SpaceTrack. org. In the current analysis, the on-orbit object counting tool in the ADEPT suite (Ref. 2) was run on these orbital element histories for the Delta I second stages, Delta II second stages, and Centaur stages to determine the number, total mass, and total area of known stainless steel tanks on orbit versus time from start of the Space Age until end of 2010. This tool determines the effective number of objects at each time point within a specified altitude range using an equation derived by Don Kessler (Ref. 3). Three altitude ranges were considered:

- 200 km to 1000 km: This range contains some atmosphere, and particles may decay into the shuttle altitude range.
- 800 km to 1000 km: This range more tightly fits the JPSS orbit. There is effectively no atmosphere above 1000 km, so particles are unlikely to decay down to JPSS orbit. Particles may eventually cross the JPSS orbit due to eccentricity growth from solar

radiation pressure, but the time spent at JPSS orbit will be diluted due to associated increase in apogee.
- 200 km to 6000 km: More comprehensive, but some objects will be retained that are far from the shuttle altitude range and JPSS orbit.

The following stainless steel tank mass and surface area estimates were used for the analysis.

- Delta I 2nd stage: mass = 229 kg, area = 28.87 m^2. Estimated from data on Delta 1000s at www.astronautix.com; reliability of data unknown. Tank mass prorated from stage mass using Delta II tank to stage mass ratio.

- Delta II 2nd stage: mass = 266.7 kg, area = 14.8 m^2. Determined from data provided by Mike Weaver.

- Centaur stage: mass from contractor data used, area = 136 m^2. Area determined from data supplied by Mike Weaver for previous upper stage lifetime analyses. This is very approximate; there are several Centaur variants.

Figures 1-3 show the effective number, total mass, and total area, respectively, of stainless steel tanks in the 200 km to 1000 km altitude range vs. year. Figures 4-6 show the same plots for the 800 km to 1000 km altitude range. Figures 7-9 show the same plots for the 200 km to 6000 km altitude range. From these figures, it can be seen that the amount of total stainless steel tank mass and area grew steadily from 1960 to 2010. Approximately 14000 kg of mass and 1600 m^2 of area were effectively available between 200 km and 1000 km by 2010. Approximately 3200 kg of mass and 350 m^2 of area were effectively available between 800 km and 1000 km by 2010. Approximately 30000 kg of mass and 4000 m^2 of area were effectively available between 200 km and 6000 km by 2010. As a result, it can be inferred that approximately 16000 kg of mass and 2400 m^2 of area were effectively available between 1000 km and 6000 km by 2010, i.e., there is approximately as much mass and area in the 1000 to 6000 km altitude range as in the 200 to 1000 km altitude range.

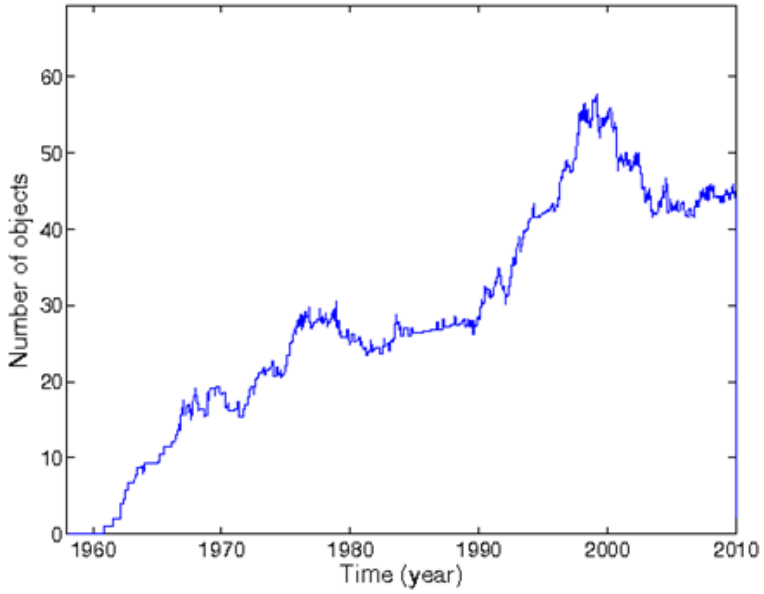

Figure 1. Effective number of Delta I, II, and Centaur stainless steel tanks in the altitude range 200 km to 1000 km vs. time.

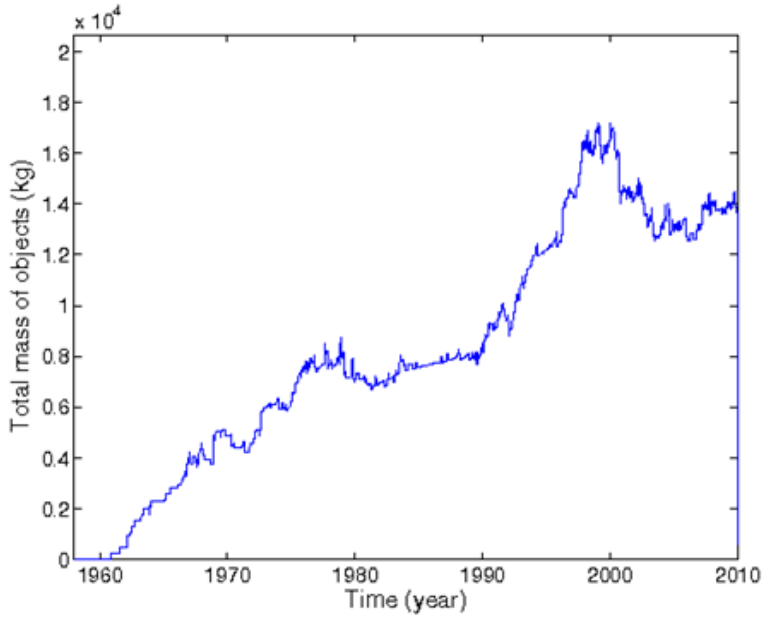

Figure 2. Effective total mass of Delta I, II, and Centaur stainless steel tanks in the altitude range 200 km to 1000 km vs. time.

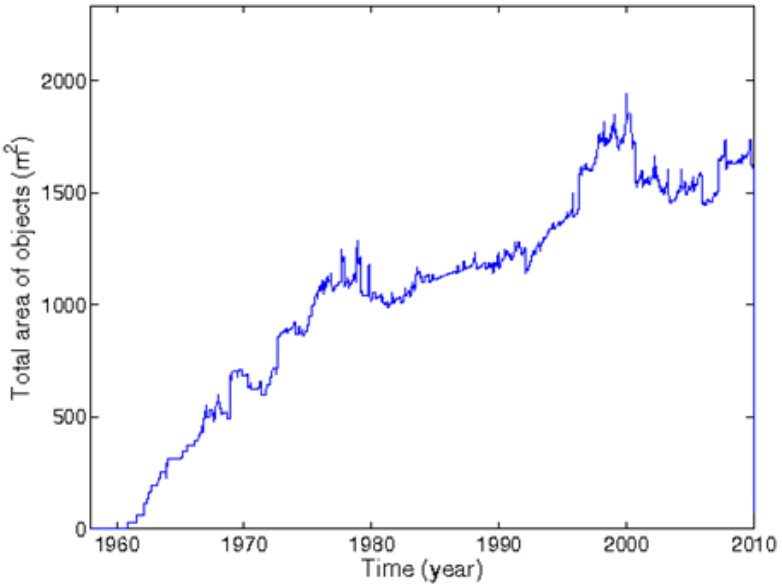

Figure 3. Effective total area of Delta I, II, and Centaur stainless steel tanks in the altitude range 200 km to 1000 km vs. time.

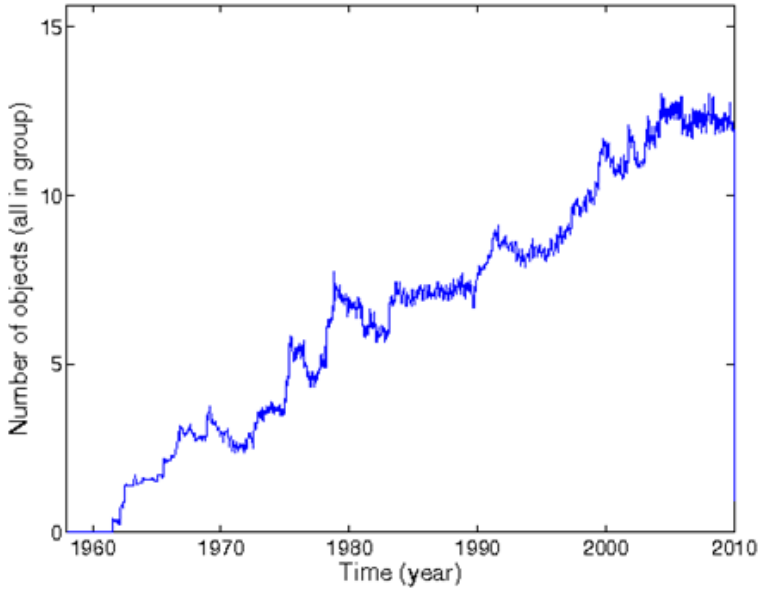

Figure 4. Effective number of Delta I, II, and Centaur stainless steel tanks in the altitude range 800 km to 1000 km vs. time.

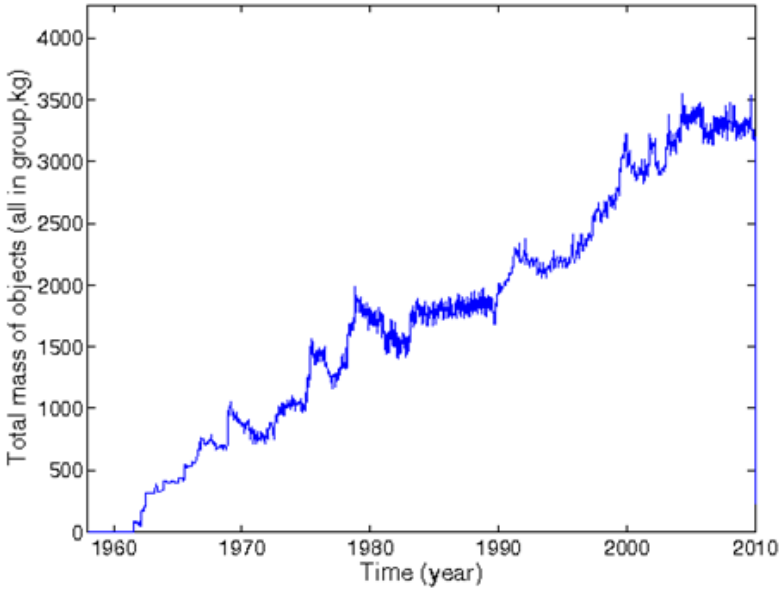

Figure 5. Effective total mass of Delta I, II, and Centaur stainless steel tanks in the altitude range 800 km to 1000 km vs. time.

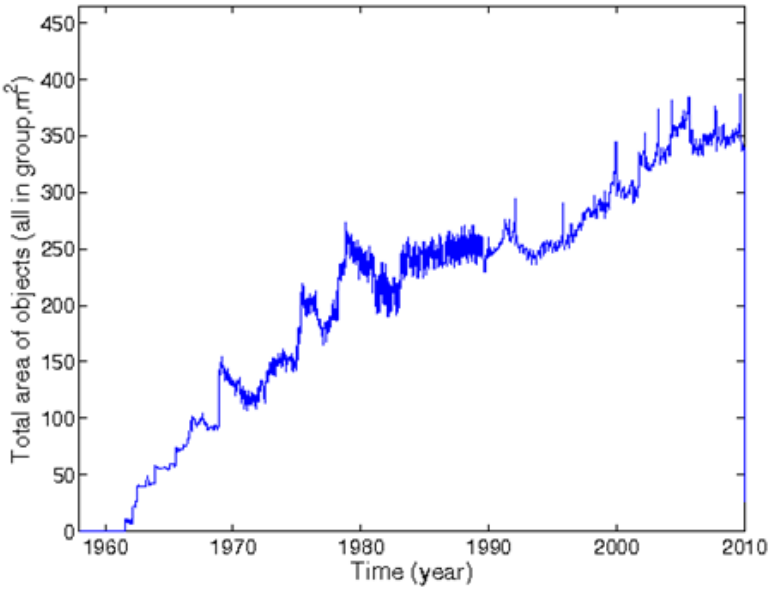

Figure 6. Effective total area of Delta I, II, and Centaur stainless steel tanks in the altitude range 800 km to 1000 km vs. time.

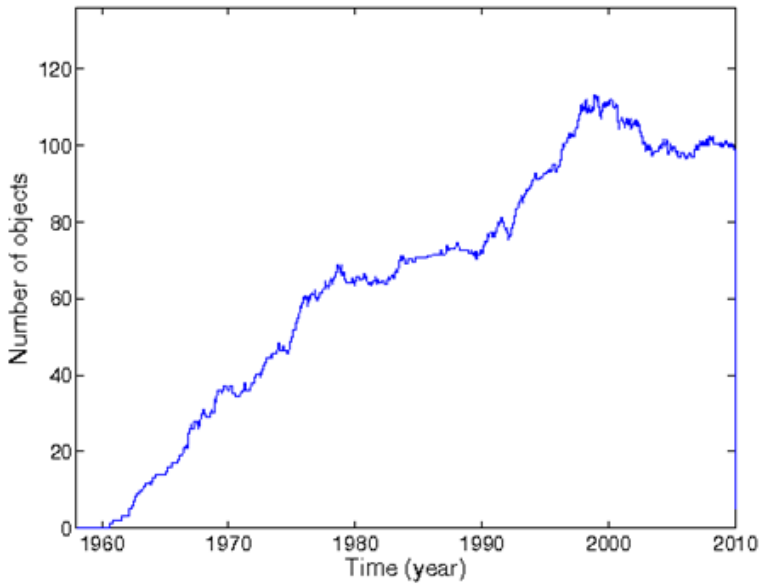

Figure 7. Effective number of Delta I, II, and Centaur stainless steel tanks in the altitude range 200 km to 6000 km vs. time.

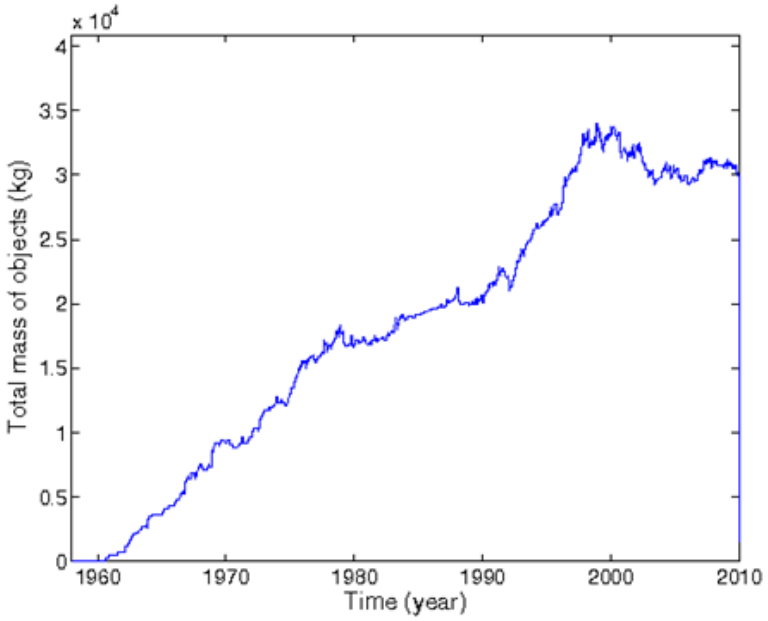

Figure 8. Effective total mass of Delta I, II, and Centaur stainless steel tanks in the altitude range 200 km to 6000 km vs. time.

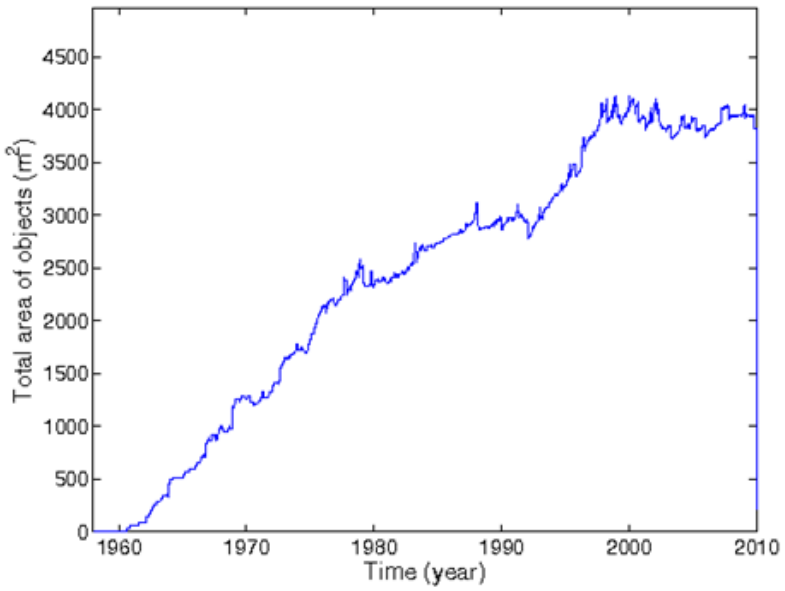

Figure 9. Effective total area of Delta I, II, and Centaur stainless steel tanks in the altitude range 200 km to 6000 km vs. time.

The meteoroid flux was computed using the Gruen meteoroid flux vs. mass model with Earth shielding and gravitational focusing factors (Ref. 4) evaluated at a single altitude of 500 km altitude. The use of flux at a single altitude is acceptable for this analysis because the variation with altitude in LEO is relatively small. The resulting flux was multiplied by the total on-orbit area at each time point to yield the impact rate vs. time. The impact rate was then integrated over time to yield cumulative number of impacts vs. time.

The Gruen flux was evaluated at three mass thresholds. The primary interest in this analysis is in impacting particles with enough mass to generate stainless steel ejecta particles of size 1 mm. The impacting particle mass thresholds were selected to correspond to equivalent stainless steel particle diameters of 0.1 mm (4.14×10^{-6} g), 1 mm (4.14×10^{-3} g), and 1 cm (4.14 g). The assumption here is that the ejected stainless steel particles will have masses which lie in a range that has an upper bound just above the mass of the impacting meteoroid.

Figures 10-12 show cumulative meteoroid impacts on effective total stainless steel tank surface area in the 200 km to 1000 km altitude range vs. year for equivalent stainless steel size thresholds of 0.1 mm, 1 mm, and 1 cm, respectively. Figure 12 shows the 1 cm curve on a log scale because the mean cumulative impacts are much less than 1 (essentially a probability instead of a count). The 0.1 mm and 1 mm curves are included to illustrate how much lower the 1 cm curve is. Figures 13-15 show the same plots for the 800 km to 1000 km altitude range. Figures 16-18 show the same plots for the 200 km to 6000 km altitude range. From these figures, it can be seen that the number of impacts on collective Delta I, II, and Centaur stainless steel tanks only

becomes significant for an equivalent stainless steel particle size threshold between 0.1 mm and 1 mm. The number of impacts at the 1 mm threshold is approximately 27 between 200 km and 1000 km, approximately 5 to 6 between 800 km and 1000 km, and approximately 62 between 200 km and 6000 km. The number of impacts at the 0.1 mm threshold is approximately 100,000 between 200 km and 1000 km, approximately 21,000 between 800 km and 1000 km, and approximately 240,000 between 200 km and 6000 km. To yield enough 1 mm stainless steel ejecta to produce a likely hit on the shuttle, impactors would have to generate larger ejecta fragments than themselves. Ejecta models, such as the one used by MASTER, could be used to further investigate this possibility.

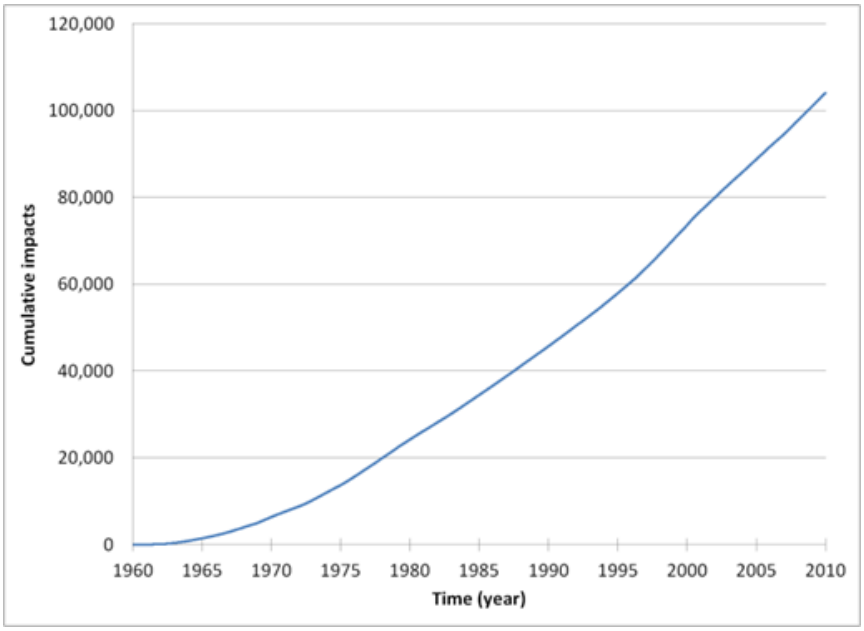

Figure 10. Cumulative meteoroid impacts on Delta I, II, and Centaur stainless steel tanks vs. time. Results are shown for an equivalent stainless steel size threshold of 0.1 mm and the altitude range 200 km to 1000 km.

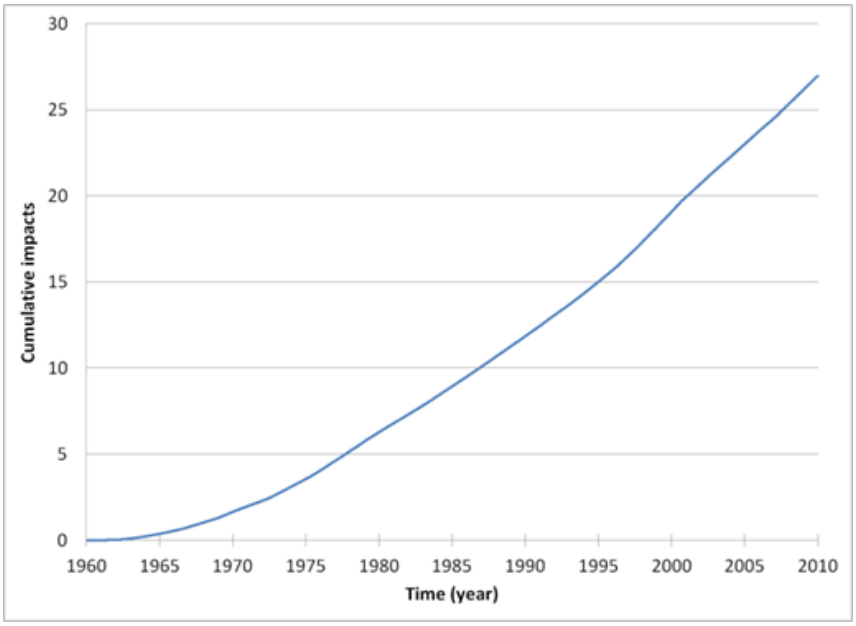

Figure 11. Cumulative meteoroid impacts on Delta I, II, and Centaur stainless steel tanks vs. time. Results are shown for an equivalent stainless steel size threshold of 1 mm and the altitude range 200 km to 1000 km.

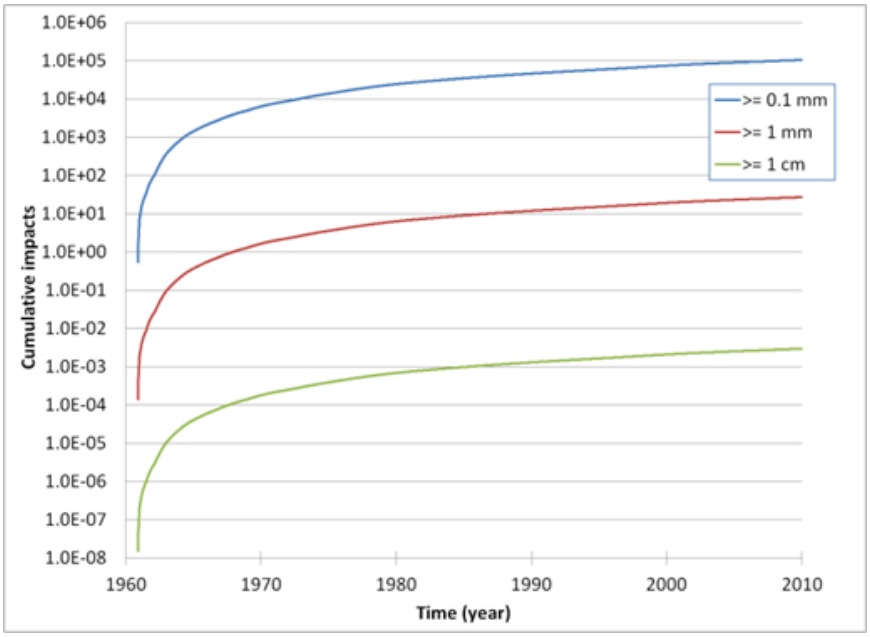

Figure 12. Cumulative meteoroid impacts on Delta I, II, and Centaur stainless steel tanks vs. time. Results are shown for equivalent stainless steel size thresholds of 1 cm, 1 mm, and 0.1 mm, and the altitude range 200 km to 1000 km.

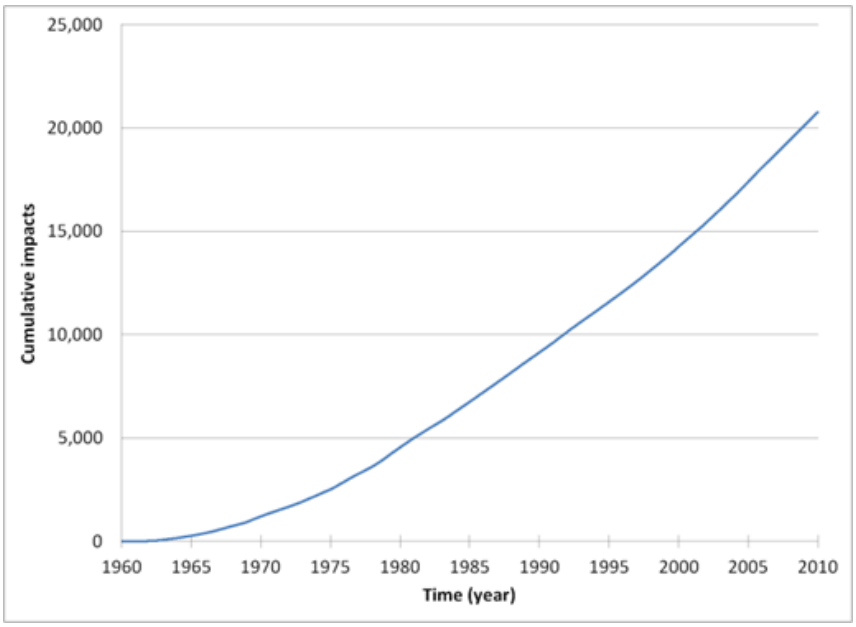

Figure 13. Cumulative meteoroid impacts on Delta I, II, and Centaur stainless steel tanks vs. time. Results are shown for an equivalent stainless steel size threshold of 0.1 mm and the altitude range 800 km to 1000 km.

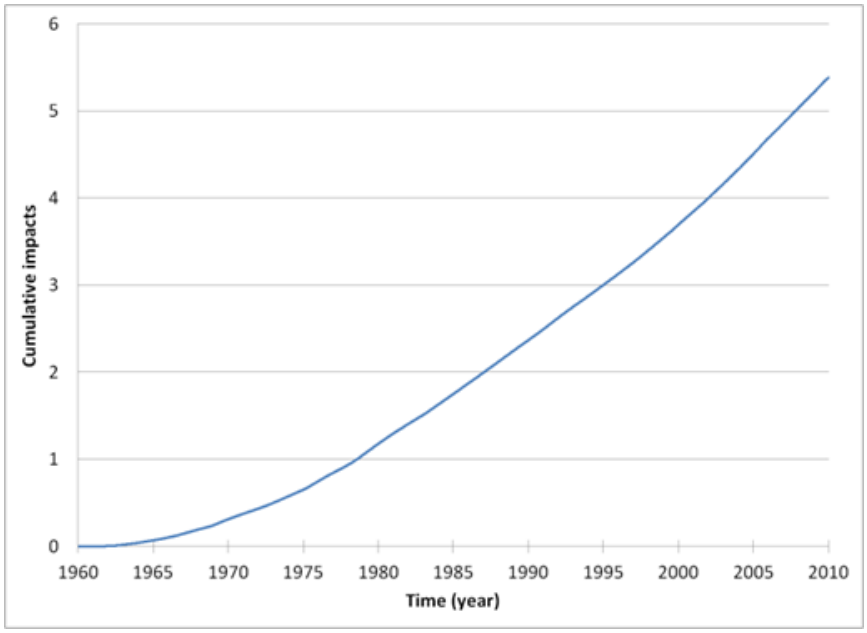

Figure 14. Cumulative meteoroid impacts on Delta I, II, and Centaur stainless steel tanks vs. time. Results are shown for an equivalent stainless steel size threshold of 1 mm and the altitude range 800 km to 1000 km.

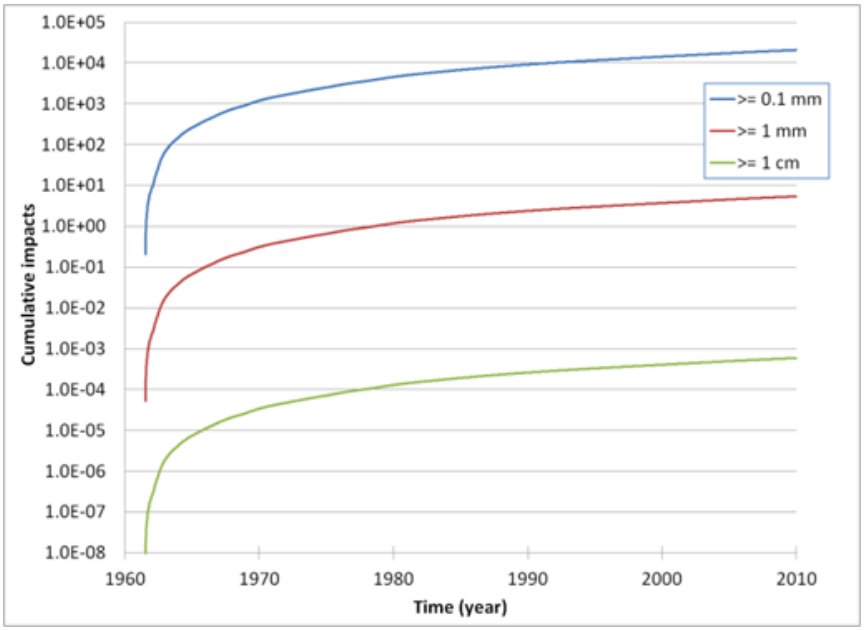

Figure 15. Cumulative meteoroid impacts on Delta I, II, and Centaur stainless steel tanks vs. time. Results are shown for equivalent stainless steel size thresholds of 1 cm, 1 mm, and 0.1 mm, and the altitude range 800 km to 1000 km.

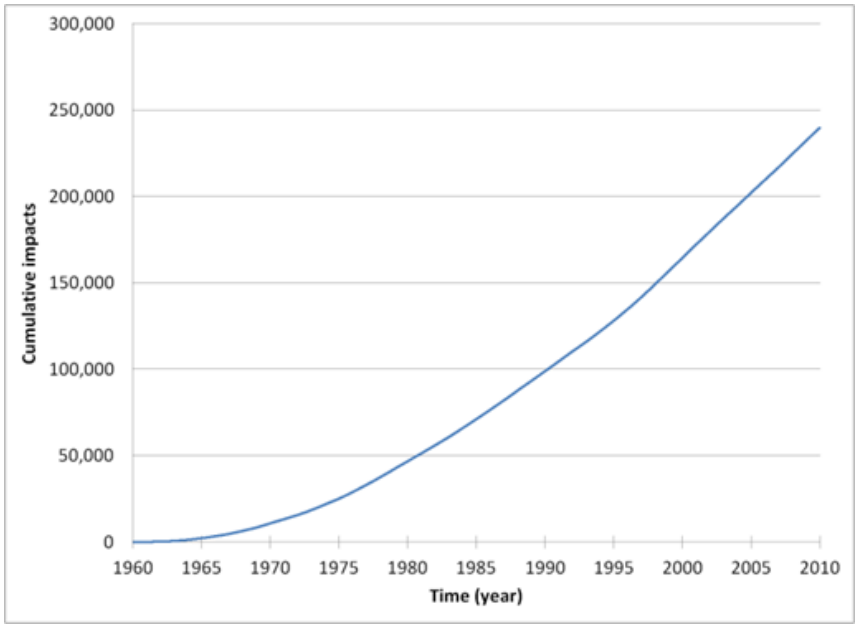

Figure 16. Cumulative meteoroid impacts on Delta I, II, and Centaur stainless steel tanks vs. time. Results are shown for an equivalent stainless steel size threshold of 0.1 mm and the altitude range 200 km to 6000 km.

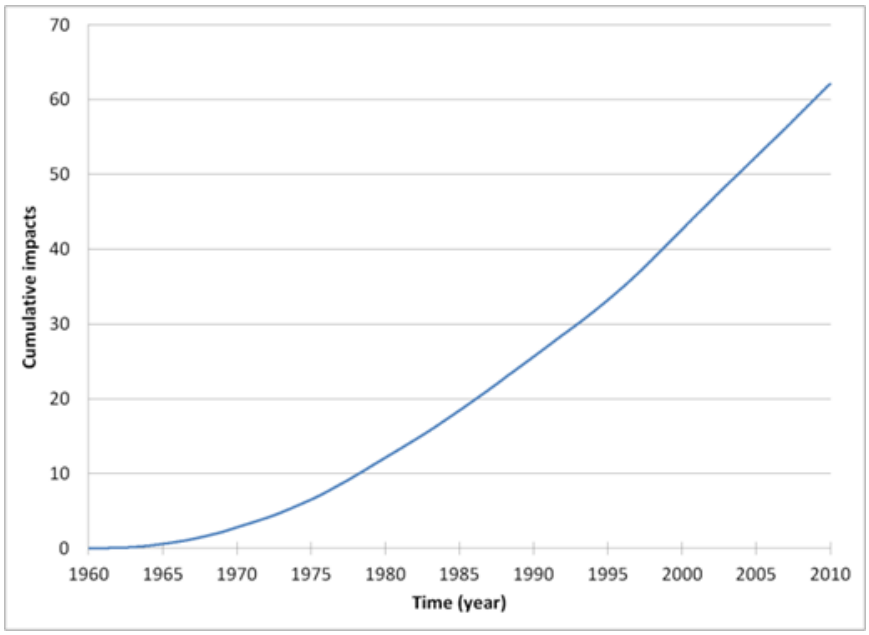

Figure 17. Cumulative meteoroid impacts on Delta I, II, and Centaur stainless steel tanks vs. time. Results are shown for an equivalent stainless steel size threshold of 1 mm and the altitude range 200 km to 6000 km.

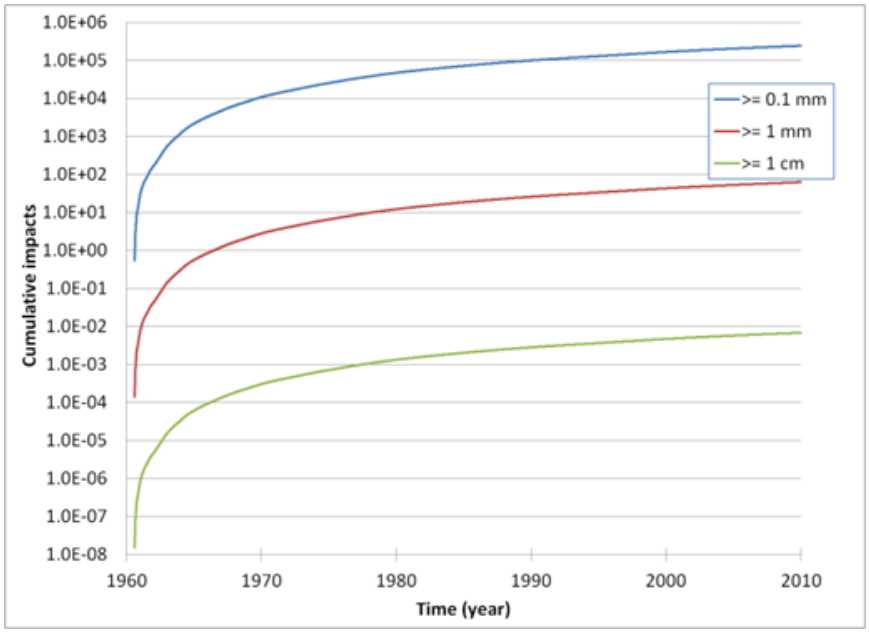

Figure 18. Cumulative meteoroid impacts on Delta I, II, and Centaur stainless steel tanks vs. time. Results are shown for equivalent stainless steel size thresholds of 1 cm, 1 mm, and 0.1 mm, and the altitude range 200 km to 6000 km.

Ejecta Model

The size distribution of cone ejecta resulting from a typical meteoroid impact was briefly investigated. The references for this are the description of the ejecta model implemented in MASTER-2009 (Ref. 5) and a report on hypervelocity impact ejecta prepared by the IADC Working Group 3 (Ref. 6).

References 5 and 6 state that there are three types of ejecta: cone ejecta, jetting ejecta, and spallation ejecta. Both references indicate that jetting ejecta account for only 1% of the total. In addition, spallation only occurs for brittle surfaces. Since stainless steel is not brittle, only coning ejecta were considered here.

The model used by MASTER-2009 (Ref. 5) was implemented in a spreadsheet. The impactor was assumed to be a meteoroid with mass of a 1 mm size stainless steel particle (4.14 mg). The meteoroid density was assumed to be 1 g/cc, and the corresponding meteoroid size was 1.99 mm. The impact was assumed to occur at 20 km/s at an angle normal to the surface. The target surface parameters were selected to represent stainless steel. These include selecting model parameters for a ductile surface and a density of 7.9 g/cc. It is noted that the model information presented in Ref. 6 was essentially the same as the MASTER-2009 model, but with variations in some parameter values derived from experimental data processed by various authors.

Figure 19 shows the resulting reverse cumulative distribution of ejecta fragments over size. The total mass ejected computed by the model was 12.9 times the impactor mass. The maximum fragment size computed by the model was 0.051 mm, which is much less than the equivalent stainless steel size of the impacting meteoroid. The figure shows that the ejecta mass consists of a large number of fragments that are much smaller than the impactor.

Since only 5 to 60 impacts by meteoroids of equivalent stainless steel size 1 mm and larger are expected to have occurred on all Delta I, II, and Centaur stainless steel tanks, and since the resulting ejecta are much smaller than the impactor due to the ductile nature of stainless steel, it appears unlikely that a significant population of stainless steel fragments has been created by meteoroid impacts on these tanks.

Whether impacts by existing orbital debris particles could have created significant amounts of stainless steel ejecta has not been determined here.

It is separately noted that Refs. 5 and 6 note that brittle surfaces can release multiple spall fragments that are larger than the impactor. This implies that meteoroid and debris impacts on spacecraft solar arrays or other brittle surfaces may generate a significant amount of spall ejecta of the same material.

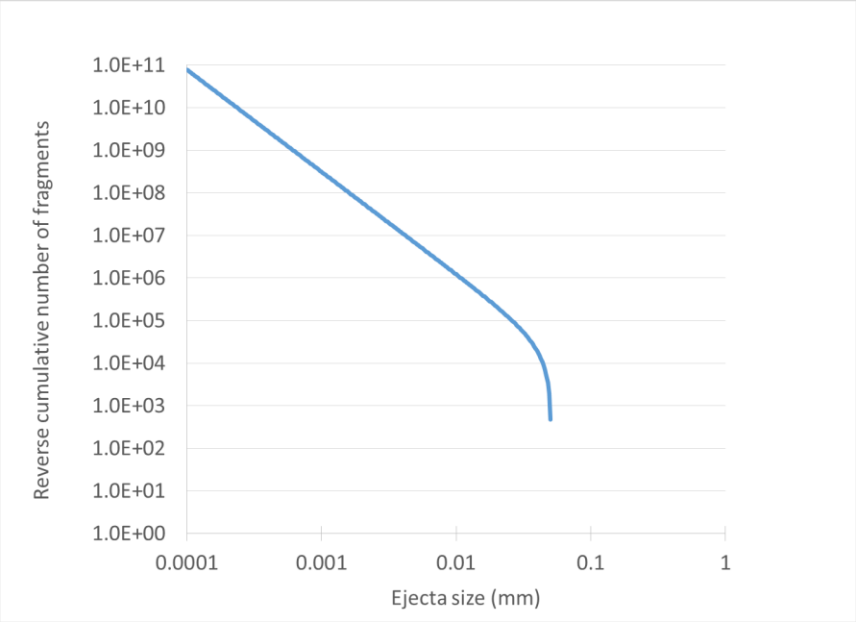

Figure 19. Reverse cumulative distribution of stainless steel ejecta fragments over size resulting from an impact by a meteoroid with equivalent stainless steel size of 1 mm with impact 20 km/s and normal incidence.

Evidence of Impacts on Stainless Steel Tanks

A reentered Delta II 2nd stage tank on display at the Aerospace main campus shows evidence of multiple impacts. This tank was on orbit from April 1996 to June 1997 for a total of 273 days. There are 15 impact craters as well as two perforations with diameters of approximately 1 to 1.5 mm. Consistent with statements in Refs. 5 and 6, none of these craters or perforations shows any evidence of spallation. No analysis has been performed to determine whether the impactors were likely meteoroids or orbital debris.

Conclusions

The possibility that Delta I and II second stage propellant tanks and Centaur propellant tanks could be sources of the stainless steel debris observed on space shuttle surfaces was investigated. It was found that the amount of total on orbit stainless steel tank mass and area available for creation of debris has steadily grown from 1960 to 2010. Approximately 14000 kg and 1600 m^2 was effectively available between 200 km and 1000 km altitude by 2010.

The number of meteoroid impacts on these tanks that may have produced stainless steel ejecta was estimated. The associated number of debris impacts on these tanks was not considered due to limited study scope. It was determined that the number of impacts only becomes significant for an equivalent stainless steel particle size threshold between 0.1 mm and 1 mm. To generate significant amounts of 1 mm stainless steel ejecta, meteoroid impactors smaller than 1 mm equivalent stainless steel particle size would have to generate larger ejecta fragments than

themselves. The MASTER-2009 ejecta model was used to investigate the ejecta created by a meteoroid equivalent to a 1 mm stainless steel particle. It was found that the largest ejecta fragment was much smaller than the impactor due to the ductile nature of stainless steel. Spallation can generate fragments larger than the impactor, but this occurs only on brittle surfaces. Evidence of actual impacts is shown on a reentered Delta II 2nd stage tank at Aerospace that was on orbit 273 days, but they showed no evidence of spallation. As a result, it appears unlikely that a significant population of stainless steel fragments has been created by meteoroid impacts on known stainless tanks.

Whether impacts by existing orbital debris particles could have created significant amounts of stainless steel ejecta has not been determined here.

References

1. "ORDEM 3.0 (Orbital Debris Engineering Model)," NASA Orbital Debris Program Office briefing package, August 2012.
2. Jenkin, A.B., Sorge, M.E., McVey, J.P., Peterson, G.E., Yoo, B.B., "MEO Debris Environment Projection Study," Proceedings of the Sixth European Conference on Space Debris, Darmstadt, Germany, April 22-25, 2013 (ESA SP-723, August 2013).
3. Kessler, D.J., "Derivation of the Collision Probability between Orbiting Objects: The Lifetimes of Jupiter's Outer Moons," Icarus 48, 1981, pp. 39-48.
4. "Natural Orbital Environment Guidelines for Use in Aerospace Vehicle Development," NASA Technical Memorandum 4527, June 1994.
5. "Final Report – Maintenance of the ESA MASTER Model," Revision 1.1, June 7, 2011.
6. "Characterization of Ejecta from HVI on Spacecraft Outer Surfaces," IADC-11-05, April 2013, accessible at http://www.iadc-online.org.

Appendix D. CTU Risk Assessment

IDA

CTU Risk Assessment

Joel Williamsen
Institute for Defense Analyses
Steve Evans
NASA-Marshall Space Flight Center

July 11, 2014

3/19/2015-1

IDA

Objectives

- Examine the structure of the CTU
- Perform hydrocode assessments of orbital debris penetration through CTU and MLI elements
- Perform independent risk assessment(s) of orbital debris failure risk using ORDEM 3.0
- Compare results to those derived from Bumper by NASA-JSC
- Suggest alternative failure criteria risk criteria, penetration equations, etc. for future NASA orbital debris risk assessments of CTU and other critical LPSS elements

3/19/2015-2

IDA

CTU Structure

- *Port side – radiator*
- *Starboard side – cables*
- *Zenith – MLI blanket*
- *Front – box shadowing*
- *Aft – shadowing*
- *Bottom – covered*

- *CTU is inclined at a15 degree angle to the velocity vector*

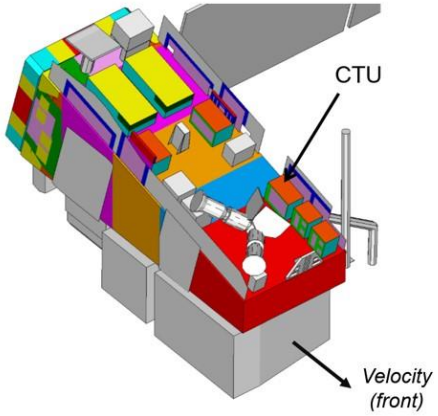

3/19/2015-3

IDA

CTU Structure

Three Critical Elements

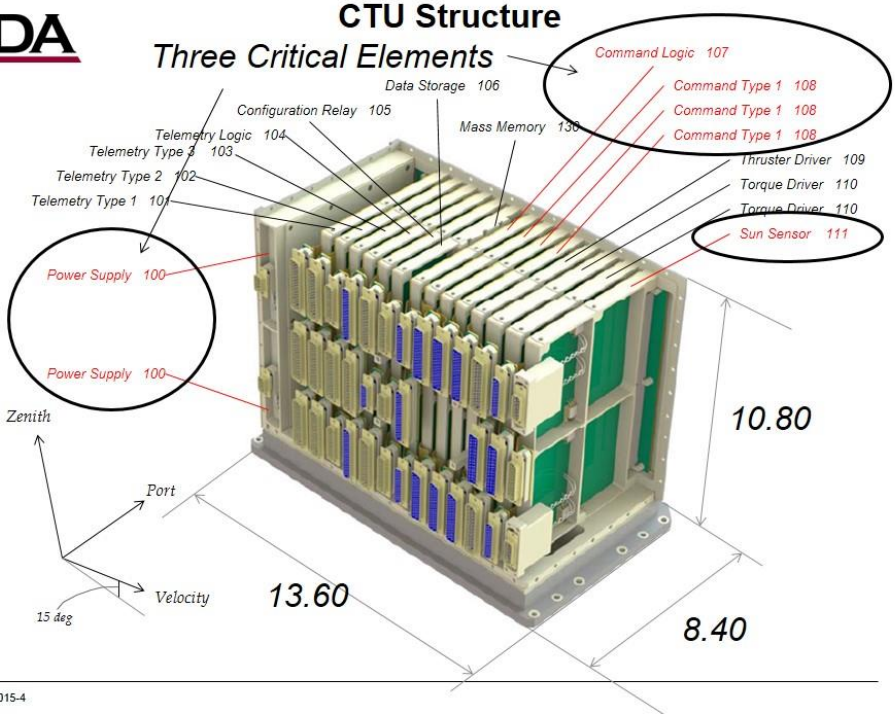

3/19/2015-4

IDA

CTU Internal Structure (Starboard Side View)

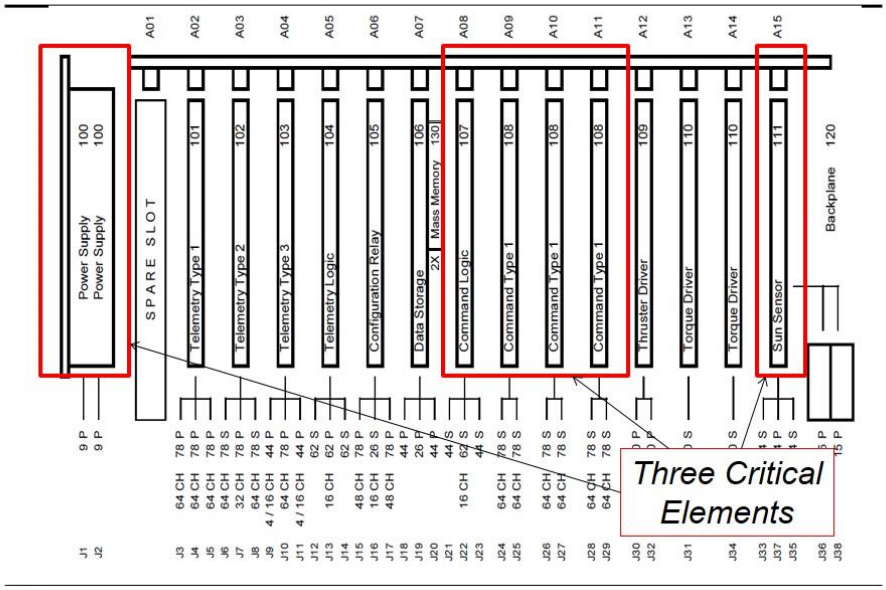

3/19/2015-5

IDA

Power Supply Internal Structure

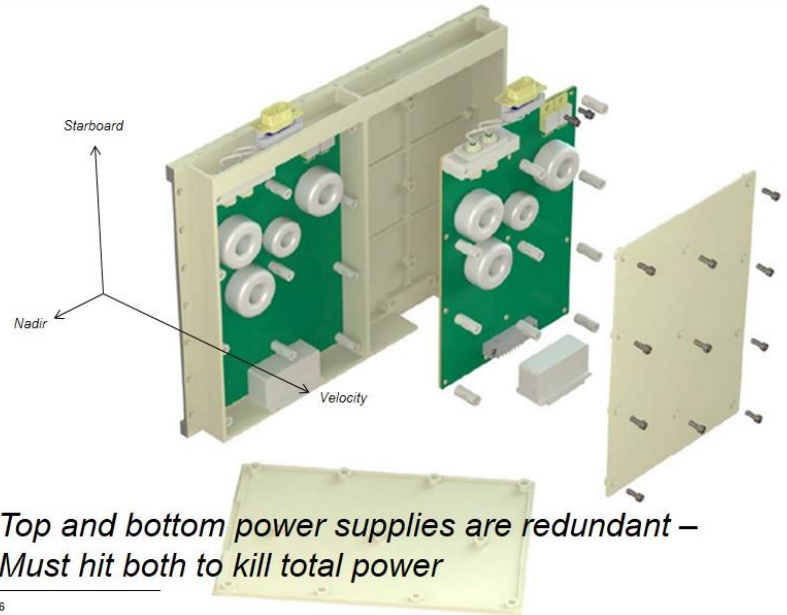

Top and bottom power supplies are redundant – Must hit both to kill total power

3/19/2015-6

CTU Internal Structure – Four Command Cards and Sun Sensor

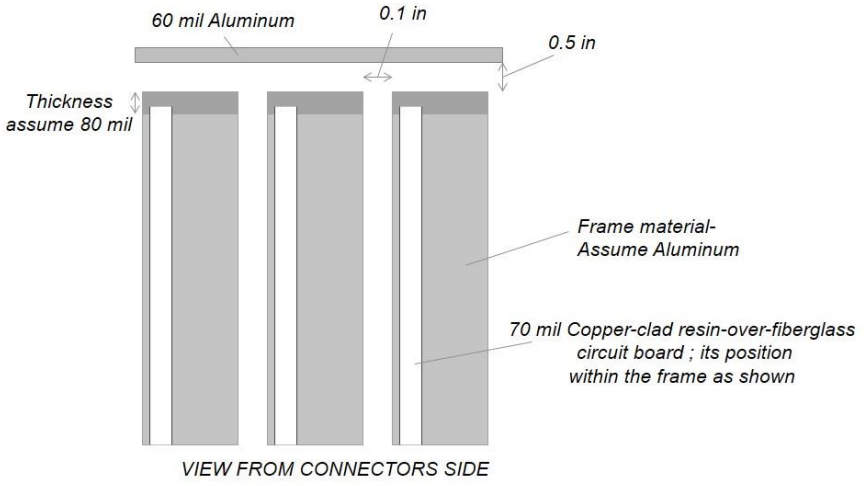

3/19/2015-7

Hydrocode Runs Top Surface of CTU, Assuming No MLI

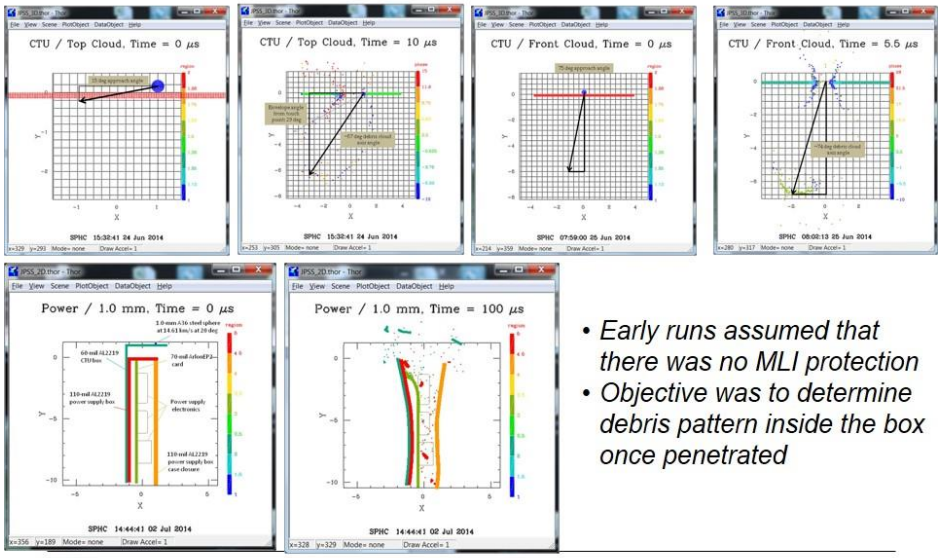

- *Early runs assumed that there was no MLI protection*
- *Objective was to determine debris pattern inside the box once penetrated*

3/19/2015-8

IDA

Hydrocode Runs
Top Surface of CTU, Assuming No MLI

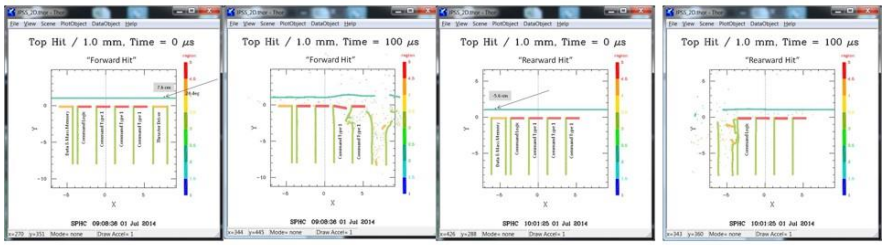

- *Given a direct hit by particle on top of CTU, hydrocode assessment establishes the following areas which may cause critical failure.*
- *This area would be used in establishing smaller critical exposed area for CTU box.*

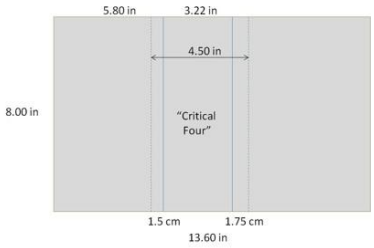

3/19/2015-9

IDA

Hydrocode Runs, 3mm Steel Particle
Front Surface of CTU, MLI Present

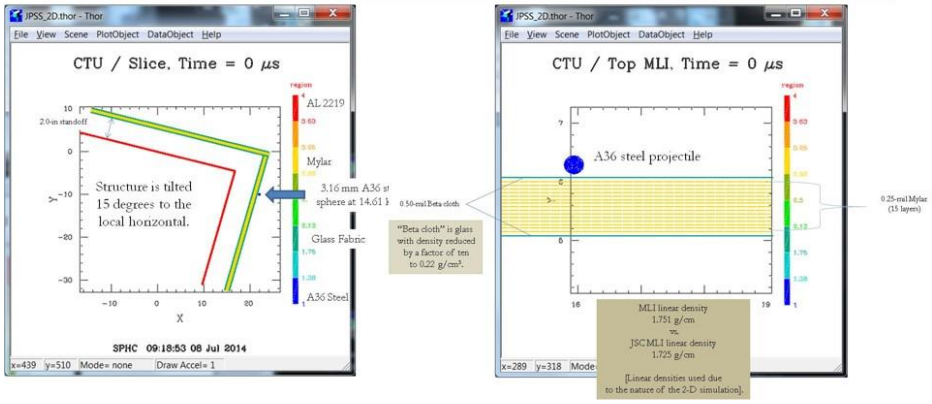

3/19/2015-10

Hydrocode Runs, 3mm Steel Particle Front Surface of CTU, MLI Present

Frontal hit onto front of CTU box (1/2)

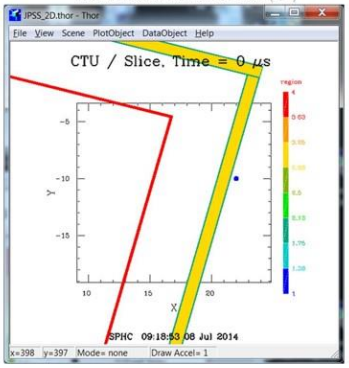

Frontal hit onto front of CTU box (2/2)

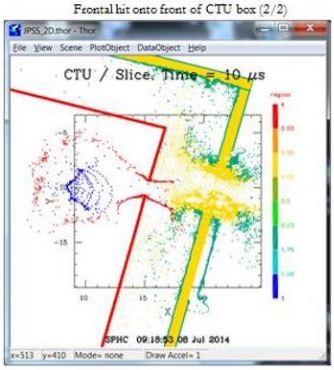

- *Penetration occurs in narrow area along shotline of original particle, not due to MLI cloud distribution*

3/19/2015-11

Hydrocode Runs, 3mm Steel Particle Top of Front Surface of CTU, MLI Present

Frontal hit onto top of CTU box (1/2)

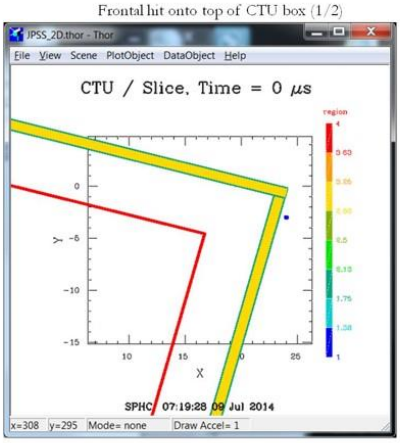

Frontal hit onto top of CTU box (2/2)

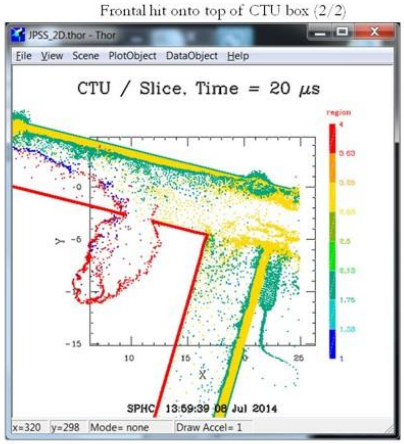

- *Penetration occurs in narrow area along shotline of original particle, not due to MLI cloud distribution*
- *Note that secondary debris cloud in CTU box turns normal to CTU box surface*

3/19/2015-12

Hydrocode Runs, 3mm Steel Particle Top Surface of CTU, MLI Present

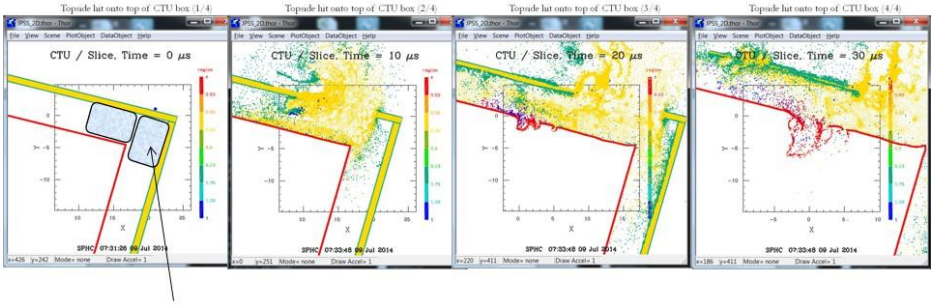

- ***Standoff is essential!***
- *It allows debris cloud to spread out and causes less damage to CTU wall.*
- *Include foam spacers > 2" high to force MLI away from the wall when in orbit.*
- *Penetration occurs in narrow area along shotline of original particle, not due to MLI cloud distribution*
- *Note that secondary debris cloud in CTU box turns normal to CTU box surface*

3/19/2015-13

Hydrocode Runs Port Surface of CTU

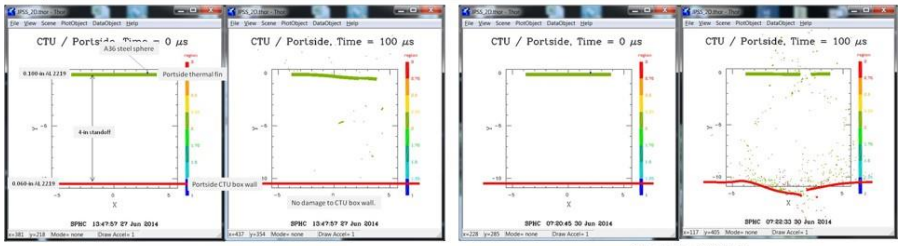

1mm, 5 deg ; 14.61 km/s

1mm; 15 deg ; 14.50 km/s

- *Early runs assumed that there was no MLI protection*
- *Objective was to determine debris pattern inside the box once penetrated*
- *Conclusion: Failure occurs over narrow area from bumper fragments*

Ballistic Limit	3.160	Yes		Yes	Yes	Yes	Yes			Yes	Yes
d (mm)	1.000	No	Yes	No	No	No	No	Yes	Yes	No	No
	0.316		No					No	No		
approach (deg)		5	15	25	35	45	55	65	75	85	95
speed (km/s)		14.61	14.50	13.53	12.27	10.69	8.71	6.45	4.10	2.20	1.67

3/19/2015-14

IDA Independent CTU Risk Assessment

Objectives: *Perform simplified orbital debris risk assessment of CTU using:*

- *ORDEM 3.0 Flux*
- *Single wall penetration equations with CTU geometry*
- *JSC Whipple shield penetration equations (JSC MLI assumptions)*
- *Reduced critical area using CTU critical internal geometry (no internal element resistance included)*
  - *Case 1: Command cards, Batteries, and Sun Sensor are critical*
  - *Case 2: Command cards and Batteries are critical, NOT Sun Sensor*
- *Higher ballistic limit equation (Modified Wilkinson) for top of CTU*

Purposes:

- *Verify BUMPER implementation of ORDEM 3.0 Flux (to a limited extent)*
- *Verify JSC assumptions regarding MLI as bumper material*
- *Determine effectiveness of reduced critical area*
- *Determine effectiveness of higher ballistic limit equation*

3/19/2015-15

IDA Case 1: CTU Areas Actually Containing Critical Internal Elements— Sun Sensor Card Baseline, Not Protected

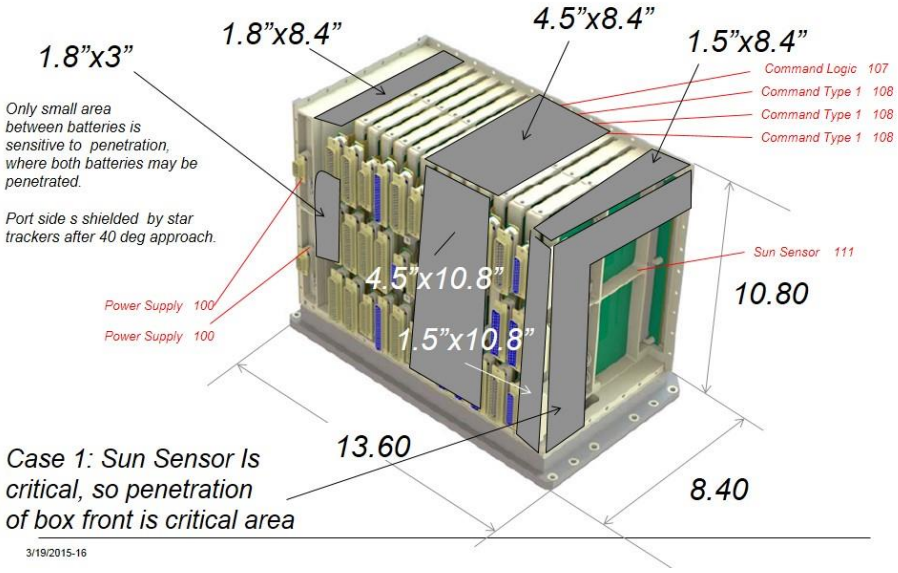

3/19/2015-16

Case 2: CTU Areas Actually Containing Critical Internal Elements— Sun Sensor Card Protected

IDA

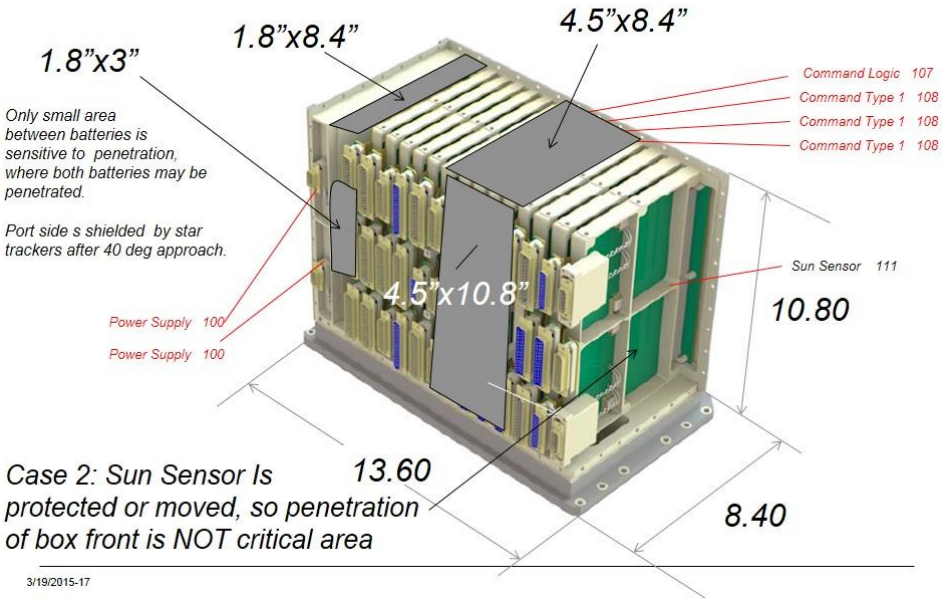

Case 2: Sun Sensor Is protected or moved, so penetration of box front is NOT critical area

3/19/2015-17

ORDEM 3.0 Flux Assumptions

IDA

99.5% of flux emerges from the orbital plane from 0 to 90 deg from velocity vector

Element	az_low	az_high	el_low	el_high	Flux NK30	Flux LD30	Flux MD30	Flux HD30	Flux IN30	Total Flux	Ave Vel	Ratio to all flux	Cum flux %
6900	-10	0	-5	5	1.12E-05	0.002979	0.308817	0.299282	3.59E-07	0.61109	14.61414	0.232308	0.232307927
7291	0	10	-5	5	1.12E-05	0.002979	0.308817	0.299282	3.59E-07	0.61109	14.61414	0.232308	0.464615854
6509	-20	-10	-5	5	1.5E-05	0.001607	0.088528	0.123581	2.48E-07	0.213731	14.50171	0.081251	0.545866575
7682	10	20	-5	5	1.5E-05	0.001607	0.088528	0.123581	2.48E-07	0.213731	14.50171	0.081251	0.627117296
6118	-30	-20	-5	5	7.52E-06	0.000859	0.051243	0.069155	1.34E-07	0.121265	13.53222	0.046099	0.673216714
8073	20	30	-5	5	7.52E-06	0.000859	0.051243	0.069155	1.34E-07	0.121265	13.53222	0.046099	0.719316132
5727	-40	-30	-5	5	5.45E-06	0.000617	0.037653	0.050869	9.43E-08	0.089145	12.27197	0.033889	0.753204804
8464	30	40	-5	5	5.45E-06	0.000617	0.037653	0.050869	9.43E-08	0.089145	12.27197	0.033889	0.787093476
5336	-50	-40	-5	5	4.43E-06	0.000497	0.030844	0.041175	7.63E-08	0.07252	10.68644	0.027569	0.814662093
8855	40	50	-5	5	4.43E-06	0.000497	0.030844	0.041175	7.63E-08	0.07252	10.68644	0.027569	0.842230709
4945	-60	-50	-5	5	4.06E-06	0.000425	0.026915	0.036063	6.72E-08	0.063407	8.712949	0.024104	0.866335174
9246	50	60	-5	5	4.06E-06	0.000425	0.026915	0.036063	6.72E-08	0.063407	8.712949	0.024104	0.890439639
4554	-70	-60	-5	5	4.5E-06	0.000378	0.024347	0.033433	6.07E-08	0.058163	6.449906	0.022111	0.912550353
9637	60	70	-5	5	4.5E-06	0.000378	0.024347	0.033433	6.07E-08	0.058163	6.449906	0.022111	0.934661067
4163	-80	-70	-5	5	3.2E-06	0.000348	0.025216	0.034377	5.72E-08	0.059944	4.09998	0.022788	0.957448956
10028	70	80	-5	5	3.2E-06	0.000348	0.025216	0.034377	5.72E-08	0.059944	4.09998	0.022788	0.980236846
3772	-90	-80	-5	5	0	0.000181	0.010253	0.010219	3.11E-08	0.020654	2.399011	0.007852	0.988088444
10419	80	90	-5	5	0	0.000181	0.010253	0.010219	3.11E-08	0.020654	2.399011	0.007852	0.995940043

3/19/2015-18

IDA

Preliminary Results—Box Penetration
CTU 6.98 years, OD Only

	Single Wall		MLI + SW		Sun Sensor Critical Reduced Area		Sun Sensor Not Critical Reduced Area		JSC
Top Surface (Cards)	0.8394		0.00667		0.00400		0.00300		
Top Surface (Cables)	0.2798	1.522	0.00222	0.01229	0.00133	0.00217	0.00100	0.0056	0.0162
Top Surface (Batteries)	0.4029		0.00336		0.00168		0.00160		
Port Surface (Cards)	0.0002		0.00027		0.000160		0.000123		
		0.0002		0.00036		0.00018		0.000137	0.0008
Port Surface (Batteries)	6E-05		0.00008		0.000014		1.41E-05		
Starboard Surface (Cables)	2.7819		0.00679		0.00246		0.001845		
		3.7833		0.00923		0.00267		0.00205	0.0167
Starboard Surface (Batteries)	1.0015		0.00244		0.00021		0.000205		
Front Surface (Cards)	2.0409		0.024995		0.024995		0		
		3.0705		0.0366		0.036597		0	0.0584
Front Surface (Batteries)	0.9797		0.011600		0.011600		0		
	8.3761		0.06195		0.04997		0.011299		0.0921

Factor of 139 Risk Reduction Due to Inclusion of MLI

20% Risk Reduction Due to Reduced Area w/Sun Sensor Card Critical

Factor 5.5 Risk Reduction w/Sun Sensor Card Protected

3/19/2015-19

IDA

Assessment does not include the following factors:

- *Resistance of internal elements—would further lower risk*
- *Shadowing by cables (see below)—would further lower risk*
- *Contamination by penetrating particles on other internal elements of CTU not impacted directly by penetrating particles. Would increase risk of eventual failure unless internal wiring and circuit boards have thick coating.*

3/19/2015-20

Another Consideration in Calculating CTU Risk: NASA's Current High Velocity Penetration Prediction Equation May be Too Conservative

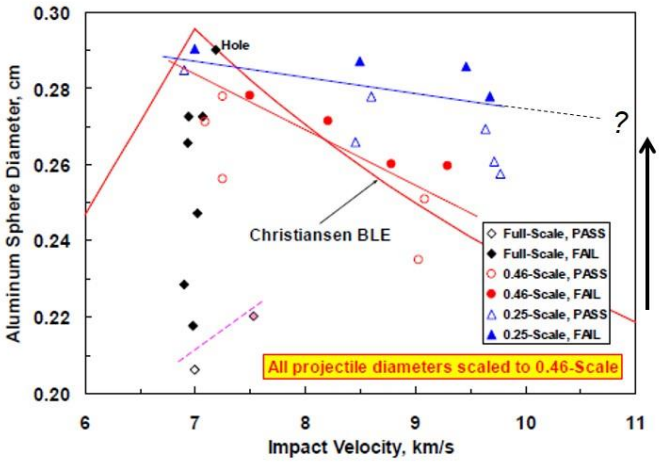

*Piekutowski and Poorman[1] (2010) show large improvements over NASA Non Optimum penetration equation at velocities above 7 km/sec in **full-scale tests** (mixed results in subscale tests).*

Similar to Modified Wilkinson Equation[2] (Bjorkman, 1993).

What would be the effect on penetration risk if adopted?

1 Piekutowski and Poorman, "Effects of scale on the performance of Whipple shields for impact velocities ranging from 7 to 10 km/s", HVIS 2010, Darmstadt GE

3/19/2015-21

High Velocity Penetration Equations MLI Over CTU

	15 deg Obliquity						
	1	3.1	7.3	9	11	13	15
NNO	0.264	0.129	0.275	0.239	0.209	0.187	0.17
Mod Wilkinson	0.264	0.129	0.321	0.305	0.29	0.278	0.268
Schmidt Housen	0.264	0.129	0.34	0.331	0.3	0.297	0.308
	45 deg Obliquity						
	2	3	4.2	9.9	11	13	15
NNO	0.279	0.216	0.174	0.277	0.258	0.231	0.21
Mod Wilkinson	0.279	0.216	0.174	0.322	0.314	0.301	0.291
Schmidt Housen	0.279	0.216	0.174	0.339	0.342	0.322	0.3
	65 deg Obliquity						
	3	5	7.1	16.55	18	20	
NNO	0.48	0.35	0.282	0.277	0.262	0.244	
Mod Wilkinson	0.48	0.35	0.282	0.322	0.315	0.307	
Schmidt Housen	0.48	0.35	0.309	0.339	0.342	0.335	

45 Deg Obliquity

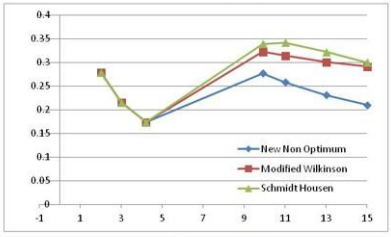

15 Deg Obliquity

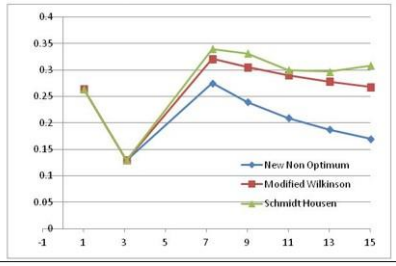

65 Deg Obliquity

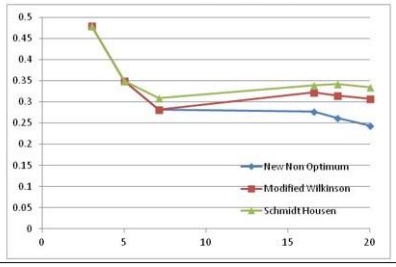

3/19/2015-22

IDA

Preliminary Results
CTU 6.98 years, OD Only

	Single Wall		MLI + SW		Modified Wilkinson		JSC
Top Surface (Cards)	0.839365		0.00667		0.00182		
Top Surface (Cables)	0.279788	1.522049	0.00222	0.01229	0.00071	0.00355	0.01621
Top Surface (Batteries)	0.402895		0.00336		0.00102		

Factor of 3.5 Risk Reduction Due to Penetration Equation Improvement

3/19/2015-23

IDA

Conclusions and Recommendations

- **CTU structure contains four command logic cards, a sun sensor and a redundant set of batteries that are critical to controlled re-entry. Other elements act as shielding.**
- **Hydrocode assessments of orbital debris penetration through CTU and MLI elements show area where impacts cause penetration of critical elements.**
- **Independent risk assessment shows reduced critical element areas reduce risk of assuring controlled re-entry differentially, based on their inclusion.**
  - **If sun sensor is critical,** we must include entire frontal area of CTU box as critical. As such, **risk only drops by 20% over baseline** (where any box penetration causes failure to re-enter).
  - **If sun sensor is moved** to a safer position **or protected internally** (such as behind control logic cards), **risk is reduced by a factor of ~5.**
    - **Additional analyses of internal features would be required** even if sun sensor is internally protected (internal hardness, potential contamination).
- **Conclusion: Consideration of internal elements of CTU will probably not be sufficient to reach factor of 12 reduction required, due largely to exposure of internal sun sensor card. Some (very thin) external blanket directly over CTU is needed.**
- **It is absolutely essential that large (≥2 inch) standoff of MLI over CTU be maintained.** Consider placing light foam spacers between CTU and MLI blanket
- **Use of alternate high velocity equation (Modified Wilkinson or similar) would reduce risk by a factor of ~3.5** (top surface, limited study). UDRI tests from 7-10 k/s verify this possibility.
  - **Considering increase in OD population and density, this is a recommendation that should benefit all spacecraft, and is worthy of NASA investment in tests to verify it.**

3/19/2015-24

Appendix E. JPSS-1 Zenith Deck Orbital Debris Wire Harness Failure Assessment

IDA

JPSS-1 Zenith Deck Orbital Debris Wire Harness Failure Assessment

October 10, 2014

Joel Williamsen
Institute for Defense Analyses
Steve Evans
NASA-Marshall Space Flight Center

3/19/2015-1

IDA

Summary

- **Task 1: Performed "generic" risk assessments of orbital debris penetration through a "typical" wire harness (cable) with baseline MLI blanket protection at normal obliquity using SPH hydrocode**
  - **36, 18, and 6 wire harness (cable) with redundant wire pairs**
  - **Considered one year, zenith/nadir wire orientation**
  - **Steel and aluminum orbital debris**
  - **2" standoff of baseline MLI to wire harness (cable)**
- **Task 2: Performed trade studies and risk assessments with MLI blanket and MMOD blanket configurations at 75 degree obliquity to determine performance and optimal configuration for zenith-facing wires using SPH hydrocode**
  - **Ultimate objective was to prevent penetration of 3mm aluminum sphere through adding enhanced MMOD blanket over zenith facing wires**
- **Both orbital debris risk assessments used ORDEM 3.0 flux levels for a variety of configurations – Meteoroids not included**

3/19/2015-2

Task 1: Generic Wire Harness Risk
JPSS-1 Wire Harness Location

- *Typical cable on "zenith deck" is similar to that emerging from the Command Telemetry Unit (CTU)*

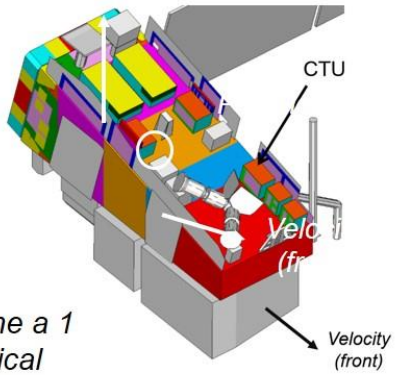

- *Examine a 1 foot typical length*
- *Perpendicular to velocity vector aligned with zenith*

3/19/2015-3

JPSS-1 Wire Harness Structure and Failure Assumptions

- *Goal: Determine the number of wire failures in a 1 foot harness for each of the following conditions*
  - *Steel OD*
  - *Aluminum OD*
- *Interpolate between results for impact velocity & diameter to determine flux vs. number of wire failures*
- *Associate probability of primary + 1 randomly placed redundant wire failure*
- *Extend analysis to other wire types, lengths, designs*
- *Initially: Assume a wire harness with 36 single 24 gauge wires*
  - *Each 24 gauge wire holds19 strands surrounded by .024" plastic*
  - *2 layers of Lamiglass and 1 layer of Kapton surrounds 37 wire bundle*
  - *MLI blanket is kapton only (no betacloth), 0.032 g/cm2 (very thin)*
  - *Perform entire assessment with and without MLI blanket*
- *Perform 18 and 6 strand wire examples based on 36 strand wire results*

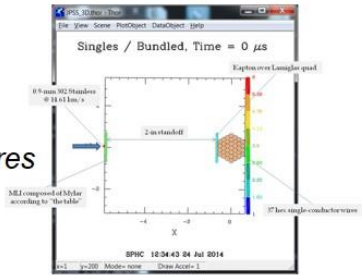

3/19/2015-4

IDA

No MLI Over Wire Harness
0.5mm Stainless Steel at 14.6 km/sec

Target

Lamiglas Layers

Teflon Insulator

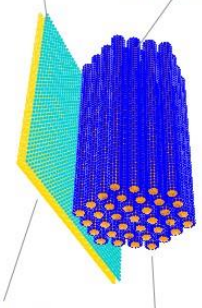

Kapton Layer

Copper Conductor

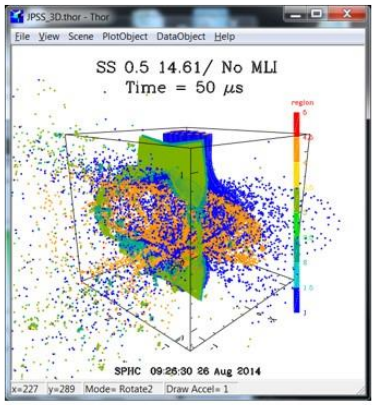

Result:

No MLI Option

Projectile diameter: 0.5-mm

Number of wires cut: 37

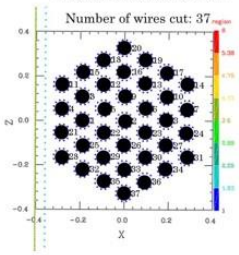

With 0.5mm Aluminum Sphere
At 7.3 and 14.6 km/sec:

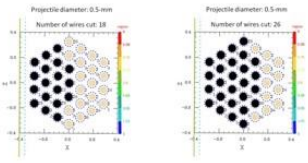

3/19/2015-5

IDA

Hydrocode Results with Baseline MLI
2 Inch Standoff Over Wire Harness

0.5 mm Stainless Steel, 14.61 k/s

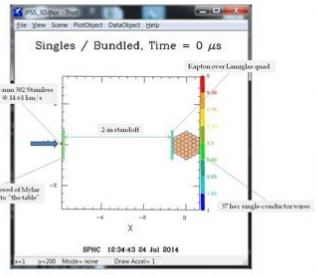

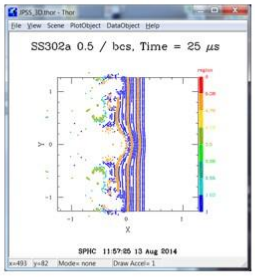

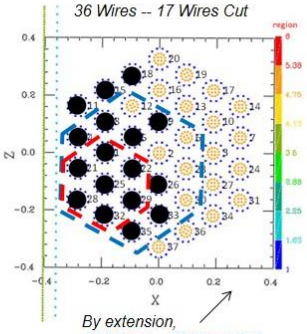

By extension,
198Wires -- 13 Wires Cut
6 Wires – 7 Wires Cut

0.9 mm Aluminum, 7.3 k/s

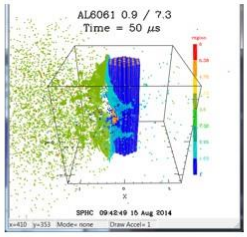

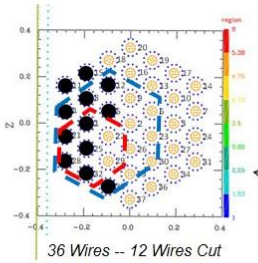

36 Wires -- 12 Wires Cut

By extension,
18 Wires -- 10 Wires Cut
6 Wires– 5 Wires Cut

(Note: "37th", "19th" and "7th" wires ignored in hex pattern)

3/19/2015-6

IDA

JPSS-1 Wire Harness Failure
Hydrocode Results
Number and Locations of Wires Cut

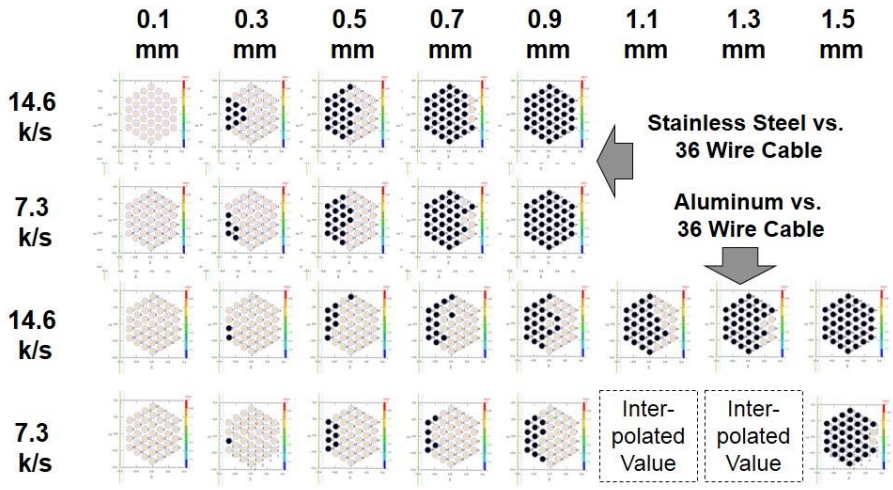

3/19/2015-7

IDA

JPSS-1 Wire Harness Failure
Summary of Results To Date

Stainless Steel -- 36 Wire Cable

Hydrocode Results Number of Wires Cut	0.1 mm	0.3 mm	0.5 mm	0.7 mm	0.9 mm
14.6 k/s	0	9	22	33	36
7.3 k/s	0	5	17	31	36

Aluminum -- 36 Wire Cable

	0.1 mm	0.3 mm	0.5 mm	0.7 mm	0.9 mm	1,1 mm	1.3 mm	1.5 mm
14.6 k/s	0	2	13	13	20	26	32	36
7.3 k/s	0	1	6	6	12	22*	32*	36

**Interpolated Value*

Results by Extension to 19 and 7 Wire Cables (Steel/Aluminum)

	Velocity	0.3 mm	0.5 mm	0.7 mm	0.9 mm	1.1 mm	1.3 mm	1.5 mm
18	14.6 k/s	8 / 2	17 / 6	18 / 10	18 / 16	18 / 18	18 / 18	18 / 18
	7.3 k/s	4 / 2	14 / 4	18 / 5	18 / 10	18/15*	18/18*	18 / 18
6	14.6 k/s	5 / 1	6 / 5	6 / 6	6 / 6	6 / 6	6 / 6	6 / 6
	7.3 k/s	3 / 1	6 / 3	6 / 3	6 / 6	6 / 6*	6 / 6*	6 / 6

3/19/2015-8

IDA ORDEM 3.0 Flux (1 mm or higher)

99.5% of flux emerges from the orbital plane from 0 to 90 deg from velocity vector. Interpolated between ORDEM predictions for 0.1 mm through 1.3 mm sizes for these 18 approach vectors..

Element	az_low	az_high	el_low	el_high	Flux NK30	Flux LD30	Flux MD30	Flux HD30	Flux IN30	Total Flux	Ave Vel	Ratio to all flux	Cum flux %
6900	-10	0	-5	5	1.12E-05	0.002979	0.308817	0.299282	3.59E-07	0.61109	14.61414	0.232308	0.232307927
7291	0	10	-5	5	1.12E-05	0.002979	0.308817	0.299282	3.59E-07	0.61109	14.61414	0.232308	0.464615854
6509	-20	-10	-5	5	1.5E-05	0.001607	0.088528	0.123581	2.48E-07	0.213731	14.50171	0.081251	0.545866575
7682	10	20	-5	5	1.5E-05	0.001607	0.088528	0.123581	2.48E-07	0.213731	14.50171	0.081251	0.627117296
6118	-30	-20	-5	5	7.52E-06	0.000859	0.051243	0.069155	1.34E-07	0.121265	13.53222	0.046099	0.673216714
8073	20	30	-5	5	7.52E-06	0.000859	0.051243	0.069155	1.34E-07	0.121265	13.53222	0.046099	0.719316132
5727	-40	-30	-5	5	5.45E-06	0.000617	0.037653	0.050869	9.43E-08	0.089145	12.27197	0.033889	0.753204804
8464	30	40	-5	5	5.45E-06	0.000617	0.037653	0.050869	9.43E-08	0.089145	12.27197	0.033889	0.787093476
5336	-50	-40	-5	5	4.43E-06	0.000497	0.030844	0.041175	7.63E-08	0.07252	10.68644	0.027569	0.814662093
8855	40	50	-5	5	4.43E-06	0.000497	0.030844	0.041175	7.63E-08	0.07252	10.68644	0.027569	0.842230709
4945	-60	-50	-5	5	4.06E-06	0.000425	0.026915	0.036063	6.72E-08	0.063407	8.712949	0.024104	0.866335174
9246	50	60	-5	5	4.06E-06	0.000425	0.026915	0.036063	6.72E-08	0.063407	8.712949	0.024104	0.890439639
4554	-70	-60	-5	5	4.5E-06	0.000378	0.024347	0.033433	6.07E-08	0.058163	6.449906	0.022111	0.912550353
9637	60	70	-5	5	4.5E-06	0.000378	0.024347	0.033433	6.07E-08	0.058163	6.449906	0.022111	0.934661067
4163	-80	-70	-5	5	3.2E-06	0.000348	0.025216	0.034377	5.72E-08	0.059944	4.09998	0.022788	0.957448956
10028	70	80	-5	5	3.2E-06	0.000348	0.025216	0.034377	5.72E-08	0.059944	4.09998	0.022788	0.980236846
3772	-90	-80	-5	5	0	0.000181	0.010253	0.010219	3.11E-08	0.020654	2.399011	0.007852	0.988088444
10419	80	90	-5	5	0	0.000181	0.010253	0.010219	3.11E-08	0.020654	2.399011	0.007852	0.995940043

3/19/2015-9

IDA Probability of Critical Failure vs. Wire Harness Size Given Randomly Placed Redundant Wire Failure

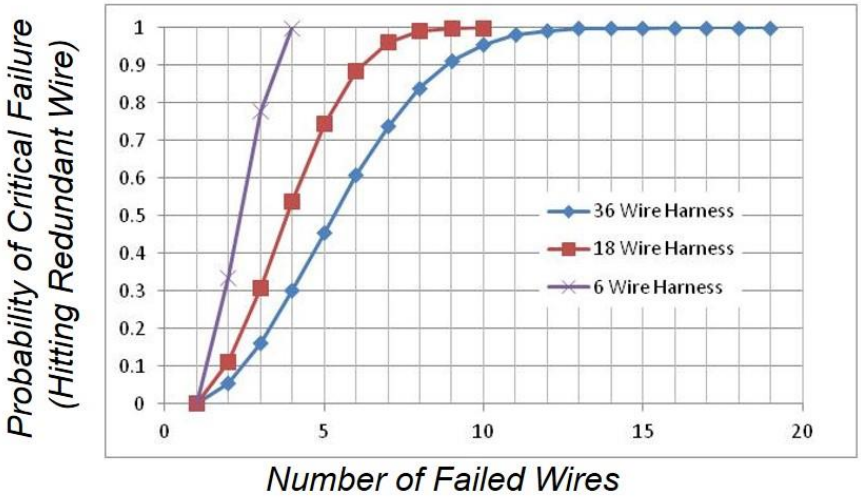

Larger Bundles Require More Wire Failures (Larger Particles) To Fail Redundant Wire and Cause Critical Component Failure

3/19/2015-10

IDA Predicted Number of 1 Foot Cable Failures / Year Steel Orbital Debris vs. 36 Wire Cable

N Wires	For a 36 wire harness, particle diameter that causes N (of 36) wire penetrations, 1 foot wire length. Velocity k/s: 14.6	14.5	13.5	12.3	10.7	8.7	7.3	<—Assume same as 7.3—> 6.4	4.1	2.4	P (Redundant Kill in N Wires)	Flux for N Failures	n Bundle Failures
36	0.90	0.90	0.90	0.90	0.90	0.90	0.90	0.90	0.90	0.90	1	2.084810	0.01009
35	0.83	0.84	0.84	0.85	0.85	0.86	0.86	0.86	0.86	0.86	1	0.562263	0.00436
34	0.77	0.78	0.78	0.79	0.80	0.81	0.82	0.82	0.82	0.82	1	0.720792	0.00349
33	0.7	0.71	0.73	0.74	0.75	0.77	0.78	0.78	0.78	0.78	1	0.925806	0.00448
32	0.68	0.69	0.70	0.71	0.72	0.73	0.74	0.74	0.74	0.74	1	0.402053	0.00195
31	0.67	0.67	0.68	0.68	0.68	0.69	0.7	0.70	0.70	0.70	1	0.461342	0.00223
30	0.65	0.66	0.66	0.67	0.67	0.68	0.69	0.69	0.69	0.69	1	0.325944	0.00158
29	0.63	0.64	0.65	0.65	0.66	0.67	0.67	0.67	0.67	0.67	1	0.366730	0.00178
28	0.62	0.62	0.63	0.64	0.64	0.65	0.66	0.66	0.66	0.66	1	0.391479	0.00190
27	0.60	0.61	0.61	0.62	0.63	0.64	0.64	0.64	0.64	0.64	1	0.417912	0.00202
26	0.58	0.59	0.60	0.61	0.61	0.62	0.63	0.63	0.63	0.63	1	0.446145	0.00216
25	0.57	0.57	0.58	0.59	0.60	0.61	0.61	0.61	0.61	0.61	1	0.476301	0.00231
24	0.55	0.56	0.57	0.58	0.58	0.59	0.60	0.70	0.70	0.70	1	0.272218	0.00132
23	0.53	0.54	0.55	0.56	0.57	0.58	0.59	0.59	0.59	0.59	1	0.779216	0.00377
22	0.52	0.53	0.53	0.54	0.55	0.56	0.57	0.57	0.57	0.57	1	0.579678	0.00281
21	0.5	0.51	0.52	0.52	0.53	0.53	0.56	0.56	0.56	0.56	1	0.673271	0.00326
20	0.48	0.49	0.50	0.51	0.52	0.53	0.54	0.54	0.54	0.54	1	0.499006	0.00242
19	0.47	0.48	0.49	0.50	0.51	0.52	0.53	0.53	0.53	0.53	1	0.812389	0.00393
18	0.45	0.46	0.47	0.48	0.49	0.50	0.51	0.51	0.51	0.51	0.999999984	0.753807	0.00365
17	0.43	0.44	0.46	0.47	0.48	0.49	0.50	0.50	0.50	0.50	0.999997071	0.8047327	0.00390
16	0.42	0.43	0.44	0.45	0.46	0.47	0.48	0.48	0.48	0.48	0.99997364	0.8838968	0.00430
15	0.40	0.41	0.42	0.43	0.44	0.46	0.47	0.47	0.47	0.47	0.999841838	0.9510521	0.00460
14	0.38	0.40	0.42	0.44	0.46	0.48	0.45	0.50	0.50	0.50	0.999288271	0.3546039	0.00172
13	0.37	0.38	0.39	0.40	0.41	0.42	0.43	0.43	0.43	0.43	0.997437775	1.75156	0.00846
12	0.35	0.36	0.37	0.38	0.39	0.41	0.42	0.42	0.42	0.42	0.992313326	1.1642548	0.00560
11	0.33	0.34	0.36	0.37	0.38	0.39	0.40	0.40	0.40	0.40	0.980234267	1.2462	0.00591
10	0.32	0.33	0.34	0.35	0.36	0.37	0.38	0.38	0.38	0.38	0.9555271	1.3238557	0.00617
9	0.3	0.31	0.32	0.33	0.34	0.36	0.37	0.37	0.37	0.37	0.911054201	1.426623	0.00629
8	0.28	0.29	0.30	0.31	0.33	0.34	0.35	0.35	0.35	0.35	0.839897562	1.9413414	0.00788
7	0.26	0.27	0.28	0.29	0.31	0.32	0.33	0.33	0.33	0.33	0.738014192	2.1165	0.00756
6	0.23	0.25	0.26	0.28	0.29	0.30	0.32	0.32	0.32	0.32	0.607021287	2.3077614	0.00678
5	0.21	0.23	0.24	0.26	0.27	0.29	0.3	0.30	0.30	0.30	0.455875629	2.5165205	0.00555
4	0.19	0.20	0.21	0.22	0.24	0.25	0.26	0.26	0.26	0.26	0.300411523	3.4141473	0.00497
3	0.17	0.18	0.18	0.19	0.20	0.21	0.22	0.22	0.22	0.22	0.160493827	3.8076557	0.00296
2	0.14	0.15	0.16	0.16	0.17	0.17	0.18	0.30	0.30	0.30	0.055555556	2.8507219	0.00077
1	0.12	0.13	0.13	0.13	0.13	0.14	0.14	0.14	0.14	0.14	0	6.1409101	0.00000
0	0.1	0.1	0.1	0.1	0.1	0.1	0.1	0.10	0.10	0.10	0	--	
	Hydrocode model values in red; all others are linear interpolations											n cable failures	0.14292

Number of wires cut

Diameter orbital debris particle causing this number of wires to be cut (at this impact V)

Highlighted diameters represent hydrocode runs; Other values are linear interpolations

Probability that a redundant wire has been cut within a bundle of 36 wires

Orbital debris flux for this combination of diameters and velocities

Expected number of cable failures with N wire failures in one year, assuming wires are:
- 1 foot long and 5/8" wide
- Oriented along the nadir/zenith
- Fully exposed to the orbital debris flux

Expected number of cable failures in one year considering 1 through 36 wire failures
Actual failures can be **fewer,** considering:
- **Alternate orientations** (less exposure)
- **Shadowing** (behind other wires or equipment)

3/19/2015-11

IDA Summary Predictions Number of Cable Failures for Three Cable Sizes (1 Foot Length, 1 Year Exposure, Zenith Orientation)

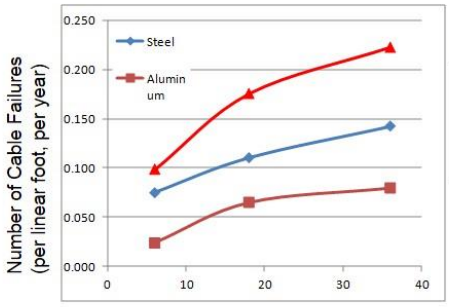

Bundle Size	Steel	Aluminum	Total
6	0.075	0.024	0.099
18	0.111	0.065	0.176
36	0.143	0.080	0.223

Expected number of cable failures in one year considering N wires per cable, assuming:
- 1 foot long and 5/8" wide (36 strands). 18 strand cable is 7/16" wide; 6 strand cable is 5/16".
- Oriented along the nadir/zenith
- Fully exposed to the orbital debris flux

Actual failures can be **fewer,** considering:
- **Alternate orientations** (less exposure)
- **Shadowing** (behind other wires or equipment)
- Fewer critical wires in a cable.

3/19/2015-12

IDA Effect of Shadowing and Reduced Criticality On Complex Wire Harness

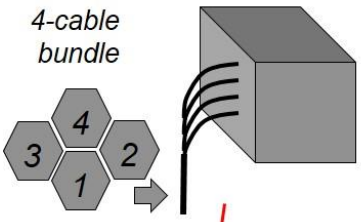

Four 36 strand wires, each 2 ft long
- Act alone over first foot
- In a 4-cable bundle for second foot
- Fourth cable shadowed by first 3
- 2nd and cable 50% shadowed completely from starboard when in 4-cable bundle
- 1st cable unshadowed when in 4-cable bundle
- All cables shadowed by CTU from port side
- All cables shadowed from front approaching debris by other cables forward
- Cables shadowed from 45 degrees to 90 degrees on starboard side from star trackers
- All cables contain 18 redundant pairs, but only 50% of pairs are critical
- Neglects effect of horizontal first foot (conservative)
- Neglects effect of additional tape (conservative)

3/19/2015-13

IDA Effect of Shadowing and Reduced Criticality On Complex Wire Harness

Cable	Length (ft)	Baseline n Fails	Portside Shadowing	Front (0 deg) Shadowing	45 deg Shadowing	Bundle Shadowing	Criticality	Realistic n fails
1	2	0.446	0.5	0.46	0.84	1	0.5	0.043084
2	2	0.446	0.5	0.46	0.84	0	0.5	0
3	2	0.446	0.5	0.46	0.84	1	0.5	0.043084
4	2	0.446	0.5	0.46	0.84	0	0.5	0
Baseline n fails		1.784			More realistic n fails in 8 ft			0.086
Failure per foot		0.223				Failures per foot		0.011
					Unshadowed baseline vs Realistic			20.7

- **Including more realistic shadowing and criticality yields a reduction of a factor of 20 on failure risk for this 8 foot example**
- **About 1% risk for eight ft cables with 50% criticality**

Earlier assessments (for the James Webb Space Telescope, ISS, etc.) assumed that any penetration of the shield caused failure of the entire harness.

The next task takes a similar approach, determining protection and risk levels for improved MLI and MMOD blanket designs (preventing MMOD blanket penetration and impact onto wires).

3/19/2015-14

IDA

Task 2: Additional Hydrocode Runs
With
Alternate MLI and Kevlar Protection

3/19/2015-15

IDA *Heavy MLI Over Wire Harness (2 Layers of Beta Cloth)*
2 Inch Standoff, to Wires, no MMOD Blanket beneath

Heavy MLI Option

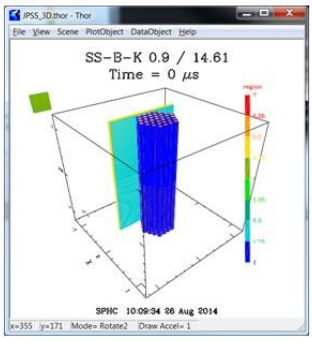

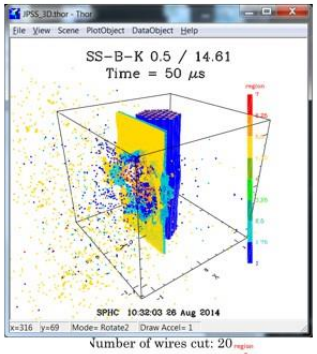

"Heavy MLI"

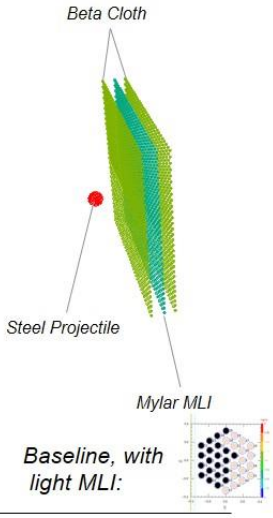

Results with heavy MLI:

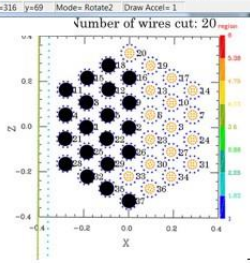

Baseline, with light MLI:

3/19/2015-16

IDA

Heavy MLI (2 Layers of Beta Cloth Added), Plus 2 Inch Standoff, Beta-Kevlar-Kevlar-Beta MMOD Blanket Over Wire Harness

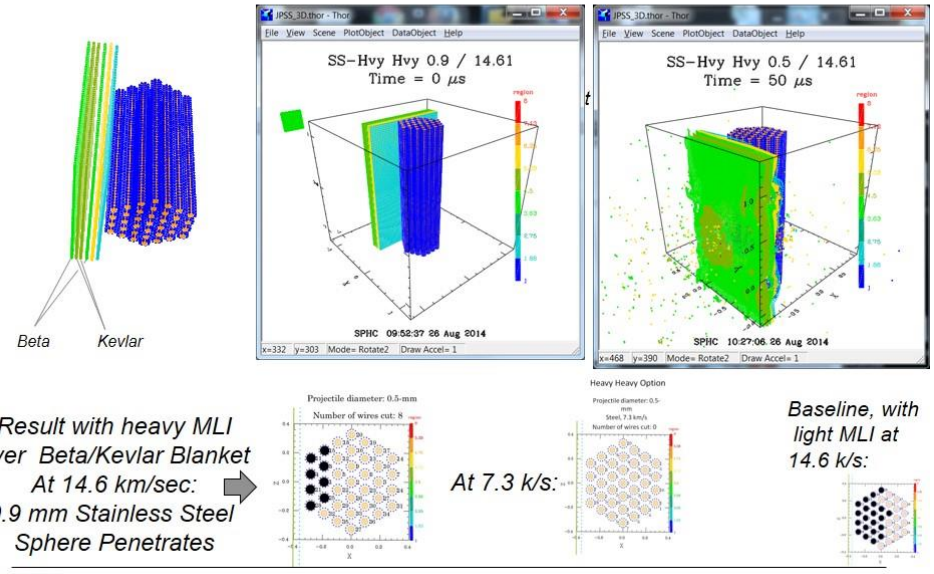

Result with heavy MLI over Beta/Kevlar Blanket At 14.6 km/sec: 0.9 mm Stainless Steel Sphere Penetrates

At 7.3 k/s:

Baseline, with light MLI at 14.6 k/s:

3/19/2015-17

IDA

Enhanced Wire Harness Shielding Considering Oblique Impact

- ***Based in part on these hydrocode results, the program decided to place an enhanced MLI/MMOD shield over zenith deck wire harness areas***
- ***As stated earlier, 99.5% of orbital debris approaches from within the X-Y (orbital) plane. Debris approaching from the Y axis would impact the deck at 14.6 km/sec and impact the blanket at 75 degrees obliquity***
- ***Program elected to implement an MLI & MMOD blanket design similar to one placed over CTU***

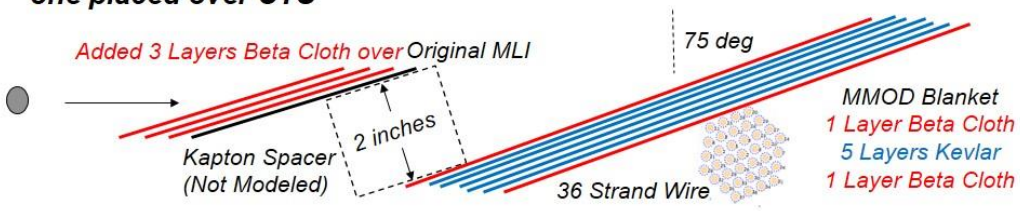

- ***Ultimate objective was to prevent penetration of 3mm aluminum sphere through adding enhanced MMOD blanket over zenith facing wires***

3/19/2015-18

IDA

Hydrocode Results
Enhanced Wire Harness Shielding

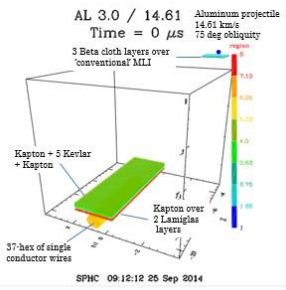

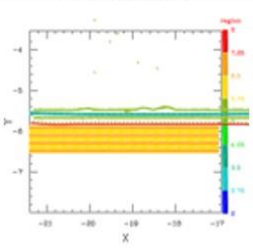

2.12 mm Stainless steel sphere at 14.61 km/sec and 75 deg obliquity marginally penetrated MMOD blanket (clipping 2 wires)

3 mm Aluminum sphere at 14.61 km/sec and 75 deg obliquity did not penetrate MMOD blanket

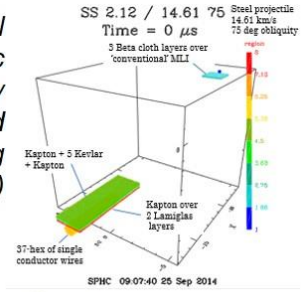

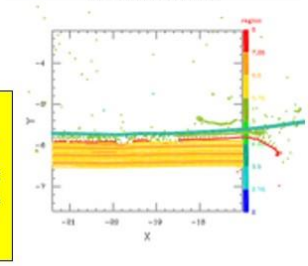

Conservatively assume ballistic limit for MLI/MMOD blanket is 2.12mm Stainless steel and 3mm Aluminum at all (lower) velocities.

3/19/2015-19

IDA

Estimating Exposed Wiring Area
JPSS Zenith Deck

		Exposed Area by Approach Direction (m^2)									
Region	Surface Area	0 deg	5	15	25	35	45	55	65	75	85
A	**0.930**	**0.241**	**0.239603**	**0.233331**	**0.219177**	**0.197053**	**0.170032**	**0.138053**	**0.102683**	**0.063927**	**0.021817**
B	**0.454**	**0.118**	**0.117139**	**0.114073**	**0.107153**	**0.096337**	**0.083127**	**0.067492**	**0.050201**	**0.031253**	**0.010666**
C	**0.527**	**0.137**	**0.135775**	**0.132221**	**0.1242**	**0.111663**	**0.096351**	**0.07823**	**0.058187**	**0.036225**	**0.012363**
D	**0.142**	**0.037**	**0.036606**	**0.035648**	**0.033485**	**0.030105**	**0.025977**	**0.021091**	**0.015688**	**0.009767**	**0.003333**
E	**0.129**	**0.033**	**0.033278**	**0.032407**	**0.030441**	**0.027368**	**0.023616**	**0.019174**	**0.014262**	**0.008879**	**0.00303**
	Obliquity	75	75.1	75.5	76.4	77.8	79.5	81.5	83.7	86.1	88.7
	Total Area	0.57	0.56	0.55	0.51	0.46	0.40	0.32	0.24	0.15	0.05

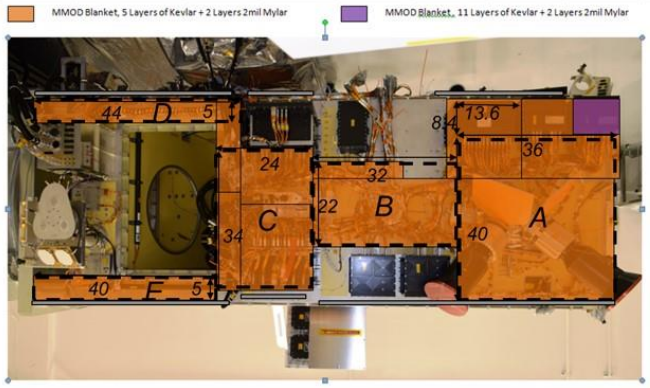

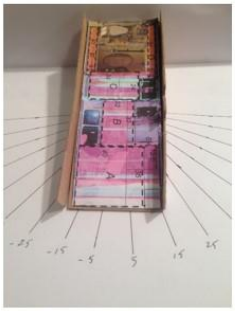

Orbital Debris Approach Angles

3/19/2015-20

IDA

Estimating Exposed Wiring Area
Effect of Shadowing by Side Thermal Panels

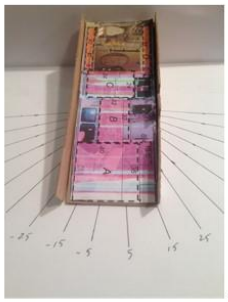

Orbital Debris Approach Angles

	Estimated Exposure by Approach Direction (%)								
Region	5	15	25	35	45	55	65	75	85
A	1	1	1	0.5	0.25	0.1	0.05	0.01	0.01
B	1	1	0.5	0	0	0	0	0	0
C	1	0.8	0	0	0	0	0	0	0
D	1	1	0	0	0	0	0	0	0
E	1	0	0	0	0	0	0	0	0

		Exposed Area Including Shadowing by Approach Direction (m^2)								
Region	Surface Area	0 deg	5	15	25	35	45	55	65	75	85
A	0.930	0.241	0.239603	0.233331	0.219177	0.098527	0.042508	0.013805	0.005134	0.000639	0.000218
B	0.454	0.118	0.117139	0.114073	0.053577	0	0	0	0	0	0
C	0.527	0.137	0.135775	0.105777	0	0	0	0	0	0	0
D	0.142	0.037	0.036606	0.035648	0	0	0	0	0	0	0
E	0.129	0.033	0.033278	0	0	0	0	0	0	0	0
	Obliquity	75	75.1	75.5	76.4	77.8	79.5	81.5	83.7	86.1	88.7
	Total Area	0.57	0.56	0.49	0.27	0.10	0.04	0.01	0.01	0.00	0.00

Exposed areas of wire harnesses by approach angle

15 Deg Approach

25 Deg Approach Angle

35 Deg Approach Angle

45 Deg Approach

3/19/2015-21

IDA

Risk Assessment of MMOD Blanket Penetration in 7 Years
Considering Obliquity and Shadowing

Steel risk with shadowing

		Steel		7 years
Approach	BL for N	Pen Flx	Area	N pens
5	2.120	0.003448	0.562	0.013563491
15	2.120	0.001757	0.488	0.006000823
25	2.120	0.000942	0.272	0.001792875
35	2.120	0.000688	0.098	0.000472185
45	2.120	0.000549	0.042	0.000161411
55	2.120	0.000484	0.013	4.40532E-05
65	2.120	0.000462	0.005	1.61581E-05
75	2.120	0.000471	0.0006	1.97961E-06
85	2.120	9.55E-05	0.0002	1.33696E-07
			Total Port	0.0221
			Total Stbd	0.0221
			Total	**0.0441**
			Ppen	**0.0431**

Aluminum risk with shadowing

		Aluminum		7 years
Approach	BL for N	Pen Flx	Area	N pens
5	3.000	0.000678	0.562	0.002668771
15	3.00	0.000503	0.488	0.001718317
25	3.000	0.000259	0.272	0.000493157
35	3.000	0.000184	0.098	0.000126244
45	3.000	0.000149	0.042	4.38661E-05
55	3.000	0.000129	0.013	1.17334E-05
65	3.000	0.000116	0.005	4.07175E-06
75	3.000	0.000114	0.0006	4.80279E-07
85	3.000	6.57E-05	0.0002	9.19177E-08
			Total Port	0.0051
			Total Stbd	0.0051
			Total	**0.0101**
			Ppen	**0.0101**

Total Risk ~ 5.3% probability of 1 or more MMOD blanket penetrations in 7 years.

3/19/2015-22

Risk Assessment of Zenith Deck Wire Failure in 7 Years Considering Obliquity and Shadowing

IDA

- *Probability (≥ 1 penetration of enhanced MMOD shield) is ~ 0.053 (5.3%).*
- *This is a conservative estimate of critical wire failure risk.*
- *Probability of critical wire failure would be lower, accounting for:*
  - *Actual wire coverage (less than coverage of MMOD blanket)*
  - *Higher ballistic limit at other approach angles (lower velocities)*
  - *Criticality and redundancy of wires (not every wire hit is critical, and even if critical, are often redundant)*
- *Considering these factors, probability of wire failure could well be beneath 1%.*

3/19/2015-23

REPORT DOCUMENTATION PAGE

Form Approved
OMB No. 0704-0188

1. REPORT DATE *(DD-MM-YYYY)*	2. REPORT TYPE	3. DATES COVERED *(From - To)*
01- 07 - 2015	Technical Memorandum	April 2015 - April 2015

4. TITLE AND SUBTITLE

Joint Polar Satellite System (JPSS) Micrometeoroid and Orbital Debris (MMOD) Assessment

5a. CONTRACT NUMBER

5b. GRANT NUMBER

5c. PROGRAM ELEMENT NUMBER

6. AUTHOR(S)

Squire, Michael D.; Cooke, William J.; Williamsen, Joel; Kessler, Donald; Vesely, William E.; Hull, Scott H.; Schonberg, William; Peterson, Glenn E.; Jenkin, Alan B.; Cornford, Steven L.

5d. PROJECT NUMBER

5e. TASK NUMBER

5f. WORK UNIT NUMBER

869021.05.07.05.32

7. PERFORMING ORGANIZATION NAME(S) AND ADDRESS(ES)

NASA Langley Research Center
Hampton, VA 23681-2199

8. PERFORMING ORGANIZATION REPORT NUMBER

L-20595 NESC-RP-14-00948

9. SPONSORING/MONITORING AGENCY NAME(S) AND ADDRESS(ES)

National Aeronautics and Space Administration
Washington, DC 20546-0001

10. SPONSOR/MONITOR'S ACRONYM(S)

NASA

11. SPONSOR/MONITOR'S REPORT NUMBER(S)

NASA/TM-2015-218780

12. DISTRIBUTION/AVAILABILITY STATEMENT

Unclassified - Unlimited
Subject Category 16 Space Transportation and Safety
Availability: NASA STI Program (757) 864-9658

13. SUPPLEMENTARY NOTES

14. ABSTRACT

The Joint Polar Satellite System (JPSS) Project requested the NASA Engineering and Safety Center (NESC) conduct an independent evaluation of the Micrometeoroid and Orbital Debris (MMOD) models used in the latest JPSS MMOD risk assessment. The principal focus of the assessment was to compare Orbital Debris Engineering Model version 3 (ORDEM 3.0) with the Meteoroid and Space Debris Terrestrial Environment Reference version 2009 (MASTER-2009) and Aerospace Debris Environment Projection Tool (ADEPT) and provide recommendations to the JPSS Project regarding MMOD protection. The outcome of the NESC assessment is contained in this report.

15. SUBJECT TERMS

Micrometeoroid and Orbital Debris; NASA Engineering and Safety Center; Joint Polar Satellite System; MASTER-2009, ORDEM; ADEPT

16. SECURITY CLASSIFICATION OF:			17. LIMITATION OF ABSTRACT	18. NUMBER OF PAGES	19a. NAME OF RESPONSIBLE PERSON
a. REPORT	b. ABSTRACT	c. THIS PAGE			STI Help Desk (email: help@sti.nasa.gov)
					19b. TELEPHONE NUMBER *(Include area code)*
U	U	U	UU	225	(757) 864-9658